Methodology for monitoring waterlogging and salt accumulation on selected irrigation schemes in South Africa

JP Nell, A van Niekerk, SJ Muller, D Vermeulen, T Pauw, G Stephenson, J Kemp

WATER RESEARCH COMMISSION
TT 648/15

Methodology for monitoring waterlogging and salt accumulation on selected irrigation schemes in South Africa

Report to the

WATER RESEARCH COMMISSION

by

JP Nell[1], A van Niekerk[2], SJ Muller[2], D Vermeulen[2], T Pauw[2], G Stephenson[2], J Kemp[2]

[1]ARC-Institute for Soil, Climate and Water

[2]Stellenbosch University

WRC Report No. TT 648/15

December 2015

Obtainable from
Water Research Commission
Private Bag X03
Gezina, 0031

orders@wrc.org.za or download from www.wrc.org.za

The publication of this report emanates from a project entitled *Methodology for monitoring waterlogging and salt accumulation on selected irrigation schemes in South Africa* (WRC project no. K5/1880).

ISBN 978-1-4312-0739-8
Printed in the Republic of South Africa

EXECUTIVE SUMMARY

BACKGROUND

There is a need for a suitable national waterlogging and salt-affected soil monitoring and evaluation system to monitor the impact of agriculture, mining, urban and industrial activities. In its absence, various *ad hoc* pieces of data, information, norms and standards that are constantly being collected will remain pieces of a large puzzle that is extremely difficult to incorporate into a holistic picture.

No reliable secondary salinity, sodicity and waterlogging information is obtainable for South Africa, nor are there monitoring programmes to track the waterlogging and salt-affected status of soils on irrigation schemes. Reliable waterlogging, salinity and sodicity information is required for various agricultural and environmental studies on a provincial and national scale. Examples include the FAO's Terrastat, Aquastat and LADA programmes, the International Commission of Irrigation and Drainage (ICID) and South Africa's State of Environment reporting.

Comprehensive and reliable sources of data, from which trends in constituents depicting the long-term sustainability of irrigated agriculture could be deduced, are lacking. It is evident from information available that the degree of degradation varies considerably between irrigation schemes and also over time within the same irrigation scheme. An increase in salinity and sodicity normally coincides with hydrologically dry years with below-average runoff and an increase in waterlogging occurs during hydrologically wet years. A review of about 3000 soil irrigation reports revealed that soils free of limitations for sustainable irrigation are limited in extent in South Africa. However, it appears that waterlogging, salinity and sodicity affects only 8-18% of the area under regular irrigation in South Africa (Nell & De Clercq, 2008). With the elevated soil salinity and sodicity levels expected to rise further in future, it will become increasingly necessary to monitor the situation on irrigation schemes and within irrigated lands in order to identify salt accumulation and waterlogging trends and associated potential problems timeously for remedial action to be taken.

The operation and management of irrigation water must include proper monitoring and reduction of seepage and other water losses in the system, particularly if there is a component of recharge by raising water tables and cause salt-affected soils. Management-related distribution losses (causing waterlogging that salinization conditions) on irrigation schemes are, among others, caused by inaccurate dam releases, faulty sluice gate control, inaccurate lag time calculations, errors in water requisition calculations and insufficient monitoring of canal end points (Benade, 1991), and over-irrigation.

RATIONALE

The high costs of measuring waterlogging and salt-affected soils on South African irrigation schemes, as well as inconsistencies in data collection and reporting methods, have resulted in incomplete and often contradictory information on the extent and distribution of salt-affected and waterlogged soils. Since the late 1980s no national effort has been made to quantify the extent of waterlogging and salt accumulation across irrigation schemes in South Africa. Indications are that soil and water quality are declining and these problems are actually escalating. To identify soils for drainage and reclamation, the extent of waterlogging and salt accumulation has to be determined.

Major capital investment was made in irrigated areas in South Africa in the past. It is, therefore, important to monitor degradation and plan rehabilitation at farm and scheme level with reliable information. Sustainability of food production and infrastructure are potentially threatened if a reliable monitoring system is not in place for South African irrigation schemes. At this stage, waterlogging and the problem of salt-affected soils are based on intelligent guesses due to lack of recent validated data.

National monitoring of waterlogging and salt accumulation is a high priority but currently no proven methodology is available to undertake this task. Therefore a methodological approach at appropriate scales has to be tested before application at national level can be implemented.

AIMS

AIM 1

To develop and test a methodological approach for identification, classification and monitoring the extent and degree of waterlogging and salt accumulation at farm, irrigation scheme and national level.

AIM 2

To develop guidelines and make recommendations for application of the methodology to monitor the extent and degree of waterlogging and salt accumulation on irrigation schemes at a national level.

AIM 3

To make available soil maps in different digital formats for at least the ten largest irrigation schemes in South Africa and establish links to the AGIS website of the National Department of Agriculture (NDA)[1].

AIM 4

To quantify the current level of waterlogging and salt accumulation and monitor changes over time at the appropriate scale on selected schemes.

AIM 5

To capture temporal and spatial data in a user-friendly geographical information database.

METHODOLOGY

Due to the costs involved in soil sampling and analysis, the only viable option for monitoring waterlogging and salt accumulation over large areas (i.e. irrigation scheme level) is to use existing soil maps (where available), terrain data and satellite imagery to identify areas where these processes are likely (or unlikely) to occur. By combining various sources of data and a priori knowledge, large areas can be eliminated from further consideration and specific areas can be highlighted as being potentially affected.

An experimental approach was taken in developing a suitable methodology for quantifying and monitoring waterlogging and salt accumulation. Various sources of data and techniques were applied and compared to empirical (reference) data to determine their potential for monitoring waterlogging and salt accumulation.

---

[1] During this project NDA became the Department of Agriculture, Forestry and Fisheries

The techniques were applied within three main strategies. The first approach attempted to use remote sensing to directly detect salt accumulation by studying the spectral characteristics of soils that are salt-affected. A satellite image with a very high spatial and spectral resolution was used for this experiment to reduce the influence of image resolution on the spectral, statistical and image classification techniques that were evaluated. The main aim of these experiments was to investigate the relationships between known affected areas (as determined using EC measurements) and a range of image features (bands and indices), with the purpose of determining whether these relationships can be used to accurately predict the spatial distribution of salt accumulation.

The second strategy was to evaluate whether an indirect remote sensing approach can effectively be used to monitor salinity levels. In this approach vegetation response to saline conditions was investigated. Two different data sources were evaluated at two different (field and scheme) scales. The first series of experiments made use of a very high resolution (0.5 m) WorldView-2 satellite image to detect changes in vegetation response to saline conditions within a single (lucerne) field. The influence of image resolution was also examined. The second series of experiments made use of high (2.5 m) resolution SPOT-5 images. These experiments were carried out on a variety of crops in two dissimilar irrigation schemes (Vaalharts and Breede River), mainly to determine to what extent statistical and classification techniques are influenced by large variations in how different types of crops respond to saline conditions.

The final set of experiments focussed on investigating the relationships between terrain data and waterlogging and salt accumulation in the Vaalharts and the Breede River study areas. A series of statistical analyses were carried out to find the continuous relationships between a large set of terrain features derived from three different digital elevation models (DEMs). Machine learning algorithms were also employed to model waterlogging and salt accumulation.

Each experiment was assessed in terms of its accuracy and in the context of finding an operational solution to quantifying and monitoring waterlogging and salt accumulation at field, farm and irrigation scheme level at national scale. The techniques and data sources that showed potential were considered for incorporation in an operational solution. Some techniques were excluded from investigation based on the outcomes of the experiments.

Three approaches to mapping waterlogged and salt-affected areas were identified as having potential for future application. The first is a modelling approach whereby hydrological, terrain and soil data is used to determine where waterlogging or salt accumulation is likely to occur. Another approach is to differentiate affected and unaffected soils by making use of remotely-sensed imagery (hyperspectral or multispectral) to analyse their spectral properties. This direct remote sensing method is consequently applied to exposed (bare) soil. The third approach, referred to as the indirect remote sensing approach, examines vegetation response (e.g. loss of biomass) to saline or waterlogged conditions. The latter approach mainly makes use of vegetation indices (VIs) derived from multispectral imagery.

RESULTS AND DISCUSSION

All three of the above approaches were evaluated in this research. For the direct remote sensing approach, a WorldView-2 (WV2) satellite image was used to investigate if there are any spectral features of affected soils that can be used in their discrimination. The WV2 image was ideal for this purpose as it had the highest possible spatial (0.5 m) and spectral (8 bands) resolution available at the time of analysis (higher resolution imagery has since become available). Although such imagery is too expensive to be used for monitoring purposes over large areas, its use in this study contributed to the establishment of a "best case scenario". Also, it enabled an investigation into how less expensive imagery (e.g. those offering only red, green, NIR bands) might perform in comparison. Statistical analyses as well as rule-based and supervised classification methods were evaluated.

Experiments with the direct remote sensing approach showed that there were a number of statistically significant relationships between image features and salt accumulation, with $NDSI_1$ being the best predictor. However, the use of WV2 imagery to identify salt-affected soils was found to be unreliable as all of the methods evaluated grossly overestimated salt accumulation. This was attributed to the inconsistencies in the visual appearance of salt-affected soils as in many cases there was no visible evidence of salt accumulation (e.g. salt precipitation). Another factor that complicates the detection of salt accumulation when bare soils are observed using remote sensing is the disturbance caused by soil preparations (e.g. ploughing) as this can alter the soil surface and reflectance. But the main limitation of the direct approach is that a relatively small proportion of fields in irrigation schemes are bare at any given time during the year. The implication is that multiple analyses will be required to map an entire irrigation scheme. This would be costly, even with the use of less expensive satellite imagery.

Field verifications of the various satellite images used were done at Vaalharts, Loskop: Olifants River, Vredendal: Olifants River, Makhathini, Sundays River, Tugela River, Limpopo River, Douglas: Vaal and Orange River irrigation schemes. Soil samples were taken at the observation points for analysis and quantification of the salt content. In the Lower Orange River the soil sampling points and areas identified as salt-affected and/or waterlogged with remote sensing by Volschenk *et al.* (2005) and Mashimbye (2005) were again visited to verify their findings. Historical soil maps and reports were also used to identify problematic areas and to compare the change in salt-affected and waterlogged soils over time.

The indirect remote sensing approach was evaluated in the Vaalharts and Breede River study areas. The WV2 image of a lucerne field at Vaalharts was used for evaluating vegetation response to saline conditions. Several experiments were also carried out to investigate the impact of reduced spatial and spectral resolution of satellite imagery – effectively testing the hypothesis that very high spatial resolution imagery is required for monitoring salt accumulation and waterlogging in South African irrigation schemes. A total of 445 WV2-derived spectral and spatial (texture) features were analysed at 0.5, 2, 6, 10, 15 and 20 m resolutions to determine their potential for distinguishing between salt-affected and unaffected soils. Regression analyses were carried out to investigate the relationships between the image features and EC values of 30 soil samples collected in the field. The results showed that there are significant and strong continuous relationships between EC and several of the features considered and that the yellow band, as well as a number of VI and texture features, produced the strongest models. Generally, the strength of these relationships diminished as the spatial resolution was reduced. Overall, the regression analysis and classification and regression tree (CART) results were very promising as they showed that VIs generated at 6 m and higher resolution can potentially be used. The results also suggested that high resolution texture features can potentially be used together with VIs for the indirect monitoring of salt-affected soils. Furthermore, the relatively high spectral resolution of the WV2 imagery is not critical as the VIs (based on red and NIR wavelengths only) performed relatively well compared to the performance of the individual bands.

It was concluded that, due to its relatively high cost, the operational use of WV2 imagery for regular monitoring of large areas is not viable. The results show that slightly lower spatial and spectral resolution imagery might produce comparable results. Notable candidates are SPOT-5 (2.5 m panchromatic; 10 m multispectral), SPOT-6 (1.5 m panchromatic; 6 m multispectral), RapidEye (5 m multispectral) and Sentinel-2 (10 m multispectral) data. Although SPOT-5 will soon be decommissioned, its large archive of imagery will be very useful for change analyses where historical baselines are required.

The models generated only considered soil samples collected in a cultivated field with a single crop. Given that crops differ in their response to saline conditions, an additional series of experiments were carried out to investigate how these variations will affect the results. These experiments were carried out in the Vaalharts and Breede River study areas using slightly lower resolution SPOT-5 imagery. It was found that the spectral responses of affected crops differed considerably between the two study areas and that none of the feature sets and/or classification algorithms stood out as being superior for monitoring salt accumulation on irrigation scheme level. Due to the large variations in how different crops respond to saline conditions, the classifications tended to produce many false positives. The accuracy levels also varied significantly according to training set size, which is problematic as the routine collection of large sets of soil samples is prohibitively expensive.

The final set of experiments investigated the efficacy of elevation data and its derivatives for modelling salt accumulation at irrigation scheme level. Vaalharts and Breede River were again chosen as the study areas and the SRTM DEM, SUDEM and DSMs derived from high-resolution stereoscopic aerial photography were used as the primary data sources. Numerous derivatives were produced from the primary datasets and several terrain analysis methods were assessed. Two rule sets based on regression modelling and CART, as well as five supervised classifiers (NN, ML, SVM, DT and RF) were considered. The kNN supervised classifier was the most successful in differentiating salt-affected from unaffected soils in both study areas, but it was concluded that the use of elevation data and its derivatives to identify salt-affected soils is ineffective and unreliable. Most of the methods evaluated either underestimated or overestimated salt-accumulation or achieved low accuracies, especially for Breede River. The low spatial resolution and quality of the DEMs might have had a negative impact on the results and other elevation data sources, such as LiDAR, should be explored in future research. However, such data may be prohibitively expensive to acquire for large irrigation schemes.

Many experiments were carried out during the course of this research project. This included the use of CART on all possible input data (satellite imagery, terrain derivatives, soil data), multi-temporal vegetation response monitoring, and object-based terrain analyses using high-resolution (2 m) DSMs. Not all of these experiments were successful, but they provided a better understanding of the complexities involved in monitoring salt accumulation and waterlogging in irrigation schemes. It became clear that image texture (heterogeneity) is an important feature for identifying areas that are likely salt-affected or waterlogged. The newly-developed within-field anomaly detection (WFAD) method is based on the principle that heterogeneous areas are in many cases indicative of waterlogging or salt accumulation. Affected areas often stand out as being spectrally different compared to the rest of a field, either because of a reduction in biomass due to saline or saturated conditions (in cultivated fields) or due to specific species of vegetation occurring in fallow fields. Although such “anomalies” can be easily identified using visual interpretation of imagery, they are not easily extracted from remotely-sensed data. Traditional remote sensing techniques involve classifying individual pixels (cells) without taking topology (relationships between spatial entities) into consideration. The WFAD method was implemented and evaluated in all of the study areas. The results showed that, compared to the other methods evaluated, WFAD produced the most promising results for monitoring and quantification purposes. WFAD not only produced accurate (74.9% on average) results, but is also the most cost-effective technique as it can be applied on both vegetated and non-vegetated fields; requires no empirical data; makes use of freely-available imagery (SPOT-5); and has the potential to be fully automated.

The WFAD method was used to quantify the extent of affected areas on nine irrigation schemes. On average, 3.3% of the areas considered were found to be affected. This estimate was adjusted to 6.27% by adding abandoned fields. Although WFAD is very successful in identifying salt-affected and waterlogged areas, one of its main limitations is that it cannot discriminate such areas from anomalies that are caused by other factors (e.g. drought, flooding, soil compaction, disease, inadequate fertilizer application). Based on the field surveys conducted in nine irrigation schemes, waterlogging and salt accumulation were the cause in 77.8% of cases. The WFAD method should consequently be regarded as a scoping mechanism that can direct attention to areas that are likely affected by salt accumulation and/or waterlogging. Such areas should preferably be visited to investigate the likely causes.

If the figure of 6.27% of areas affected is applied to the 1.5 million hectares under irrigation in South Africa, the area that is salt-affected and waterlogged on South African irrigation schemes is 94 050 ha. The areas affected by waterlogged and salt-affected soils on the different irrigation schemes studied were: Vaalharts 849 ha (3.1%), Loskop 2 345 ha (5.7%), Tugela 2103 ha (7.4%), Limpopo River 564 ha (6.4%), Makhathini 361 ha (7.8%), Olifants River 665 ha (5.6%), , Breede River 2215 ha (7.3%), Sundays River 741 ha (3.9%) and Douglas (Vaal and Orange Rivers) 2124 ha (9.1%).

CONCLUSIONS

In this project various data sources and methodologies for the identification of areas prone to salt accumulation and waterlogging were investigated. This includes land cover mapping, bare soil analysis (i.e. direct approach), multi-temporal crop condition monitoring (i.e. indirect approach), terrain analysis, within-field anomaly detection, and machine learning.

The occurrence of salt accumulation and waterlogging in generally small patches in South African irrigation schemes poses unique challenges and will require a robust modelling strategy.

It is important to note that no model based on remotely-sensed data will ever replace in-field monitoring. The purpose of this study was to develop a method to detect potential areas of salt accumulation or waterlogging so that in-field monitoring can be performed.

Various factors have to be considered when selecting a specific source of satellite imagery for a classification project. The spatial, spectral and temporal resolutions are important factors, as is cost.

Despite the efforts of the science community, there is currently no robust model for accurately and consistently extracting soil water content or soil salinity from synthetic aperture radar (SAR) imagery. This science is very much still in an experimental phase, and most authors agree that great strides still need to be made before such an application can be operational.

The direct and indirect remote sensing approaches show the most promise as they can be applied to high resolution, multispectral satellite imagery. Statistical methods such as regression, partial least squares regression and multi-regression have been shown to be successful in a number of studies and should be investigated further. Surprisingly little attention has been given to the use of modern image classification and machine learning algorithms (e.g. classification and regression trees, decision trees, support vector machines and random forest) for mapping waterlogged and salt-affected areas. Such algorithms are very effective for this purpose – as demonstrated in this research – but they require sufficient in situ (soil samples) data that is often not available or expensive to collect.

From the review of the literature it is clear that there is a large body of work that is focussed on finding practical solutions for monitoring waterlogging and salt accumulation. However, none of the methods stood out as being the ultimate solution, with each having some kind of limitation for operational application. It is consequently likely that the solution lies not in one technique but in a combination of methods. However, to find the best combination of methods for monitoring waterlogging and salt accumulation, each of the most promising techniques must be evaluated in a South African context to better understand their individual strengths and limitations. It is critical that the uncertainties in the outputs of the different techniques must be taken into consideration before they are incorporated into a modelling strategy.

Due to the costs involved in soil sampling and analysis, the only viable option for monitoring waterlogging and salt accumulation over large areas (i.e. irrigation scheme level) is to use existing soil maps (where available), terrain data and satellite imagery to identify areas where these processes are likely (or unlikely) to occur. By combining various sources of data and *a priori* knowledge, large areas can be eliminated from further consideration.

RECOMMENDATIONS FOR FUTURE RESEARCH

- South Africa must adopt standardized monitoring, assessments, modelling and mapping methodologies/procedures to improve the quantification and qualification of salt-affected and waterlogged soils on a scheme and national scale.
- Viable permanent irrigated agriculture requires periodic information on salts and water tables. A network of representative monitoring points (benchmark soil sites) should therefore be established on irrigation schemes in conjunction with remote sensing.
- Assessment and monitoring of salt-affected soils with remote sensing should include associated salts/metals, e.g. magnesium, iron, boron, manganese, chloride, etc.
- Identify areas on existing irrigation schemes that were abandoned due to waterlogging and salt-affected soils using historical aerial photography and satellite images. Because the WFAD method only considers cultivated or fallow fields, it does not incorporate fields that have been abandoned due to salt accumulation or waterlogging. This exclusion can have a significant effect on the overall quantification of affected areas.

ACKNOWLEDGEMENTS

The Water Research Commission (WRC) is acknowledged for initiating, funding and managing this project under the directed call for proposals.

The authors would like to thank the Reference Group of the WRC Project for the guidance and the constructive discussions during the duration of the project:

Dr GR Backeberg	Water Research Commission (Chairman)
Prof JG Annandale	University of Pretoria
Dr WP de Clercq	Stellenbosch University
Mr HM du Plessis	Independent Consultant
Mr D Haarhoff	GWK
Dr M Lück-Vogel	CSIR
Mr RK Mampholo	Department of Agriculture, Forestry and Fisheries
Dr T Volschenk	ARC Infruitec-Nietvoorbij

The project was made possible with the co-operation and help of many individuals:

- Dr DJ Beukes from the ARC-Institute for Soil, Climate and Water for his valuable guidance, support and discussions.
- Ms V Roberts from the ARC-Institute for Soil, Climate and Water and Mr F Reeders from Nvirotek laboratories for conducting the chemical analyses of the soil.
- Prof LD van Rensburg from the University of the Free State, Mr PMJ Verwey from DAFF and the late Mr C van Niekerk of the Vaalharts experimental farm for help and advice on identifying problematic areas on Vaalharts.
- Farmers at the various irrigation schemes for providing access to their irrigated areas for soil sampling and verification of images and for their intuitive insight to problem areas.
- Dr TP Fyfield from the ARC-Institute for Soil, Climate and Water for editorial assistance.

This page was left blank intentionally

TABLE OF CONTENTS

LIST OF FIGURES

LIST OF TABLES

LIST OF ABBREVIATIONS

AGIS	Agricultural Geo-referenced Information System
AI	Artificial Intelligence
Ar	Anomaly Ratio
ASTER	Advanced Spaceborne Thermal Emission and Reflection Radiometer
AUROC	Area Under the Receiver Operating Characteristic
CART	Classification And Regression Tree
CB	Coastal Blue
CEC	Cation Exchange Capacity
CNBL	Channel Network Base Level
COSRI	Combined Spectral Response Index
dB	Decibels
DEM	Digital Elevation Model
DSM	Digital Surface Model
DT	Decision Tree
EC	Electrical Conductivity
EMI	Electromagnetic Induction
EO	Earth Observation
ESP	Exchangeable Sodium Percentage
FAO	Food and Agriculture Organization of the United Nations
GCPs	Ground Control Points
GEOBIA	GEographical Object-Based Image Analysis
GIS	Geographical Information System
HAND	Height Above Nearest Drainage
HIS	Intensity Hue and Saturation
ICID	International Commission on Irrigation and Drainage
IRS	Indian Remote Sensing
JM	Jeffries-Matusita
kNN	k-Nearest Neighbour
LADA	LAnd Degradation Assessment in Drylands
MCDM	Multi-Criteria Decision Making
ML	Maximum Likelihood
MSAVI	Modified Soil Adjusted Vegetation Index
NDSI	Normalized Difference Salinity Indices
NDVI	Normalized Difference Vegetation Index
OBIA	Object-Based Image Analysis
OA	Overall Accuracy
PCA	Principal Component Analysis
RADAR	Radio Detection and Ranging

RE	Red Edge
RF	Random Forest
ROC	Receiver Operating Characteristic (ROC)
SAGA	System for Automated Geoscientific Analyses
SANSA	South African National Space Agency
SAR	Sodium Absorption Ratio
SAR	Synthetic Aperture Radar
SAVI	Soil-Adjusted Vegetation Index
SEaTH	SEparability and Thresholds
SPOT	Satellite Pour l'Observation de la Terre
SRTM	Shuttle Radar Topography Mission
SUDEM	Stellenbosch University Digital Elevation Model
SVM	Support Vector Machine
TDS	Total Dissolved Solids
TMS	Table Mountain Sandstone
TWI	Topographic Wetness Index
VDTCN	Vertical Distance To Channel Network
VI	Vegetation Index
VIL	Variable Importance List
VIS	Virtual Intelligent Sensor
WFAD	Within-Field Anomaly Detection
WFAD	Within-Field Anomaly Detection
WRC	Water Research Commission
WV2	WorldView-2

1 INTRODUCTION AND OBJECTIVES

1.1 Introduction

There is a need for a suitable national waterlogging and salt accumulation monitoring and evaluation system, to monitor the impact of agriculture, mining, urban and industrial activities on South African irrigation schemes. In its absence, various *ad hoc* pieces of data, information, norms and standards that are constantly being collected will remain pieces of a large puzzle that is extremely difficult to incorporate into a holistic picture.

No reliable secondary salinity, sodicity and waterlogging information is obtainable for South Africa, nor are there monitoring programmes to track the waterlogging and salt-affected status of soils on irrigation schemes. Reliable waterlogging, salinity and sodicity information is required for various agricultural and environmental studies on a provincial and national scale. Examples include the FAO's Terrastat, Aquastat and LADA programmes, International Commission on Irrigation and Drainage (ICID) and South Africa's State of Environment reporting.

Theoretically all land could be irrigated provided the necessary financial resources and management skills, but the consequences of incorrect management or incorrect selection of irrigation areas can be disastrous, causing irrigation areas to become waterlogged and/or salt-affected, thus rendering them unfit for continued sustainable irrigation. There is a lack of comprehensive and reliable sources of data from which trends in constituents depicting the long-term sustainability of irrigated agriculture could be deduced. It is evident from information available that the degree of degradation varies considerably between irrigation schemes and also over time within the same irrigation scheme in South Africa. An increase in salinity and sodicity normally coincide with hydrologically dry years with below-average runoff, and an increase in waterlogging during hydrologically wet years. A review of about 3 000 reports at the Agricultural Research Council – Institute for Soil, Climate and Water (ARC-ISCW) revealed that soils free of limitations for sustainable irrigation are limited in extent in South Africa. However, it appears that severe waterlogging, salinity and sodicity affects only 8-18% of the area under regular irrigation in the country Backeberg *et al*. (1996). With the elevated soil salinity and sodicity levels expected to rise in future, it will become increasingly necessary to monitor the situation on irrigation schemes and within irrigated lands in order to identify salt accumulation and waterlogging trends and associated potential problems timeously for remedial action to be taken.

Conventionally, soil salinity has been measured by collecting *in situ* soil samples and analysing those samples in the laboratory to determine their solute concentrations or electrical conductivity. However, these methods are time-consuming and costly since dense sampling is required to adequately characterize the spatial variability of an area. The detection of soil salinity and waterlogging are mostly time consuming, but remote sensing data and techniques offer more efficiently and economically rapid tools and techniques for monitoring and mapping soil salinity and waterlogging.

Remote sensing can contribute a great deal to monitoring salt accumulation and waterlogging because of its ability to capture information at both spatial and temporal scales (Abbas et al., 2013). Bastiaanssen *et al*. (2000) states that remote sensing has the potential to predict soil salinity, perform diagnosis and assess its impact. Compared to regular field surveys this ability can save labour, time and effort (Eldiery et al., 2005). Considering that there are no current programmes in place to monitor salt-affected areas in South Africa, remote sensing provides a promising alternative to regular field-based surveys.

1.2 Aims

AIM 1
To develop and test a methodological approach for identification, classification and monitoring the extent and degree of waterlogging and salt accumulation at farm, irrigation scheme and national level.

AIM 2
To develop guidelines and make recommendations for application of the methodology to monitor the extent and degree of waterlogging and salt accumulation on irrigation schemes at a national level.

AIM 3
To make soil maps available in different digital formats for at least the ten largest irrigation schemes in South Africa and establish links to the AGIS website of the National Department of Agriculture, Forestry and Fisheries.

AIM 4
To quantify the current level of waterlogging and salt accumulation and monitor changes over time at the appropriate scale on selected schemes.

AIM 5
To capture temporal and spatial data in a user-friendly geographical information database.

1.3 Structure of the report

The introduction and objectives are presented in Chapter 1. A wide-ranging literature study, which includes review papers on South African irrigation schemes and definitions – because no universally accepted definitions exist for the various salt and waterlogging parameters – is provided in Chapter 2. The nine different study areas are detailed in Chapter 3. The reference data collection procedures and methodological framework are given in Chapter 4. The different remote sensing approaches (direct and indirect) and terrain analyses at irrigation scheme level are described in Chapter 5. Chapter 6 provides a detailed overview of within-field anomaly detection method, with an accuracy assessment and quantification of affected areas, whilst Chapter 7 discusses the role of Geographic Information Systems. Chapter 8 comprises a summary and conclusions. Recommendations and areas for future research are given in Chapter 9.

2 LITERATURE REVIEW

2.1 Salt accumulation

There are many local names and terms for the different kinds of salt-affected soils in the world and it is difficult to find correlations, if any, between them.

The term salinity has become so ambiguous that its usefulness at a scientific level has become seriously endangered. There is no universally accepted definition for saline soils because the definition depends on the discipline and the type of measurement (Fitzpatrick, 2002). Soil scientists and geo-hydrologists, for example, distinguish between primary and secondary salinity; plant scientists use the distribution of salt-tolerant plant species and/or the approximate range of electrical conductivity (EC) levels to distinguish slightly, moderately or severely affected soils and/or plants; and scientists in other disciplines may use measurements of pH (>9), presence of sodium carbonate and high EC to distinguish between alkaline saline soils; while others use pH (<3.5) and the presence of sulphur and high EC to distinguish acid sulphate soils (Fitzpatrick, 2002).

Hall & Du Plessis (1984) use the word mineralization – a term they prefer to salinization – and sometimes mineral content for salinity. They defined mineralization as the progressive accumulation of dissolved solids by surface water and groundwater in passing through the land phase of the hydrologic cycle.

The traditional division between saline and non-saline soils in soil science has been set at a saturated electrical conductivity (EC_e) of 400 mS/m. According to Bresler *et al.* (1982), the terminology committee of the Soil Science Society of America recommended that this limit be decreased to 200 mS/m because of the large number of crops and ornamentals which can be affected by salinity even in the saturated paste EC range of 200 to 400 mS/m. This recommendation was not accepted and they are still using the 400 mS/m value (SSSA, 2007).

An excessive accumulation of salts in the soil profile causes a decline in agricultural productivity. Soil salinity is the term used to designate a condition in which the soluble salt content of a soil reaches a level harmful to crops (Childs & Hanks, 1975). Soil salinity affects plants directly through the reduced osmotic potential of the soil solution and the toxicity of specific ions such as chloride and sodium. If the salts are primarily sodic salts, their accumulation increases the concentration of sodium ions in the soil's exchange complex, which in turn affects soil properties and behaviour. Thus, salinity can also have indirect effects on plant growth through deleterious modification of such soil properties as swelling, porosity, water retention and permeability (Hillel, 1998).

The salt tolerance thresholds for crops vary between species. Maas & Hoffman (1977) summarized previous published work and carried out a comprehensive review of crop salt tolerance data, which was subsequently updated by Maas (1990). Salt tolerance data has inherent uncertainties concerning plant responses to spatial and temporal variations in root zone salinity (Hopmans & Bristow, 2002; Meiri & Plaut, 1985). Different kinds of plants can be expected to react differently to total salt concentration and to the composition of the soil solution under different soil-water regimes and climatic conditions. According to Tanji (1990), with the advent of new methods of irrigation and water management, the time has come for re-examination of salinity criteria, which ought to be based on dynamic (rather than static) concepts related to the movement as well as the state of water and salts in the soil.

The historical criterion to distinguish between sodic and non-sodic conditions has been an exchangeable sodium percentage (ESP) equal to 15% or more of the soil cation exchange capacity (CEC). Because of numerous potential errors in traditional CEC and ESP determinations, however, there are many situations where measured ESP values may be seriously in error. As a result, and to lessen the time and expense of diagnosis, some practitioners use the sodium adsorption ratio of the saturation extract for sodic soil characterization. Although exchangeable sodium percentage and sodium adsorption ratio are not exactly equal numerically, a ratio of 15 has been maintained for the sake of convenience as the threshold between sodic and non-sodic (Bresler *et al.,* 1982). However, this assumption is seriously in error for South African conditions as Nell (1991) established a 2:1 relationship between ESP and sodium adsorption ratio for most South African conditions. Therefore, the problem of defining what characteristics a sodic soil should possess has not yet been resolved satisfactorily to give a universally accepted definition. In some literature (Agassi *et al.,* 1985), the term sodic has even been applied to soils with low but no fixed ESP. In view of the continuous effect of sodium, from low to high levels, on soil behaviour, the establishment of a critical level of ESP or sodium adsorption ratio is very arbitrary and has caused considerable confusion. According to Sumner (1993), it would appear that the terms sodic and sodicity should become obsolete as their definition has become imprecise. Rather, soils should be described in terms of behaviour.

The definition of alkalinity was previously also problematic because it was considered synonymous with sodicity. Alkalinity is mostly expressed as a soil pH value greater than 7. For a soil to have a pH >7 it must be calcareous (pH>8.3), dolomitic or sodic. The basic chemical definition of alkalinity is the sum of the bases that can be titrated with strong acid.

Under irrigation, saline soils are formed primarily when high salinity water is used for irrigation. Soil salinity is determined by interaction between total dissolved solids (TDS) of irrigation water and leaching. Saline soils can, however, also be formed when salts from an elevated water table (which frequently form under irrigated land as a result of over-irrigation) are concentrated in the soil profile by surface evaporation.

At the very first South African Irrigation Congress held in 1909, much concern was expressed at the extent of salt-affected soils and the sediment content of water supplies (Kanthach, 1909). At the National Irrigation Symposium 82 years later, Scotney & Van der Merwe (1991) had the same concerns and said that the long-term viability of soil and water resources is in jeopardy. Major threats to these resources result from, among others, salinity, sodicity and waterlogging.

No data is available on a systematic survey or the monitoring of salt-affected soils on national scale for South African irrigation schemes. Backeberg *et al*. (1996) estimated that approximately 18% of the irrigated area in South Africa experiences some degree of detrimental effects caused by waterlogging and/or salt accumulation (Table 2.1).

Table 2.1 Estimated percentage of waterlogged or salt-affected irrigated land in the different provinces (Backeberg *et al*., 1996)

Province	Waterlogged or salt-affected		
	Severely %	Moderately %	Total %
Eastern Cape	6	13	19
Free State	6	18	24
Gauteng	5	15	20
KwaZulu-Natal	5	9	14
Mpumalanga	1	5	6
Northern Cape	4	20	24
Limpopo	12	14	26
North West	3	5	8
Western Cape	9	15	24

Ghassemi *et al*. (1995) citing Van Pletsen (1989) stated that a survey of five major irrigation schemes indicated that, on average, 28% of irrigated land shows signs of either waterlogging or harmful high salt contents or both. Salt-affected and waterlogged figures of 18-28% for South Africa seem unrealistic if compared to countries such as India, Pakistan, Iran and Egypt with known salt-affected and waterlogging problems. A figure of 10% or even less seems more realistic (Table 2.1 and Table 2.2).

Table 2.2 Global estimate of secondary salinization in some of the world's irrigated lands (Ghassemi *et al*., 1995)

Country	Irrigated area (Mha)	Salt-affected land in irrigated area (Mha)	Share of salt-affected to irrigated land (%)
China	44.83	6.7	15.0
India	42.10	7.0	16.6
USA	18.10	4.2	23.0
Pakistan	16.08	4.2	26.2
Iran	5.74	1.7	30.0
Thailand	4.00	0.4	10.0
Egypt	2.69	0.9	33.0
Australia	1.83	0.2	8.7
Argentina	1.72	0.6	33.7
South Africa	1.13	0.1	8.9
World	227.11	45.4	20.0

According to Görgens & Foster (1989), many of the serious salinity problems experienced in South Africa to date have occurred during, or as a result of, extreme climatic events. For example, the rapid rise in the salinity of water in the dams of the middle and lower Vaal catchment as well as certain dams in the Eastern Cape Province was directly related to the 1979-84 drought, and the rise in the salinity of Lake Mentz (Darlington Dam) during 1975-78 was a direct result of successively heavy seasonal rains in the Sundays River catchment. It should be noted that the salinization impact of extreme events is often more pronounced in systems where water utilization and human activity are the greatest (Ghassemi *et al*., 1995). In essence, an increase in salinity during drought conditions is primarily a result of the shortage of dilution water which under normal circumstances is generally available to maintain salinities at non-problem levels. If dilution water shortages occur while the discharge of saline effluent remains relatively constant, then salinity levels will increase.

Stream salinity caused by irrigation return flow occurs in several river systems in South Africa (Volschenk *et al*., 2005; Rose, 2002; Du Preez *et al*., 2000; Rossouw, 1997; Herold & Bailey, 1996; Moolman *et al*., 1983; Cass, 1980; Hall *et al*., 1980; Hall & Görgens, 1978).

2.2 Waterlogging

Waterlogging is the lowering in land productivity through the rise in groundwater close to the soil surface. Also included under this heading is the severe form, termed ponding, where the water table rises above the surface. Waterlogging is linked with secondary salt-affected soils, both being brought about by incorrect irrigation management. Waterlogging is characterized by too much water in the root zone and limits the oxygen availability. This causes anaerobic conditions and symptoms such as stunting, discolouration of foliage, defoliation, wilting and death in some cases (McGhie & Ryan, 2005). Van der Walt & Van Rooyen (1995) definition of waterlogging is: “Soil or land saturated with water, it may result from excessive rain, irrigation or seepage, coupled with inadequate drainage, and is detrimental to the growth of most crop plants”.

A good irrigation management plan strives to apply sufficient water to meet crop water demand plus the leaching requirement without wastage. Salinity problems encountered in irrigated agriculture are very frequently associated with an uncontrolled water table, within 1-2 m of the ground surface (FAO, 1985, 2002).

Over-irrigation and leaking water supply canals that result in water seepage which promote water table formation and subsequent salinization, occur in many irrigation projects (Rhoades & Loveday, 1990). The leakage from canals and pipelines of the older irrigation schemes in South Africa often exceeds planning norms. The design norm for concrete-lined canal systems in South Africa is 1.9-l/s.1000 m^{-2} of wetted lining, compared to the design norm of 0.35 l/s.1000 m^{-2} as quoted by overseas authors. Research in South Africa has indicated losses varying from 12-27% from some concrete-lined canals and an average allowance of 25% for earthen canals. Leakage losses in excess of 30% out of an earthen canal have been measured in one case (Backeberg *et al.,* 1996).

Ninham Shand (1985) estimated that there were some 148 000 ha of waterlogged irrigated land in South Africa in 1975 and some 37 000 ha in 1980. The large waterlogged area in 1975 is attributed to abnormally high rainfall during 1974-76.

Table 2.3 provides a summary of an investigation carried out by Streutker (1982) and quoted by Ninham Shand (1985) and Ghassemi *et al*. (1995), concerning the occurrence of waterlogging in a number of irrigation schemes. It shows that of 135 868 ha of irrigated land in the surveyed schemes, some 11 946 ha or 9% of irrigated land were waterlogged. However, on a national level the percentage of waterlogged areas would be much lower because it seems that the most problematic schemes were selected for the survey.

Table 2.3 Occurrence of waterlogging in a number of South African irrigation schemes#.

Irrigation scheme	Irrigated area (ha)	Waterlogged area (ha)	Waterlogged (%)	Year
Oudtshoorn	1 900	50	26.31	1982
Klaasvoogds	545	405	74.31	1982
Hex River	5 000	40	0.80	1982
Elgin	15 000	0	0	1982
Olifants River (Western Cape)	12 000	200	16.67	1982
Golden Valley	2 523	1 800	71.34	1980
Douglas	1 200	512	48.61	1978
Vaalharts (North Canal)	25 000	1 500	6.00	1977
Riet River (B-Farms)	2 600	2 000	7.69	1974
Hartbeespoort	22 000	154	0.70	1982
Marico	4 600	135	2.93	1980
Loskop	25 200	1 250	4.96	1980
Pongola	9 200	2 300	25.00	1978
Sterk River	2 500	600	24.00	1980
Blyde River	6 600	1 000	15.15	1979
Total	135 868	11 946	8.79	

#Adapted from Streutker (1982)

Drainage of water from the soil profile is necessary to prevent excessive soil water conditions (waterlogging) in the root zone of crops, to control salinity and to ensure trafficability of fields for execution of farming activities.

On some small-scale farming projects, waterlogging is common. Irrigation projects in South Africa for small-scale farming have been imposed, conceived and rehabilitated essentially on the basis of civil engineering and crop technology criteria, and without adequate knowledge of soil, environmental and socio-economic parameters. Nell (1997) found in the Nkomazi irrigation scheme for small-scale farmers that waterlogging, salinity and sodicity has reduced the agricultural productivity to such an extent, after just one year of irrigation, that reclamation of these soils has become essential for sustainable agriculture. Nell (2007) found that only 41% of the area investigated on the 30 irrigation schemes for small-scale farmers that form part of the RESIS project in the Limpopo Province can be regarded as irrigable, mainly because of very shallow effective depth and signs of wetness and waterlogging. This is an alarming percentage because the surveys were done on existing irrigation schemes.

2.3 Ground-based methods for waterlogging and salt accumulation monitoring

The aims of salt accumulation and waterlogging mapping and monitoring are to know temporal subtle salt accumulation and waterlogging differences in the landscape and to develop salt and waterlogging zones to help design management plans for sustainable use of soil resources. In agriculture regions, salt accumulation and waterlogging varies widely vertically, horizontally, and temporally, depending on such conditions as variation in soil texture, plant growth, quality of irrigation water, hydraulic conductivity and irrigation and drainage systems in place.

Waterlogging and salt accumulation are difficult to map and monitor at field scales and larger spatial extents because of its spatial and temporal heterogeneity. The optimum strategy for mapping waterlogged salt-affected soil depends on the scale and resources available. Users need to make best use of existing information and then integrate a range of the available mapping methods to that they best address their specific problem (Spies & Woodgate, 2005).

Technological advances in recent years have revolutionized, soil salinity assessment. These revolutions have been in RS/GIS and development of a number of electromagnetic induction (EMI) instruments for providing reasonable in situ estimates of salinity (Corwin & Rhoades, 1982; Slavich, 1990). The apparent electrical conductivity (EC_a) measured by EMI can be rapidly measured on a second-by-second basis; therefore, data population is relatively large, and landscape or farming land can be covered more comprehensively in short time than by conventional survey tools and methods.

A limitation in the use of conventional soil sampling/laboratory analysis methodology for characterizing the spatial variability of soil properties is the high labour requirement involved and high laboratory cost. Typically for farming applications, a grid of 100 by 100 metres is used (one sample per ha), which often is not intensive enough. According to Rhoades *et al.* (1999) the proper grid spacing depends on the variability of the property of interest, which, of course, is unknown at the outset. Thus, the proper locations to collect the samples and the number of samples required cannot easily be determined by the conventional approach. As a result, too few samples are frequently taken to properly characterize the variability that often exists in fields for prescription farming purposes. No cost effective, scientific approach for determining grid size has been developed using such grid-point methods. Thus, directed sampling and remote sensing techniques are being sought and advocated, in order to site optimum soil-test locations and to minimize sampling needs. But traditional methods of directed sampling and remote sensing often do not provide enough, or sufficiently quantitative, information about the various soil properties described above for the needs of prescription farming.

According to Rhoades et al. (1999) there are three primary cost advantages associated with the mobilization of the various salinity survey instruments. The first advantage is the speed in which the survey process can be completed. Mechanized systems can almost always be used to survey more land than hand held systems simply because of their increased travel speed. Second, mechanized systems can be used to collect significantly more survey data. Indeed, many of the commercial systems currently available can collect survey data in a nearly continuous fashion. And third, when hand held units are mounted or adapted into mobilized platforms, they tend to last longer. Rhoades et al. (1999) also indicate measurements of EC_a and of geospatial position can be obtained rapidly with geophysical sensors and used to determine optimum soil-test sites. Additionally, EC_a can be used to infer a number of soil properties, besides salinity, that are useful to prescription farming purposes and thus to create much more detailed and affordable soil-property maps than those obtained by the use of conventional soil/grid-point sampling methods (Kachanoski et al., 1988; Lesch et al., 1992; Doolittle et al., 1994; Jayne, 1996).

Primary saline, sodic, and calcareous soils were mapped or described for South Africa in the past by Barnard *et al*. (2002), Ellis (1988), MacVicar (1972), Mountain (1967), Nell & Henning (2003), Nell (2010), Samadi *et al*. (1998), and Van der Merwe (1942).

2.4 Remote sensing

Remote sensing is the practice of deriving information about the Earth's land and water surfaces using images acquired from an overhead perspective, by employing electromagnetic radiation in one or more regions of the electromagnetic spectrum, reflected or emitted from the Earth's surface (Campbell, 2007). A distinction is made between the two main types of remotely-sensed data, namely those derived from passive and active sensors.

Passive sensors mainly operate in the visible and the infrared regions of the electromagnetic spectrum. The visible spectrum contains those wavelengths of radiation that can be perceived by human vision, i.e. from violet to red light. Wavelengths longer than those of the visible spectrum (but shorter than those of microwave radiation) are termed infrared, and this spectrum can be subdivided into near-, mid- and far-infrared. The primary source of near- and mid-infrared radiation is the sun and they are reflected by the Earth's surface like visible light. Hence, the near- and mid-infrared wavebands, together with the visible bands, are sometimes collectively known as the optical bands. Far-infrared radiation is emitted by the Earth's surface in the form of heat, or thermal energy, and is sometimes known as thermal infrared radiation. Thermal infrared bands are generally less common in VIR sensors than visible and near- and mid-infrared bands (Campbell, 2002; Mather, 2004).

The longest wavelengths commonly used in remote sensing fall within the microwave spectrum, in which solar irradiance is negligible although the Earth itself emits some microwave energy. However, this emitted energy is rarely measured in remote sensing as most microwave sensors are active sensors. Active sensors use their own energy to illuminate target objects and then measure the portion of energy reflected back to them, whereas passive sensors measure energy generated by an external source (usually the sun) (Campbell, 2002; Mather, 2004). Active microwave sensors are RADAR (radio detection and ranging) sensors. An imaging RADAR system consists of the following basic components: a transmitter, a receiver, an antenna array and a recorder. The transmitter transmits repetitive microwave pulses at a specific frequency through the antenna array, which controls the propagation of the electromagnetic wave through devices known as waveguides. Usually, the same antenna then receives the echo of the signal. This is then accepted by the receiver, which filters and amplifies it as required, and passes it on to the recorder (Campbell, 2002).

2.4.1 Principles of EO using optical remote sensing

In optical remote sensing the spectral characteristics of objects on the Earth's surface are measured using a sensor and analysed to automatically or semi-automatically recognize objects. The spectral characteristics, or signatures, contain unique patterns of absorption and reflection at specific wavelengths. For instance, Figure 2.1 shows that clear water moderately reflects the blue, green and red wavelengths and strongly absorbs near-infrared (NIR) and longer wavelengths (Mather, 2004).

The spectral properties of most soil types show a consistent increase in reflectivity as wavelength increases in the visible and NIR portions of the spectrum (Jensen, 2007). Increasing soil moisture will result in a strong reduction in reflectance in all wavelengths, also the NIR region (Jensen, 2007).

In actively photosynthesizing green leaves, reflection in the green wavelengths dominates with a strong absorption in the blue and red wavelengths (Buschmann *et al.*, 2000). The overall reflectance from plant leaves increases sharply between 0.7μm and 1.2μm. These increases in the NIR wavelengths are unique to plants and are caused by the cell structure. As plant cover decreases and more soil is detected through the vegetation, the spectral curve changes to a typical soil spectral curve. This provides the basis for estimations of cover density from image data (Huete *et al.*, 1985).

The spectral profiles of water, soil and vegetation form the basis of many EO techniques. For instance, soils and vegetation are effectively discriminated by studying the relationship between the reflectance of objects in the red and NIR regions of the spectrum, while water's low reflection in the NIR band is the basis of its discrimination from both soil and vegetation. These relationships are the focus of image classification procedures.

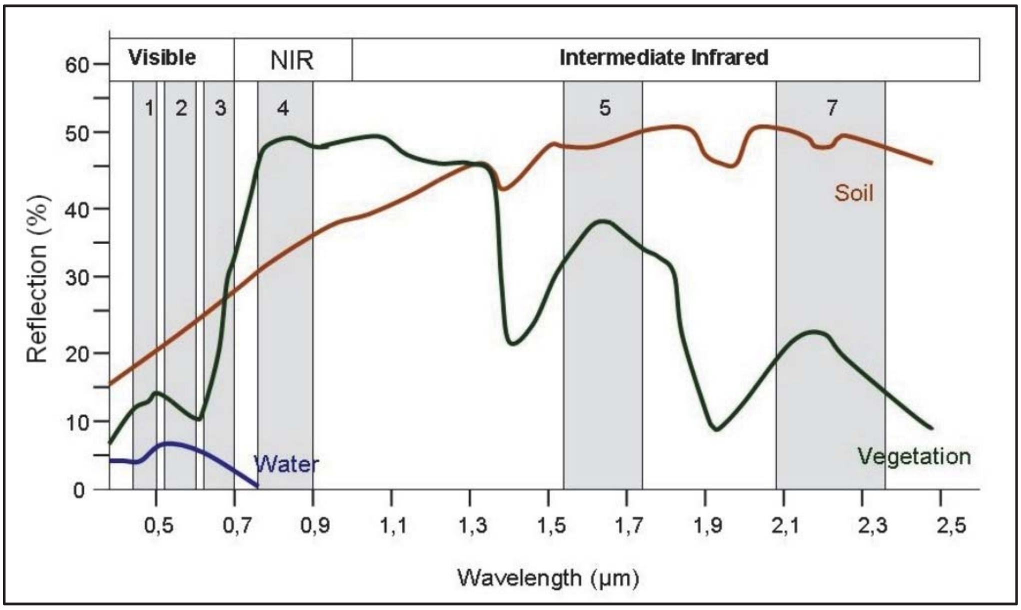

Figure 2.1 Spectral profiles of water, soil and vegetation in relation to the visible, near-infrared (NIR) and intermediate infrared regions of the electromagnetic spectrum (with Landsat 7 bands depicted in grey for reference) (SEOS 2014).

2.4.2 Image classification approaches

2.4.2.1 Unsupervised classification

Unsupervised classification is defined by two distinct steps. The first step is the automatic classification of pixels into a user-specified number of image classes according to their spectral properties. The second step is the manual labelling of the classes, usually depicted in images as areas of homogeneity, according to real-world information (Campbell, 2007). Although the automated nature of the spectral delineation renders this classification method less user-intensive than others, it is not truly unsupervised. As Mather (2004) puts it, unsupervised classification is a useful exploratory tool, where repeated unsupervised area delineations with different parameters allow a user to “get a feel” for which real-world (informational) classes are spectrally distinct and which are spectrally similar. This understanding of image features can inform the construction of the set of informational classes to be used in the classification, rendering unsupervised classification extremely useful where *a priori* information regarding the study area or the classification structure is unavailable or not pre-determined. Conversely, where a real-world class structure is already established it is rare that it will correspond with the automatically delineated spectral classes, resulting in the lowering of the accuracy of the outcome (Campbell, 2007). This is especially true for high-resolution imagery where features of interest commonly comprise multiple spectral classes shared by more than one information class. This is the primary disadvantage of unsupervised classification, and for this reason its use often has limited practical value.

2.4.2.2 Supervised classification

Supervised classification is defined by the application of *a priori* information of real-world informational classes to determine the identity of unknown image elements. Data for the real-world classes are acquired from an external source and entered into the classifier in the form of designated and labelled polygons termed “training areas” or “training data”. These training areas are used to generate statistical information regarding the spectral properties of each class, which is used by a classification algorithm to identify the class of unknown pixels (Mather, 2004; Campbell, 2007). Classification algorithms are widely varied, but are all designed to compare the features of each of the classes with those of an unknown pixel in geometric space, and assign a class based on the results of that comparison. The most widely used algorithm is the maximum likelihood (ML) classification algorithm, due to its ready accessibility, robustness, strong theoretical foundation, and high accuracies for a wide range of remote sensing applications (Bolstad & Lillisand, 1991; Brown de Colstoun *et al*., 2003; Tseng *et al*., 2008). Because of these traits, a number of studies use ML as the benchmark with which to compare newly developed classification methods (Liu *et al*., 2002; Nangendo *et al*., 2007; Myburgh & Van Niekerk, 2013, 2014a). The ML classifier assumes the provided training data is normally distributed to determine the means and variances of the classes (Harris, 1987; Gibson & Power, 2000). The probabilities of each class are then determined from these estimates (Rees, 2001; Albert, 2002; Lillesand *et al*., 2004). Myburgh & Van Niekerk (2013) showed that the accuracy of the ML classifier decreases as the number of input features increases.

Other popular classifiers used in remote sensing applications include k-nearest neighbour (kNN), support vector machines (SVM), decision trees (DT) and random forest (RF). The kNN algorithm is a simple distance-based classifier that labels each unknown pixel based on the labels of its k neighbouring known pixels (Cover & Hart, 1967; Gibson & Power, 2000). Although kNN is effective for classifying data that is not normally distributed, the method has the disadvantage of assuming equal importance (weight) of all features. Given that certain features may have higher priority for a particular target class, this assumption can produce incorrect class assignments and diffused clusters (Cunningham & Delany, 2007). To avoid ties (known pixels with identical spectral values) the value of k must be set to an odd value (Campbell, 2007). A value of k=1 is often used when a small set of training samples are available.

By focussing on the training samples (support vectors) close to the edge of the class descriptors, SVM determines the optimal separating hyperplane between classes that will minimize misclassifications (Novack *et al*., 2011). Kernels such as the radial basis function (RBF) are used to project samples non-linearly into a higher dimensional space so that the classifier can accommodate non-linear relationships (Li *et al*., 2010). SVM has been shown to be very effective for land cover mapping (Petropoulos *et al*., 2012; Lizarazo, 2008; Li *et al*., 2010). Myburgh & Van Niekerk (2013) demonstrated that SVM produces more accurate results than NN and ML using SPOT-5 imagery. See Vapnik (2000) and Huang *et al*. (2002) for a detailed explanation of the SVM algorithm.

A decision tree (DT) is a non-parametric classifier that identifies relationships between a continuous response variable known as the dependent variable, and multiple, continuous variables known as the independent variables. DTs hierarchically split a dataset into increasingly homogeneous subsets known as nodes (Gomez *et al*., 2012; Lawrence & Wright, 2001; Pal & Mather, 2003; Punia *et al*., 2011; Novack *et al*. 2011). By recursively splitting the feature datasets, a leaf node with an associated class is assigned to the observation (Pal & Mather, 2003). According to Pal & Mather (2003) and Novack *et al*. (2011), because each node splits the feature space orthogonal to the axis of the selected feature, DT classifiers are less sensitive to errors in training data. Owing to DT's ability to capture non-linear relationships, the input data does not have to be normally distributed (Gómez *et al*., 2012; Hladik & Alber, 2014). Each branch of the DT consists of divisions (or rules) of the most probable class and by applying these rules the most likely class will be assigned to a pixel (Lawrence & Wright, 2001). DT classifiers have been shown to be susceptible to model over-fitting – generating a model that is very effective in classifying the training data, but that is not transferable to other datasets. A pruning step involving cross-validation is therefore required. Essentially the dataset is divided into subsets that are then validated against each other (Campbell, 2007; Lawrence & Wright, 2001).

Several studies have demonstrated the utility of DTs for a range of remote sensing applications (Gomez *et al*., 2012; Hladik & Alber, 2014; Novack *et al*., 2011; Pal & Mather, 2003; Punia *et al*., 2011). Pal & Mather (2003) showed that, although the performance of DTs increases with an increase in training dataset size (up to a certain point), they are also effective even with small training datasets. Novack *et al*. (2011) found that DTs produced more reliable and accurate results than SVM classifiers.

Classification and regression tree (CART) (by Salford Systems) is an implementation of a DT classifier and provides an indication of the importance of each feature or variable provided as input. CART uses cross-validation to automatically prune the resulting DT and the user can interactively select from a list of the most appropriate trees based on a number of assessment measures.

Random forest (RF) has been increasingly applied in remote sensing classifications (Duro *et al*., 2012; Gislason *et al*., 2006; Lawrence *et al*., 2006; Immitzer *et al*., 2012) and has also been shown to be superior to other classification techniques in a number of studies (Gislason *et al*., 2006; Lawrence *et al*., 2006; Rodriquez-Galiano *et al*., 2012a, 2012b; Novack *et al*., 2011). RF is considered an enhancement of DTs (Immitzer *et al*., 2012) as it generates multiple DTs by randomly selecting vector samples. A vote is cast by each of the generated DTs (Breiman, 2001; Bosch *et al.,* 2007; Pal, 2005) and the most popular class is assigned to the input variable (Breiman, 2001; Rodriquez-Galiano, 2012a). Because RF makes use of bagging (Breiman, 1996; and Rodriquez-Galiano, 2012a) to generate training sets, the classifier not very sensitivity to training set size (Rodriquez-Galiano, 2012a).

RF requires two parameters to be set, namely the number of trees and the number of active (predictive) variables. Rodriquez-Galiano (2012a) showed stability in accuracy is achieved at 100 trees. They also found that a small number of active variables is best as it reduces generalization error and correlations between trees. The number of trees and active variables has been shown by Duro *et al*. (2012) to have an insignificant impact on overall accuracy (OA). A more detailed discussion of the RF classifier can be found in Breiman (1996), Breiman (2001), Pal (2005) and Rodriquez-Galiano (2012a).

Despite the advantages shown by supervised classification, it does have a number of drawbacks. The main disadvantage is the requirement for suitable training data. Poorly developed training areas result in weak classification accuracies, and thus training data must be meticulously prepared. This can be expensive in terms of both time and money, especially for projects of a wide extent that span multiple images (Albert, 2002).

2.4.2.3 Rule-based (expert system) classification

A rule-based (or expert system) classification applies a set of rules, defined based on *a priori* knowledge, on input data (e.g. images) to infer a classification result. The term "expert system" is used in many ways in remote sensing and it can represent a number of different techniques. Tsatsoulis (1993) defines the categories of expert systems as user-assistance systems, classifiers, low-level processing systems, data fusion systems and GIS applications. All pertain to different procedures in remote sensing analysis, but all are defined as "expert" in that they all employ artificial intelligence (AI) inference structures which use expert knowledge (Cohen & Shosheny, 2002). For this reason, expert systems are also known in the literature as knowledge-based systems.

Various approaches have been proposed for the construction of rules. Rules are often created manually based on analyst experience, which is then essentially an expert system approach according to Chuvieco & Huete (2010). Supervised approaches where statistical procedures are used to infer the rules from training data are also commonly used. The statistical procedures used are known as learning algorithms (Friedl & Brodley, 1997; Chuvieco & Huete, 2010). Learning algorithms can be differentiated according to whether the set of algorithms used to estimate the splits at non-terminal nodes are uniform or heterogeneous and further, in the former case, whether a single variable is used for each split (univariate decision tree), or multiple variables (multivariate decision tree). If a heterogeneous set of algorithms is used, the tree is known as a hybrid decision tree. Such a tree can use various algorithms in different subtrees, potentially combining for example uni- or multivariate decision trees with parametric supervised classifiers (Friedl & Brodley, 1997).

2.4.3 Geographical object-based image analysis

Geographical object-based image analysis (GEOBIA) aims to delineate and classify meaningful spatial units in an integrated way (Lang, 2008). This can be contrasted with the more traditional pixel-based classification approaches which regard each pixel separately. It can be argued that a major limitation of pixel-based approaches is their disregarding of spatial concepts (Blaschke *et al*., 2000). Lang (2008) states that in such approaches geographical features are characterized only by their spectral attributes or related statistical attributes such as texture. This statement arguably disregards alternative pixel-based classifiers which have the capacity to integrate ancillary data. Conversely, each image object in GEOBIA is aware of its context, neighbourhood and sub-objects. This means that geographical features can be characterized by their spatial, structural and hierarchical properties in addition to their spectral properties (Bock *et al*., 2005; Lang, 2008). Furthermore, objects offer additional spectral information that single pixels lack, including mean, median, minimum, maximum and variance values (Blaschke, 2010). Using objects as classification units rather than pixels reduces spectral variation within classes and removes the so-called “salt-and-pepper” effect (Liu & Xia, 2011). Also, the increased availability of fine spatial resolution satellite imagery has exposed further limitations of pixel-based techniques. For many applications the pixels of these images are significantly smaller than most objects of interest. In such cases it becomes more likely that most pixels will belong to the same classes as their neighbours (Blaschke *et al*., 2000; Lang, 2008).

The building blocks of GEOBIA are termed segments (Blaschke, 2010). They are created through the process of segmentation which divides an image into non-overlapping objects (Chen *et al*., 2009). Before the advent of GEOBIA this process was seen as being separate from classification; images were first segmented and then classified. However, this workflow disregards the role of scale. Segmentation attempts to delineate objects which are both homogenous and semantically significant, but the scale at which an object obtains semantic significance is dependent on the class represented in that object. Often, objects created at different scales need to be considered within the same image in order to perform an effective classification. Therefore, GEOBIA is an iterative process rather than a linear one and it is inextricably linked to concepts of multi-scale analysis (Lang, 2008; Blaschke, 2010).

The following sub-sections will first regard the various segmentation algorithms available and then briefly discuss how image classifiers can be applied in GEOBIA.

2.4.3.1 Segmentation algorithms

Segmenting an image into a given number of objects is a problem with a very large set of possible solutions (Blaschke *et al*., 2000) and various algorithms exist that attempt to arrive at effective segmentations. The following groups are distinguished: point-based, edge-based and region-based algorithms, as well as combined algorithms (Blaschke, 2010).

Point-based approaches use global threshold values to identify groups of homogenous elements (pixels) throughout a scene. Segmentation is performed in two steps: firstly, the category in which each element falls relative to the given thresholds is identified, and secondly, all spatially connected elements falling in the same categories are grouped into regions. Threshold values can be static or dynamic (histogram-based). However, this approach is less suitable for remote sensing applications as spectral values for a given object will vary for different locations within a scene (Schiewe, 2002).

In edge-based approaches, edges are regarded as object boundaries. They are identified through an edge-detection filter (e.g. a Sobel filter) and then transformed to object outlines through a contour-generating algorithm. The main drawback of such approaches is their sensitivity to noise (Blaschke *et al*., 2000; Schiewe, 2002).

Region-based approaches compare available elements (pixels or existing regions) with other elements in an image to determine whether they are similar. Two approaches are distinguished: region growing (bottom up) starts with seed pixels and grows into neighbouring elements, whereas region splitting (top down) starts with the entire scene and recursively splits it into smaller objects. Splitting algorithms can sometimes lead to over-segmentation, as non-homogenous regions are split into a predetermined number of sub-regions. However, some algorithms can remerge newly formed subregions if they are similar (Schiewe, 2002). One region-based approach that has been widely applied is the multiresolution segmentation (MRS) algorithm implemented in the widely-used GEOBIA software package eCognition (Trimble, 2011b).

MRS is a pair-wise region-merging algorithm which can take pixels or existing objects as input. Input elements are merged into a set of objects in such a way that the average heterogeneity for the set is minimized, while the respective homogeneities of the objects are maximized. A mutual-best-fitting approach is used for merging. In this approach the neighbourhood of a given seed object is evaluated and its best-fitting neighbour is identified. The neighbourhood of that neighbour object is then evaluated and if the seed object is also the best-fitting neighbour of that object they are merged, if not that object becomes the new seed. A merge is only performed if its cost is less than a specified degree of fitting (this threshold is termed the scale factor in eCognition). The algorithm continues looping until no more merges are allowed. The degree of fitting is defined according to a spectral homogeneity measure and a shape homogeneity measure (Baatz & Schäpe, 2000; Trimble, 2011a). eCognition allows one to specify homogeneity in terms of two parameters: shape and compactness. The shape criterion determines the degree of influence that object shape has compared to colour, while the compactness criterion determines the degree of influence that compactness has in comparison to smoothness. These values are specified as fractions of 1 (Trimble, 2011b).

2.4.3.2 Classifiers in GEOBIA

Several classifiers have been successfully applied to object-based classifications. Rule-based expert systems feature prominently in the literature on GEOBIA. Lang (2008) lists rule-based classification as one of the two methodological pillars of GEOBIA, implying that no other classifier is true to the principles of the paradigm. As discussed in section 2.3.2.3, expert systems attempt to model the complex network of knowledge and experience that humans use to understand the information in an image, a network largely based on our perception of that image as a series of objects (Blaschke *et al*., 2000). Many of the wealth of additional features available in GEOBIA correspond to the features that enable us to understand such objects, making expert systems inherently suitable for GEOBIA. Several studies report good results when using expert systems in object-based classification. Whiteside & Ahmad (2005) found an object-based expert system to significantly outperform a pixel-based supervised classification in land cover classification, and Chen *et al*. (2009) found the same for an urban study using a combination of LIDAR and Quickbird data. Dragut & Blaschke (2006) showed that an object-based expert system can be successfully applied to landform classification. Van der Sande *et al*. (2003) described an object-based expert system that performed well in a complex land cover classification for flood-risk assessment.

Some limitations of rule-based expert systems have been noted. For instance, creating an effective rule base is complicated and takes a lot of time, and expert systems are adversely influenced by increasing dimensionality of data. For these reasons, various studies have applied either other alternative classification algorithms or traditional supervised algorithms to GEOBIA. Li *et al*. (2010) compared a SVM classifier to a nearest-neighbour supervised classifier for object-based classification and the SVM was found to be more accurate. Mallinis *et al*. (2008) compared a decision tree to a nearest-neighbour supervised classification and revealed the decision tree to produce a significant increase in accuracy. Straatsma & Baptist (2008) successfully used a linear discriminate analysis supervised classifier in an object-based classification for the purpose of floodplain roughness parameterization. Platt & Rapoza (2008), in a study evaluating different aspects of object-based classification, found a maximum likelihood classifier to achieve a significantly higher user's accuracy than a nearest-neighbour classifier, but a slightly lower producer's accuracy. Yet, the nearest-neighbour classification could be significantly improved by integrating it with an expert system. Several studies have applied the principle where a nearest-neighbour (or other statistical) classification based on spectral values is combined with an expert system formalizing known spatial or structural relationships (Bock *et al*., 2005; Conchedda *et al*., 2008).

The GEOBIA paradigm can be applied to a large variety of data and has been shown to be effective in combining (fusing) disparate types (e.g. optical and radar) of data. The next section overviews synthetic aperture radar data.

2.4.4 Synthetic aperture radar (SAR)

Synthetic aperture radar (SAR) is a remote sensing technology that transmits microwave radiation towards the Earth's surface and measures the amplitude and phase of the backscattered waves. In this respect it falls under "active" remote sensing. SAR sensors are side-looking, with commonly used sensors capable of producing radar waves at incidence angles of between 15° and 60°.

SAR sensors are designed to transmit and receive vertically (V) and/or horizontally (H) polarized microwaves. This is normally denoted by a double-letter annotation, with the first letter indicating the polarization of the transmitted wave and the second letter indicating the polarization of the received wave. For example, a signal that was sent in a horizontal polarization but received in a vertical polarization would be denoted as HV. The four possible combination are then HH & VV (like-, or co-polarized) and HV & VH (cross-polarized).

The microwave region of the electromagnetic spectrum is fairly broad, ranging from 0.3 to 300 GHz. Generally, only frequencies between 1 and 12 GHz are used in microwave remote sensing and these relate to wavelengths between 2.5 and 30 cm through the formula:

$$f = \frac{C}{\lambda}$$ Equation 2.1

where f is the frequency;

C is the speed of light; and

λ is wavelength.

Similar to the assignment of wavelengths to bands in optical remote sensing (section 2.3.1), the microwave region can be broken up into different frequency/wavelength bands. Commonly used SAR bands together with their frequency and wavelength ranges are shown in Table 2.4.

Table 2.4 Commonly used SAR bands including frequency and wavelength ranges

Band Designator	Frequency (GHz)	Wavelength (cm)
L band	1 to 2	30.0 to 15.0
S band	2 to 4	15.0 to 7.5
C band	4 to 8	7.5 to 3.8
X band	8 to 12	3.8 to 2.5

SAR imagery is constructed through complex processing employing the timing of raw radar echoes and signal reconstruction through the use of the Doppler effect (a process called "focusing"). The intensity of the returning echoes is called radar backscatter and each pixel in a SAR image therefore contains a backscatter value. Radar backscatter is computed using a metric known as the normalized radar cross-section to indicate the amount of backscattered energy per unit area, and is expressed by the scattering coefficient σ0 or sigma-naught. Sigma-naught is usually expressed as decibels (dB). Typical values of σ0 for natural surfaces range from +5 to -40 dB. These values would be very bright and very dark, respectively, on a SAR image.

SAR backscatter (σ0) is influenced by a wide range of factors related to the sensor type, the imaging geometry and the ground conditions. The most influential factors are:

- Surface roughness (as a function of wavelength)
- Dielectric constant
- Incidence angle
- Wavelength
- Polarization
- Scattering mechanism

As a general rule of thumb, SAR backscatter increases with increasing surface roughness and dielectric constant and decreases with increasing incidence angle. The interdependence of backscatter, surface roughness, incidence angle and wavelength is shown in Figure 2.2.

The L-band response in Figure 2.2 indicates that higher backscatter is received from steeper incidence angles. It also shows that, at least for incidence angles larger than 10°, increases in surface roughness relate to increases in radar backscatter. Reading Figure 2.2 from left to right shows that the effect of incidence angle on backscatter becomes less pronounced as frequency increases (and wavelength decreases) from L-band to C-band to X-band. The sensitivity of radar backscatter to surface roughness also decreases. Comparing the X-band with the L-band, it is clear that, generally, higher backscatter can be expected from images acquired with shorter wavelengths (X) than with longer wavelengths (L).

The link between radar backscatter and soil water content is also well established and an example from Rombach & Mauser (1997) is shown in Figure 2.3. The graph shows the strong positive correlation between volumetric soil water content and the radar backscatter response.

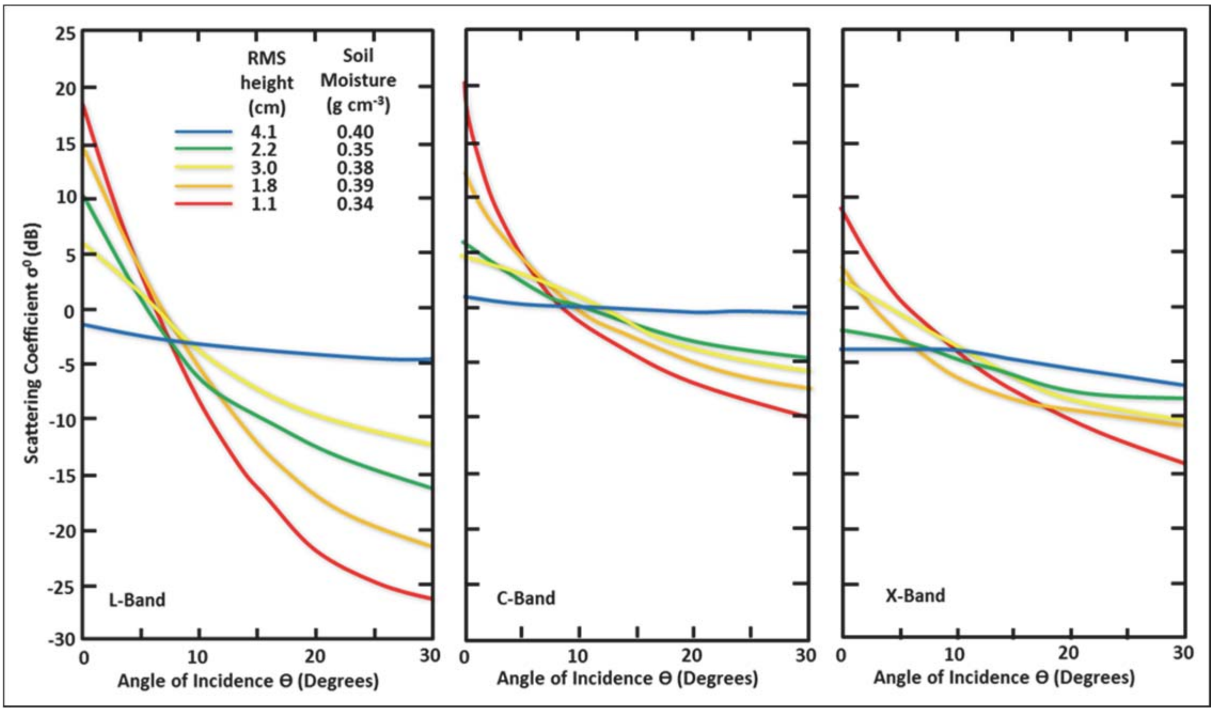

Figure 2.2 Relationship between backscatter, surface roughness, incidence angle and wavelength (adapted from Ulaby *et al*., 1986).

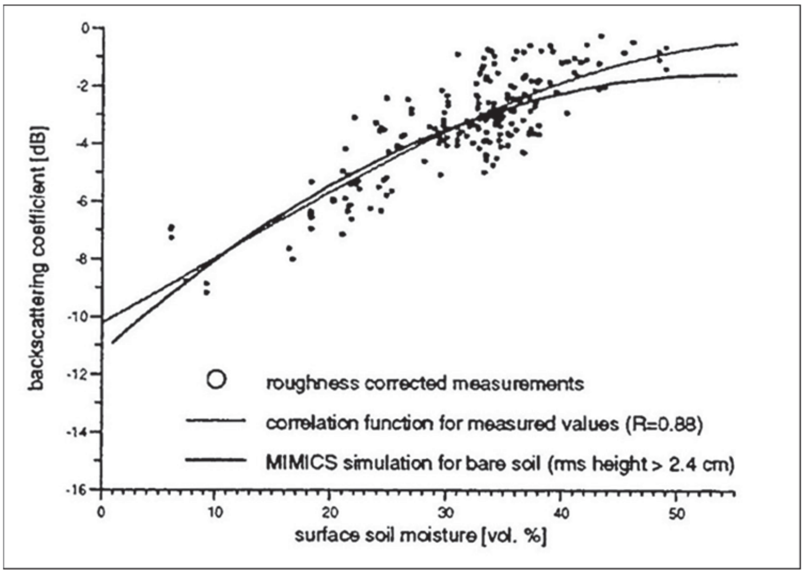

Figure 2.3 Relationship between C-band backscatter and soil water content (from Rombach & Mauser, 1997).

2.4.4.1 The dielectric constant

The dielectric constant (ϵ) (more correctly known as the complex permittivity) of a medium is a measure of how the medium responds to electromagnetic waves. It quantifies the resistance that is encountered when an electric field is formed in the material. Expressed as a complex value, the dielectric constant consists of a real (ϵ´) and an imaginary part (ϵ´´) and can be formulated as:

$$\epsilon = \epsilon' - i \cdot \epsilon'' \qquad \text{Equation 2.2}$$

where ϵ is the dielectric constant of an object;

ϵ' is the real part and corresponds to the stored energy within the medium; and

ϵ'' is the imaginary part which is related to the dissipation of energy within the medium.

The dielectric constant is a function of many variables, including frequency, temperature, volumetric soil water content, soil texture and salinity (Dobson *et al.*, 1985; Hallikainen *et al.*, 1985). Furthermore, the different components (ϵ´ and ϵ´´) of the dielectric component are sensitive to different variables. Most significantly, as the salinity of soil increases, the real component ϵ´ decreases and the imaginary component ϵ´´ increases. This relationship has been established by several authors (Dobson *et al.*, 1985; Yun *et al.*, 2003; Behari, 2005; Lasne *et al.*, 2008) and is shown in Figure 2.4. Since the complex permittivity is not a measurable quantity, this value is approximated through modelling.

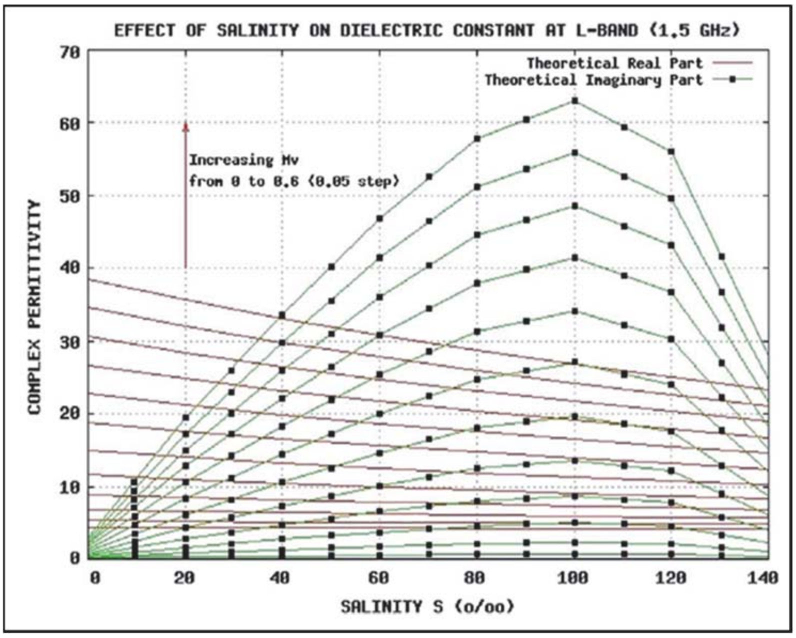

Figure 2.4 Relationships between soil salinity (dS/m), soil water content and the real (red) and imaginary (green) parts of the dielectric constant (for an L-band case) (Lasne *et al.*, 2008).

Figure 2.4 shows that as soil salinity (S) increases, there is a corresponding increase in imaginary part, ϵ´´. The effect on ϵ´, however, is minimal, with the real part only showing a mild decrease in response to higher salinity levels. This established response of the imaginary part of the dielectric constant to salinity is the basis for current research on soil salinity retrieval algorithms.

The strength of the correlation between ϵ´´ and salinity is, however, subject to soil water content, frequency and soil texture. What is evident from Figure 2.4 is the increased sensitivity of the imaginary component to salinity in the presence of higher volumetric soil water content (Mv). As soil water content increases from 0 to 0.6, the slope of the green ϵ´´ lines increases, showing that the effect of soil salinity on the dielectric constant is greatly increased in wet soils.

The frequency-dependence of the salinity / ϵ´´ relationship is shown in Figure 2.5. This graph shows the dramatic decrease of ϵ´´ sensitivity to soil salinity as microwave frequency increases. In this figure, values ranging from a to h correspond to increasing levels of salinity, while keeping soil water content constant.

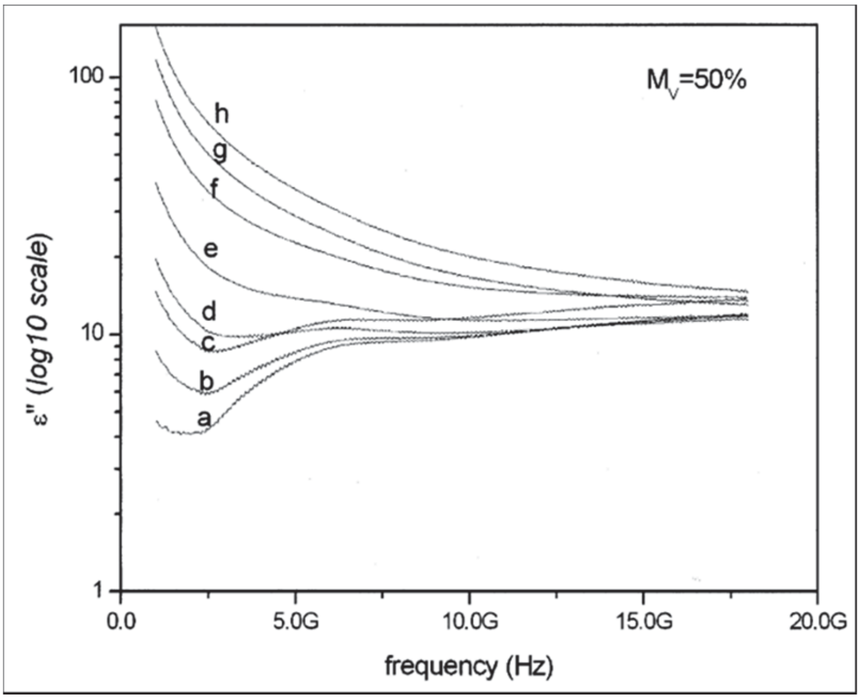

Figure 2.5 Relationships between e'', microwave frequency and soil salinity for soil containing 50% volumetric soil water content. The values a, b, c, d, e, f, g and h denote the % salinity (0, 5, 10, 20, 50, 100, 200 and saturated NaCl, respectively) (from Shao *et al.*, 2003).

Finally soil bulk density, or compactness, affects the sensitivity of ϵ´´ to salinity. Abdel-Razak Mohamed *et al.* (2003) showed that the effect of salinity on ϵ´´ is smaller in finer textured soil (silty clay) than in a coarser textured soil (sandy loam). This effect is attributed to the effect of water on the dilution of salts, which increases its reaction as an electric conductor and consequently affects the dielectric permittivity of the soil.

While the imaginary part of the dielectric constant has been shown (subject to different environmental variables) to be significantly more sensitive to soil salinity than the real part, soil water content strongly affects both the real and the imaginary parts (Yun *et al.,* 2003).

This means that the dielectric constant as a whole is highly sensitive to changes in soil water content. The challenge in creating an algorithm for the extraction of soil salinity (as well as soil water content) from SAR imagery lies in relating the SAR backscatter (σ0) to the different components of the dielectric constant.

2.4.4.2 SAR backscatter

SAR backscatter is directly, but not linearly, impacted by changes in the dielectric constant (Bindlish & Barros, 2000). Figure 2.6 shows the exponential relationship between backscatter (in dB) and the dielectric constant.

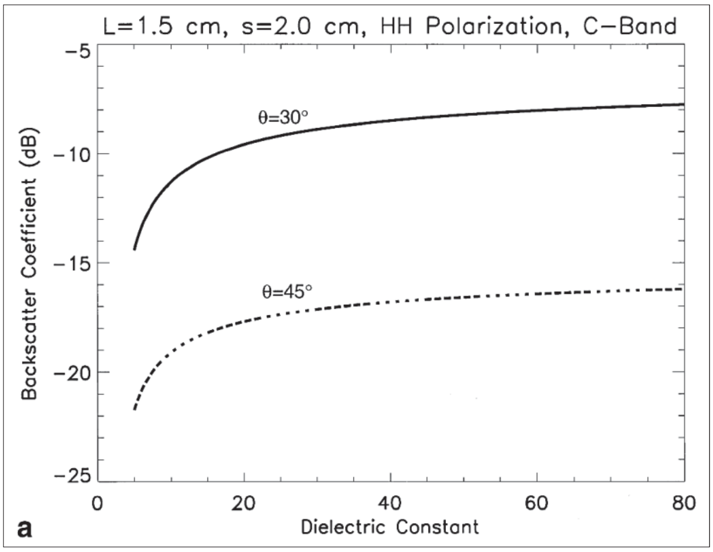

Figure 2.6 Relationship between backscatter, dielectric constant and incidence angle for HH C-band data (from Bindlish & Barros, 2000).

Since both soil water content and soil salinity are positively correlated with the dielectric constant, both of these factors impact the SAR backscatter response. Using RADARSAT-1 backscatter, Shao *et al.* (2003) showed a 79% correlation between soil salinity and ϵ´´, a 70% correlation between backscatter and ϵ´´ and a 69% correlation between backscatter and salinity. While backscatter is known to be strongly correlated with soil water content (Ulaby *et al.*, 1978), Yun *et al.* (2003) found that the correlation between backscatter and ϵ´ was only 0.27, concluding that ϵ´´ might be the dominant factor in determining the backscatter response from the dielectric constant.

Retrieval (also called inversion) of soil salinity and soil water content from SAR backscatter then rests on accurately modelling the effect of these parameters on the dielectric constant as a whole as well as extracting a value for the dielectric constant from the SAR backscatter intensity. During this process, the effects of surface roughness, incidence angle and wavelength need to be taken into account. The next section provides an overview of the SAR and optical data that is available for EO.

2.4.5 Sources of satellite imagery

Various factors have to be considered when selecting a specific source of satellite imagery for a particular application (see Table 2.5). The spatial, spectral and temporal resolutions are important, as is cost.

Landsat and ASTER are by far the most popular sensors for scientific purposes mainly because archival data from these sensors are available free over the Internet. Landsat-8 imagery has recently become freely available for download, opening up many new avenues for research. ASTER acquisitions are only done on request, which means that very few areas in South Africa are covered by recent data. Furthermore, since May 2008, ASTER's shortwave infrared sensor (which acquires the most useful information for soil science) is no longer operational.

Table 2.5 Commonly used medium to very high optical EO satellite sensors and their characteristics

Sensor	Bands	Spatial Resolution	Scene Footprint	Estimated cost per km^2
Worldview-3	Pan: 450-800 nm MS: Coastal 400-450 nm; Blue 450-510 nm; Green 510-580 nm; Yellow 585-625 nm; Red 630-690 nm; Red edge 705-745 nm; NIR1 770-895 nm; NIR2 860-1040 nm 8 x SWIR bands: 1195-2365 nm 12 x CAVIS Bands (desert clouds, aerosol-1, aerosol-2, aerosol-3, green, water-1, water-2, water-3, cirrus, snow): 405-2245 nm	Pan: 0.31-0.34 m MS: 1.24-1.38 m SWIR: 3.7-4.1 m CAVIS: 30 m	Info not yet available (launched 13 August 2014)	Info not yet available
GeoEye-1	Pan: 450-800 nm MS: Blue: 450-510 nm; Green 510-580 nm; Red 655-690 nm; NIR 780-920 nm	Pan: 0.41 m MS: 1.65 m	225 km^2	$25 (pan or MS or pan/MS bundle)
Worldview-2	Pan: 450-800 nm MS: Coastal 400-450 nm; Blue 450-510 nm; Green 510-580 nm; Yellow 585-625 nm; Red 630-690 nm; Red edge 705-745 nm; NIR1 770-895 nm; NIR2 860-1040 nm	Pan: 0.46-0.52 m MS: 1.85-2.07 m	224 km^2	$14 (pan) $35 (MS) $39 (pan/MS bundle)
Quickbird	Pan: 450-900 nm MS: Blue 450-520 nm; Green 520-600 nm; Red 630-690 nm; NIR 760-900 nm	Pan: 0.61-0.72 m MS: 2.44-2.88 m	272 km^2	$14 (pan or MS) $17 (pan/MS bundle)
Ikonos	Pan: 450-900 nm MS: Blue 450-530 nm; Green 520-610 nm; Red 640-720 nm; NIR 770-880 nm	Pan: 1 m MS: 4 m	11 km (swath width)	$20 (pan or MS or pan/MS bundle)
SPOT-6	Pan: 450-745 nm MS: Blue 450-520 nm; Green 530-590 nm; Red 625-695 nm; NIR 760-890 nm	Pan: 1.5 m MS: 6 m	3600 km^2	Info not yet available
SPOT-7	Pan: 450-745 nm MS: Blue 450-520 nm; Green 530-590 nm; Red 625-695 nm; NIR 760-890 nm	Pan: 1.5 m MS: 6 m	3600 km^2	Info not yet available
SPOT-5 (Decommissioned in 2015)	Pan: 450-690 nm MS: Green 500-590 nm; Red 610-680 nm; NIR 790-890 nm; SWIR 1580-1750 nm	Pan: 2.5 m MS: 10 m SWIR: 20 m	3600 km^2	$0.95 (10 m MS); $1.89 (2.5 m pan) Archived data free for academic use

Table 2.5. (continued)

Sensor	Bands	Spatial Resolution	Scene Footprint	Estimated cost per km^2
IRS-P6 (LISS-IV)	Pan: Any MS band MS: Green 520-590 nm; Red 620-680 nm; NIR 770-860 nm	5.8 m	490 km^2	$1.16 (MS)
Landsat 7	Pan (ETM+): 520-900 nm MS: Blue 450-520 nm; Green 520-600 nm; Red 630-700 nm; NIR 750-900 nm; SWIR5 1550-1750 nm; SWIR7 2080-2350 nm; Thermal: 10400-12500 nm	Pan: 15 m (ETM+) MS: 30 m TIR: 120 m (TM); 60 m (ETM+)	185 km (swath width)	Free (USGS)
Landsat 8	Pan (ETM+): 500-680 nm MS: Coastal aerosol 430-450 nm; Blue 450-510 nm; Green 530-590 nm; Red 640-670 nm; NIR 850-880 nm; SWIR1 1570-1650 nm; SWIR2 2110-2290 nm; Thermal1: 10600-11190 nm Thermal2: 11500-12510 nm	Pan: 15 m MS: 30 m Thermal: 100 m	185 km (swath width)	Free (USGS)
ASTER	VNIR: B1 520-600 nm; B2 630-690 nm; B3N/3B 780-860 nm; SWIR: B4 1600-1700 nm; B5 2145-2185 nm; B6 2185-2225 nm; B7 2235-2285 nm; B8 2295-2365 nm; B9 2360-2430 nm; TIR: B11 8475-8825 nm; B12 8925-9275 nm; B13 10250-10950 nm; B14 10950-11650 nm	VNIR: 15 m SWIR: 30 m TIR: 90 m	3600 km^2	$0.03

Apart from data accessibility issues, the relatively low spatial resolutions (30 m) of the Landsat and ASTER sensors makes them less suitable for monitoring waterlogging and salt accumulation, particularly in South Africa where the affected areas are often concentrated in very small (often less than 10 m in width) areas. Modern, very high resolution (VHR) sensors such as Ikonos, Quickbird, WorldView and GeoEye offer sub-metre spatial resolution (in panchromatic bands at least) and are consequently much more suitable for detecting affected areas. But compared to sensors with slightly lower spatial resolutions (e.g. SPOT-5), the VHR sensors have smaller image footprints and are significantly more expensive. Archival SPOT-5 data is available free of charge for South African academic and research use, making it an ideal source of imagery for this research. It should be noted that the shortwave infrared band of SPOT-5 is resampled from 20 to 10 m upon retrieving the data from the sensor, so that it matches the other bands. Cubic convolution resampling is used.

Table 2.6 Characteristics and estimated cost of data from currently available SAR sensors

Sensor	Bands	Polarizations	Spatial Resolution	Estimated cost per km^2
ERS-2 SAR (decommissioned)	C	VV	30 m	$0.05
Envisat ASAR (decommissioned)	C	VV; HH; VV+HH; HV+HH; VH+VV	30 m	$0.05
RADARSAT-1	C	HH	Fine: 8 m; Std: 30 m; Wide swath: 30 m	$1.41 (Fine) $0.35 (Std) $0.15 (Wide)
RADARSAT-2	C	HH; VV; HV; VH; HH+HV; VV+VH; HH+VV+HV+VH	Single pol: 3 m, 10 m Dual pol: 10 m, ~28 m (depending on incidence angle) Quad pol: 10 m, ~28 m	$13.19 (3 m single-pol) $1.40 (10 m single-pol) $1.49 (10 m dual-pol) $0.35 (25 m single-pol) $0.37 (25 m dual-pol) $8.44 (any quad-pol)
TerraSAR-X	X	HH; VV; HH+VV; HH+HV; VV+VH; HH+HV+VH+VV (designated missions only)	1 m, 3 m or 16 m, depending on mode	$85.30 (1 m single- or dual-pol) $42.65 (2 m single- or dual-pol) $1.57 (3 m single- or dual-pol) $0.12 (16 m single- or dual-pol) (Prices from Astrium)
ALOS PALSAR (decommissioned)	L	HH; VV; HH+HV; VV+VH; HH+HV+VH+VV	Single pol: 7-44 m Dual pol: 14-88 m Quad pol: 24-89 m	$0.13 (Fine resolution) $0.32 (Polarimetric) (Prices from ALOS-Pasco)
COSMO-Skymed	X	HH, HV, VH, VV;	Spotlight: 1 m Stripmap Himage: 3-30 m Stripmap PingPong: 10-20 m ScanSAR Wide: 14-30 m ScanSAR Huge: 14-100 m	$61.31 $1.47 $1.39 $0.10 $0.03

Table 2.6 provides a list of commonly used SAR sensors, their characteristics and their estimated cost in 2012. While archived scenes for decommissioned sensors such as ERS-1, ERS-2, ENVISAT and ALOS are available, a monitoring system would need to employ

currently active satellites, preferably having high-resolution, fully-polarimetric (HH, HV, VH and VV) capabilities. The sensors currently fulfilling those specifications would be RADARSAT-2, TerraSAR-X and COSMO-Skymed. While prices in Table 2.6 are provided in US$ per km^2, scenes covering between 100 and 1 000 km^2 would be acquired for any one specific date and area.

2.5 Terrain analysis and land component mapping

Terrain analysis is the study of the nature, origin, morphological history and composition of landforms, the result of which is a landform or land component map. Land components can be mapped by studying topographical maps, interpreting aerial photographs (Speight, 1977) and making field measurements (Graff & Usery, 1993). Such terrain analysis techniques are considered to be an art without formal theory and often rely on the interpreter's implicit terrain-related knowledge of the area being studied (Irvin *et al*., 1997). Such skill is the product of lengthy, expensive training and experience (Argialas, 1995). The subjective nature of terrain analysis is a major drawback because in most cases it is impossible to make any useful comparisons between land component maps produced by different analysts or even by the same analyst at different times (Speight, 1977). The interpretation and mapping of land components is extremely time-consuming, labour-intensive and expensive (Adediran *et al*., 2004) and is difficult to verify in the field owing to the fractal nature of topography (Hengl *et al*., 2004). Consequently, more objective and automated methods are needed to map land components. Computer analysis of geomorphometry is a convenient option.

2.5.1 Digital elevation models and its derivatives

Digital elevation models are essentially elevation rasters generated by interpolating the elevation of a given raster cell from nearby cells with known elevations. The known elevations are typically digitized from topographical maps, but they can also be surveyed elevations (including GPS measurements) obtained using photogrammetry or by processing radar or LIDAR (light detecting and ranging) data (Campbell, 2007; DeMers, 2009). A DEM records elevations of the Earth's surface for each cell in a grid, hereby converting a continuous data variable to a discrete representation. This simple model is extremely versatile and highly efficient for computer analysis (Longley *et al*., 2002).

Terrain analysis is usually performed on digital terrain models (DTMs) and not on digital surface models (DSMs) (see Figure 2.7). A DTM is a digital model of terrain elevation (i.e. ground positions), whereas a DSM represents the elevations of the ground and objects on the Earth's surface (PCI Geomatics, 2012). A DSM, therefore, includes vegetation, buildings, etc., whereas a DTM only includes the topography of a region. It is important to note that a DTM and DSM can be stored as a DEM (raster) or a TIN (triangular irregular network). In this research, only the DEM formats for storing DTMs and DSMs were used.

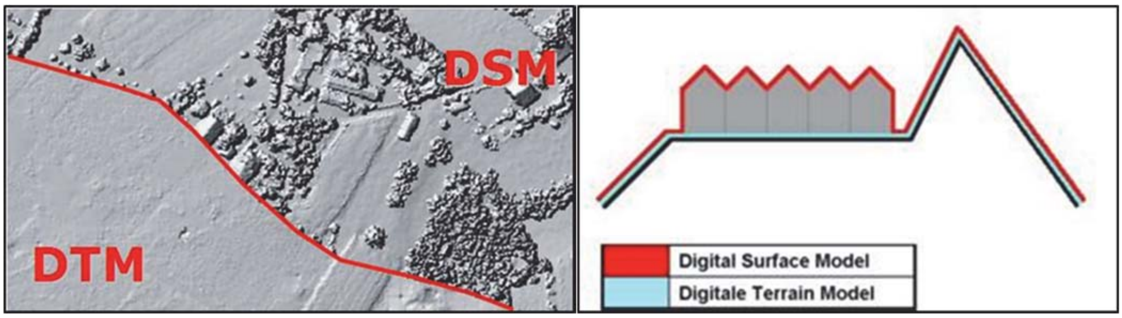

Figure 2.7 Difference between digital terrain model (DTM) and digital surface model (DSM).

Slope gradient is defined as the angle between the surface tangent and the horizontal and it controls the gravitational force available for geomorphic work (Van Niekerk & Schloms, 2001). Slope gradient is especially useful for evaluating agricultural land uses as it imposes limitations on cultivation (Mitchell, 1991). Most governments, including South Africa's, have laws that prevent agricultural developments on steep slopes (James, 2001). Slope gradient is also used in environmental modelling owing to the strong relationship between slope gradient and land cover (Pickup & Chewings, 1996; Hoersch *et al*., 2002; Adediran *et al*., 2004).

Slope aspect is the direction in which a slope faces and therefore determines its exposure to illumination from the sun. In the southern hemisphere, northern slopes receive more solar radiation than southern slopes, especially during winter. Slope aspect, in combination with gradient, determines the amount of solar radiation that reaches an area. It affects the temperature of the soil, the rate of temperature change, vegetation composition, evapotranspiration and other influences on soil properties (Irvin *et al*., 1997). Solar radiation is essential for plant development due to its role in photosynthesis, making it an important factor to consider in agricultural and forested land uses.

Curvature is the rate of change of slope gradient over a given distance and is an indication of where surface runoff will accumulate or disperse. Because of the three-dimensional nature of terrain, slopes can curve in infinite directions. For hydrological analyses and soil-landscape modelling it is useful to know whether an area is concave or convex along the slope direction (profile curvature) and/or perpendicular to the slope (plan curvature) (Irvin *et al*., 1997; Van Niekerk & Schloms, 2001).

Owing to the developmental limits imposed by slope gradient, the effect of aspect on plant growth (Dendgiz *et al*., 2003) and the influence of curvature on hydrological and soil formation processes, it is essential that these two terrain derivatives are considered for modelling waterlogging and salt accumulation. Zhou & Liu (2004) showed that the accuracy of these derivatives is highly dependent on the quality of the DEM from which they are generated. Care should therefore be taken in the selection of an appropriate DEM.

The spatial distribution of soil water content and groundwater flow often follows surface topography. The topographic wetness index (TWI), introduced by Beven & Kirkby (1979), can be derived from a DEM to determine where surface and sub-surface water may likely accumulate. TWI is defined by Sørensen *et al*. (2006) as:

$$Ln(\frac{a}{TanB})$$ Equation 2.3

where A a is the local upslope area drainage through a certain point per contour length in m; and

$Tan\ B$ is the local upslope of the ground surface.

The upslope area per contour length (a) is defined as (Sorensen & Seibert, 2007):

$$a = \frac{A}{L}$$ Equation 2.4

where A is the upslope area in m^2; and

L is the contour length in m.

By calculating soil wetness with TWI, large upslope areas will receive a high index value, whereas a low index value will be allocated to small upslope areas. Furthermore, a small index value will be calculated for steep locations, whereas gently sloped areas will receive a higher index value (Sorensen & Seibert, 2007).

According to Sorensen & Seibert (2007) the resolution of the input DEM influences the resulting TWI in several ways, namely:

- larger grid sizes results in the disappearance of fine-scale features, resulting in different patterns when TWI is calculated;
- as grid resolution increases, the values for specific upslope area also increases;
- at lower resolutions, *Tan B* is more even, which means that gentle slopes were steeper and steeper slopes were less steep;
- the estimation of upslope area is more affected by DEM resolution than that of slope;
- for landscape analyses and modelling, lower resolution DEMs might be more useful; and
- the optimal resolution for a particular study depends on which features are important to represent in the DEM.

2.5.2 Land components and geomorphometry

Land components are essentially subdivisions of landscapes and are frequently used in suitability analysis as a basic mapping unit (i.e. land unit). Although 'landscape' has been variously defined, it can be conceptualized in the terrain analysis context as a hierarchical collection of terrain forms comprising land regions, land systems, land forms, hillslopes, land components and land elements.

A land element is the smallest practical terrain unit at a given scale of mapping. McDonald *et al*. (1984) suggest that such elements should not be less than 150 x 150 m in size (i.e. <2.25 ha) at 1:50 000 scale, but can potentially be much larger in homogeneous landscapes. Land elements can be combined to form land components which are typically associated with ridge crests, fallfaces, midslopes, and footslopes (Argialas, 1995; Dymond *et al*., 1995).

Hillslopes (also called profiles) are sequences of land components orientated in the slope direction (Figure 2.8). The sequences of components differ according to number and type. Fallfaces are, for instance, not present on low hills while midslopes are absent on mesas. Complex hillslopes can include multiple occurrences of a particular type of component.

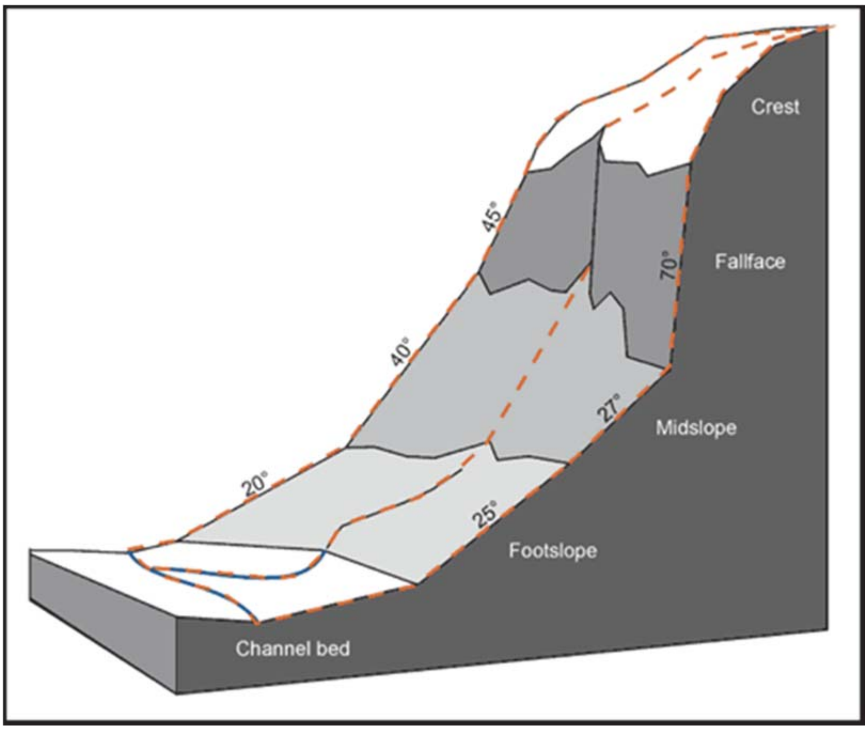

Figure 2.8 Two hypothetical hillslopes, each consisting of a sequence of five land components (Van Niekerk & Schloms, 2001).

Landforms (e.g. hills, mesas, escarpments) are essentially sequences of hillslopes arranged perpendicular to the slope direction and they are, in many cases, the main focus of terrain analysis. However, landforms have little value in land suitability analysis because land properties can vary considerably within a landform. In the southern hemisphere, temperatures will, for instance, be considerably higher on north-facing than on south-facing hillslopes, while soils will be deeper in channel beds than on crests. Land components are thus the most appropriate demarcations to use as the basis for suitability analysis.

Geomorphometry, the numerical representation of topography, combines mathematics, engineering and computer science. In the past, geomorphometry concentrated on the geometry of terrain, but technical advances in computing, analytical algorithms, input-output devices and large sets of topographic data have shifted the focus to digital representation of terrain, process modelling and generalization (Adediran *et al*., 2004).

Recently, the increasing availability of DEMs has promoted the use of computer technology for the calculation and discrimination of terrain properties. DEM-derived datasets such as slope, aspect, hydrographical pattern and shaded relief are being increasingly exploited in terrain analysis. These morphometric parameters are not only less prone to human error but can be used to objectively and quantitatively compare terrain units (Dymond *et al*., 1995; Giles & Franklin, 1998).

2.6 Existing geospatial methods for monitoring waterlogging and salt accumulation

According to Zink (2000), the impact of salt accumulation can be reduced by sensible land and water management practices and by closely monitoring salt-affected areas. Monitoring involves identifying areas where salts concentrate and detecting the temporal and spatial changes in this occurrence (Zink, 2000). Salt accumulation is a dynamic process and remote sensing data can contribute a great deal to monitoring these processes, mainly because of its ability to capture information in both spatial and temporal scales (Abbas, 1999). Generally, remote sensing has the potential to predict soil salinity, performance diagnosis and impact assessment (Bastiaanssen *et al.*, 2000). Compared to gathering field data, a remote sensing approach can save cost, time and effort (Eldiery, 2005). By integrating remotely-sensed data with GIS and spatial statistics, more accurate models can be developed to predict the distribution, presence and pattern of soil salinity (Kalkhan *et al.*, 2000).

According to Farifteh *et al*. (2006), there are two types of indicators that can be used for detecting salt-affected soils, namely soil-related indicators and performance-orientated indicators. Soil-related indicators (i.e. direct methods) include white salt crusts, puffy soil, dark greasy surfaces, dehydrated cracks and coarser topsoil, while performance-orientated indicators (i.e. indirect methods) include spotty growth of crops, presence of dead trees, blue-green tinge and moisture stress. This is consistent with the view of Mougenot *et al*. (1993) that soil salinity can be detected from remotely-sensed data either directly on bare ground or indirectly through vegetation type and growth. The following sections will discuss these two remote sensing approaches to monitoring salt accumulation in more detail.

2.6.1 Direct approach

According to Elnaggar & Noller (2009) and Metternicht & Zinck (2003), salt-affected soils with salt encrustations at the surface are smoother than non-saline surfaces and cause high reflectance in the visible and the near-infrared (NIR) regions of the spectrum. Farifteh *et al*. (2006) found that the main factors influencing the spectral reflection of salt-affected soils are the:

- quantity and mineralogy of salts, which determines the presence (or absence) of absorption bands in the spectrum (Metternicht & Zinck, 2003);
- colour of the soil; and
- surface roughness of the soil.

A variety of remote sensing data have been used for identifying and monitoring salt-affected soils. Broadband (multispectral) remote sensing data are more frequently used for monitoring salt-affected soils, mainly because they are more readily available than narrow-band (hyperspectral) data (Sharma & Bhargarva, 1988; Rao *et al*., 1995; Dwivedi, 1992; Verma *et al*., 1994). The following sections provide an overview of both approaches. Notwithstanding, multispectral sensors have been successful in distinguishing severely salt-affected from non-affected soils (Farifteh *et al*., 2006; Weng *et al*., 2010).

2.6.1.1 Hyperspectral remote sensing

Hyperspectral remote sensing has the ability to provide near-laboratory quality reflectance spectra for each pixel, allowing for the discrimination of subtle differences between materials and permitting investigation of phenomena and concepts that greatly extend the scope of traditional multispectral remote sensing (Campbell, 2007). Weng *et al*. (2010) developed a univariate regression model to estimate soil salt content using a soil salinity index constructed from continuum-removed reflectance at 2052 and 2203 nm. When applied to a Hyperion image, a moderate relationship between salt content and the index was achieved (R^2= 0.627). Using partial least square regression (PLSR), Farifteh (2007) obtained prediction R^2 values between 0.78 and 0.98. Mashimbye *et al*. (2012) showed that good predictions of salinity could be made with bagging PLSR using first derivative reflectance (FDR) (R^2 = 0.85), PLSR using untransformed reflectance (R^2 = 0.70), NDSI (R^2= 0.65), and the untransformed individual band at 2257 nm (R^2 = 0.60) predictive models. These results indicate that hyperspectral remote sensing holds much potential for mapping salt accumulation. However, the relative cost of this type of data is still prohibitive for mapping large areas.

2.6.1.2 Multispectral remote sensing

Multispectral imagery, such as WorldView-2 images, normally encompasses the visible, near-infrared (NIR) and the thermal regions of the electromagnetic spectrum. A multispectral sensor consists of multiple discrete spectral bands encompassing a great range of the electromagnetic spectrum (Lillesand *et al*., 2004). Multispectral remote sensing has been widely used to study salt-affected soils (Ben-Dor *et al*., 2001; Németh *et al*., 2006).

Metternicht & Zinck (2003) found that an increase in soil salinity is masked by the blue band (450-510 nm), owing to the interference of these wavelengths with the ferric oxides within the soil. Several salinity indices (SI) have been developed to help identify salt-affected soils from multispectral imagery (Abbas, 2007).

$$S_1 = \frac{B_1}{B_3} \qquad \text{Equation 2.5}$$

$$S_2 = \frac{B_1 - B_3}{B_1 + B_3} \qquad \text{Equation 2.6}$$

$$S_3 = \frac{B_2 \times B_3}{B_1} \qquad \text{Equation 2.7}$$

$$S_4 = \sqrt{B_1 \times B_3} \qquad \text{Equation 2.8}$$

$$S_5 = \frac{B_1 \times B_3}{B_2} \qquad \text{Equation 2.9}$$

$$S_6 = \frac{B_3 \times B_4}{B_2} \qquad \text{Equation 2.10}$$

where B_1 is the blue band;

B_2 is the green band;

B_3 is the red band; and

B_4 is the NIR band.

In addition, Abood *et al*. (2011) proposed several normalized difference salinity indices (NDSI) for WorldView-2 images. They are:

$$NDSI_1 = \frac{Yellow - NIR_1}{Yellow + NIR_1}$$ Equation 2.11

$$NDSI_2 = \frac{Yellow - NIR_2}{Yellow + NIR_2}$$ Equation 2.12

$$NDSI_3 = \frac{Red - NIR_1}{Red + NIR_1}$$ Equation 2.13

$$NDSI_4 = \frac{Red - NIR_2}{Red + NIR_2}$$ Equation 2.14

$$NDSI_5 = \frac{RE - NIR_1}{RE + NIR_1}$$ Equation 2.15

$$NDSI_6 = \frac{RE - NIR_2}{RE + NIR_2}$$ Equation 2.16

where $Yellow$ is the yellow band;

Red is the red band;

$NIR1\ and\ NIR2$ are the NIR bands; and

RE is the red-edge band.

NDSI1 was found to effectively highlight salt-affected soils, mainly due to their high reflectance in the yellow band. NDSI2 and NDSI3 produced slightly better results, possibly a result of high reflectance from vegetation and low reflectance from moisture and water in the NIR2 band. NDSI4 and NDSI5 performed poorly, which was attributed to the low reflectance of salts in the red and RE bands. Overall, NDSI3 produced the most accurate results (Abood *et al*., 2011).

Abood *et al*. (undated) used a random forest ensemble classification algorithm (Breiman, 2001) to produce classified land cover images for all their proposed indices in an attempt to highlight salt-affected areas. The random forest is a non-parametric classification algorithm that consists of multiple decision trees. This regression approach can accommodate a large number of variables and predictors with a healthy execution time and a highly accurate output.

Fernandez-Buces *et al.* (2006) proposed a combined spectral response index (COSRI), which is used to enunciate the combination of spectral responses of bare soil and vegetation. COSRI is defined as:

$$COSRI = \frac{Band_1 + Band_2}{Band_3 + Band_4} \times NDVI$$ Equation 2.17

where $Band_1$ is the blue band;

$Band_2$ is the green band;

$Band_3$ is the red band; and

$Band_4$ is the NIR; and

$NDVI$ is the normalized difference vegetation index.

In the COSRI, vegetated areas are associated with high values due to their high reflectance in the NIR bands and low reflectance in the visible bands. Negative index values are indicative of clouds, water or salt-affected soils because they have high reflectance in the visible spectrum and low reflectance in the NIR bands. Small concentrations of salt on the surface will result in index values close to zero (Fernandez-Buces *et al.*, 2006).

Al-Khaier (2003) accurately (R^2 = 0.86) detected salt-affected soils using a normalized salinity index on bare agricultural soils using ASTER bands 4 (near-infrared) and 5 (shortwave infrared). The index was defined as:

$$\frac{SWIR - NIR}{SWIR + NIR} \qquad \text{Equation 2.18}$$

where $SWIR$ is the shortwave-infrared band of the SPOT-5 sensor; and

NIR NIR is the near-infrared band of the SPOT-5 sensor.

According to Myers *et al.* (1970), the following issues complicate the detection of salt-affected soils using remote sensing:

- the pattern of salinity is generally very erratic in nature;
- abrupt changes from unaffected to barren soil may occur over a lateral distance of a few metres; and
- certain crops have a high salt-tolerance.

In addition, Metternicht & Zinck (2003) state that the observation of salt accumulation is only possible when the soil water content is low. It is, therefore, advisable to obtain remotely-sensed data at the end of the dry season. However, it is recognised that there will always be fields that are not bare, particularly in irrigation schemes where crops are rotated.

2.6.1.3 Synthetic Aperture Radar

While a large body of literature is devoted to the use of SAR for measuring soil water content (and by extension, waterlogging), very little research into the use of SAR for salt-affected soil has been done. Since these two phenomena have been shown to affect radar backscatter in different ways, they will be discussed separately here.

SAR backscatter imagery has been extensively researched as a tool for mapping surface soil water content (Kasischke *et al*., 2003; Svoray & Shoshany, 2004; Western *et al*., 2004; Álvarez-Mozos *et al*., 2005; Holah *et al*., 2005; Zribi *et al*., 2005a, 2005b; D'Urso & Minacapilli, 2006; Turesson, 2006; Rahman *et al*., 2008; Engelbrecht, 2009; Gibson *et al*., 2009). Generally, the approaches to this problem can be grouped as: 1) the use of regression or inversion models, 2) single-wavelength multi-temporal change detection approaches and 3) classifications using multiple wavelengths and multiple polarizations.

The use of theoretical approaches (regression or inversion models) has seen much attention in literature, as the search for an accurate model of soil water content derivation from SAR backscatter intensified. While many authors quote “acceptable” results from these models, the variability of soil surface roughness, (together with the effect of vegetation biomass) remains the single biggest confounding factor of experimental models (Wagner & Pathe, 2004; Moran *et al.,* 2006).

Using a multi-temporal approach to soil water content retrieval seems to yield promising results (Moran *et al.,* 2006). Researchers using this model typically employ a long time series of SAR imagery for the same area, using the same wavelength to measure the change in soil water content, rather than absolute soil water content. Generally it has been found that observing only temporal changes in radar backscatter, the effect of vegetation cover and surface roughness can be neglected ,if they can be assumed to remain constant throughout the observation period (Macelloni *et al.,* 1999; Moeremans & Dautrebande, 2000; Moran *et al.,* 2000; Wickel *et al.,* 2001; Kelly *et al.,* 2003; Mathieu *et al.,* 2003). This approach assumes that changes in radar backscatter are only due to changes in surface condition. Without the ability to normalize differences due to sensor configuration, this approach is limited to the use of a single SAR sensor, with a fixed configuration (incidence angle, polarization, etc.) (Moran *et al.,* 2006).

The third approach employed in soil water content retrieval is the (semi-) empirical use of multiple wavelengths and multiple polarizations to map areas affected by high soil water content. Polarimetric decomposition separates the contribution of different scattering mechanisms to the radar backscatter, and research in this area aims at separating the contributions of surface roughness and soil water content (Allain *et al.,* 2002; Hajnsek *et al.,* 2003). Different types of analyses on fully polarimetric data have been used with varying levels of success towards the mapping of soil water content (Western *et al.,* 2004; Holah *et al.,* 2005; D'Urso & Minacapilli, 2006).

While waterlogging is logically expected to correspond to an increase in soil water content, very few authors apply SAR explicitly to mapping of waterlogging – and when they do, this is commonly referred to as “flooding and waterlogging”. The phenomenon of waterlogging is more complex than merely measuring an increase in soil water content, or identifying open stands of water (Csornai *et al.,* 2004). In this regard, a handful of studies stand out which studied the complex nature of waterlogging. Kasischke *et al.* (2003) studied the hydrological patterns in Florida wetlands using C-band SAR. The authors showed that, while an increase in soil water content would lead to an increase in backscatter, inundation of the soil would lead to a drastic drop in backscatter, due to the specular reflection of microwave energy on water. As water depth increases, backscatter decreases. This is further complicated by the fact that standing biomass (crops) in a field reduces the sensitivity of backscatter to soil water content and that the double-bounce effect of crops standing in water could, in fact, increase the backscatter of inundated areas (Kasischke *et al.,* 2003).

Tswai (2011) also studied the use of fully polarimetric RADARSAT-2 SAR data on mapping of waterlogged areas in the Vaalharts irrigation scheme. The author employed polarimetric decomposition algorithms, specifically the Entropy/Anisotropy/Alpha (H-A-α) decomposition based on the Wishart Distribution (Pottier & Lee, 1999). Using known areas of waterlogging, the polarimetric decompositions could be classified and a map of waterlogged areas could be extracted, although no measure of accuracy is provided. The author points out the effect of very high rainfall prior to image acquisition which affected the results negatively.

The published literature on direct salt-affected soil extraction based on SAR imagery is minimal. Similar to the research on soil water content, three groups of research approaches to soil salinity specifically can be distinguished: 1) modelling correlations between radar backscatter and soil salinity, 2) mapping soil salinity through extraction of the dielectric constant and 3) mapping soil salinity by mapping which those factors related to it.

The first category of research is devoted to increased understanding of the relationship between radar backscatter, the dielectric constant and soil salinity. These studies are aimed at creating models for salinity extraction, but do not attempt to map salinity to any degree of accuracy (Abdel-Razak *et al.,* 2003; Yun *et al.,* 2003; Behari, 2005; Aly *et al.,* 2007; Lasne *et al.,* 2008). Generally, the outlook regarding these models is bleak, and their ability to express the dependence between soil water content, soil salinity and the backscattering coefficient has been described as “weak” (Aly *et al.,* 2007).

The second category of research is devoted to applying these theoretical and empirical backscatter models to actual SAR imagery in an attempt to extract values of the dielectric constant from them. This can then be related to soil salinity (Taylor *et al.,* 1996; Bell *et al.,* 2001). Conclusions reached from this avenue of research generally state that this approach can achieve good accuracies, but only under very specific conditions (normally the conditions for which the particular model was developed). They are therefore usually restricted to areas of uniform roughness, using a single wavelength and only for areas of high soil water content and a single land cover.

The third category of research generally takes a broader approach to mapping soil salinity, including features such as surface roughness and vegetation. These studies attempt to map areas of saline soils using indicators of salinization. Metternicht (1998) used a fuzzy classification of L-band SAR imagery to identify general classes based on their surface roughness, vegetation cover, soil salinity and crusting. The author achieved a 80.7% classification accuracy using this method, although no Kappa value (Campbell, 2007) was provided and serious omission and commission errors overwhelmed some of the classes (up to 87% confusion). This was ascribed to the effect of surface roughness. Grissa *et al.* (2011) attempted to produce an empirical model for salinity mapping, citing the complicated nature of theoretical models. The authors generated an unvalidated soil salinity map, and admit that their model only describes cases of low salinity distribution. Finally, in an integrated study by Del Valle *et al.* (2009), object-based image analysis of multiple-wavelength and multiple-polarization data was used to create salinity maps. Significant effort is employed to identify the correct combination of features to include, and these features are subjected to principal components analysis and multi-resolution segmentation. No classification is performed *per se*, but the segmentation is assessed for its accuracy. Accuracies based on four classes reached values of between 79.4% and 81.4%, with Kappa values ranging between 0.78 and 0.80. This stands out as one of the only studies to provide reasonable results for salinity mapping. However, this study employed a very specific combination of datasets, specifically using SIR-C data, for which only archival datasets of a short time period in 1994 are available. This study, while significant, can therefore not be used as a model for a monitoring system using currently available sensors.

Although research into the retrieval of soil water content and soil salinity data from SAR backscatter has been on-going for nearly three decades, no breakthroughs have been achieved. Researchers from both sides (moisture and salts) conclude that there are no robust, transferable retrieval algorithms currently available (Yun *et al.,* 2003; Wagner &

Pathe, 2004). Much hope is being placed on the use of advanced new sensor types, including fully polarimetric datasets, full waveform LIDAR and polarimetric interferometry.

In order for a waterlogging and soil salinization monitoring system to be viable it must be capable of identifying and quantifying the extent and severity of these phenomena. From the literature it can be seen that, should such a system be based on SAR, the following challenges will need to be overcome:

- Finding a way to accurately and consistently extract soil water content and soil salinity data from SAR backscatter (something which has not been achieved yet).
- Minimizing the effect of surface roughness.
- Minimizing the effect of sensor configuration (incidence angle, wavelength, etc.).
- Minimizing the effect of vegetation cover and vegetation change.
- Minimizing the effect of variations in soil water content due to rainfall.

In a South African context, two further concerns dominate, namely data availability and cost. As stated earlier, a monitoring system would need to employ currently active satellites, preferably having high-resolution, fully-polarimetric (HH, HV, VH and VV) capabilities. The sensors currently fulfilling those specifications would be RADARSAT-2, TerraSAR-X and COSMO-Skymed. Scenes covering between 100 and 1 000 km^2 would need to be acquired for any one specific date and area. This, together with the fact that the use of several images are needed to account for variations in backscatter, would make a monitoring system based on spaceborne SAR observations prohibitively expensive.

In conclusion, despite the efforts of the science community, there is currently no robust model for accurately and consistently extracting soil water content or soil salinity from SAR imagery. This science is very much still in an experimental phase, and most authors agree that great strides still need to be made before such an application can be operational.

2.6.2 Terrain analyses

In the previous section various remote sensing approaches for directly identifying and monitoring waterlogged and salt-affected areas were reviewed. According to Dwivedi (1997) and Dwivedi *et al*. (1999) the main limitation of such approaches is that subsurface processes do not directly influence the spectral response of the topsoil, which may make it difficult to map waterlogged or saline regions using a direct approach. A more robust approach may therefore be to make use of elevation data to model where waterlogging might occur. Elnaggar & Noller (2009) found a significant correlation between soil EC and elevation, slope and wetness indices. They also found that a 5 m DEM was able to more accurately identify important landforms consisting of saline soil than a 10 m DEM. Sulebak *et al*. (2000) found strong correlations between terrain data and soil moisture, with slope, aspect and profile curvature providing the best fit regression models (R^2 = 0.8), while weaker correlations were found between soil moisture and wetness indices (R^2 = 0.5). Sulebak *et al*. (2000) attributed this to the flatness of the terrain in their study area, which resulted in high wetness values throughout. Akramkhanov *et al*. (2011) found significant correlations between soil EC and environmental factors such as distance to drainage, profile curvature, slope and groundwater table depth. Weaker relationships were found with total dissolved solids in the soil. Stepwise multiple regression analysis was performed in both cases (Akramkhanov *et al*., 2011).

Furby *et al*. (2010) incorporated their multi-temporal approach with a conditional probability network (CPN). A CPN is a Bayesian network, which provides a computational framework to combine uncertain classified satellite image data from several growing seasons with landform data. The network can be represented as a graph, as shown in Figure 2.9, where the circles and rectangles represent the nodes of the graph. The overall accuracy for their land monitor project was 95%.

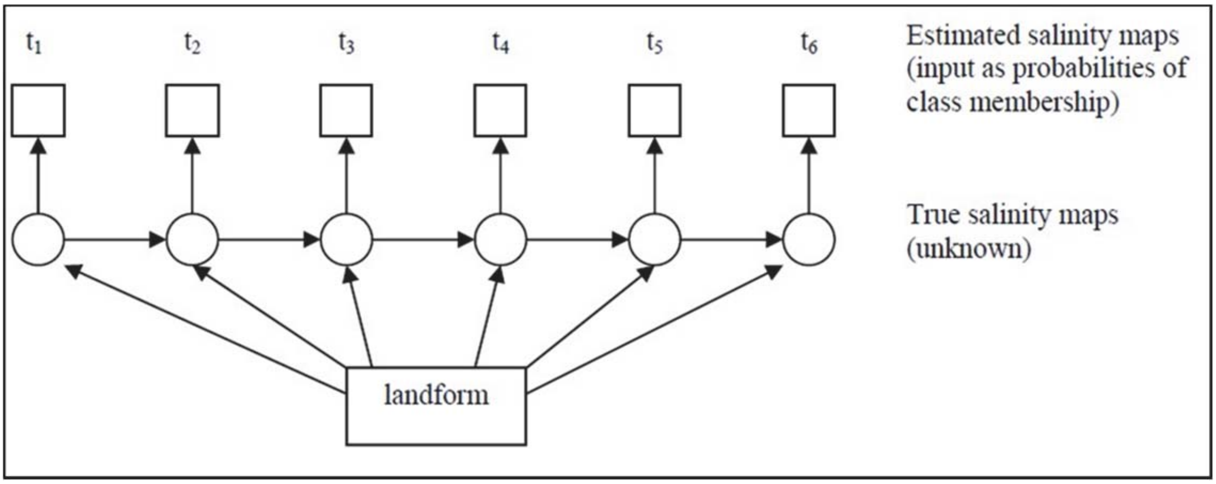

Figure 2.9 Conditional probability network used by Furby *et al*. (2010) to combine multi-temporal classification maps based on satellite images and landform data.

Based on the literature it seems that terrain analyses hold much potential for modelling waterlogged and saline conditions. However, the availability of suitable elevation data is critical and will have to be investigated.

2.6.3 Geostatistics and spatial modelling

Geostatistics and spatial modelling are widely used for salt accumulation studies. According to Eldiery (2005), choosing the correct statistical method is very important for determining the quality of the results. Geostatistics is mainly used in interpolating soil salinization from soil sample analysis results. For instance, Mohamed *et al.* (2010) employed common kriging using 150 samples of known salinity as input data. This yielded a correlation coefficient of $R^2 = 0.65$. Aldakheel (2010) also found that ordinary kriging produces the best results when interpolating EC values. Douaoui (2011) used ordinary kriging and regression kriging to interpolate a salinity map. The output revealed a good correlation compared to the salinity map obtained using WorldView-2 data. They also found that the regression-kriging method produces high levels of accuracy in the spatial estimation of salinity. However, in some cases kriging cannot be used, particularly when input samples are clustered. Lobell *et al.* (2010) showed that relatively good results can be obtained by using spatial analysis of variance (spatial ANOVA).

2.6.4 Indirect approach

Plants usually require small quantities of salts (and nutrients) to carry out the complex metabolic processes involved in photosynthesis and respiration. Salts also play an important role in the movement of water between the soil and root. A concentration of salts around the root zone will consequently reduce the plant's capability to take up water. This can lead to dehydration and wilting of plant leaves and stems. The lack of water also limits the plants metabolic processes such as photosynthesis. This impact of salts is referred to as the osmotic effect. Salts can also have a toxic effect when the plant absorbs water to compensate for water loss during transpiration. If this process continues over a long period, the salt concentrations within the plant may become so high that it becomes toxic.

Different plant species vary in their salt sensitivity or salt tolerance. Some plants are affected by low concentrations of salt, while others (halophytes) will tolerate high salt concentrations. A common symptom of the toxic effects of salts is that the leaf tips of plants turn yellow. In addition, waterlogging can have a negative effect on plant growth. Waterlogging is characterized by too much water in the root zone and limits the oxygen availability. This causes anaerobic conditions and symptoms such as stunting, discolouration of foliage, defoliation, wilting and death in some cases (McGhie & Ryan, 2005).

The effect that waterlogging and salt accumulation have on plants (refer to Section 2.1) can be used to indirectly infer where these processes are occurring within fields. This section focuses on how remote sensing can be used to detect the possible salt stress effects of waterlogging and salt accumulation.

Remote sensing indices are commonly used for mapping land cover/use, standing biomass and green leafy biomass (Abood *et al.,* 2011). An index is formed from combinations of several spectral values that are added, divided or multiplied in a manner designed to yield a single value (Campbell, 2007). Vegetation indices (VIs) are the most popular and scientifically-proven tools for analyzing remote sensing data (Verstraete & Pinty, 1996; Ceccato *et al.,* 2002). VIs attempt to measure biomass or vegetative vigour using the spectral response of different surface features (Campbell, 2007). The Normalized Difference Vegetation Index (NDVI) is the most common vegetation index used and is defined as:

$$NDVI = \frac{N - R}{N + R} \qquad \text{Equation 2.19}$$

where N is the reflectance in the near-infrared (NIR) band; and

R is the reflectance in the red band.

It should be noted that although NDVI is useful for a wide range of applications, it is very sensitive to soil background brightness (Huete, 1988; Bausch, 1993). In order to adjust the soil background brightness constraint inherent in the NDVI spectral index, Huete (1988) proposed using a soil-adjustment factor (L). This factor accounts for first-order, non-linear, differential NIR and red radiative transfer through a canopy (Jiang *et al.,* 2008). The resulting soil-adjusted vegetation index (SAVI) is defined as:

$$SAVI = (1 + L)\frac{N - R}{N + R + L} \qquad \text{Equation 2.20}$$

where N is the reflectance in the near-infrared (NIR) band;

R is the reflectance in the red band; and

L is the soil-adjustment factor.

The soil-adjustment factor can vary from 0 to 1 depending on the amount of visible soil. The thicker the vegetation, the less soil is exposed and the lower the L value. However, 0.5 is a reasonable approximation for the L value when the amount of soil scene is unknown (Koshal, 2010). SAVI provides better results than NDVI at low vegetation cover because of its ability to eliminate the soil background effect (Koshal, 2010). Modifications of the SAVI, in the form of MSAVI (Qi *et al.*, 1994a) and MSAVI2 (Qi *et al.*, 1994b), have also been developed.

The Enhanced Vegetation Index (EVI) was developed to optimize the vegetation signal with improved sensitivity in high biomass regions and improved vegetation monitoring by disconnecting the canopy background signal and a reduction in atmospheric influences (Jiang *et al.,* 2008). EVI is defined as:

$$EVI = G\frac{N - R}{N + C_1R - C_2B + L} \qquad \text{Equation 2.21}$$

where N is the reflectance in the near-infrared (NIR) band;

R is the reflectance in the red band;

B is the reflectance in the blue band;

G is a gain factor;

L is the soil-adjustment factor; and

$C1,C2$ are aerosol resistance coefficients.

The values as adopted in the MODIS EVI algorithm are L = 1; C1 = 6; C2 = 7.5 and G = 2.5 and are used as a *de facto* standard for other sensors as well.

Many researchers have compared NDVI and soil salinity (Wiegand *et al.,* 1994; Eldiery, 2005; Tajgardan *et al.,* 2007; Elnaggar & Noller, 2009; Lobell *et al.,* 2010; Abood *et al.*, 2011). Elnaggar & Noller (2009) found no significant statistical correlation between Landsat-derived NDVI and electrical conductivity (EC)[2]. The relatively low resolution of the Landsat imagery was offered as a possible explanation for this result. Aldakheel (2010) only found a weak, non-linear statistical correlation between Landsat-derived NDVI but noted that low NDVI values generally corresponded to high EC values, indicating that salinity had some impact on growth. Although Lobell *et al.* (2010) also found some correlation between EC values and MODIS-derived NDVI, the NDVI was bested by the EVI in the correlation with EC values. The results showed that the EVI nearly always provided a larger absolute correlation than the NDVI, which supports the notion that EVI represents a more robust measurement of vegetation condition than NDVI. Results using SAVI were very similar to those of NDVI (Alhammadi & Glenn, 2008).

The use of normalized VIs for saline soil detection has been limited partly due to the spectral resolution of the multispectral sensors currently utilized (Metternicht & Zinck, 2003). Abood *et al.* (2011) took advantage of the new spectral bands and high spatial resolution of the WorldView-2 satellite to design six different NDVI and SAVI indices. The NDVI no. 3 index proved to be the best in distinguishing saline soils from non-saline soils. The index uses the WorldView-2 yellow band (585-625 nm). The NDVI no. 3 is defined as:

---

[2] EC in this document refers in most cases to EC_e which relates to the electrical conductivity of the saturation extract of the soil.

$$NDVI\ no.3 = \frac{NIR1 - Yellow}{NIR1 + Yellow}$$ Equation 2.22

where $NIR1$ is the reflectance of WorldView-2's first near-infrared band; and

$Yellow$ is the reflectance of WorldView-2's yellow band.

Abood *et al.* (2011) also developed six new SAVI indices to test the effect of a higher spatial resolution and additional spectral bands of the WorldView-2 satellite in the mapping of soil salinity. The yellow band proved again to be the most successful in distinguishing between heavy vegetated areas and saline soils. The adjusted SAVI index (SAVI no. 2) is defined as:

$$SAVI\ no.2 = NIR1 - \frac{Yellow\ \times (1 + 0.5)}{NIR1 + Yellow + 0.5}$$ Equation 2.23

where $NIR1$ is the reflectance of WorldView-2's first near-infrared band; and

$Yellow$ is the reflectance of WorldView-2's yellow band.

SAVI no. 2 produced better results than the NDVI no. 3. Koshal (2010) also made use of VIs, mainly IRS-derived SAVI in detecting salt accumulation. The thresholds used in distinguishing the soil salinity are provided in Table 2.7. The results showed that the classified SAVI image was very useful for distinguishing between healthy crops and crops affected by severe salinity. He concluded that a combination of VIs and water indices (WIs) improves the assessment of salt-affected plants.

Table 2.7 Soil-adjusted vegetation index (SAVI) values for various land cover classes (Koshal, 2010)

No.	Land cover classes	Value range
1	Crop affected by salinity (Severe/moderate salinity)	0.50-0.68
2	Waterlogged area/canal	0-0.50
3	Normal crop	>0.68
4	Settlement/fallow (sand dunes)	<0.18

Zhang *et al.* (2011) derived several VIs from the recorded hyperspectra and assessed their predictive power for salinity detection. A mixture of halophytes and salt-sensitive plants were studied. They suggested that the ambiguity of VIs may originate from the different spectral responses of various plants to salinity. This is because different species have different tolerance thresholds to stress (Lauchli & Luttge, 2002), implying that spectra gathered over a salt-affected area may have species-dependent thresholds. This also explains why inconsistent results are often found when using NDVI.

The nine narrow band indices that were assessed are shown in Table 2.8, along with their potentials for estimating salinity within different vegetation species. Corn, cogon, grass and (to a lesser extent) cotton are the more saline sensitive species while reed, saltcedar, suaeda and aeluropus are more hylophytic in nature. It is clear that the selected VIs were not sensitive to all species, with an overall R^2 of 0.28. However, when considering the individual results, the narrow band SAVI produced the best overall result. Better results were achieved for cotton, corn and cogon grass, which emphasises the difficulties of employing VIs on halophytic vegetation.

Table 2.8 Nine narrow band vegetation indices assessed along with their R^2 values for each vegetation species (Lauchli & Luttge, 2002)

Performance of narrow band vegetation indices for predicting soil salinity across dominant species in the YRD, with coefficient of determination (R^2) of linear regression.

VIs	Cotton	Corn	Cogon grass	Reed	Saltcedar	Suaeda	Aeluropus
$NDVI_{680}$	0.32**	0.35**	0.32**	0.27**	0.18**	0.17**	0.16*
$NDVI_{705}$/CI	0.10**	0.26*	0.34**	0.36**	0.23**	0.31**	0.27*
SR_{680}	0.30**	0.34**	0.29**	0.21**	0.18**	0.15**	0.12*
SR_{705}	0.10*	0.29*	0.33**	0.23**	0.22**	0.27**	0.15*
PSRI	0.25**	0.19*	0.30**	0.35**	0.16**	0.22**	0.22**
SIPI	0.25**	0.18*	0.32**	0.33**	0.17**	0.18**	0.20**
PRI	0.18**	0.31**	0.01	0.03	0.003	0.08*	0.05*
REP	0.20**	0.42**	0.12**	0.04	0.10*	0.09*	0.02
$SAVI_{800}$	0.44**	0.66**	0.53**	0.41**	0.40**	0.42**	0.30**

* $p < 0.05$.
** $p < 0.01$.

Zhang *et al.* (2011) conducted a statistical analysis to identify salt-sensitive bands for various species. They identified seven band zones as the most sensitive to salt stress through partial least square. These bands range from the visible spectrum (395-410, 483-507, 632-697 nm) to the NIR spectrum (731-762, 813-868, 884-809, 913-930 nm). Of these, the NIR spectral regions in the red edge were found to be the most responsive to salt stress. However, they found that none of the VIs were sensitive enough to all species and that there was generally a weak relationship with soil salinity. Only the non-halophytes showed a relatively high relationship with salinity. A number of new SAVI-based salinity indices were consequently developed using 156 080 different band combinations. Linear regressions were used to test all of these indices. Four new salinity indices, called SASI1-4, were developed using this approach. SASI is defined as:

$$SASI = (1 + L) \times \frac{\lambda_2 - \lambda_1}{\lambda_2 + \lambda_1 + L} \quad \text{Equation 2.24}$$

where L = 0.5; and for

$$SASI_1: \lambda_1 \rightarrow average(546 - 575);\ \lambda_2 \rightarrow average(560 - 590)$$

$$SASI_2: \lambda_1 \rightarrow average(655 - 764);\ \lambda_2 \rightarrow average(690 - 780)$$

$$SASI_3: \lambda_1 \rightarrow average(655 - 764);\ \lambda_2 \rightarrow average(800 - 868)$$

$$SASI_4: \lambda_1 \rightarrow average(655 - 764);\ \lambda_2 \rightarrow average(889 - 903)$$

The SASI indices showed superior results (Table 2.9) when compared to other VIs for all of the species because they were constructed by the most sensitive bands.

Table 2.9 Performance of SASI indices when compared to other VIs

R^2 of linear regression	All species	Halophyte species	Salt-sensitive species
$SASI_1$	0.53^{**}	0.47^{**}	0.60^{**}
$SASI_2$	0.50^{**}	0.44^{**}	0.55^{**}
$SASI_3$	0.58^{**}	0.43^{**}	0.66^{**}
$SASI_4$	0.58^{**}	0.43^{**}	0.69^{**}
$NDVI_{680}$	0.13^{**}	0.17^{**}	0.46^{**}
$CI/NDVI_{705}$	0.36^{**}	0.25^{**}	0.39^{**}
$SAVI_{800}$	0.48^{**}	0.27^{**}	0.52^{**}

Halophyte species: reed, saltcedar, suaeda, and aeluropus.
Salt-sensitive species: cotton, corn, and cogon grass.
** $p < 0.01$.

$SASI_3$ and $SASI_4$ are of particular interest because the band ranges of many popular sensors cover their adopted bands (Zhang *et al.,* 2011). Examples of these are: bands 1 and 2 of MODIS, bands 3 and 4 of Landsat TM and bands 2 and 3 of SPOT.

From the literature it is evident that VIs produce valuable information for indirect detection of salt accumulation. However, Lenney *et al.* (1996) caution that crops with low density cover can easily be confused for crops affected by salt accumulation. They showed that this can be overcome by using a multi-temporal approach. The principle of this approach is that, if an area within a field is highlighted as being stressed (possibly due to salt accumulation) at multiple dates, it is unlikely that the cause of this stress is related to farming practices. Lobell *et al.* (2010) emphasize the importance of a multi-temporal approach and support the notion that factors other than salinity affecting vegetation tend to exhibit more variable spatial patterns from year to year.

2.6.5 Biophysical approach

The biophysical approach to salt accumulation mapping is based on detecting crop reaction to soil salinity through osmotic forces and increasing surface resistance due to stomatal closure. This method, proposed by Al-Khaier (2003), is based on surface resistance, which is the combined vapour flow of the transpiring crop and evaporating soil when the soil is not completely covered by a canopy.

To calculate the surface resistance, Al-Khaier (2003) used the Penman-Monteith equation along with the SEBAL (Surface Energy Balance Algorithm for Land) algorithm developed by Bastiaanssen (1998). The Penman-Monteith equation is defined as:

$$\lambda E = \frac{s_a(R_n - G_0 + \frac{p_a c_p \Delta e}{r_a})}{s_a + \gamma(1 + \frac{r_s}{r_a})}$$ Equation 2.25

where λE is the actual evaporation determined by SEBAL;

Sa is the slope of the saturated vapour pressure curve (mbar K^{-1});

Pa is the moist air density (kg m^{-3});

Cp is the air specific heat at constant pressure (J kg^{-1} K^{-1});

Δe is the air vapour deficit from saturation (mbar);

ra is the aerodynamic resistance (S/m); and

rs is the surface resistance (S/m).

Since the surface resistance is the only unknown variable, it could be solved from the inversion of the Penman-Monteith equation. Al-Khaier (2003) showed that the higher the surface resistance, the lower the osmotic pressure will be, and the lower the osmotic pressure, the higher the salinity will be.

The result of the surface resistance map was promising. As shown in Figure 2.10, when the salinity of the soil is less than 7.7 dS.m^{-1} (770 mS/m) there is less correlation between the EC and rs values. However, between the values 7.7 and 27 dS.m^{-1} (770 and 2700 mS/m) the correlation between the EC and rs values is strong. This indicates that the more saline the soil is (the higher the EC value) the more difficult it is for the crop to obtain water from the soil, and thus the greater the surface resistance becomes (Al-Khaier, 2003). The overall correlation coefficient was R^2 = 0.86, which indicates high correlation accuracy. It should be noted that the salinity levels in this experiment are significantly higher than what is normally encountered in South Africa, which means that this index will likely be less effective in local conditions.

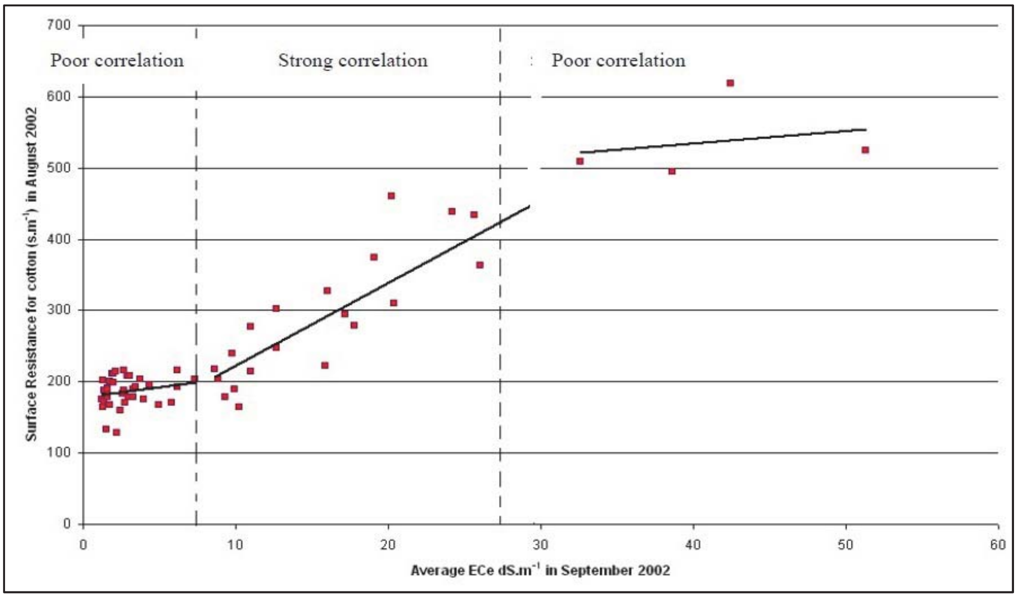

Figure 2.10 Result of the surface resistance map (Al-Khaier, 2003).

The main limitation of the biophysical approach to monitoring salt accumulation or waterlogging is its dependence on satellite imagery with a thermal band. Such data is restricted to medium to low resolution sensors (e.g. ASTER, Landsat, MODIS) which produce at best thermal images at a resolution of 100 m (Landsat 8). It is therefore very unlikely that the biophysical approach will pick up small (<10 m) variations in salt accumulation.

2.6.6 Conclusions

The previous sections reviewed the published literature on existing remote sensing and modelling methods for mapping and monitoring waterlogging and salt accumulation. The existing body of work can be summarized according to the data sources and the techniques used. The following conclusions can be drawn:

Hyperspectral data is currently still prohibitively expensive and SAR-based approaches require multi-temporal datasets that are unlikely to be attainable for large areas. In a data-scarce country such as South Africa, it seems that for the remote sensing techniques that rely on high resolution, multispectral satellite imagery such as those produced by SPOT-5/6/7 hold the most potential, as such data is the most accessible and available at national level. The recent release of 30 m SRTM DEM elevation data of Africa may also be a very useful source of data for terrain analyses techniques. Other sources of elevation data include the 5 m resolution Stellenbosch University Digital Elevation Model (SUDEM) and the 2 m resolution Stellenbosch University Digital Surface Model (SUDSM). The value of these datasets for modelling waterlogging and secondary salt accumulation needs to be investigated further.

The direct and indirect remote sensing approaches show the most promise as they can be applied to high resolution, multispectral satellite imagery. Statistical methods such as regression, partial least squares regression and multi-regression have been shown to be successful in a number of studies and should be investigated further. Surprisingly little attention has been given to the use of modern image classification and machine learning algorithms (e.g. classification and regression trees, decision trees, support vector machines and random forest) for mapping waterlogged and salt-affected areas. Such applications will likely be very effective given their success in other remote sensing applications (e.g. land cover mapping).

The review of the literature reflects a large body of work that is focussed on finding practical solutions for monitoring waterlogging and salt accumulation. However, none of the methods provided being the ultimate solution, with each having some kind of limitation for operational application. Most likely, that the solution does not lie in one technique but in a combination of methods. In order to find the best combination of methods for monitoring waterlogging and salt accumulation, each of the most promising techniques must be evaluated in a South African context to better understand their individual strengths and limitations. It is critical that the uncertainties in the outputs of the different techniques must be taken into consideration before they are incorporated into a modelling strategy.

2.7 Critical evaluation of remote sensing detecting salt-affected soils

In the past decades, the use of remote sensing was widely investigated for collecting information on soil properties such as salinity (Farifteh, 2007). Considering the complexity of the salinization process and its influence on different soil properties (both physical and chemical), detecting salt-affected soils with remote sensing is not an easy task. The main limitations of remote sensing in salinity studies can be summarized as follows (Irons *et al*., 1989; Csillag *et al*., 1993):

- Variations in the reflectance spectra of soils cannot be attributed to a single soil property.
- Remote sensing data do not contain information on the third dimension of the soil body (the profile and other subsurface properties).
- Salinization is hidden at its inception and thus can often go undetected by remote sensing sensors.
- Many of the salts diagnostic spectral signatures occur in water regions at around 1400 and 1900 nm and are hence obscured by the presence of water.
- In general, most absorption features indicative of salt minerals are in the far infrared, whereas spectral features in the visible, near and shortwave infrared (400-2500 nm) are very weak and limited.
- Salt concentrations in soils need to be high to influence the soil reflectance.
- Moisture content of soils and salts (depending on the types) have similar effects on soil reflectance spectra and causes large anomalies in predicting salinity levels from remotely-sensed data.

2.8 Geographical information systems and agricultural geo-referenced information system

A geographical information system (GIS) can be defined as a computer-enhanced information system that aids decision-making by referencing data to spatial or geographical co-ordinates (Schoolmaster & Marr, 1992). GIS-based information systems on land and water are world-wide becoming an integral component of institutionalized programmes for integrated natural resource planning, management, conservation and agricultural development.

GIS is often used to support geomorphometry and land component mapping. The most common approach is to use GIS overlaying techniques to combine DEM derivatives such as slope and aspect to create unique, homogeneous morphological units (Adediran *et al*., 2004). Classification is required to convert the continuous slope and aspect raster surfaces into regions (polygons). Once the slope and aspect rasters have been classified, they are usually converted to vector format and overlaid to create new polygons representing combinations of aspect and slope. The overlay operation is, in many cases, followed by a conflation operation to get rid of insignificantly small polygons.

The use of overlay techniques to delineate morphological land units is simple, fast and can be done with standard GIS software. The problem with this technique is the way in which terrain is generalized during the classification process. Slope aspect is usually classified into nine standard aspect classes representing north, north-east, east, south-east, south, south-west, west, north-west, and no aspect (level) (Dymond *et al*., 1995), while slope gradient is usually classified into a number of equal-interval classes. The effect of applying such classification schemes over the entire extent of the slope gradient and aspect rasters (i.e. as a global raster operation) is that class breaks will not likely coincide with local terrain transitions. This is especially problematic for slope breaks because small transitions in slope gradient can have drastic effects on land properties such as soil and vegetation cover.

Until recently, the analysis, storage, organization and presentation of spatial data have been the primary function of a GIS, but the rapid development of the object orientated programming genre and associated GIS components have broadened the capacity of the GIS suggests that to fulfil GIS potential as a suitable aid to environmental monitoring, the introduction of knowledge-based concepts and methods into GIS software should be encouraged.

AGIS (Agricultural Geo-referenced Information System) was the official portal for the dissemination of data for the Department of Agriculture in South Africa. The vision of AGIS was: "Making South Africa's Agricultural information available on the Internet". AGIS went live in 1999 and was officially launched at the World Summit on Sustainable Development in 2002. AGIS contains a large amount of information related to the environment and agriculture (Rust *et al.*, 1999). The operational objective of AGIS was to increase the quality, efficiency and accountability of the decision-making processes. A schematic representation of AGIS is given in Figure 2.11.

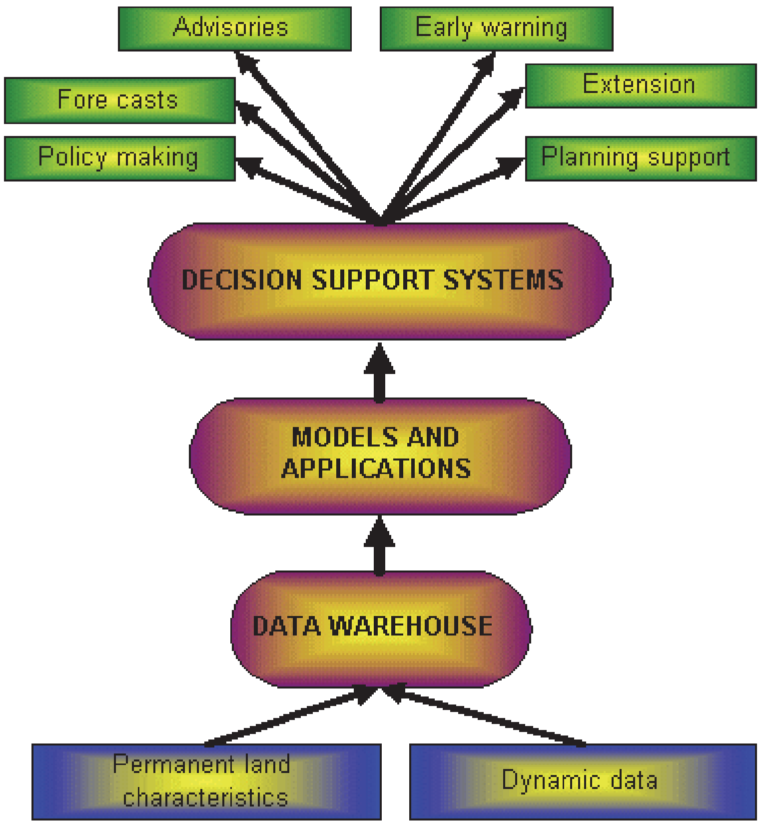

Figure 2.11 Schematic representation of AGIS.

The South African AGIS web application was developed in the ArcGIS Server environment. ArcGIS Server allows geographical data to be published online and provides web users with access to the data through the internet.

2.9 Review papers on South African irrigation schemes

Although old, the review papers of Scotney & Van der Merwe (1991), Du Plessis (1991), Schoeman & Van Deventer (2004) and Policy Proposal for Irrigated Agriculture in South Africa by Backeberg *et al.* (1996) are still relevant to salt-affected soil and waterlogging for South African irrigation schemes today.

Schoeman & Van Deventer (2004) reviewed environmental impacts on soils due to agriculture. They point out that:

- Due to elevated soil salinity levels expected in future, it would become increasingly necessary to monitor the situation on irrigation schemes in order to timeously identify salinization trends and potential problems.
- There is a need for a suitable national environmental monitoring and evaluation system. In its absence, various *ad hoc* pieces of environmental data, information, norms and standards that are constantly being collected will remain pieces of a large puzzle and extremely difficult to incorporate into a holistic picture.
- Despite its obvious advantages, irrigated agriculture continues to contribute to soil degradation in the form of salinization, sodicity, waterlogging, structural breakdown, crusting and compaction. Contributing causes are deteriorating water quality, low suitability of the soil, sub-optimal management, poor planning and the indirect consequences of economic pressures.

The review of Scotney & Van der Merwe (1991) points out that:

- Long-term viability of many irrigation schemes is in jeopardy. Studies suggest that the extent of soil degradation exceeds 10% of the total area irrigated. Many State schemes are being seriously threatened by the rapid decline in water quality. Little is known of the extent of degradation on private schemes but it is evident that the economic viability of many schemes is in doubt.
- Growing competition for limited soil and water resources will force all industries, including agriculture, to meet the demands for maintaining higher standards of environmental quality. Farmers will need to appreciate that society will demand higher standards of resource management in future.
- Positive steps are needed to counteract the continuing degradation of soil and water resources under irrigation. This implies acceptance of the ‘sustainability’ concept much debated and rhetorical.
- The adverse effects of off-site damage to downstream consumers, including health hazards, are rarely appreciated. Deteriorating water quality, sedimentation and damage by flooding are all aspects of particular relevance to the long-term viability of irrigation schemes.
- Understanding the interaction between soil properties and water quality is fundamental to reclaiming degraded land.
- Water supply and quality are crucial issues for future irrigation development. Promoting water use efficiency, affecting control over water tables and preventing salinization are major needs. While much can be achieved through improved

management, special attention should be given to communal drainage networks, on-farm drainage and preventing leakage.
- Sub-optimal farm management and deficiencies in physical and financial planning, together with fragmented research and extension efforts, are important reasons for poor water use efficiency and resource degradation. Such limitations have persisted over many years.
- Degradation should be approached on a ’prevention is better than cure ‘basis. However, properly planned drainage systems together with soil amelioration have proved highly successful in improving crop performance on degraded areas and should be encouraged.
- The future poses many special challenges if long-term viability of irrigated land is to be safeguarded. Greatest among these is the need to match technology with the natural resource base and the managerial skills of the farmer.

The review by Du Plessis (1991) concluded that:
- Although waterlogging appears to be an incessant problem countrywide and even serious on some irrigation projects, the situation seems to be largely under control from a national perspective.
- Salinization of both water and soil resources appears, on the other hand, to pose an increasing threat to sustainable irrigated agriculture.
- Progress has been made with regard to understanding permeability problems and the factors that play a role. The implementation of the acquired knowledge in practice is, however, still mostly lacking.
- No programme exists to determine the extent of waterlogged conditions on South African irrigation schemes on a regular basis.
- Up to now soil salinization in South Africa seems to have been largely associated with shallow water tables.
- Although there are obvious exceptions, soils generally appear to recover fairly rapidly from excess salinity after installation of drainage to remove the high water tables and allow the leaching of accumulated salts. The rapid recovery can probably be ascribed to the combined effect of soil selection criteria, over-irrigation with relatively low salinity water and the addition of gypsum where needed.
- The salinity of irrigation water will increase in future and improved management of water applications will reduce over-irrigation. Under these conditions soil salinity is bound to rise and it will become increasingly important to control soil salinity and the negative effects it has on crop production.
- With the elevated soil salinity levels expected to arise in future, it will become increasingly necessary to monitor the situation on irrigation schemes and within irrigated lands in order to identify salinization trends and potential problems timeously for remedial action to be taken.

A number of aspects of the discussion paper Policy Proposal for Irrigated Agriculture in South Africa by Backeberg *et al.* (1996) are also relevant to salt-affected soil and waterlogging problems on South African Irrigation Schemes. They recommended that:
- Rehabilitation of existing schemes should be prioritized above development of new schemes.

- Emphasis be placed on the prevention of deterioration in water quality and increasing health threats as caused by point and non-point pollution of water and protection of river ecosystems and the natural landscape in order to maintain biodiversity.
- Better soils should receive priority for irrigation.
- Environmental damage must be minimized through sustainable irrigation practices, and ecological and social responsibility must be developed among irrigators.
- Water use should be moved from crops with low physical and economic water use efficiencies to those which perform better.
- Water saving practices should be encouraged.
- Very few small-scale farmer irrigation schemes have succeeded – a multi-disciplinary task team should investigate the cause of failure, make innovative changes and develop training programmes for both project managers and farmers.
- National water resources development and irrigation policies and strategies must be reviewed and reformed to meet the objective of sustainable agricultural development in the small-scale farming sector.

3 STUDY AREAS

3.1 Introduction

The irrigation schemes were selected considering, amongst others the following factors: known problem areas regarding waterlogging and salt accumulation, availability of soil information, summer and winter rainfall, and inland and coastal areas to develop a methodology for identification, classification and monitoring the extent and degree of waterlogging and salt accumulation on South African Irrigation schemes. The irrigation schemes selected for the study were in the following Water Management areas: Limpopo, Olifants, Pongola-Mtamvuna, Vaal, Orange, Breede-Gouritz and Berg-Olifants.

3.2 Irrigation potential

Irrigation potential maps were produced for Vaalharts, Loskop and Makhathini. Procedures for the assessment of land for irrigation development in South Africa were done according to Irrigation Planning Staff (1980), Hensley & Laker (1980), Bester & Liengme (1989), Dohse *et al.* (1991) and Nell (1991).

The following irrigation classes were used to produce the irrigation potential maps:

- **Class 1** – Highly suitable for irrigation with few or no limitations or preconditions. Topography is flat, soils are well drained, of moderate permeability and are deep, medium textured with good available water-holding capacity.
- **Class 2** – Suitable for irrigation with slight limitations such as undulating topography, moderately well drained soils, moderately slow or moderately rapid permeability or moderate depth of soil.
- **Class 3** – Low suitability for irrigation with moderately severe limitations such as significantly rolling topography, imperfect or somewhat excessively drained soils, slow or rapid permeability, or shallow soils.
- **Class 4** – Not suitable for irrigation under most conditions with severe limitations.
- **Class 5** – Soils with severe limitations, not recommended at all, such as soils in natural waterways or in the river floodplain, soils presently eroded or soils showing the presence of any permanent or potential water table.

Soils of irrigation classes 1 and 2 can be recommended for irrigation. Soils of irrigation class 3 is normally not recommended for large-scale irrigation development under average conditions, but small areas may be considered if they adjoin or are enclosed by areas of soils having irrigation classes 1 and 2.

Soil depth provides the volume of soil material for root development, water storage and nutrient uptake. Effective soil depth can be considered as the depth freely permeable to plant roots and water. The derived irrigation potential classes used in terms of soil depth are:

- Class 1 – 900 to 1500 mm
- Class 2 – 600 to 900 mm
- Class 3 – 300 to 600 mm
- Class 4 – 150 to 300 mm
- Class 5 – 0 to 150 mm

The main criteria used to assign irrigation potential classes included soil depth and texture, whereas certain specified conditions rendered soils non-irrigable:

Soils with more than 10% and less than 35% clay and without significant different textural layers are considered irrigable (irrigation class 1). Soils with distinct different textural layers, less than 10% clay and more than 35% clay were classified as irrigation class 3 or higher.

Non-irrigable soils (irrigation class 5) were identified using the following criteria:

- Soils in natural waterways
- Soils in the floodplain of the river
- Soils presently eroded
- Soils showing the presence of any permanent or potential water table.

3.3 Vaalharts Irrigation Scheme

The Vaalharts irrigation scheme (Figure 3.1) is located on the border of the Northern Cape, North West and Free State provinces. Nearby towns include Jan Kempdorp, Hartswater and Pampierstad. At 36 950 ha in size (Gerber, 2006), Vaalharts is the largest irrigation scheme in South Africa, but is relatively small in comparison to irrigation schemes in the United States, Canada, Australia, Sudan and Egypt.

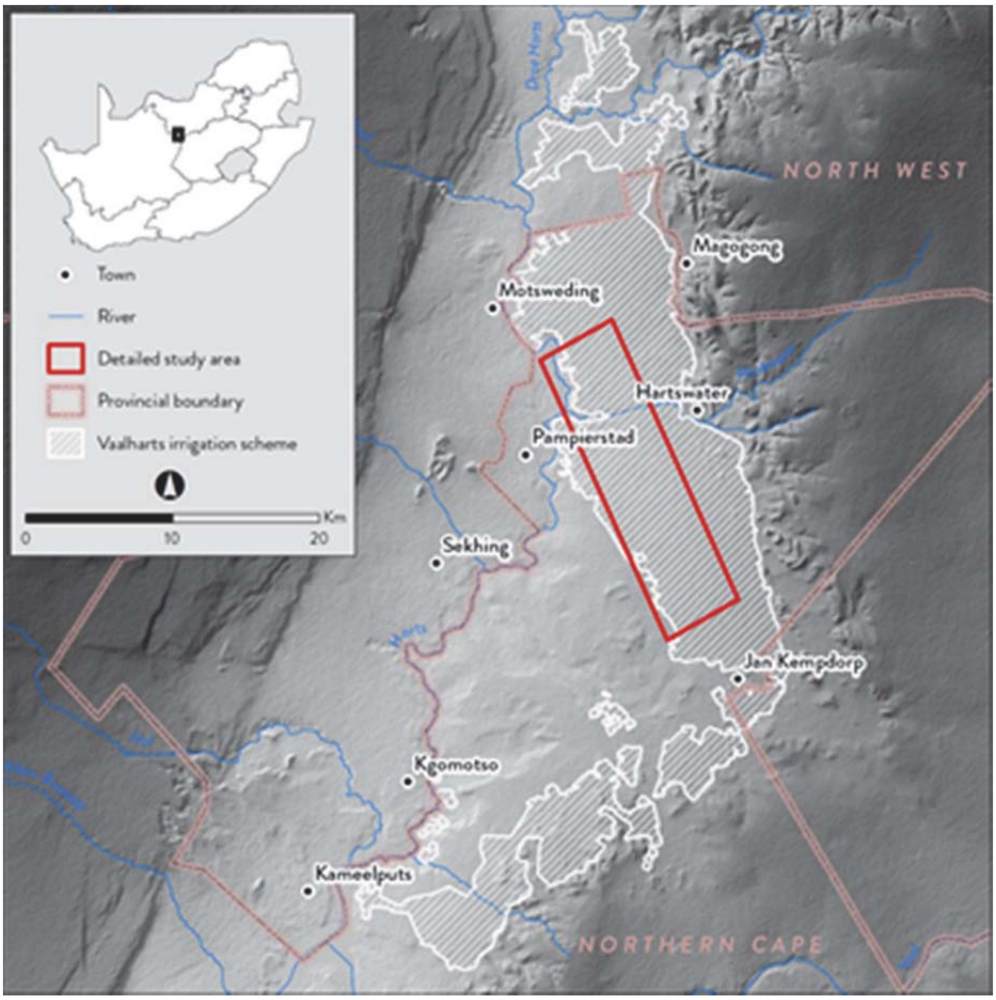

Figure 3.1 Vaalharts irrigation scheme.

Vaalharts was selected because it is the irrigation scheme in South Africa with the most available information and data (including digitized soil maps). Vaalharts is also known to have waterlogging problems, although an intensive drainage system is in place. Several waterlogging studies have been done on this scheme, which can be used as reference for this study. Waterlogging is a much bigger problem than salt accumulation at Vaalharts for two reasons: the good quality irrigation water (and good quality drainage water) and the fact that calcium is the dominant cation in the soil and water.

The Vaalharts area is known for its sandy soils (Figure 3.2), which are prone to waterlogging and salinization as well as compaction (Maisela, 2007). Typically the soils in the scheme consist of 8% clay, 2% silt, 68% fine sand and 22% medium and coarse sand (Streutker, 1977). The main crops planted in the area are maize, wheat, barley, lucerne and groundnuts (Kruger *et al*., 2009). These annual cash crops are mostly planted on a rotational basis. Large areas were planted with permanent crops such as pecan nuts in the last 5 years. The majority of the soils on the Vaalharts irrigation scheme are irrigation potential class 1 and class 2 soils (Figure 3.2). The scheme receives its irrigation water from the Vaal and Harts Rivers. The irrigation comprises mostly flood irrigation (45%), while pivot irrigation contributes up to 41% (Aurecon, 2010). Vaalharts is situated at an altitude of 1175 m above mean sea level and is known for its long warm summers and cold winters with occurrence of frost, hail and storms (Gerber, 2006). The area receives a mean annual rainfall of 450 mm with most (89%) of this precipitation occurring from October to April (Maisela, 2007).

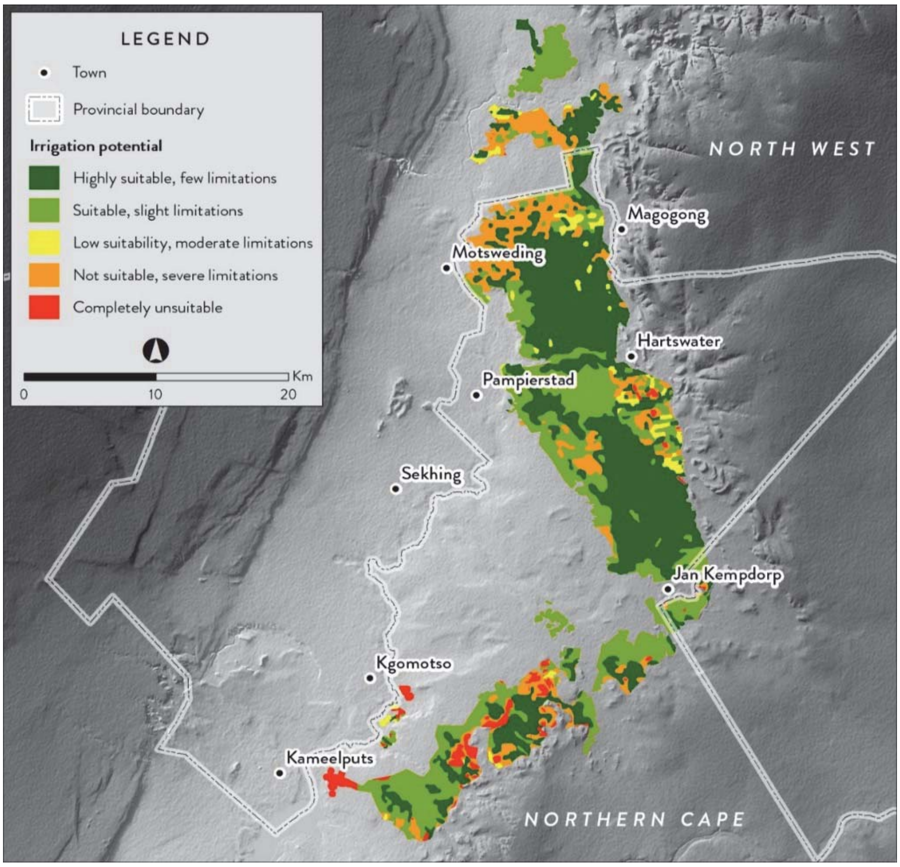

Figure 3.2 Irrigation potential of soils at Vaalharts.

3.4 Loskop Irrigation Scheme

The Loskop Dam, built on the farms Loskop and Vergelegen, is situated in the Olifants River approximately 32 km south of Groblersdal in the Mpumalanga and Limpopo Provinces (Figure 3.3). The largest part of the catchment area is situated on the Highveld plateau at an altitude of more than 1 500 m above mean sea level; the remaining part is on slopes of the plateau in the Lowveld. The mean annual runoff is approximately 451 million m^3. The catchment area of the dam is 12 300 km^2 and at full supply level its surface area is 2 350 ha.

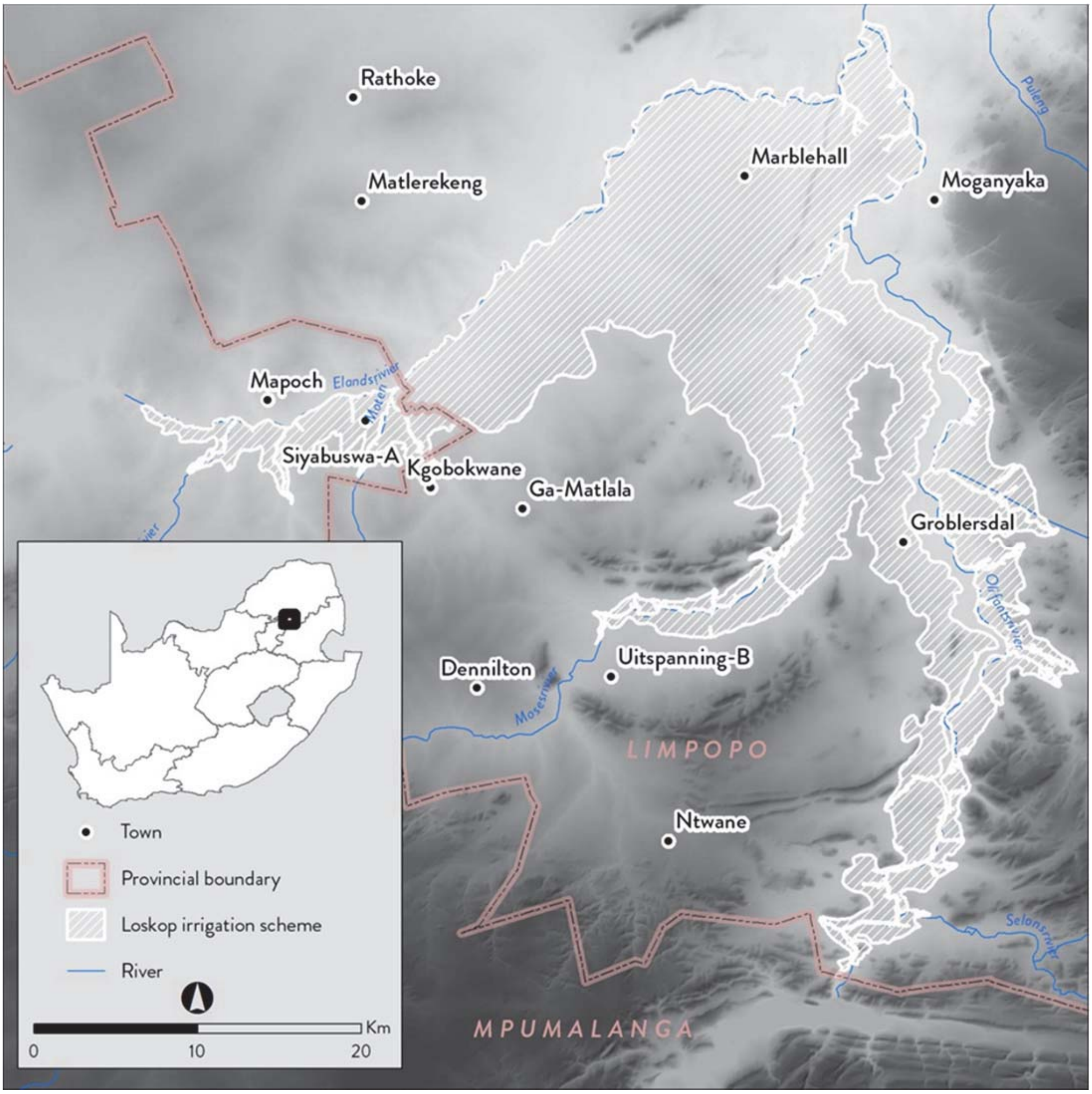

Figure 3.3 Loskop irrigation scheme.

In 1917 the first private dam was completed on the farm Rooikraal. Around 1925, after the successes of small irrigation schemes, the Hereford Irrigation Board was founded to supply irrigation water to an area of about 2 140 ha situated a few kilometres downstream of the present Loskop Dam. The early success of this scheme gave rise to a petition which resulted in studies of the Hereford Scheme, as well as in a soil and a topographical survey of the dam basin. This paved the way for the commencement of construction of the Loskop dam in 1934.

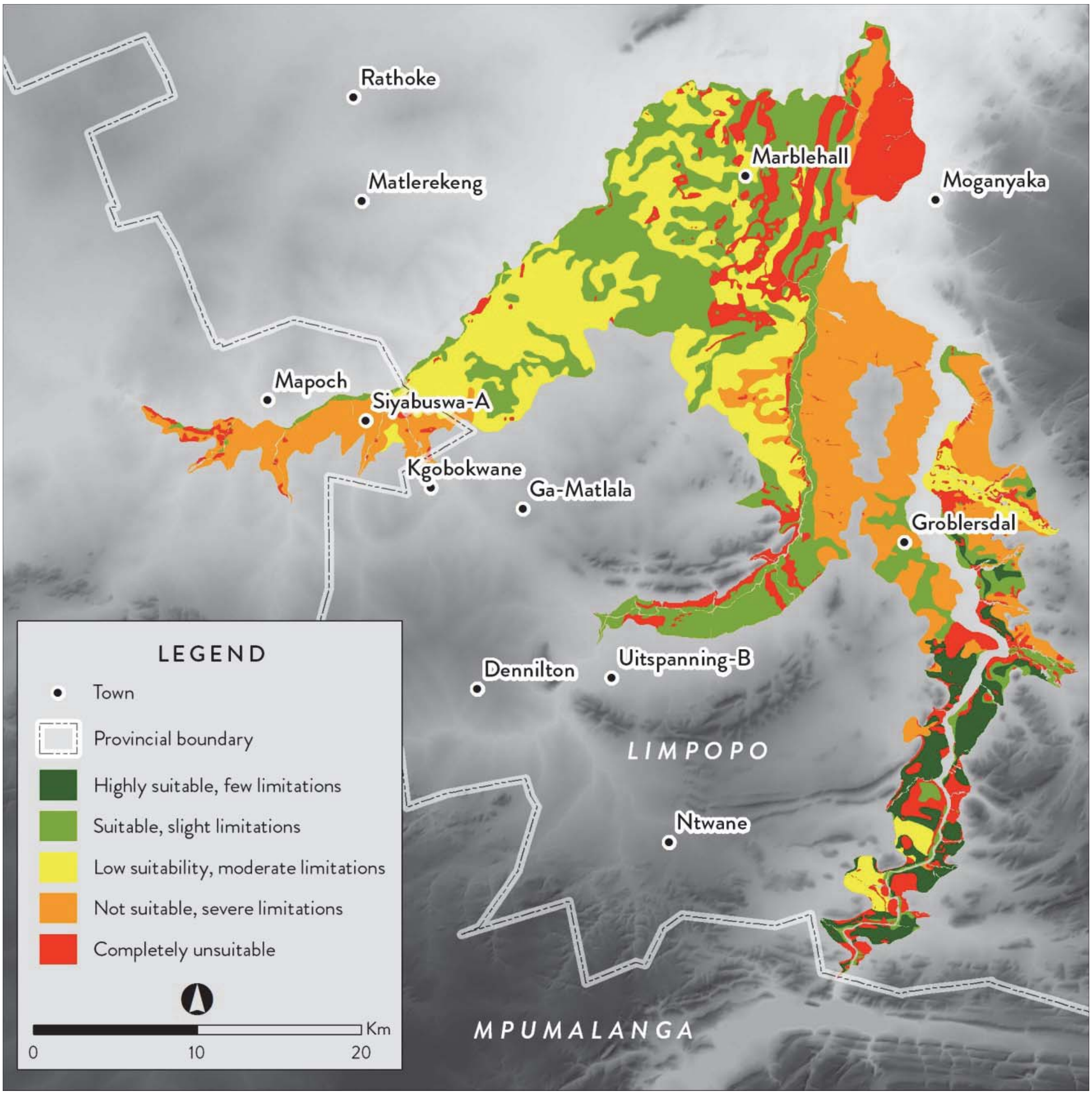

Figure 3.4 Soil irrigation potential at Loskop.

The original soil survey, done on a 1:12 000 scale by Van der Merwe (1934), was used for the planning of the Loskop irrigation scheme and base map for developing the irrigation potential map. Several hundred observations were made and samples were analysed during this soil survey. The majority of the soils in the study area have a clay topsoil content of about 20% and a clay subsoil content of 28%. The effective depth is mostly between 400 and 800 mm. The scheme is characterized by large areas of plinthic soils and other areas of very stony, shallow soil. The southern section of the scheme has the highest irrigation potential, while the north-western section has the lowest irrigation potential. Waterlogging conditions (mostly perched/hanging water tables and natural fluctuating water tables) are common on the scheme. A large number of reports about waterlogging and "salinity" in the Loskop irrigation scheme have been made over the last 70 years which is indicative of the relatively low irrigation potential of the area.

The main crops grown on the Loskop irrigation scheme are citrus, table grapes, maize, wheat, soya bean, cotton, tobacco and groundnuts.

3.5 Makhathini Irrigation Scheme

The Makhathini Flats cover the floodplains on either side of the Pongola River, stretching from just below the Jozini Dam to the confluence of the Pongola and Usuthu River on the Mozambique border (Figure 3.5). The Makhathini Flats cover about 677 800 ha, of which 106 000 ha have relatively high agriculture potential. At present only 3 900 ha are under irrigation, where 276 farmers are settled leasehold on individual plots (Engineering News, 2002).

The main crops planted in the area include sugarcane, maize, cotton and a variety of vegetables.

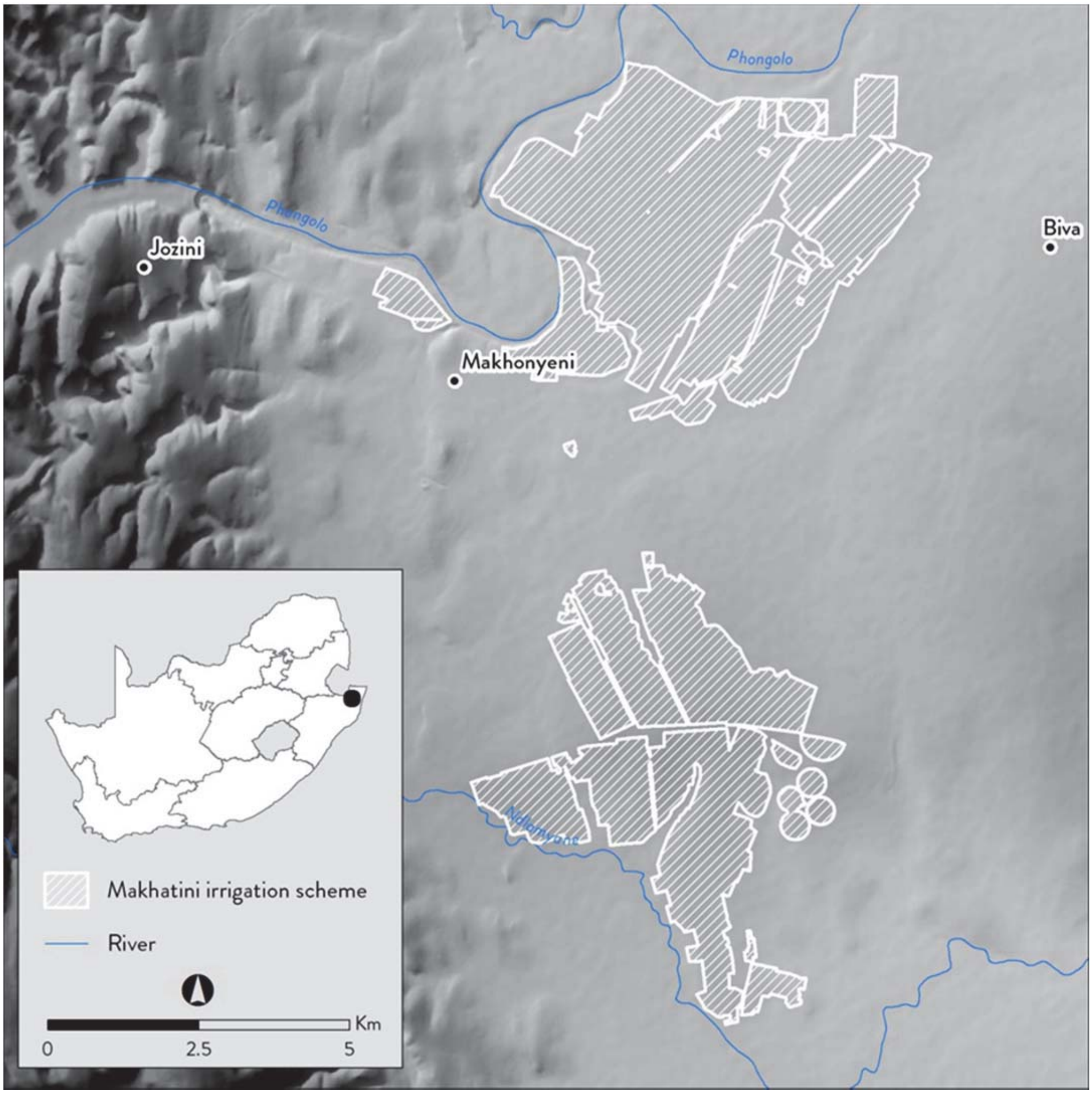

Figure 3.5 Makhathini irrigation scheme.

The majority of the soils on the irrigation scheme are characterized by a relatively high silt and clay content (silt plus clay content between 20 and 45%) (Figure 3.6). The geology of the area is strongly influenced by recent marine deposition and the localized areas that are salt-affected can be directly associated with the geological material.

The high silt plus clay content of the soil has a negative influence on the internal drainage capacity and the infiltration rate of the soils. Temporary perched water tables can be directly associated with the low infiltration and hydraulic conductivity of the soil. Poor project management (poor irrigation equipment and water works maintenance) and irrigation planning in the area are a major cause of localized waterlogging and salt accumulation (Figure 3.7).

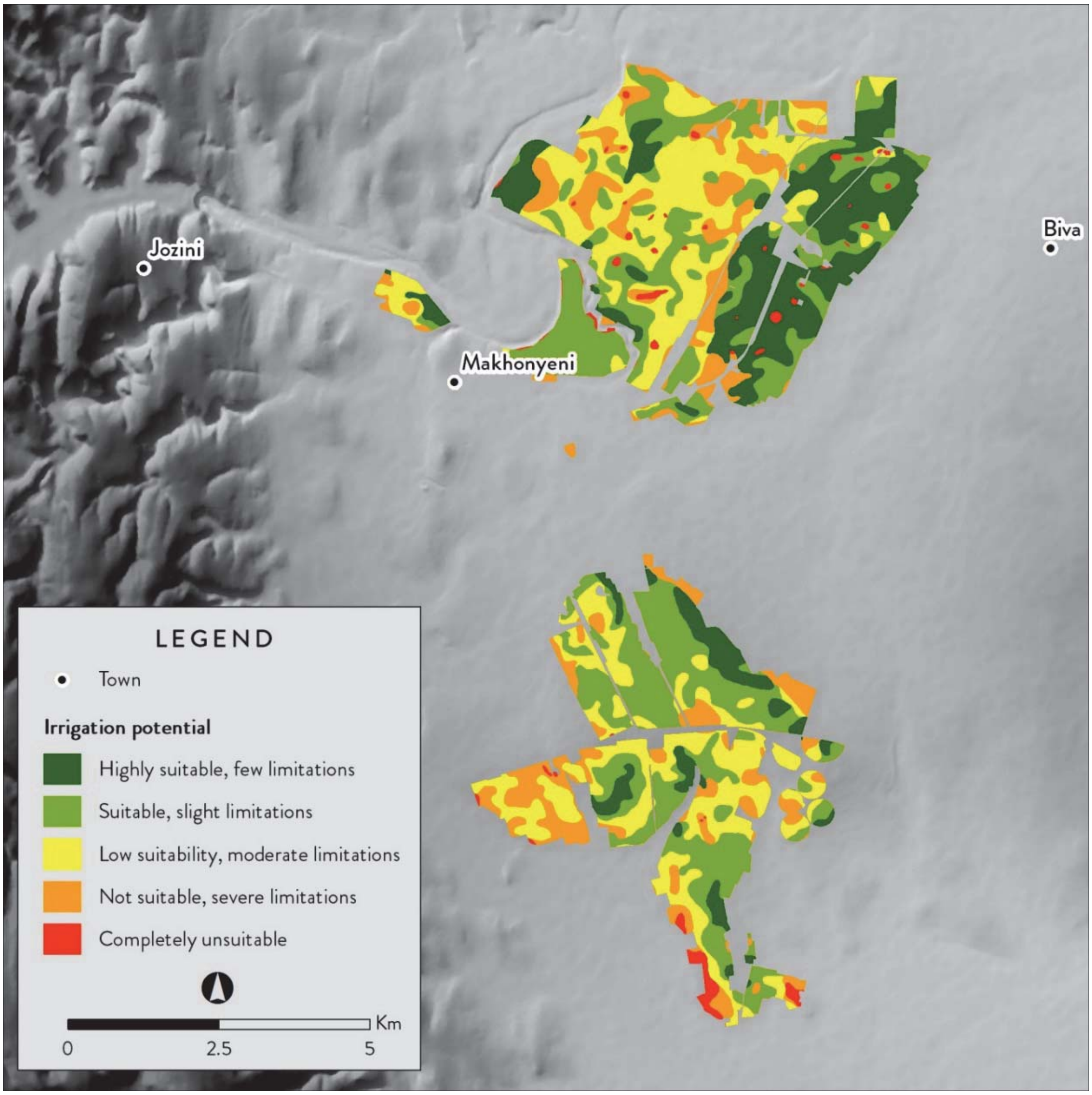

Figure 3.6 Soil irrigation potential at Makhathini.

Figure 3.7 Waterlogged and salt-affected soils on the marine sediments of the Makhathini flats.

3.6 Olifants River Irrigation Scheme

Olifants irrigation scheme (Figure 3.8) was selected because it is the biggest irrigation scheme in the winter rainfall region in South Africa. Economic activity in the Olifants River catchment is concentrated on commercial, irrigated agriculture with approximately 90% of the total water used for irrigated agriculture.

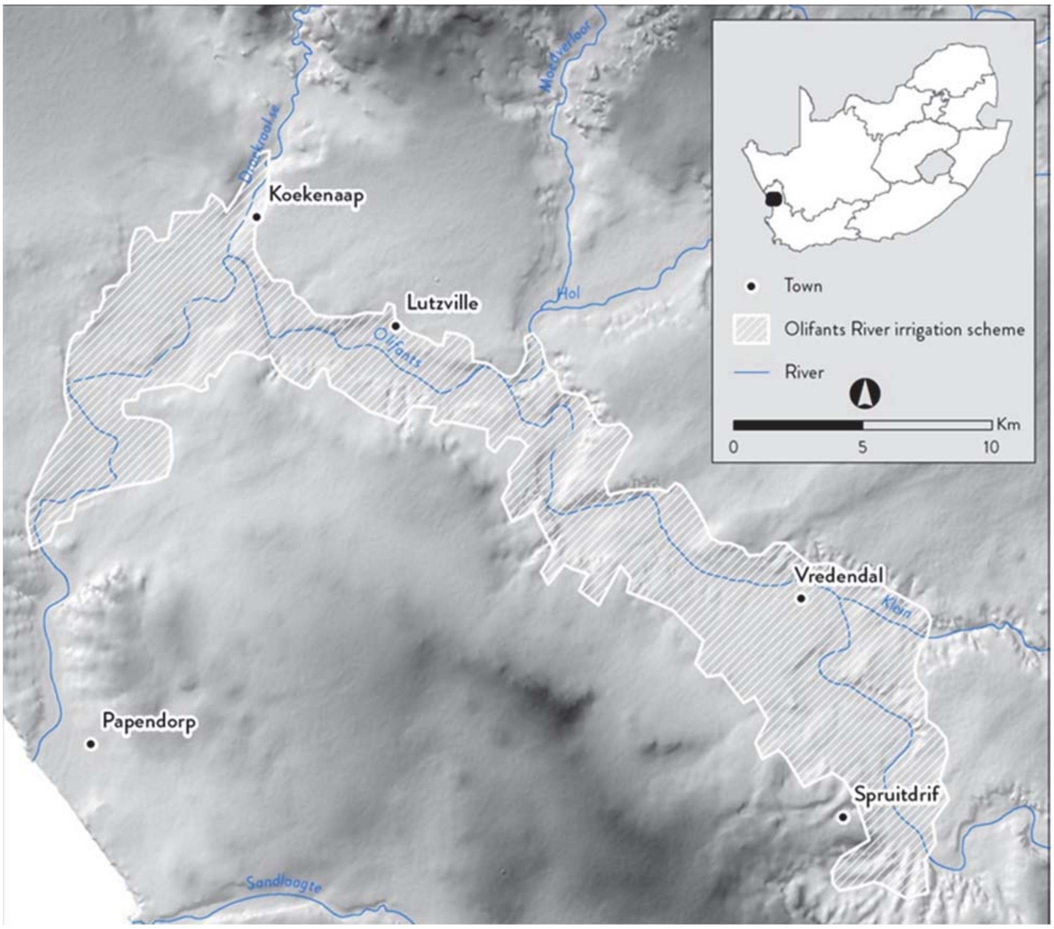

Figure 3.8 Olifants irrigation scheme.

The Olifants irrigation scheme lies along the west coast of South Africa, beside the cold Benguela current of the Atlantic Ocean and is situated near the towns of Klawer, Vredendal, Lutzville and Koekenaap in the Western Cape Province. The Olifants River catchment is the second largest in South Africa, covering over 46 000 km^2. The river originates in the Cederberg mountain range 100 km north of Cape Town and enters the Atlantic Ocean near Strandfontein (Morant, 1984).

The summer months, November to February, are very warm and dry, and are characterized by extremely high evaporation losses. Climate is extreme, with summer temperatures reaching 45°C in the Vredendal/Koekenaap area. According to Rudman *et al.* (1978) the annual rainfall for Lutzville is 127 mm and for Klawer is 218 mm. The study area receives winter rainfall, with almost all the rainfall between May and August. The lowest temperatures in winter are 5-10°C. Frost occurs in winter, but is rare. The highest temperatures in summer are mainly between 25 and 30°C, but it is not unusual to record temperatures above 40°C.

The main storage dam in the catchment area is the Clanwilliam Dam situated on the Olifants River (with a capacity of 127 million m^3) upstream of the town of Clanwilliam. The irrigation scheme is serviced by an open concrete canal system. The main canals stretch over 280 km (60 km for secondary canals). The system operates on a ”just-in-time” basis, using a water demand scheduling system managed by the Lower Olifants River Water User Association.

The majority of the irrigated area is found on alluvium and calcrete of Quaternary age, with soils of the Hutton, Oakleaf, Kimberley, Plooysburg and Gamoep soil forms dominant. Shallower soils are mostly associated with schist and limestone of the Gifberg Formation, Van Rhynsdorp Group. Shallow “dorbank” soils of the Garies form are common in the area, but have a relatively high irrigation potential after deep cultivation (Figure 3.9).

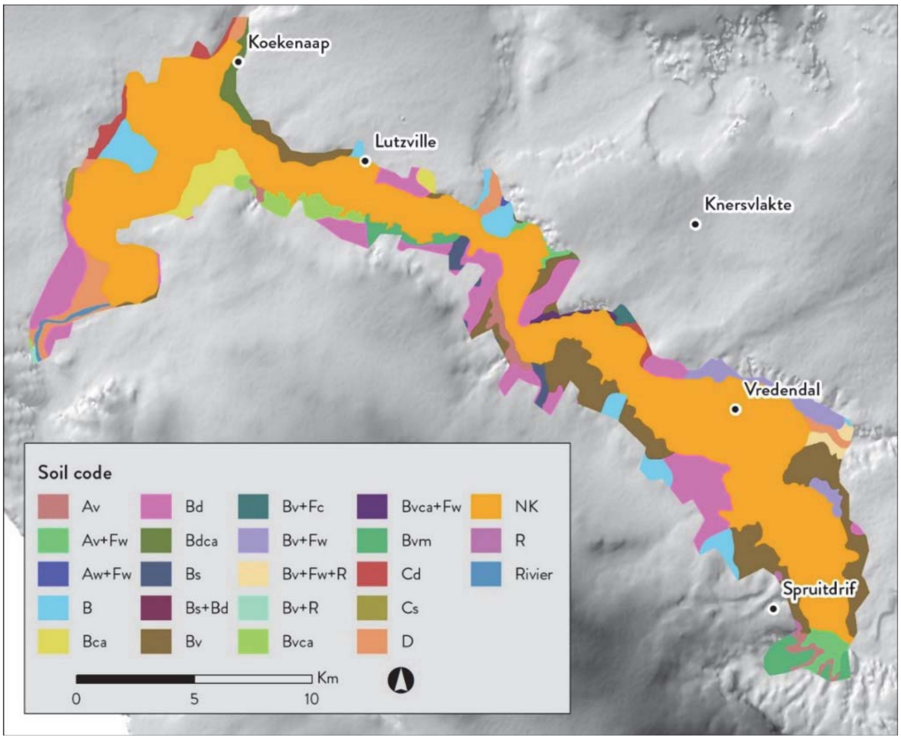

Figure 3.9 Olifants River catchment soil types.

Waterlogging is a bigger problem than salt accumulation in the Olifants River catchment because some of the irrigation plots are located in the flood plain of the river and drainage of the higher lying terraces occurs to the lower terraces (Figures 3.10 and 3.11). The highest concentration of salts is found west of Lutzville. The majority of the salinity, sodicity and alkalinity surveys for the area were done between 1930 and 1950. The use of good quality water of the Olifants River resulted in the leaching of harmful salts that were problematic in the past.

Figure 3.10 Waterlogged and salt-affected soils near Vredendal.

Figure 3.11 Terraces in the Olifants irrigation scheme.

3.7 Tugela River Irrigation Scheme

The Tugela irrigation scheme (Figure 3.12) is characterized by a relatively high rainfall resulting in natural waterled conditions. Irrigation and dryland farming are intertwined. Farmers use water directly from the Thukela, Little Thukela and UMtshezi Rivers or the canals running therefrom. The Little Thukela supplies a canal in which gravity delivers irrigation water for approximately 10 km. Over the last 30 years farming practices have changed from furrow irrigation (<30% water efficient) and overhead sprinkler irrigation (45-55% water efficient) to an almost exclusive use of centre pivot systems (80-85% water efficient).

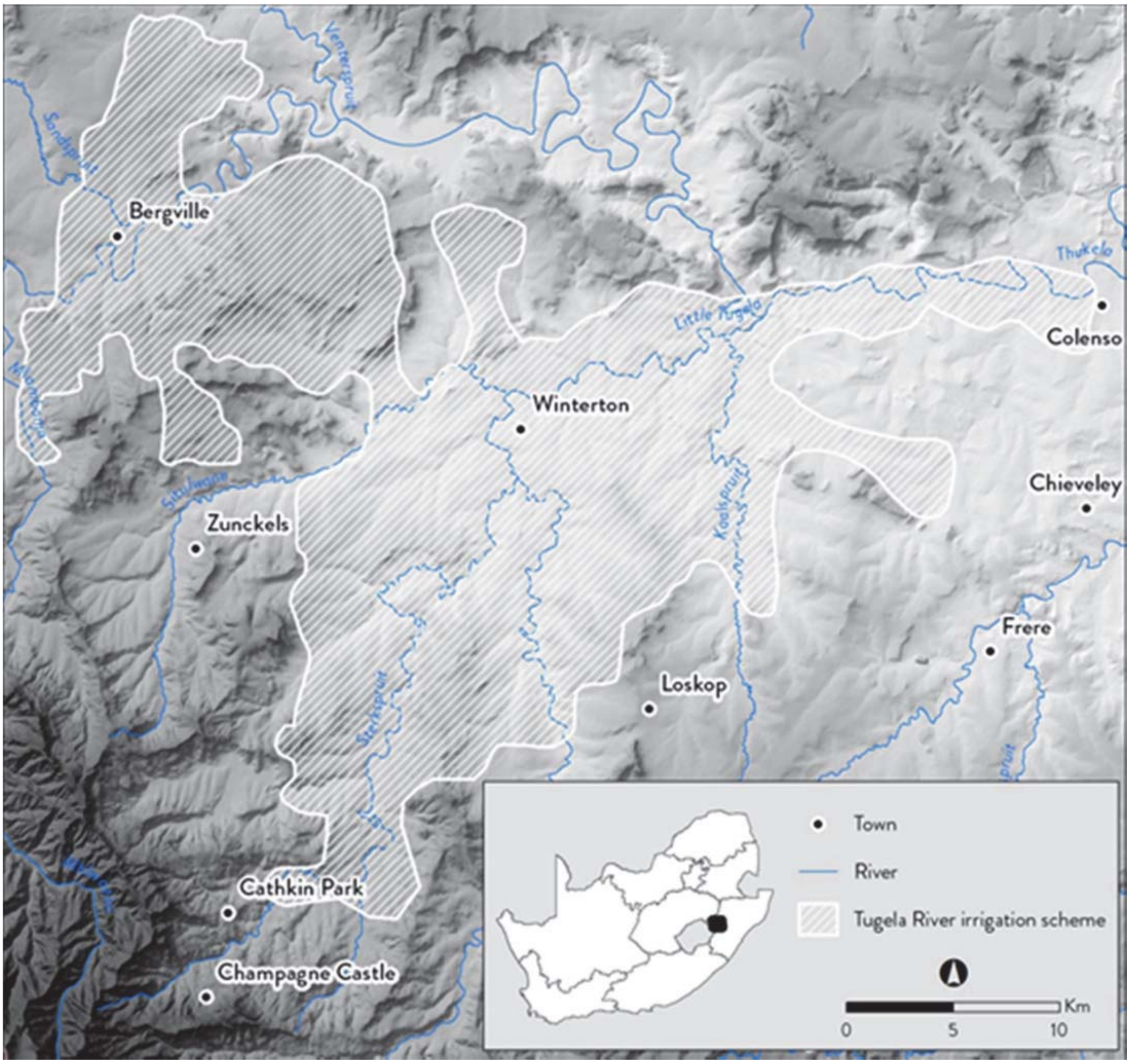

Figure 3.12 Tugela irrigation scheme.

No detailed soil survey is available for the study area. However, the well-known study "Soils of the Tugela Basin" by Van Der Eyck *et al*. (1969), that forms the foundation of the current South African soil classification as done in the area. A large section of the study area falls within land type Ac437 (red-yellow apedal, freely drained soils), with a small south-eastern section in land type Ca115 (Plinthic catena: upland duplex and/or margilitic soils common). The geology of these land types consists mostly of shale, siltstone and mudstone of the Estcourt Formation, and unconsolidated layered sediments of the Masotcheni Formation with small areas of dolerite and alluvial deposits. In land type Ac437 the dominant soil type consists of deep (800-1200 mm) Hutton soils which comprise 37% of the land type. These Hutton soils have 25-35% clay in the A-horizons and 30-50% in the B-horizons, with the texture ranges from clay loam to clay. Various sub-dominant soil forms also occur, including the deep Clovelly soil form (22% of land type with 20-35% clay), shallow Mispah and Glenrosa soil forms (11.6% of land type), deep Dundee and Oakleaf forms (8% of land type) and the medium depth Westleigh and Avalon soil forms (7% of land type). In the south-eastern section of the study area, land type Ca115 consist of numerous soil types of which the dominant form is the medium depth Avalon soil form (24% of land type) with 28-35% clay in the A horizon and 30-50% clay in the B-horizons. These soils have textures ranging from fine sandy clay loam to clay and are characterized by Apedal B-horizons. The sub-dominant soil types are from the medium depth Longlands form (13% of land type), the shallow Westleigh form (11% of land type), soils from a duplex soil association, namely Swartland (6%) and Valsrivier (3%) soil forms, and patches of Estcourt (5%), Clovelly (4%), Cartref (3.5%) and Oakleaf (3%) soil forms (Stronkhorst *et al.*, 2010).

The study area falls within the Moist Tall Grassveld Bioclimatic Region of KwaZulu-Natal or, according to Mucina and Rutherford (2006), in the Northern KwaZulu-Natal Moist Grassland or KwaZulu-Natal Highland Thornveld. The area has an average annual rainfall of 840 mm, ranging between 710 and 1 120 mm. The mean annual temperature is 17 ºC with average maximum and minimum temperatures of 24 and 10 ºC, respectively. Frost is moderate with occasional severe frosts during winter. The study area mainly has summer rainfall during the months of August to May (Stronkhorst *et al.*, 2010). Due to the relatively high rainfall, pastures is mostly only under supplementary irrigation. The relatively high rainfall and low evapotranspiration also result in natural waterlogging conditions in some clayey soils and in the lower lying terrain units.

The geological history of the area has resulted in poor quality, shallow, steep, rocky and highly erodible soils in the south and east. Soils in the central and northern areas are less susceptible, partly because the topography tends to be undulating rather than broken or steep. A large portion of soils in the Winterton and Bergville areas, together with similar soils at Jozini, make up most of the Land Capability Class I soils that constitute only 2% of KZN soils. The irrigation potential of the soils is, however, considerably lower, because of the tendency of the soils to have shallow water tables.

3.8 Breede River Irrigation Scheme

The Breede River irrigation scheme is one of South Africa's primary vine and deciduous fruit growing areas. The greater portion of the irrigated lands, is situated in the middle part of the Breede River Valley between Worcester and Bonnievale (Figure 3.13).

Irrigation in the valley began in the 18th century. As the valley lies in the winter rainfall region, most of the runoff occurs during the winter months, while water is mainly needed during the irrigation season between October and April. The Brandvlei Dam was built in 1922 to supply irrigation water for the middle part of the Breede River Valley. When the demand increased, the walls of the Brandvlei and Kwaggaskloof Dams were raised in 1983 to combine the two dams into the Greater Brandvlei Dam with full supply level capacities of 303.8 x 10^6 m^3 and 170.9 x 10^6 m^3 respectively, i.e. a total of 474.7 x 10^6 m^3 (Kirchner, 1995).

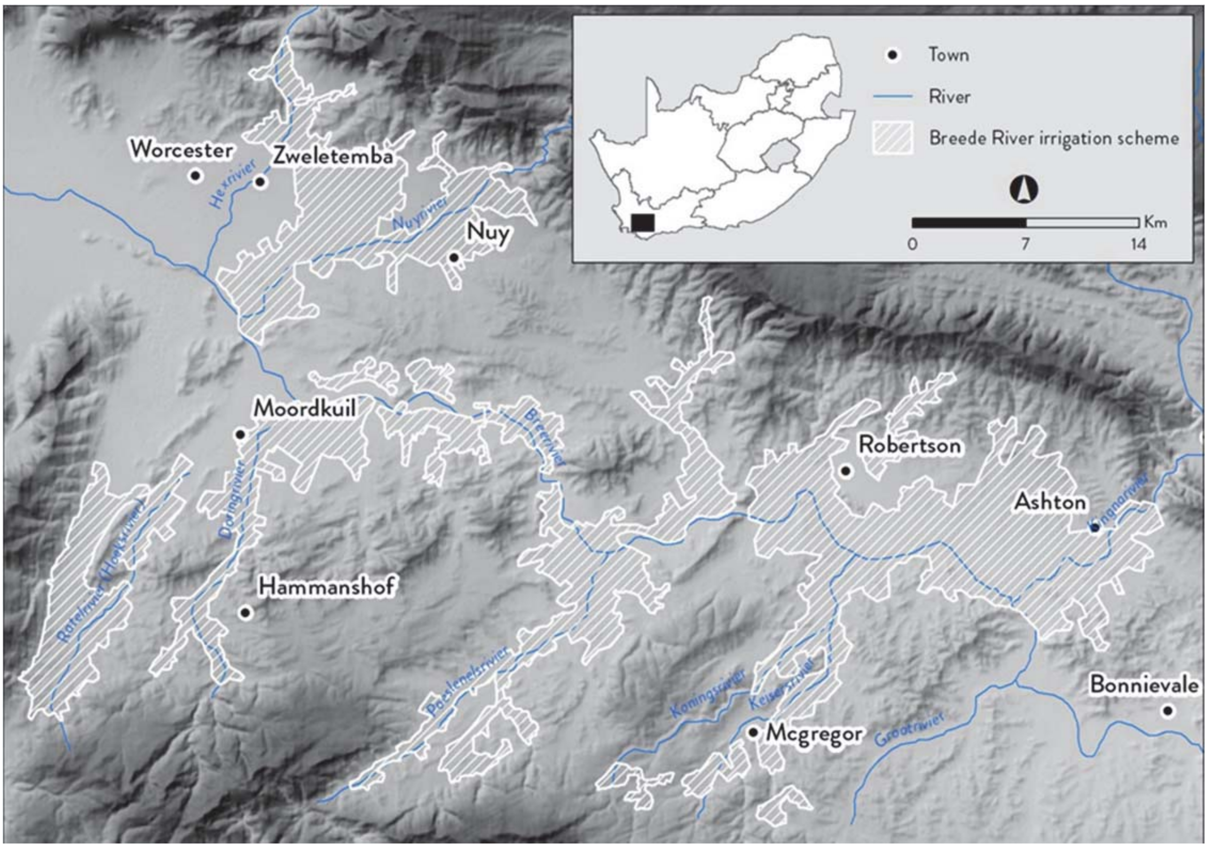

Figure 3.13 Breede River irrigation scheme.

The Breede River originates in the Ceres Valley, approximately 100 km north-west of Cape Town, and flows in a south-easterly direction where it reaches the Indian Ocean after 320 km at Witsand. The middle part of the valley lies between the Riviersonderend Mountains in the south and the Langeberg Mountains in the north. The mean annual rainfall measured in the area between 1966 and 1986 was 273 mm, while the A-pan evaporation reached about 1790 mm per year (Kirchner, 1995).

During the last 30 years, various research projects dealt with different aspects of and factors possibly contributing to the growing salt load in the river. The Water Research Commission took a very active role in the co-ordination and funding of these projects which aimed at the better understanding and quantification of the salinization processes in the Breede River (Bertram, 1989; Bester *et al.,* 1990; Flugel, 1989a, 1989b; Greeff, 1989, 1990, 1991; Jolly, 1990; Kienzle, 1988, 1989; Kienzle *et al.,* 1990; Moolman & Weber, 1979; Moolman, 1982; Moolman *et al.,* 1983; Ninham Shand, 1985). Zietsman *et al.* (1996) also did a study on the identification of irrigated land by means of satellite remote sensing in the Breede River valley.

According to Lambrechts (1979), soils of the Hutton 22, Clovelly 22, Constantia 12, La Motte 12 and Champagne 10 developed on quartzitic fold mountain ranges in the area. On pediments and valley floors the soils consist of: Clovelly 21/22, Constantia 11/12, La Motte 11/12, Fernwood 32 and Champagne 11. In contrast, Glenrosa, Swartland, Sterkspruit, Estcourt and Kroonstad are likely on heavy-textured or duplex soils derived from granites and shales in the area (Figure 3.14). Alongside the Breede River some irrigation also occurs on Dundee, Oakleaf and Fernwood soils.

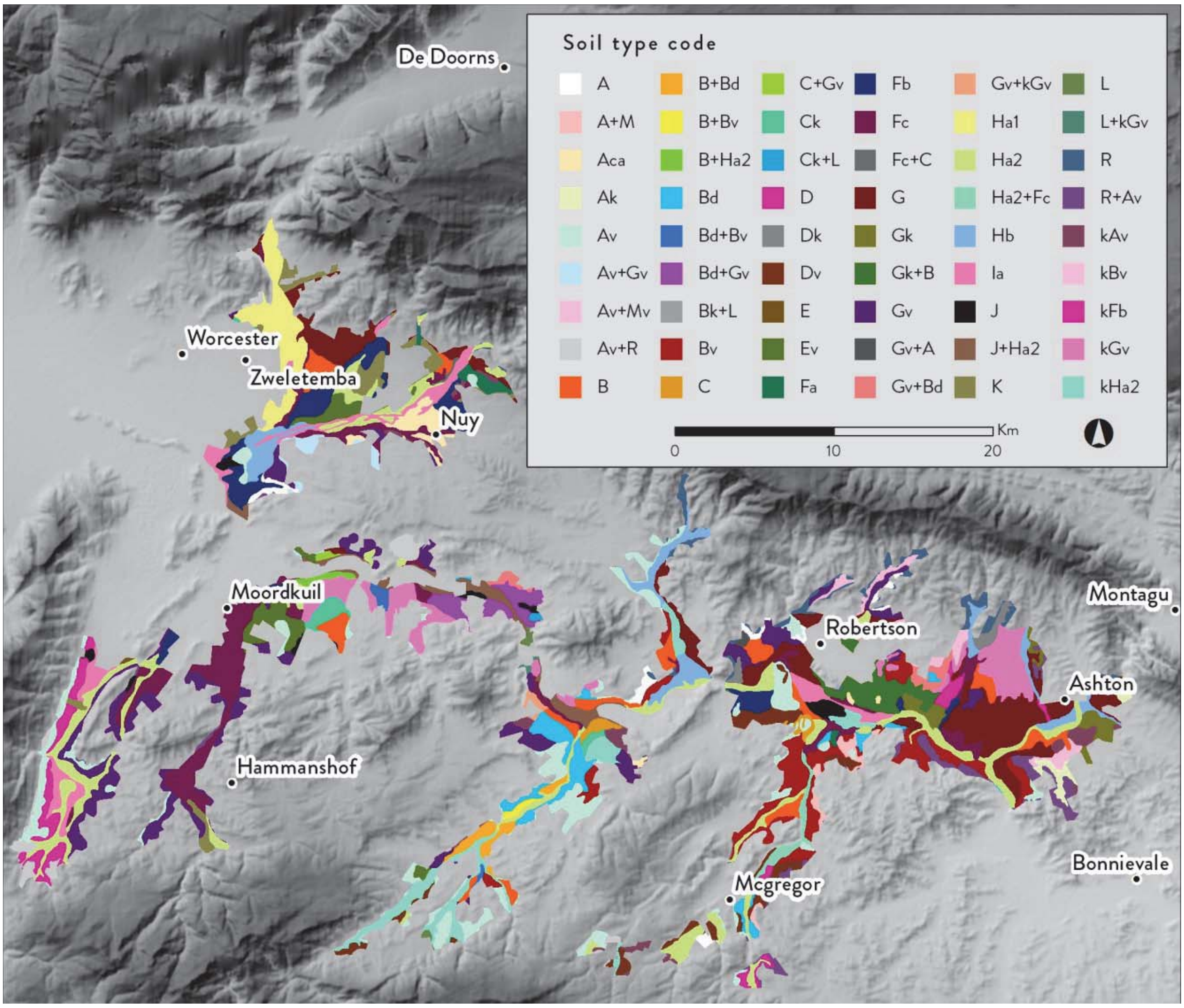

Figure 3.14 Breede River soil types.

Groundwater encountered in some of the formations adjacent to the Breede River upstream of the Zanddrift and the Angora Canal off-takes is brackish or saline. One of the factors influencing the salinity of the water in the Breede River might therefore be a contribution from these formations (Bertram, 1989). Groundwater is encountered in rocks of all geological ages. With the exception of the alluvium, all aquifers are secondary aquifers, i.e., the groundwater moves primarily along faults, fractures and joints. Table Mountain Sandstone (TMS) which forms the mountain ranges is an important, if not the most important aquifer in the area. Because it consists of pure, fractured sandstone, TMS water has a low salt concentration and the aquifer has a comparatively high transmissivity. Where it is overlain by less permeable formations, it becomes confined and water may drain along joints, fractures and faults into overlying aquifers (Kirchner, 1995).

Figure 3.15 Visual evidence of secondary salt accumulation due to waterlogging in the Breede River valley.

3.9 Sundays River Irrigation Scheme

To secure water supply to the Sundays River Valley, water from the Orange River Project was linked to Darlington Dam in 1978. This water dilutes the salinated water from the Sundays River and therefore presents an immediate benefit by improving the water quality for citrus farming in the lower Sundays River Valley. Approximately 25% of South Africa's navel oranges and 50% of the country's lemons are produced in the Sunday's River valley. The area under irrigation is about 17 000 ha.

The Sundays River irrigation area (Figure 3.16) has been subject to the problems of salinization and waterlogging of the soil under irrigation from as early as 1930 (Hartmann & Nell, 1993). As far back as 1927 farm mismanagement was blamed for impaired drainage and declining soil quality (Shone, 1976). In 1981 the problems of chlorosis, defoliation, die-back, unseasonal fruit set, root disease, varying yields and quality deterioration among others led to an attempt to establish the causal factors. Physical characteristics of the soil were identified as responsible for poor soil drainage. Management practices such as orchard traffic and extensive levelling increase soil compaction, and heavy irrigations then exacerbate the problem and retard gas exchange. These conditions need light frequent irrigation applications, and hence a finer resolution of control over the amount and timing of water applied.

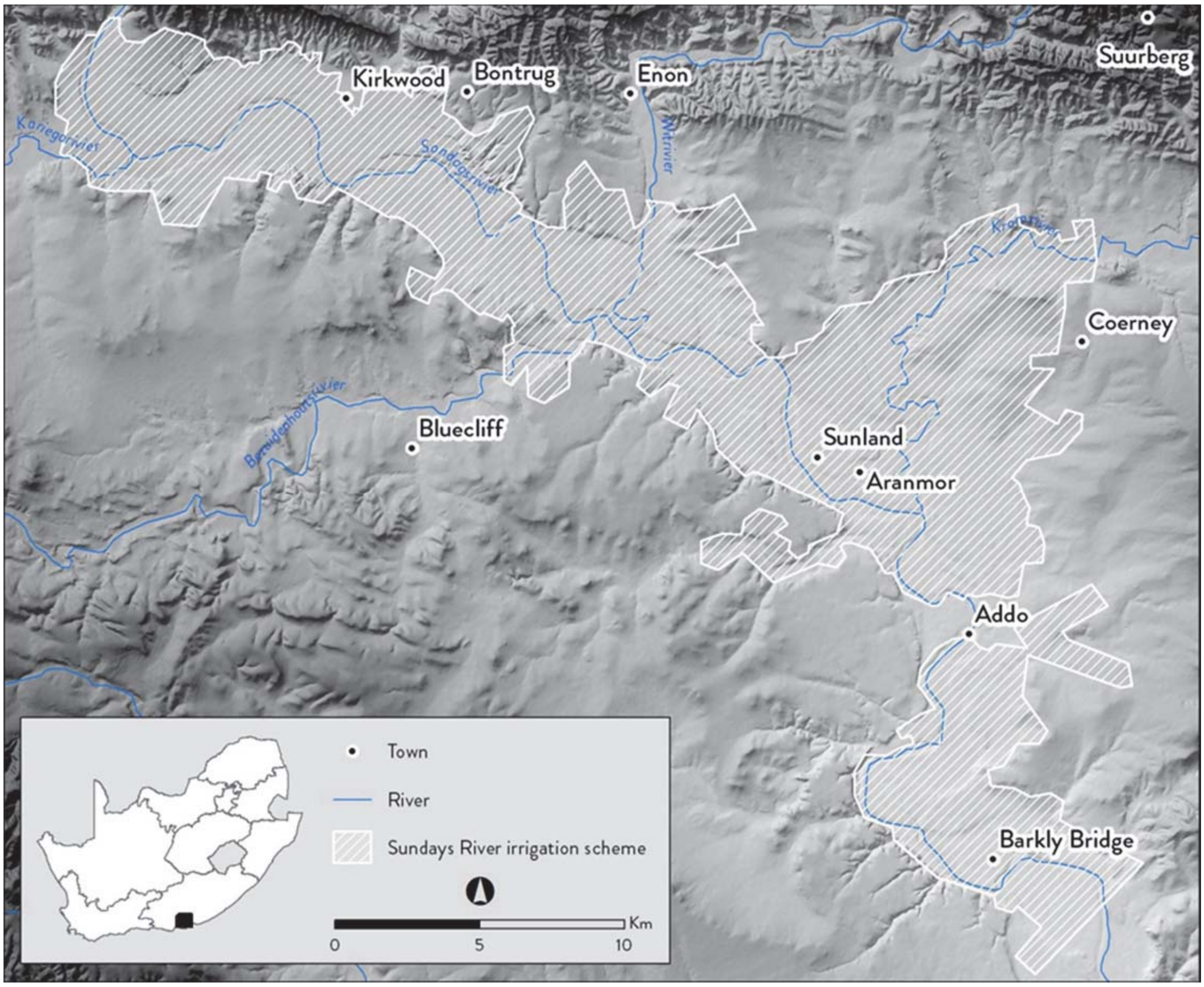

Figure 3.16 Sundays River irrigation scheme.

The soils in the Sundays River Valley are generally calcareous, being derived from transported materials and limestone. Weathering and soil formation appears largely to be *in situ* with slight influence of locally transported material on the steeper slopes (Figure 3.17). Soils are divided predominantly in two series of alluvial terraces: lower terraces in close proximately to the Sundays River and upper higher level terraces situated further away from the river. The lower terrace soils are typically composed of deep, well drained, apedal to weakly structured loamy sands to sandy loams. The upper terrace soils are typically composed of shallow loamy sands overlying weakly to strongly structured sandy clay to sandy clay loams. The strongly structured soils typically exhibit signs of restricted internal drainage (Van der Merwe *et al.,* 1989). They have been classified mainly in the Valsrivier soil form (Nell & Childs, 1992; Nell, 1993a, 1993b).

The morphology of the Sundays River Valley area has been determined by the tectonic and drainage history of the region, which has resulted in a series of terraces developing in the Cretaceous rocks and river alluvium. Different terraces have been recognised, each consisting of an alluvial deposit overlying a boulder bed, which is thought to represent a former stream channel subsequently infilled by finer alluvium as the river migrated laterally (Ruddock, 1947).

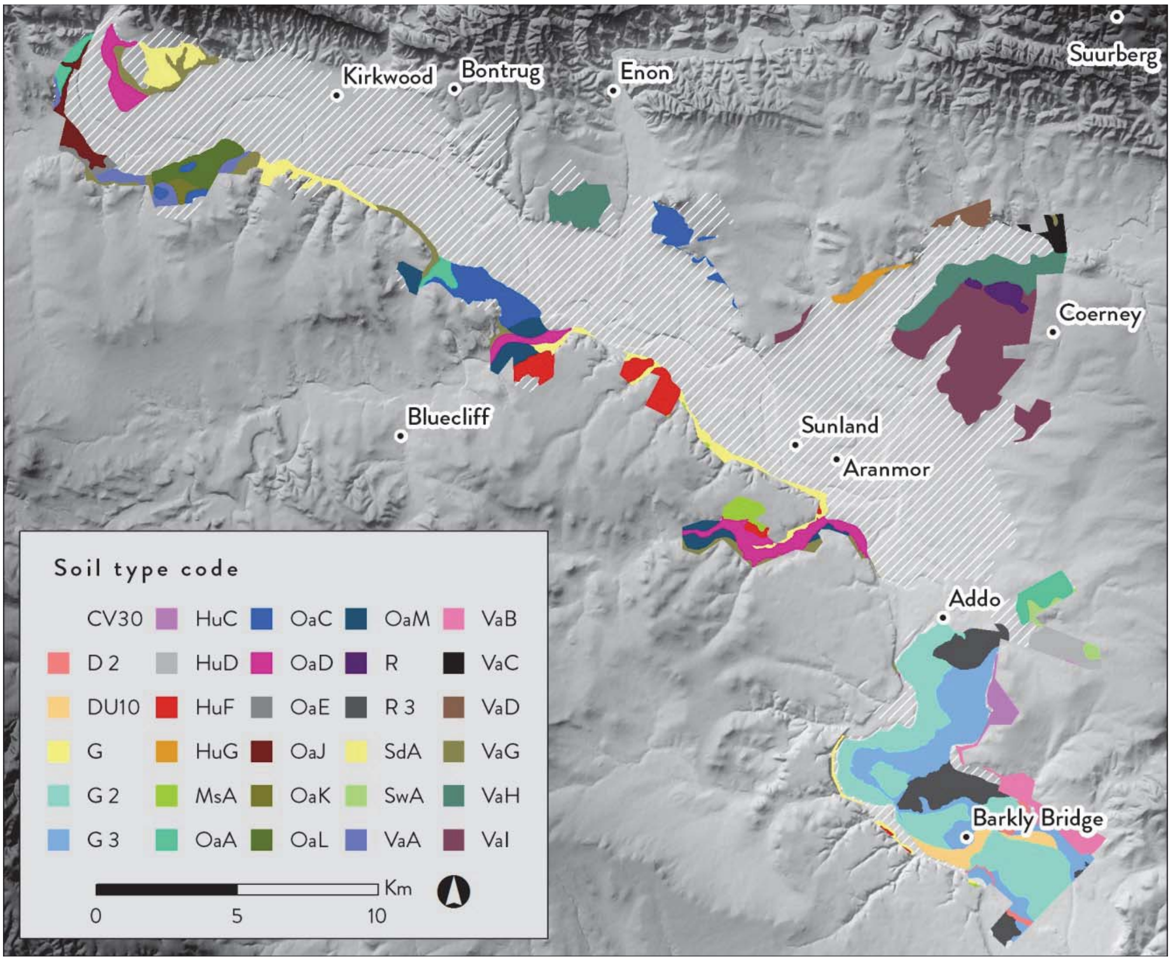

Figure 3.17 Sundays River soil types.

The Sundays River area falls within the transitional belt between the spring and winter rainfall maxima that exist to the north and south of the area, respectively (Stone, 1988). Consequently, rainfall occurs fairly evenly throughout the year, with slight maxima in spring and autumn. Average annual rainfall is between 300 and 400 mm, although extreme values ranging from 162 to 735 mm have been recorded (Schulze, 1965). Mean maximum daily temperatures range from 26°C in January to 19°C in July, and minima range from 15°C in January to 7°C in July. Extreme temperatures range from -4°C in winter to 42°C in summer (Schulze, 1965). Moisture loss through evaporation is high in the valley, with a mean monthly pan evaporation of 118 mm (Pearce, 1987).

Figure 3.18 Visual evidence of salt accumulation and waterlogging in the Sundays River irrigation scheme.

3.10 Limpopo River Irrigation Scheme

The Limpopo River irrigation scheme is located in the Limpopo Province and covers a total area of 8 538 ha. The study area borders with Zimbabwe and Botswana and is west of Musina and east of Pontdrift (Figure 3.19). The Limpopo Water Management Area is the northern-most water management area in the country and represents part of the South African portion of the Limpopo Basin which is also shared by Botswana, Zimbabwe and Mozambique.

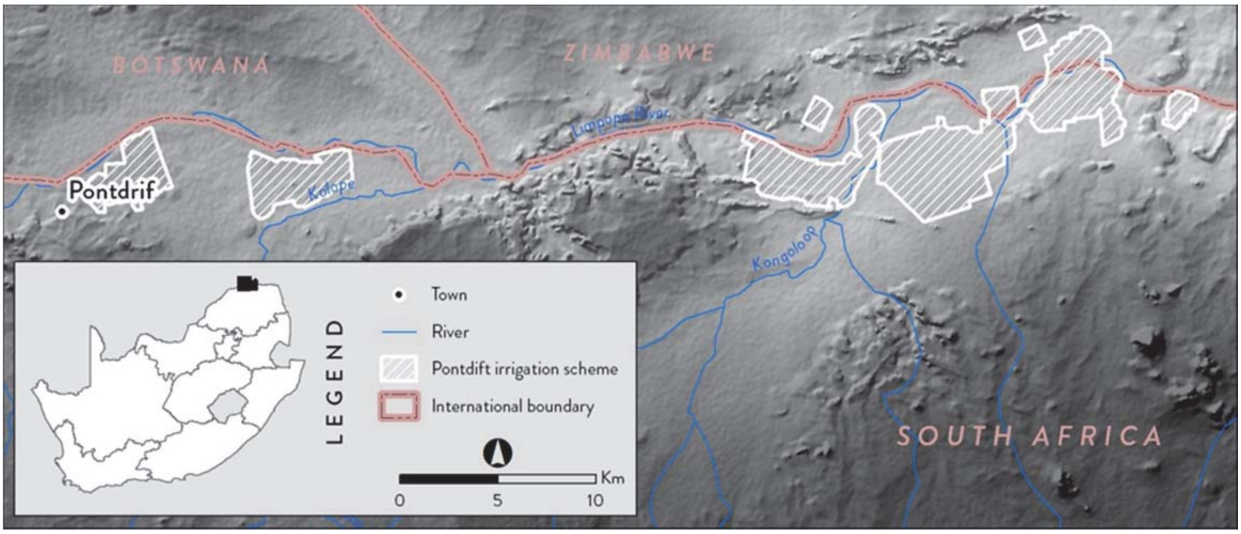

Figure 3.19 Limpopo River irrigation area.

The majority of aquifers in southern Africa are associated with secondary porosity, the Limpopo River Basin features some of the few alluvial aquifers in the region, with subsurface flow of the Limpopo River and some of the tributaries providing groundwater to irrigation farmers, towns and mines along the main stem river during periods of low flow. The groundwater quality in the riverbed of the Limpopo River decrease with depth, with negative consequences, especially during dry periods. According to Nell (1994, 1998) there is an increase in mineralization of the Limpopo River water from Pontdrift (median EC 74 mS/m) to Oosgrens (median EC 137 mS/m). Salinity is especially problematic during the dry months, between August and November. The area is a flat to undulating plain at an altitude of 250-650 m, falling away towards the Limpopo River. Paleo-drainage channels of the Limpopo River are the most prone to waterlogging and salt accumulation, especially in the Pontdrift area (Figure 3.20).

The area is underlain mainly by gneiss and other igneous rocks of the Beit Bridge Complex, with some basalt of the Letaba Formation. The irrigated area are dominated by alluvial deposits of the Quaternary System. According to Botha *et al*. (1988), the soils alongside the river consist of a loamy sand texture and belong to the Vaalrivier Series (Oa33) or Letaba Series (Oa26) of the Oakleaf Form, which is relatively stable. Just outside the floodplain of the river, however, the soil is dominantly duplex (sandy topsoil and clayey subsoil which is prone to erosion) and belongs to the Lindley Series (Va41) of the Valsrivier Form with a sandy clay loam to sandy clay texture. The soils formed from alluvium are moderately deep to deep, dark brown, weakly structured, mainly calcareous, sandy clays and clays. The gneiss gives rise to shallow or moderately deep non-saline soils, mainly reddish-brown apedal, eutrophic to calcareous sandy loams with zones of lithosols.

Figure 3.20 Waterlogging and salt precipitation in paleo drainage channels of the Limpopo River.

3.11 Vaal and Orange Rivers Irrigation Schemes near Douglas

The Douglas Irrigation Scheme is located in the Northern Cape Province, about 100 km south-west of Kimberley. It covers a total area of 30 869 ha (Figure 3.21).

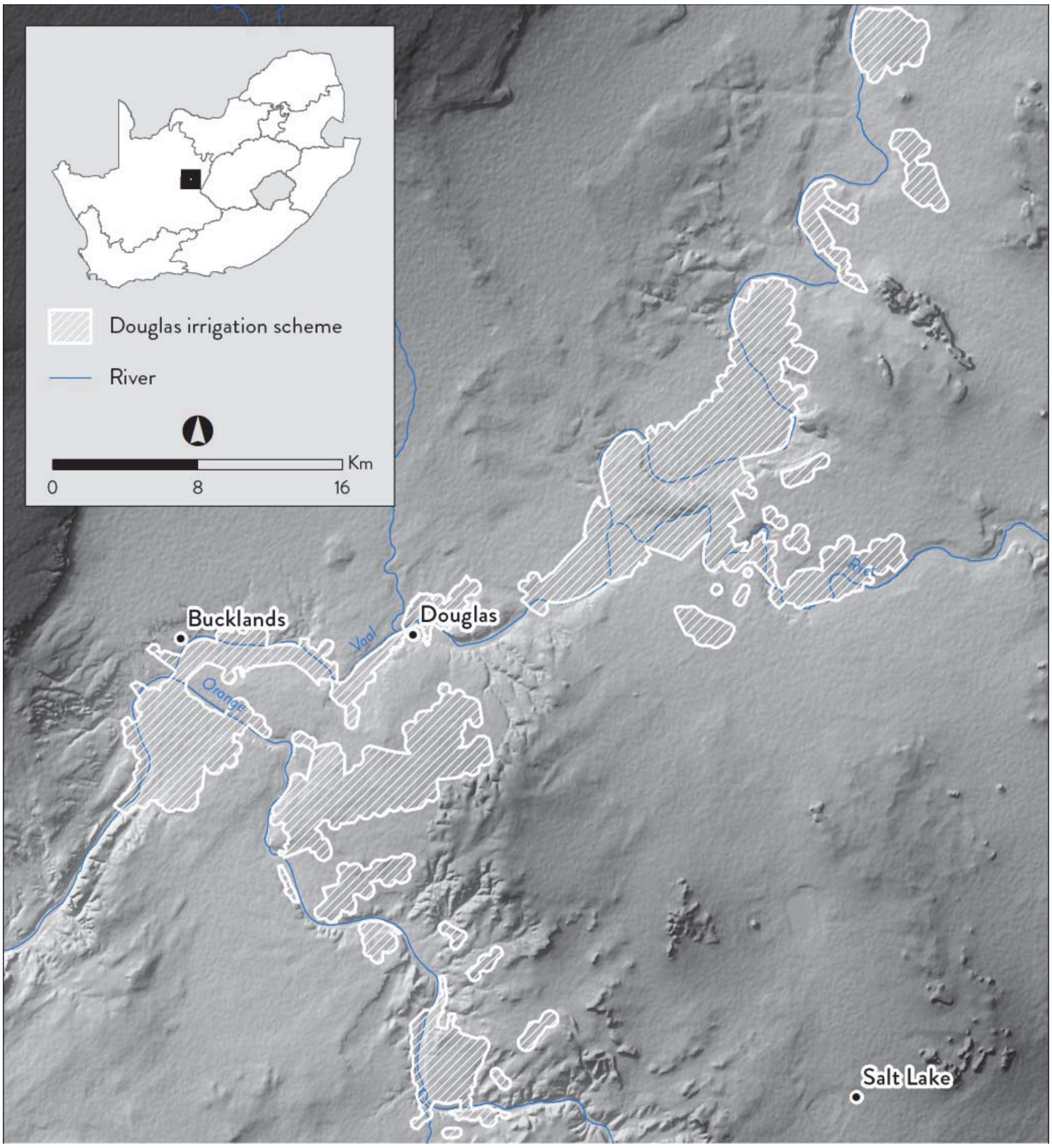

Figure 3.21 Vaal and Orange Rivers irrigation areas near Douglas.

The Douglas Weir on the lower Vaal River and the Orange-Riet Irrigation Scheme on the Riet River were built by the Department of Water Affairs specifically to provide irrigation water to farmers along the lower Vaal River and the Riet River downstream of Jacobsdal. However, farmers in the area have complained that the high salt content of the irrigation water is leading to yield losses and a gradual salinization of the soils. At present, both irrigation schemes are operated to be conservative with water, and only sufficient water is supplied to meet irrigation demands. This means that they are operated as closed systems and salts tend to accumulate in some parts of these schemes. As a result, high salinities are recorded in these areas.

The Douglas Weir together with the Louis Bosman Canal, and the old Orange-Riet Government Water Scheme together with the Orange-Riet Canal, are the two main water transfer and storage schemes in operation in the study area. Both these schemes involve the pumping of Orange River water into canals and the transfer of this water to irrigators along the Vaal and Riet Rivers, respectively (Moolman & Quibell, 1995).

According to Armour (2002), 28% of the area is flood irrigated and 70% is sprinkler irrigated. The trend is towards conversion to centre pivot irrigation, which is a potential problem as it is difficult to leach for salinity management with centre pivot irrigation systems. In other areas where salinity is a problem, flood irrigation on laser-levelled lands seems to be the most efficient and effective. Most of the vineyards in the study region, which predominantly occur in Bucklands and Atherton, are irrigated with micro and drip irrigation systems. The larger farms which occur in Olierivier, Vaallus and New Bucklands predominantly have centre pivot irrigation systems.

According to Nell (1995), 54% of the entire area under irrigation is situated on high irrigation potential (class 1) soils, whilst 12% is on medium (class 2) soils and 34% on poor (class 3) soils. However, these soils are not evenly distributed throughout the system. The Riet River Settlement is dominated by good soils (81%) while the soils along the Riet River are of mostly poorly (47%) and moderately (30%) suited for irrigation. Irrigation along the Riet River Arm is situated on predominantly medium (53%) and some poor soils (4%), while as much as 72% of the Bucklands and Atherton section is on poor soils. Although only 43% of the farms along the Douglas Weir Basin are irrigating poor and medium soils, two-thirds of the Vaallus estates are situated on poorly suited for irrigation soils.

Figure 3.22 Ponding in wheel rut on problematic duplex soils (Douglas).

According to Moolman & Quibell (1995), water from the Orange River entering the Riet River and the Douglas Weir via the Orange-Riet and Louis Bosman canals is dominated by calcium and carbonate (CO_3) ions, while the industrial and mining effluents from higher upstream in the Vaal River produce water dominated by the sulphate (SO_4) ion. When the water is used for irrigation, the calcium and carbonate ions tend accumulate in the soil. However, the sodium and chloride ions are more mobile and are thus, typically, the most common ions in irrigation return flows. As a result of this the water in the Riet River becomes increasingly sodium chloride (NaCl) dominated downstream, as the volume of return flows becomes larger. Boron concentrations in the irrigation return flows are high, being highest in the lower reaches of the Riet River and in the region of Vaallus. Ninham Shand (1985) estimated that 512 ha out of 1 200 ha near Douglas were waterlogged.

4 REFERENCE DATA COLLECTION

4.1 Methodological Framework

Due to the costs involved in soil sampling and analysis, the only viable option for monitoring waterlogging and salt accumulation over large areas (i.e. irrigation scheme level) is to use existing soil maps (where available), terrain data and satellite imagery to identify areas where these processes are likely (or unlikely) to occur. By combining various sources of data and a priori knowledge, large areas can be eliminated from further consideration and specific areas can be highlighted as being potentially affected.

An experimental approach was taken in developing a suitable methodology for quantifying and monitoring waterlogging and salt accumulation. Various sources of data and techniques were applied and compared to empirical (reference) data to determine their potential for monitoring waterlogging and salt accumulation (Chapter 6). The techniques were applied within three main strategies (Figure 4.1).

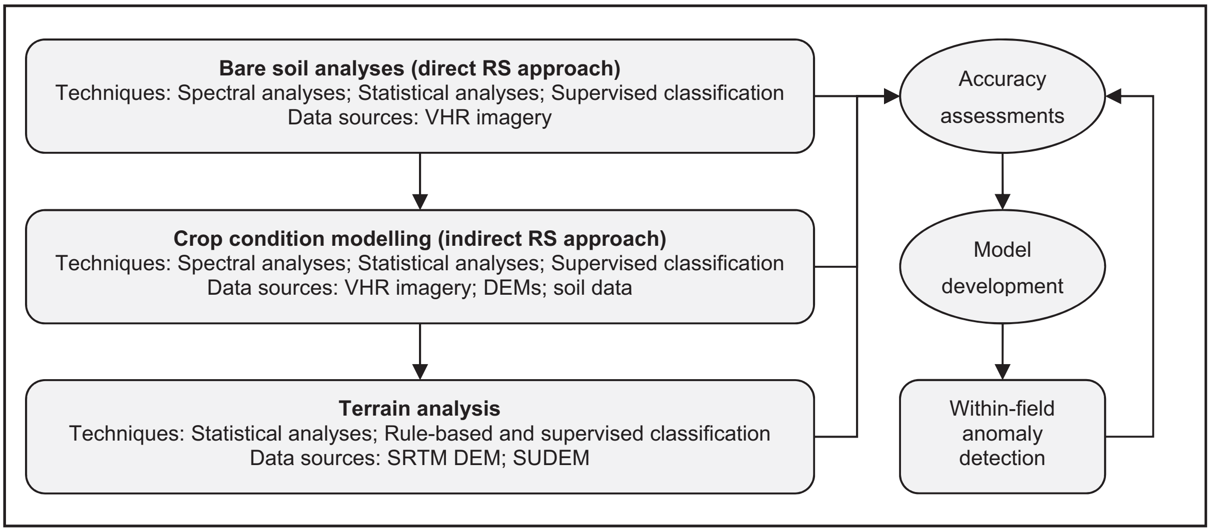

Figure 4.1 Model development strategy

The first approach attempted to use remote sensing to directly detect salt accumulation by studying the spectral characteristics of soils that are salt-affected. A satellite image with a very high spatial and spectral resolution was used for this experiment to reduce the influence of image resolution on the spectral, statistical and image classification techniques that were evaluated. The main aim of these experiments was to investigate the relationships between known affected areas (as determined using EC measurements) and a range of image features (bands and indices), with the purpose of determining whether these relationships can be used to accurately predict the spatial distribution of salt accumulation

The second component of the methodological framework was to evaluate whether an indirect remote sensing approach can effectively be used to monitor salinity levels. In this approach vegetation response to saline conditions was investigated. Two different data sources were evaluated at two different scales (field and scheme). The first series of experiments made use of a very high resolution (0.5 m) WorldView-2 satellite image to detect changes in vegetation response to saline conditions within a single (lucerne) field (section 5.2). The influence of image resolution was also examined. The second series of experiments made use of high (2.5 m) resolution SPOT-5 images. These experiments were carried out on a variety of crops in two dissimilar irrigation schemes (Vaalharts and Breede River), mainly to determine to what extent statistical and classification techniques are influenced by large variations in how different types of crops respond to saline conditions (section 5.3).

The final set of experiments focussed on investigating the relationships between terrain data and waterlogging and salt accumulation in the Vaalharts and the Breede River study areas (section 5.4). A series of statistical analyses were carried out to find the continuous relationships between a large set of terrain features derived from three different DEMs. Machine learning algorithms were also employed to model waterlogging and salt accumulation.

Each experiment was assessed in terms of its accuracy and in the context of finding an operational solution to quantifying and monitoring waterlogging and salt accumulation at field, farm and irrigation scheme level at national scale. The techniques and data sources that showed potential were considered for incorporation in an operational solution. Some techniques were excluded from investigation based on the outcomes of the experiments.

Initially the principle of "conversion of evidence" was used for developing an operational solution. This strategy assumes that if a particular area is identified as being susceptible for salt accumulation by more than one of the model components, then that area will receive a higher overall susceptibility score than an area for which only one (or none) of the components registered a likelihood of waterlogging and salt accumulation. This is a common geographical information system (GIS) and multi-criteria decision making (MCDM) approach to spatial analysis. However, during the course of the study it became clear that this strategy is only sensible if the output of each component is of acceptable quality, as errors can easily be propagated. Also, the effort and cost of using multiple data sources and applying multiple approaches and techniques over large areas also needed to be taken into consideration in designing an operational solution. The "conversion of evidence" strategy was consequently abandoned in favour of a method that makes use of a single data source that is available at national level and that combines direct and indirect remote sensing methods. The resulting method, called within-field anomaly detection (WFAD), is discussed in detail in Chapter 6.

4.2 Field survey

Three field surveys were carried out to collect suitable reference data (ground truth) in the Vaalharts Irrigation Scheme (5th and the 8th June 2012; 12th and the 14th September 2012; and 2nd and the 5th April 2013), two field surveys were carried out in the Loskop Irrigation Scheme (9-11 January 2013; and 25-28 February 2013). The Olifants River Irrigation Scheme near Vredendal was visited between the 5th and the 8th June 2013; Tugela Irrigation Scheme between Bergville and Winterton between 5th and 8th August 2013; Breede River Irrigation Scheme between Worcester and Robertson between the 21st and 25th January 2014; Sundays River Irrigation Scheme between Addo and Kirkwood between the 14th and 19th January 2014; Limpopo River Irrigation Scheme between Mussina and Pontdrift between 30th July and the 4th August 2014; Makhathini Irrigation Scheme between the 16th

and 18th January 2013 and again between the 6th and 9th March 2013; and the Vaal and Orange River Irrigation Scheme near Douglas between the 6th and 9th August 2014.

The survey was conducted using a hand auger to a depth of 1.2 m, or shallower if a restricting layer such as rock was encountered to determine the depth and watertable depth The soil was considered as waterlogged if the water table was shallower than 1.2 m. The position of the observation and verification points was determined by GPS.

4.3 Laboratory analyses

Soil samples were analysed in the laboratories of the ARC-ISCW and Nvirotek according to methods described by the Non-Affiliated Soil Analysis Work Committee (1991). A saturation extract was prepared and the values for electrical conductivity (EC_e), Na, Ca, Mg, (SAR) were determined. The soil was considered as saline if the EC_e was higher than 400 mS/m. About 900 samples were analysed (Appendix B to Appendix G).

5 EXPERIMENTS TOWARDS AN OPERATIONAL SOLUTION FOR MONITORING SALT ACCUMULATION AND WATERLOGGING

This chapter provides an overview of four series of experiments. The first set of experiments (section 5.1) focuses on the direct method and compares remotely-sensed multispectral imagery of bare soil with *in situ* data (soil analyses) to investigate whether such an approach can be used for operational salt accumulation monitoring in South African irrigation schemes. The next two sets of experiments focus on the indirect remote sensing approach. The first set concentrates on monitoring vegetation responses to saline conditions at field scale (section 5.2), while the second set focuses on the same approach but at scheme level (section 5.3). The fourth and final set of experiments investigates the relationships between affected areas and terrain data (section 5.4).

The chapter concludes with a synthesis in which the strengths and weaknesses of each of the evaluated methods are discussed. Each method is also assessed in terms of its value for operational monitoring of salt accumulation and waterlogging at scheme level. Suggestions on how some of the limitations of the evaluated techniques can be addressed are also made.

5.1 Remote sensing direct approach: Bare soil analyses at sub-scheme level[3]

As explained in Section 2.5.1.2, salt-affected soils have higher reflectance values in the visible and near-infrared (NIR) regions of the electromagnetic spectrum and that salt-affected soils with visible surface salt encrustations are smoother than non-saline surfaces and cause high reflectance in the visible and the NIR regions of the spectrum. The colour and the surface roughness of salt-affected soils influence their spectral properties, but increased moisture, ferric oxides and clay decreases reflectance and makes it difficult to identify salt-affected soils (Metternicht & Zinck, 2003). These findings led to the development of several salinity indices (SIs) calculated from image bands which have been shown to be effective in discriminating saline soils from unaffected soils (Fernandez-Buces et al., 2006; Abbas & Khan, 2007; Abood et al., 2011; Abbas et al., 2013).

Most studies that investigated the use of remote sensing methods for detecting and monitoring salt-affected areas were carried out using medium resolution, multispectral imagery such as those acquired by Landsat (30 m), ASTER (15 m) or SPOT-5 (10 m). A notable exception is Abood *et al*. (2011) who made use of very high resolution (VHR) WorldView-2 imagery for detecting salt-affected soils in Mesopotamia using normalized difference salinity indices (NDSIs) and random forest (RF) supervised classification. The results were very promising and given that salt-accumulation in South Africa usually occurs in small patches, VHR imagery also holds much potential for detecting and delineating such areas.

The aim of this component of the research was to evaluate the use of WorldView-2 (WV2) imagery for mapping salt accumulation in conditions where salt accumulation is relatively moderate. The study expands on the work by Abood *et al*. (2011) by evaluating both

[3]. The content of this section was adapted from the MSc thesis of Divan Vermeulen and an article that was submitted for publication in a scientific journal.

supervised and rule set classification approaches. The rule sets are based on three methods, *viz.* 1) Jeffries-Matusita (JM) distance, 2) regression modelling, and 3) classification and regression trees (CART), while five supervised classification algorithms, *viz.* 1) k-nearest neighbour (kNN), 2) maximum likelihood (ML), 3) support vector machine (SVM), 4) decision tree (DT) and 5) RF are assessed.

5.1.1 Study area and data collection

The analyses were conducted in a 100 km^2 section of the Vaalharts study area (Figure 5.1). A WV2 image, captured on 23 May 2012, was used. The image has a spatial resolution of 0.50 m (0.46 m at nadir) for the panchromatic band and 2 m (1.84 m at nadir) for the multispectral bands (DigitalGlobe, 2015). WV2 was chosen because it offered the highest combination of spatial and spectral resolution at the time. The sensor provides eight multispectral bands, namely coastal blue (CB), blue, green, yellow, red, red edge (RE), near-infrared1 (NIR1) and NIR2 (DigitalGlobe, 2015).

A total of 51 *in situ* soil samples were collected during two field surveys which took place from June to September 2012. A clustered, random sampling scheme was used. Soil samples were collected along transects or in regular grids in six sampling sites (Figure 5.1).

5.1.2 Image pre-processing

Pre-processing refers to those operations that are preliminary to the main analysis and typically includes radiometric calibration, atmospheric correction of the digital numbers, and geometric rectification (Campbell, 2002; Lillesand *et al.*, 2004).

Twelve ground control points (GCPs) collected during the field survey and the 5 m resolution Stellenbosch University digital elevation model (SUDEM) (Van Niekerk, 2012) were used to orthorectify the WV2 image. The ATCOR-2 model was used for radiometric and atmospheric corrections (Richter, 2011). All pre-processing operations were performed by making use of PCI Geomatica 2013 software.

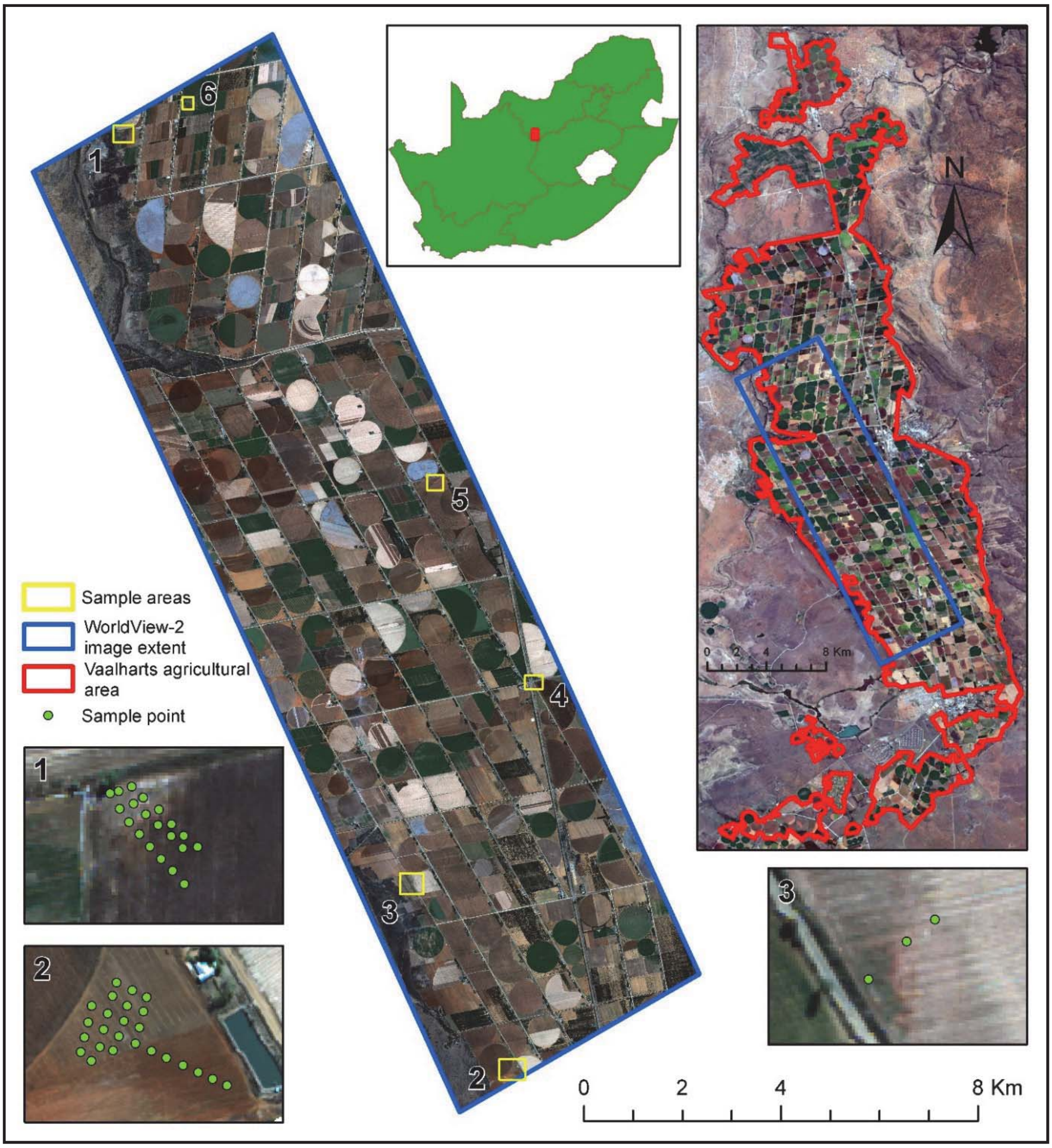

Figure 5.1 Location of the six sample collection sites within the Vaalharts irrigation scheme and WorldView-2 image.

5.1.3 Feature set development

A feature set comprising 68 input variables was considered for differentiating salt-affected from unaffected areas (Table 5.1). All of the WV2 bands and several SIs developed specifically for the direct detection of salt-affected soil (Abbas & Khan, 2007; Abbas *et al.*, 2013; Abood *et al.*, 2011; Fernandez-Buces *et al.*, 2006; Khan *et al.*, 2005; Setia *et al.*, 2013; Sidike *et al.*, 2014) were included in the feature set. They are:

$S_1 = Blue/Red$

$S_2 = (Blue - Red)/(Blue + Red)$

$S_3 = (Green \times Red)/Blue$
$S_4 = \sqrt{Blue \times Red}$
$S_5 = (Blue \times Red)/Green$
$S_6 = (Red \times NIR)/Green$

where S_1 to S_6 are the proposed SIs;
Blue is the blue and CB bands;
Green is the green and yellow bands;
Red is the red and RE bands; and
NIR is the NIR_1 and NIR_2 bands.

In a comparison of SIs, Abbas & Khan (2007) found S_3 to have the highest correlation with observed soil EC, while Abbas *et al*. (2013) found that S_4 provides better results. The normalized difference salinity index (NDSI) has been successfully employed in several studies (Abood *et al*., 2011; Iqbal, 2011; Khan *et al*., 2005). The index uses the red and NIR regions of the spectrum and can be calculated as follows:

$$NDSI = (Red - NIR)/(Red + NIR) \qquad \text{Equation 5.1}$$

Table 5.1 Features considered for the direct analysis

Type		Features	# of features
Spectral features	Mean	CB, blue, green, yellow, red, RE, NIR_1, NIR_2	8
Salinity indices	Mean	S_1, S_2, S_3, S_4, S_5, S_6, $NDSI_1$, $NDSI_2$, $NDSI_3$, $NDSI_4$, $NDSI_5$, $NDSI_6$, $COSRI_1$, $COSRI_2$, $COSRI_3$, $COSRI_4$, $COSRI_5$, $COSRI_6$, $COSRI_7$, $COSRI_8$	14
Salinity indices (S_1, S_2, S_3, S_4, S_5, S_6) modified for WV2 bands	Mean	S1a, S1b, S1c, S1d, S2a, S2b, S2c, S2d, S3a, S3b, S3c, S3d, S4a, S4b, S4c, S4d, S5a, S5b, S5c, S5d, S6a, S6b, S6c, S6d	24
Texture features (3×3; 5×5; 7×7)	GLCM	Contrast, entropy, homogeneity, variance	21
	Histogram	Energy, entropy, variance	
Image transformations	Mean	PCA1	1

Abood *et al.* (2011) proposed several variations of the NDSI based on selected WV2 bands. The six NDSI indices included in our feature set are:
$NDSI_1 = (Yellow - NIR_1)/(Yellow + NIR_1)$
$NDSI_2 = (Yellow - NIR_2)/(Yellow + NIR_2)$
$NDSI_3 = (Red - NIR_1)/(Red + NIR_1)$
$NDSI_4 = (Red - NIR_2)/(Red + NIR_2)$
$NDSI_5 = (RE - NIR_1)/(RE + NIR_1)$
$NDSI_6 = (RE - NIR_2)/RE + NIR_2$
where Yellow is the yellow band;
Red is the red band;
RE is the red-edge (RE) band; and
NIR_1 and NIR_2 are the NIR bands.

Abood *et al.* (2011) found that the high soil reflectance in the visible bands (especially in the yellow band) makes $NDSI_1$ useful in delineating salt-affected soils, but that $NDSI_2$ provided better results due to the relatively low reflectance of wet soils and water in the NIR_2 band. $NDSI_4$ and $NDSI_5$ performed poorly, which was attributed to the low reflectance of salts in the red and RE bands.

Fernandez-Buces *et al*. (2006) proposed a combined spectral response index (COSRI) to enunciate the combination of spectral responses of bare soil and vegetation. COSRI is defined as:

$$COSRI = ((Blue + Green)/(Red + NIR)) \times NDVI \qquad \text{Equation 5.2}$$

Vegetated areas will result in large CORSI values due to high reflectance in the NIR bands and low reflectance in the visible bands, whereas negative index values will be yielded for clouds, water or salt-affected soils which have high reflectance values in the visible spectrum and low reflectance values with the NIR bands. Small concentrations of salt on the surface will result in index values close to zero (Fernandez-Buces *et al*., 2006). Wang *et al*. (2013) found COSRI to provide a good estimate of measured soil EC values (R^2 = 0.72).

For the purposes of this study, COSRI was modified for WV2 imagery. The CORSI based indices included in our feature set are:

$$COSRI_1 = ((CB + Green)/(Red + NIR_1)) \times NDVI$$
$$COSRI_2 = ((CB + Green)/(Red + NIR_2)) \times NDVI$$
$$COSRI_3 = ((CB + Green)/(RE + NIR_1)) \times NDVI$$
$$COSRI_4 = ((CB + Green)/(RE + NIR_2)) \times NDVI$$
$$COSRI_5 = ((Blue + Green)/(Red + NIR_1)) \times NDVI$$
$$COSRI_6 = ((Blue + Green)/(RE + NIR_1)) \times NDVI$$
$$COSRI_7 = ((Blue + Green)/(RE + NIR_2)) \times NDVI$$
$$COSRI_8 = ((Blue + Green)/(Red + NIR_2)) \times NDVI$$

where CB is the coastal blue band;
Blue is the blue band;
Green is the green band;
Red is the red band;
RE is the red edge band;
NIR_1 and NIR_2 are the NIR bands; and
NDVI is the normalized difference vegetation index.

Texture measures contain information on the spatial distribution of tonal variations, where tone is based on the varying shades of grey of cells in an image (Haralick *et al.,* 1973). Baraldi & Parmiggiani (1995) define texture as the visual effect that is produced by the spatial distribution of tonal variations over relatively small areas, while Irons & Petersen (1981) describe tone as the brightness or darkness of a surface. Texture has been found to be useful for many remote sensing applications (Cai *et al*., 2010; Haralick *et al*., 1973; Odindi & Mhangara, 2013) including salt accommodation monitoring. Cai *et al*. (2010) classified salt-affected soils by making use of a SVM classifier and texture features. Results showed an improved overall accuracy (OA) with the inclusion of a single texture measure, but the best results were achieved by including a combination of several texture measures. The mean, variance and homogeneity texture measures were found to provide the best results for mapping soil salinity. Puissant *et al.* (2005) found that window sizes larger than

7×7 will contribute less to the separation of classes and that homogeneity is the optimal texture measure for remote sensing classifications.

A principal component analysis (PCA) was performed on the multispectral WV2 bands to condense most (96%) of the spectral variance into a single component (Campbell, 2002). The resulting first principal component (PCA1) was included in the feature set and used as input to the texture measures. Texture measures were also carried out on the panchromatic band and each of the multispectral bands. This combination of input variables allowed the texture calculations to be assessed at all possible spatial and spectral resolutions offered by the WV2 image. Texture measures based on histogram statistics and second-order statistics computed from grey level co-occurrence matrices (GLCM) (Clausi, 2002; Haralick *et al*., 1973) were evaluated. The histogram measures considered were energy, entropy and variance; the GLCM measures were contrast, entropy, homogeneity and variance. Three window sizes, namely 3×3, 5×5 and 7×7, were used for generating the texture measures. PCI Geomatica 2013 software was used to perform all the texture calculations.

5.1.4 Separability analysis

Feature selection has been shown to improve classification accuracies (Lu & Weng, 2007; Myburgh & Van Niekerk, 2013), especially when the number of training sets is disproportionally to the number of features (Myburgh & Van Niekerk, 2014a; Oommen *et al*., 2008; Pal & Mather, 2004). The JM distance measure, as implemented in the SEaTH (SEparability and THresholds) software package (Nussbaum *et al*., 2006), was used to score the features according to class separation. The algorithm firstly identifies features that have the best separability between classes, and secondly the threshold of separation for each feature is determined (Gao *et al*., 2011; Heumann, 2011; Nussbaum *et al*., 2006). The JM distance is calculated as (Nussbaum *et al*., 2006):

$$J = 2(1 - e^{-B}) \qquad \text{Equation 5.3}$$

where J is the JM distance; and
B is the Bhattacharya distance.

The Bhattacharya distance (*B*) is the mean and standard deviation of the training samples of the two classes (Bhattacharya, 1943). The resulting J value ranges from 0 to 2, where J = 0 indicates that the two classes are completely correlated and therefore inseparable, while J = 2 indicates that the two classes are completely uncorrelated and separable. Lower values of J will consequently produce more classification errors (Gao *et al*., 2011; Heumann, 2011; Nussbaum *et al*., 2006). According to Nussbaum *et al*. (2006), Heumann (2011) and Odindi & Mhangara (2013), a J value of 2 indicates excellent intra-class separation; a value equal to or greater than 1.9 good separation; and a value below 1.7 indicates poor separation. J values less than 1 suggest a requirement for new training data (Heumann, 2011; Nussbaum *et al*., 2006).

A limitation of the JM distance is the assumption that sample values within classes are normally distributed. In cases where this is not true, the threshold value might be substantially different, but the separability measure is still likely to be valid (Gao *et al*., 2011).

A more detailed discussion on the JM distance can be found in Nussbaum *et al*. (2006), Gao *et al*. (2011), Heumann (2011) and Odindi & Mhangara (2013).

Each of the features in Table 5.1 was included in the separability analysis. Two classification schemes, namely a binary and a senary (six-class) scheme, were used for the separability analysis. The binary scheme is based on the quantitative soil EC measurements only and consists of a salt-affected (EC ≥400 mS/m) and an unaffected (EC <400 mS/m) class, while the senary scheme combines the soil EC measurements and the high, low or absent qualitative expression of visible salt accumulation manifestations (i.e. evidence of salt precipitation) on the soil surface at each sample location. The motivation for including the qualitative expressions was to better understand the importance of surface salt accumulation manifestations in distinguishing salt-affected soil from unaffected soil. The conjecture was that, because only the reflection of the soil surface can be observed using multispectral imagery, soils with visible manifestations of salt accumulation will be easier to discriminate from unaffected soils with no such manifestations. The features which provided the highest class separation (J value) and the accompanying threshold values were used to develop a set of rules which were then implemented in the eCognition 8.9 software package.

5.1.5 Statistical modelling

Regression analyses were used to analyze the statistical relationship between the measured soil EC and the spectral bands, SIs and texture measures. This was accomplished with IBM SPSS v20.0 software. Linear, logarithmic, inverse, quadratic, cubic, power and exponential regression models were employed. Stepwise multiple regression and partial least squares (PLS) regressions were also carried out. The latter has been shown to be very effective for salt accumulation modelling using spectral data (Mashimbye *et al*., 2012) as it reduces a large number of measured collinear spectral variables to a few non-correlated latent variables. This is done by utilizing a bilinear calibration method and using data compression (Cho *et al*., 2007; Hansen & Schjoerring, 2003; Mashimbye *et al*., 2012). A linear relationship is specified between a set of dependent variables and predictor variables, thereby extracting the orthogonal predictor variables and accounting for as much of the variation of the dependent variables as possible (Cho *et al*., 2007; Mashimbye *et al*., 2012).

5.1.6 Supervised classification

A supervised classification approach uses samples of known identity to classify pixels of unknown identity (Campbell, 2002; Rees, 2001). The classifiers considered in this study were kNN, ML, SVM, DT and RF. The kNN algorithm assigns a class to a pixel according to the k nearest trained pixels (Cover & Hart, 1967; Gibson & Power, 2000). It is therefore recommended to set k to be an odd value, so as to avoid ties (Campbell, 2002). The kNN algorithm is effective in classifying data that is not normally distributed, but assigns equal weight to all features even though some features are often more important than others. This can result in incorrect class assignments, especially if the input features were not carefully selected or if the samples do not adequate represent the target class (Cunningham & Delany, 2007).

The ML classifier makes use of training data to estimate the means and variances of the classes by assuming the training data is normally distributed (Gibson & Power, 2000; Harris, 1987). These estimates are then used to determine the probabilities for each class (Albert, 2002; Lillesand *et al*., 2004; Rees, 2001). According to Campbell (2007), ML is very sensitive to the quality of the training data and a decrease in accuracy has been observed with an increase in input features (Myburgh & Van Niekerk, 2013).

The efficiency of SVM classifiers for remote sensing applications has been demonstrated by Lizarazo (2008), Li *et al*. (2010) and Petropoulos *et al*. (2012). Myburgh & Van Niekerk (2013) showed that SVM produces more accurate results than NN and ML for land cover mapping using SPOT-5 imagery. SVM determines the optimal separating hyperplane between classes (Novack *et al*., 2011) by focussing on the training samples close to the edge (support vector) of the class descriptors (Lizarazo, 2008; Tzotsos & Argialas, 2006). In cases where the relationship between classes and features are non-linear, the radial basis function (RBF) kernel is often applied (Li *et al*., 2010). See Vapnik (2000) and Huang *et al*. (2002) for a detailed mathematical formulation of SVM.

A DT identifies relationships between multiple response (dependent) variables and an independent variable. DTs hierarchically split a dataset into increasingly homogeneous subsets known as nodes (Gómez *et al*., 2012; Novack *et al*., 2011; Pal & Mather, 2003; Punia *et al*., 2011). The algorithm reaches a leaf node by recursively partitioning the feature data. When a leaf node is reached, the class associated with the node is assigned to the observation (Pal & Mather, 2003). Each DT node is limited to a split in feature space orthogonal to the axis of the selected feature (Novack *et al*., 2011; Pal & Mather, 2003). Because DT classifiers capture non-linear relationships between variables, the data does not have to be normally distributed. It is also resistant to errors in the training data (Gómez *et al*., 2012; Hladik & Alber, 2014). Each branch of the DT consists of divisions (or rules) of the most probable class. The most likely class of a pixel can therefore be classified by applying these rules (Lawrence & Wright, 2001). Some implementations of DTs also provide an indication of the importance of each feature. According to Campbell (2007) and Lawrence & Wright (2001), DTs often over-fit models and a pruning step is required. This involves cross-validation during which the data is divided into subsets and results from some subsets are validated against other subsets (Campbell, 2002; Lawrence & Wright, 2001).

Recently there has been a notable increase in the application of the RF classifier for remote sensing applications (Duro *et al*., 2012; Gislason *et al*., 2006; Immitzer *et al*., 2012; Lawrence *et al*., 2006) and it has been shown to be effective for many classification tasks (Lawrence & Wright, 2001; Gislason *et al*., 2006; Novack *et al*., 2011; Rodriquez-Galiano *et al*., 2012a, 2012b). RF is an ensemble classifier based on DTs, where each DT is generated using a random vector sampled independently from the input vector. Each DT casts a vote (Bosch *et al.,* 2007; Breiman, 2001; Pal, 2005) and contributes to the assignment of the most popular class to the independent variable (Breiman, 2001; Rodriquez-Galiano *et al*., 2012a). The RF classifier requires two parameters: the number of trees and the number of active (predictive) variables. Rodriguez-Galiano *et al*. (2012a) found that stability in accuracy is achieved at 100 trees and that a small number of split variables are preferable to reduce generalization error and correlation between trees. They also found that RF has a low sensitivity (even lower than DT classifiers) to the training set size. This is attributed to the use of bagging during training dataset and feature selection (Breiman, 1996; Rodriquez-Galiano *et al*., 2012a). Duro *et al*. (2012) showed that the number of trees and the number of variables considered at each split have an insignificant effect on OA. A more detailed discussion on the RF classifier can be found in Breiman (1996), Breiman (2001), Pal (2005) and Rodriguez-Galiano *et al*. (2012a). Novack *et al*. (2011) demonstrated that RF is superior to DTs (Rodriquez-Galiano *et al*., 2012b) and SVM, while Immitzer *et al*. (2012) successfully applied RF for classifying WV2 imagery.

The kNN, SVM, DT and RF classifications were performed within eCognition 8.9, which makes use of OpenCV implementations of the classifiers (Bradski, 2000). ENVI 5.0 was used to apply the ML classifier. A pixel-based approach was followed during the classifications to avoid distorting the values of the training features. A k value of 1, 3 and 5 was used for the kNN classifications. Odd values were used to avoid ties (Campbell, 2002). The radial basis function was chosen as the kernel type for the SVM classifier, as recommended by Hsu *et al*. (2010). The maximum number of trees for the RF classifier was set to 100. The number of active variables, which is the number of randomly selected features used to find the best splits at each node, was set to eCognition's 3. Default parameters were used for the ML and DT classifiers.

Thirty-one (60%) of the soil samples were used for classifier training, whilst 20 (40%) were kept for accuracy assessment. Vegetated areas were excluded from the analyses by using an NDVI threshold of 0.35.

5.1.7 Accuracy assessment

Maps were created form the rule-based and supervised classification outputs to identify problem areas within the study area. Confusion matrices were used to calculate the OA, producer accuracy and user accuracy. The Kappa coefficient and the receiver operating characteristic (ROC) curve were also calculated to show whether the accuracies were by chance.

5.1.8 Results

The result (Fig.5.2) of the analyses of samples representing bare soil are shown in Fig.5.2. The majority (60.8%) of the samples were salt-affected, but this is not a true reflection of the salt accumulation levels in the scheme as the sampling sites were specifically selected to include salt-affected areas. The 2:3 balance between salt-affected and unaffected samples was considered suitable for classifier training and accuracy assessment purposes.

Salt accumulation does not occur continuously (Fig.5.3), but is concentrated in relatively small patches that would be difficult to detect using medium (e.g. Landsat 8) or even high (SPOT-5) resolution imagery.

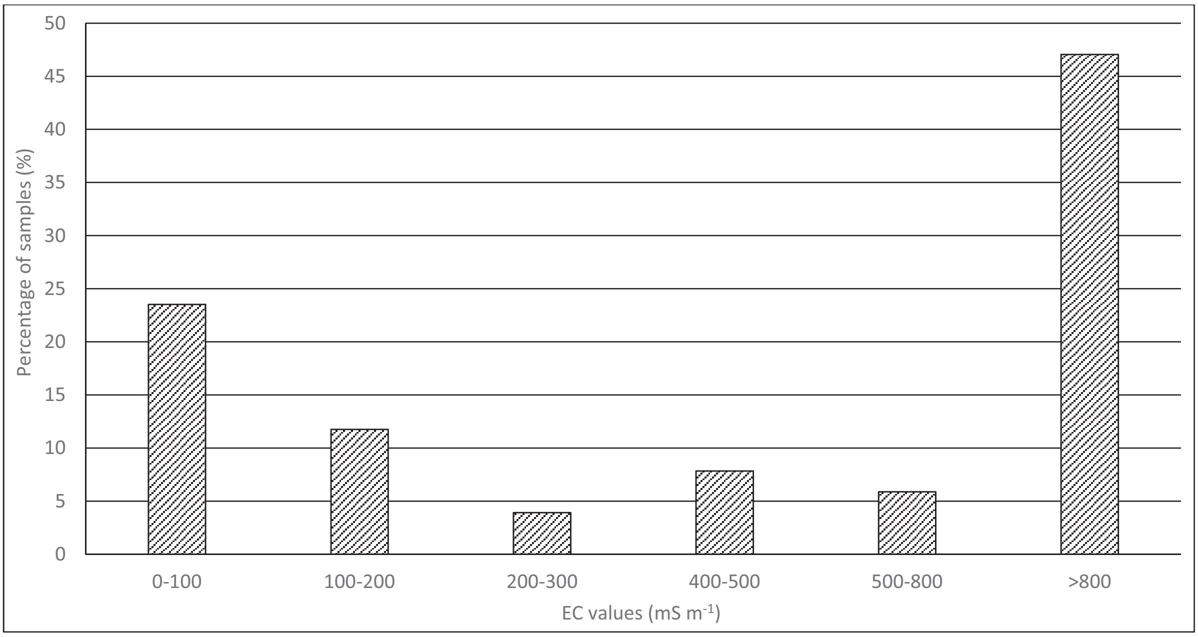

Figure 5.2 EC values of soil samples collected during the June and September field surveys.

Figure 5.3 Examples of salt precipitation patches in the study area at Vaalharts.

The result (Table 5.2) when the visual evidence of salt precipitation was combined with the measured EC values to classify the field observations into a senary classification scheme (Table 5.2). None of the soil samples that showed clear evidence of salt accumulation were found to have EC values of less than 400 mS/m, resulting in class B1 (unaffected, high salt precipitation) to be empty. There were only eight (15%) cases of salt-affected soils with high (clearly visible) salt precipitation. Most (75%) of the salt-affected soils had no or very little evidence of salt precipitation. For classes A2 and B2 the level of salt precipitation was judged (in the field) to be too low to be clearly noticeable on satellite imagery, but the relatively high number of cases (20%) in B2 (unaffected, low salt precipitation) will likely lead to some confusion in discriminating salt-affected from unaffected areas. Similarly, the lack of any visual cues of salt accumulation in classes A3 and B3 (of which there are 10 and 9 cases, respectively) is expected to also reduce classification accuracy.

Table 5.2 Senary scheme classes provided as input for the JM distance measures

Topsoil condition	Salt-affected (EC_e ≥400 mS/m) (n = 32)	Unaffected (EC_e <400 mS/m) (n = 19)
High salt precipitation	A1 (n = 8)	B1 (n = 0)
Low salt precipitation	A2 (n = 14)	B2 (n = 10)
No salt precipitation	A3 (n = 10)	B3 (n = 9)

5.1.8.1 Spectral profiles and separability analysis results

The binary and senary scheme spectral profiles in Figure 5.4 compare the percentage reflectance of salt-affected and unaffected soils in each of the WV2 bands. The spectral properties of salt-affected and unaffected soils (Figure 5.4(a)) are very similar in the CB and blue bands, with more noticeable differences in the remaining bands. In contrast to Rao *et al*. (1995), Metternicht & Zinck (2003), Abbas & Khan (2007) and Elnaggar & Noller (2009), salt-affected soils had lower reflectance values in the longer wavelengths (510-690 nm) of the visible spectrum for the binary scheme profile. This was not the case for the senary scheme profile (Figure 5.4(b)), where soils with clear evidence of salt precipitation (class A1) produced noticeably higher reflectance values than the other classes, especially in the RE, NIR1 and NIR2 bands. Conversely, salt-affected soil with little evidence of salt precipitation (class A2) consistently recorded lower reflectance values than the other classes. Salt-affected soils with no evidence of salt precipitation (class A3) recorded reflectance values less than the unaffected classes in all bands except NIR1 and NIR2. The standard deviation error bars shown in the binary scheme profile show that there is much overlap between the recorded reflectance values of samples, which will make it difficult to distinguish salt-affected from unaffected soils based solely on the spectral characteristics. This was confirmed when separability was quantified using the JM measure. The highest JM value was achieved in band 4 (J = 0.38), indicating that the classes are not separable using an individual band.

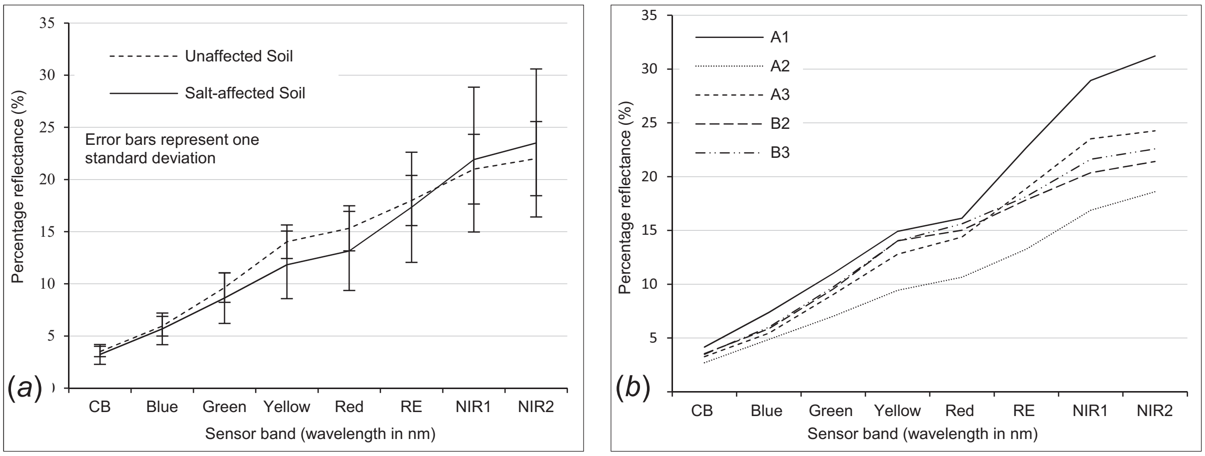

Figure 5.4 Spectral profiles of salt-affected and unaffected soils for the (a) binary and (b) senary classification schemes as extracted from the WorldView-2 Image.

Better separability was achieved when multiple bands were combined as SIs. Of all the SIs evaluated, $NDSI_3$ produced the highest separability between the salt-affected and unaffected classes, with a J value of 0.91 for the binary classification scheme. However, this separability is still relatively low and is unlikely to produce an accurate classification.

Table 5.3 lists the highest J values obtained for each of the five classes when visible evidence of salt accumulation was combined with the EC-based classification. Class pairs A1~B2 (J = 1.75), A2~B2 (J = 1.73) and A1~A2 (J = 1.65) achieved the highest separability using NDSI1, NDSI2 and NIR2 respectively. The other class combinations all attained separability scores of less than 1.50. Classes A2 (salt-affected, low salt precipitation) and A3 (salt-affected, no salt precipitation) were the most difficult to separate (J = 0.89). Classes A3 (salt-affected, no salt precipitation) and B3 (unaffected, no salt precipitation) received the second lowest J value (0.93) as no visual evidence of salt accumulation on the soil surface was present. Generally, the J values decrease with a reduction in salt precipitation levels.

None of the features considered in the JM separability analysis of the senary classification scheme stood out as being the most successful in separating the classes, although the NDSI-based indices produced the best separability on four occasions. Texture features, especially histogram-based entropy, were found to be the best discriminators on three occasions.

The features and thresholds identified by the JM separability analysis were implemented as image classification rules to produce a map of salt-affected and unaffected areas. Separate rule sets were created for the binary and the senary classification schemes.

Table 5.3 Best JM distance results for the senary scheme

Class 1	Class 2	Feature	J	Threshold
A1	B2	$NDSI_1$	1.75	-0.23
A2	B2	$NDSI_2$	1.73	-0.24
A1	A2	NIR_2	1.65	24.47
A1	B3	COSRI3	1.48	0.07
A2	B3	Entropy (Histogram – 7×7)	1.47	5.6
B2	A3	$NDSI_2$	1.20	-0.23
A1	A3	Contrast (GLCM – 7×7)	1.18	0.13
B2	B3	Entropy (Histogram – 5×5)	1.03	4.63
A3	B3	$NDSI_3$	0.93	-0.20
A2	A3	S_3	0.89	-0.51

5.1.8.2 Regression modelling

Table 5.4 shows the results of the regression modelling of EC measurements and the individual WV2 image bands, SIs and texture measures. For the sake of brevity, only features that achieved an R^2 of 0.40 or more in any of the models are included in the table. None of the WV2 bands or texture measures met this requirement. The best fit was achieved by $NDSI_1$ (R^2 = 0.64, p <0.001), with the cubic model providing the best description of this relationship.

Table 5.4 Regression models with strongest relationship between EC and WorldView-2 features

Salinity Index	Goodness-to-fit (R^2) per regression model [a]						
	Linear	Logarithmic	Inverse	Quadratic	Cubic	Power	Exponential
$NDSI_1$	0.26	-	0.27	0.47	0.64	-	0.34
$NDSI_2$	0.23	-	0.30	0.45	0.49	-	0.34
$NDSI_3$	0.18*	-	0.39	0.56	0.56	-	0.25
$NDSI_4$	0.16*	-	0.27	0.41	0.41	-	0.25
$COSRI_1$	0.19	0.28	0.33	0.43	0.43	0.38	0.28
$COSRI_2$	0.23	0.30	0.33	0.42	0.43	0.41	0.33
$COSRI_3$	0.24	0.31	0.34	0.44	0.51	0.41	0.32
$COSRI_4$	0.27	0.32	0.35	0.42	0.48	0.43	0.37
$COSRI_5$	0.19	0.29	0.34	0.43	0.43	0.40	0.28
$COSRI_6$	0.22	0.30	0.34	0.43	0.43	0.42	0.33
$COSRI_7$	0.24	0.32	0.35	0.46	0.49	0.42	0.33
$COSRI_8$	0.27	0.33	0.35	0.44	0.47	0.44	0.37

[a] All results were significant at 0.001 level, except for those indicated with * which were significant at 0.01 level.

The results from the stepwise regression analyses showed that the NIR_2 band was the first variable to be taken into account (R^2 = 0.39, p <0.001), followed by $COSRI_8$ and $COSRI_1$. The resulting model produced a R^2 of 0.51 (p <0.001). The best PLS regression model had a goodness of fit of 0.39 (R^2) and took 38 variables into account.

The cubic model in Table 5.4 that best described this relationship between soil EC and $NDSI_1$ is formulated as:

$$EC = b_0 + (b_1 \times x) + (b_2 \times x^2) + (b_3 \times x^3) \quad \text{Equation5.4}$$

where EC is the predicted soil EC
x the raster (e.g. $NDSI_1$) containing the calculated index
b_0 = 9746.258
b_1 = 161093.441
b_2 = 753892.151 and
b_3 = 907884.290.

Figure 5.5 compares this model to the calculated $NDSI_1$ and measured soil EC (mS/m) values. Samples with an $NDSI_1$ value greater than -0.23 were in most cases found to be associated with unaffected soils, with a sharp increase in salinity observed when $NDSI_1$ dropped below -0.25 (Figure 5.5 (a)). Two outliers (labelled A and B in Figure 5.5(a)) were identified and removed, resulting in a slight improvement in the goodness-to-fit (R^2 = 0.68; p <0.001) of the model. Figure 5.5(b) shows that 20 (77%) of the samples with $NDSI_1$ values greater than -0.23 had EC measurements less than 400 mS/m (unaffected).

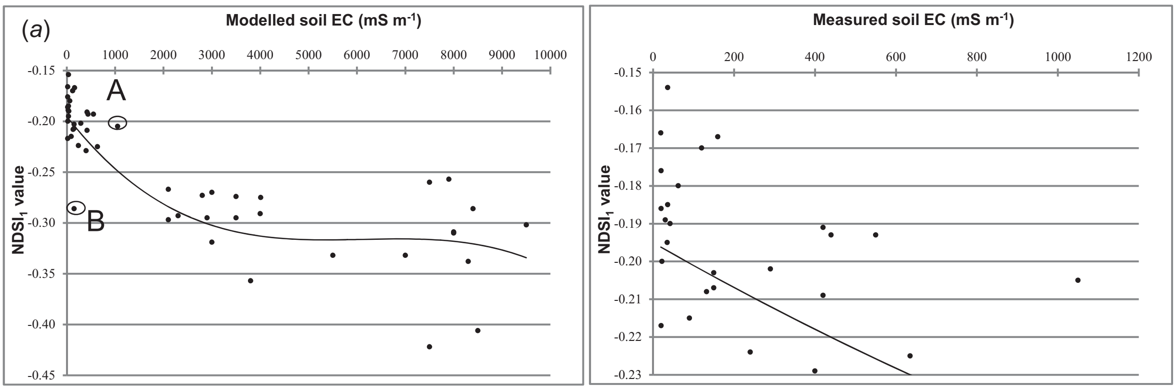

Figure 5.5 Relationship between $NDSI_1$ and measured soil EC.

A threshold value of 400 mS/m was applied to the regression model to produce a classification of salt-affected and unaffected areas. $NDSI_1$ values larger than this threshold were classed as salt-affected. A rule set was created from these results and applied in eCognition 8.9.

5.1.8.3 CART rule set

The CART analysis identified a single feature as primary splitter, namely $NDSI_1$. Low $NDSI_1$ values (≤-0.22) were shown to mostly consist of salt-affected samples. High values (>-0.22) were classed as unaffected. A rule set was created from these results and applied in eCognition 8.9.

5.1.8.4 Classification results

The accuracy assessment results of the classifications, based on an independent set of reference samples (40% of the samples collected), are shown in Table 5.5. The highest accuracy (OA = 90%; Kappa = 0.8; AUROC = 0.9) was achieved by the SVM classifier. However, the algorithm classified an unrealistically small percentage (0.023%) of the study area as salt-affected, indicating that the SVM algorithm was unable to provide a meaningful result, most likely due to training data over-fitting. The SVM results were consequently excluded from further evaluation. The rule set based on the $NDSI_1$ threshold that was obtained from the CART analysis produced the most realistic and accurate classification with an OA of 80%, Kappa of 0.6 and AUROC of 0.8. The salt-affected class recorded a very high user's accuracy (90%), but the producer's accuracy (PA) was lower (75%). The opposite was true for the unaffected class, which scored a high (87.5%) PA and a low (70%) user's accuracy (UA) and 77% of the study area was classified as being salt-affected.

Both the JM distance binary and senary scheme rule-based classifications achieved an OA of 75%, with the binary scheme attaining a slightly higher Kappa (0.51) and AUROC (076). A much higher PA for the salt-affected class was achieved with the senary scheme (83.3%) than the binary scheme (66.7%). The reverse is true of the UA for the salt-affected class, with the binary scheme (88.9%) outperforming the senary scheme (76.9%). The rule-based classification of the $NDSI_1$ regression model achieved an OA of 75% and AUROC of 0.74, with a high PA (83.3%) and a UA (76.9%) for the salt-affected class. The relatively low Kappa of 0.47 suggests a high agreement by chance.

The kNN supervised algorithm attained an OA of 80%, Kappa of 0.58 and AUROC of 0.79, which is only marginally lower than the CART rule-based classification. The DT resulted in an OA of 75% and AUROC of 0.76, although the Kappa of 0.51 indicates a high agreement by chance. RF performed slightly better with an OA of 80%, AUROC of 0.79 and Kappa of 0.58, with $NDSI_1$ being the most important variable. The worst-performing supervised classifier was ML, which achieved an OA of 70%. The low Kappa (0.35) and AUROC (0.69) indicate a very high agreement by chance (Evangelista, 2006; Garrett & Viera, 2005; Johnson *et al*., 2012).

The % salt-affected column in Table 5.5 shows that all the methods, apart from SVM, classified the majority of the study area as being salt-affected. This suggests that there was a general overestimation of salt-affected soils as the level of salt accumulation in the study area is known to be moderate. The overestimation of salt-affected soils is also evident in Figure 5.6 and Figure 5.7, which show the maps produced from the rule-based and supervised classification approaches respectively. Based on local knowledge, the JM distance binary scheme approach (Figure 5.6(b)) seems to be the most realistic representation of salt accumulation in the study area (52.3% salt-affected). Overestimation of salt-affected areas was highest for the ML classification (86.8%) (Figure 5.7(d)). The maps produced from the $NDSI_1$ cubic regression model (Figure 5.6(c)) and CART analysis (Figure 5.6(d)) are almost identical as $NDSI_1$ was used in both cases. Only small differences are evident in the maps produced by the kNN (Figure 5.7(a)) and DT (Figure 5.7(b)) supervised classifiers, while RF (Figure 5.7(c)) classified fewer fields as salt-affected.

Table 5.5 Accuracies of methods evaluated

Method	Approach	Class	Producer's accuracy (%)	User's accuracy (%)	Overall accuracy (%)	Kappa	AUROC	% Salt-affected
JM distance (senary scheme)	Rule set	Salt-affected	83.3	76.9	75	0.47	0.74	86.8
		Unaffected	62.5	71.4				
JM distance (binary scheme)	Rule set	Salt-affected	66.7	88.9	75	0.51	0.76	52.3
		Unaffected	87.5	63.6				
Regression analysis ($NDSI_1$)	Rule set	Salt-affected	83.3	76.9	75	0.47	0.74	74.5
		Unaffected	62.5	71.4				
CART	Rule set	Salt-affected	75	90	80	0.60	0.8*	77
		Unaffected	87.5	70				
kNN (k = 3)	Classifier	Salt-affected	84.6	91.7	80	0.58	0.79*	73.4
		Unaffected	85.7	75				
DT	Classifier	Salt-affected	66.7	88.9	75	0.51	0.76*	61
		Unaffected	87.5	63.6				
RF	Classifier	Salt-affected	83.3	83.3	80	0.58	0.79*	73.1
		Unaffected	75	75				
ML	Classifier	Salt-affected	83.3	71.4	70	0.35	0.69	93.39
		Unaffected	50	50				
SVM	Classifier	Salt-affected	83.3	100	90	0.8	0.9	0.023
		Unaffected	100	80				

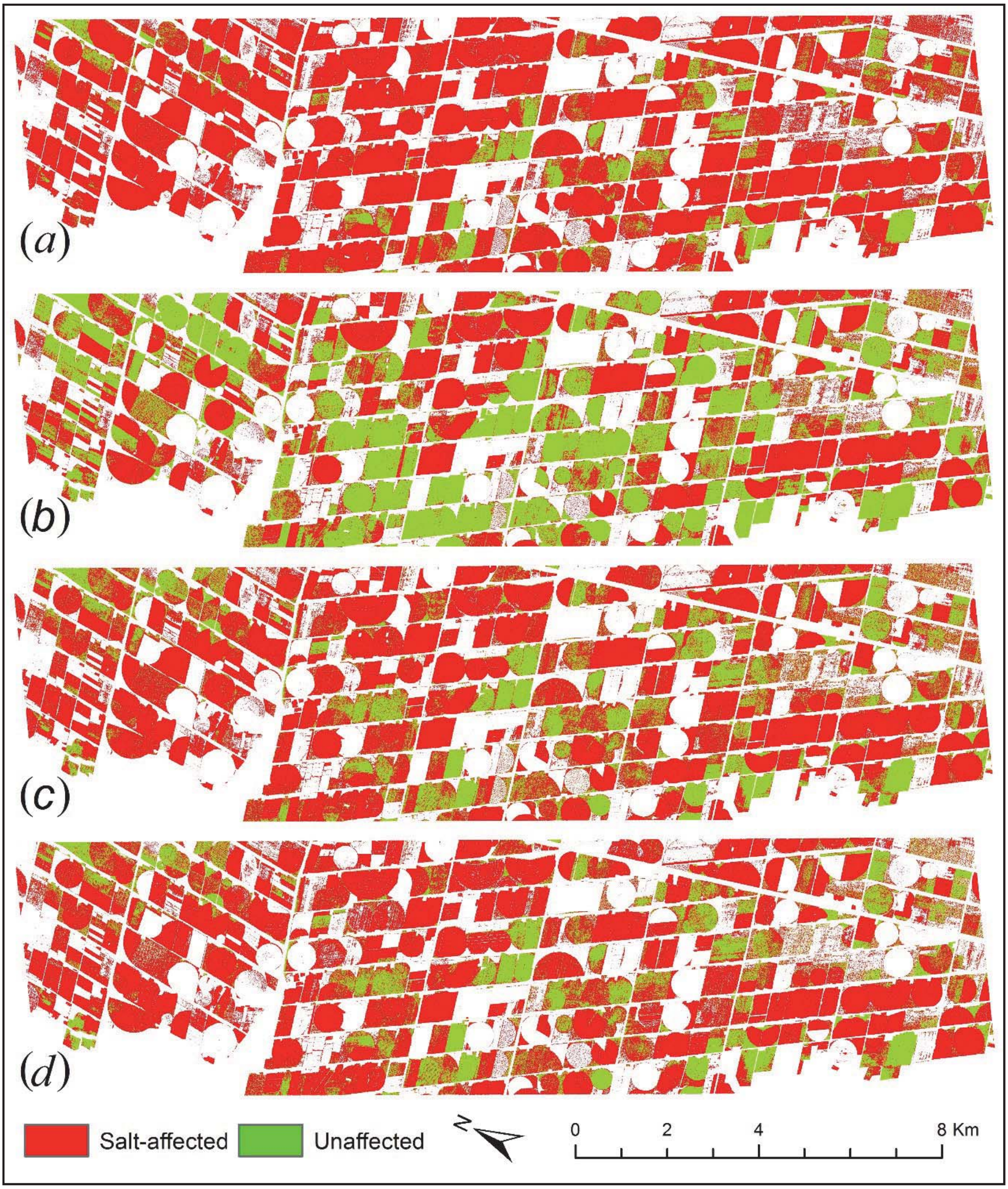

Figure 5.6 Maps produced from the rule-based (a) JM distance senary scheme, (b) JM distance binary scheme, and (c) $NDSI_1$ cubic regression model, and (d) CART.

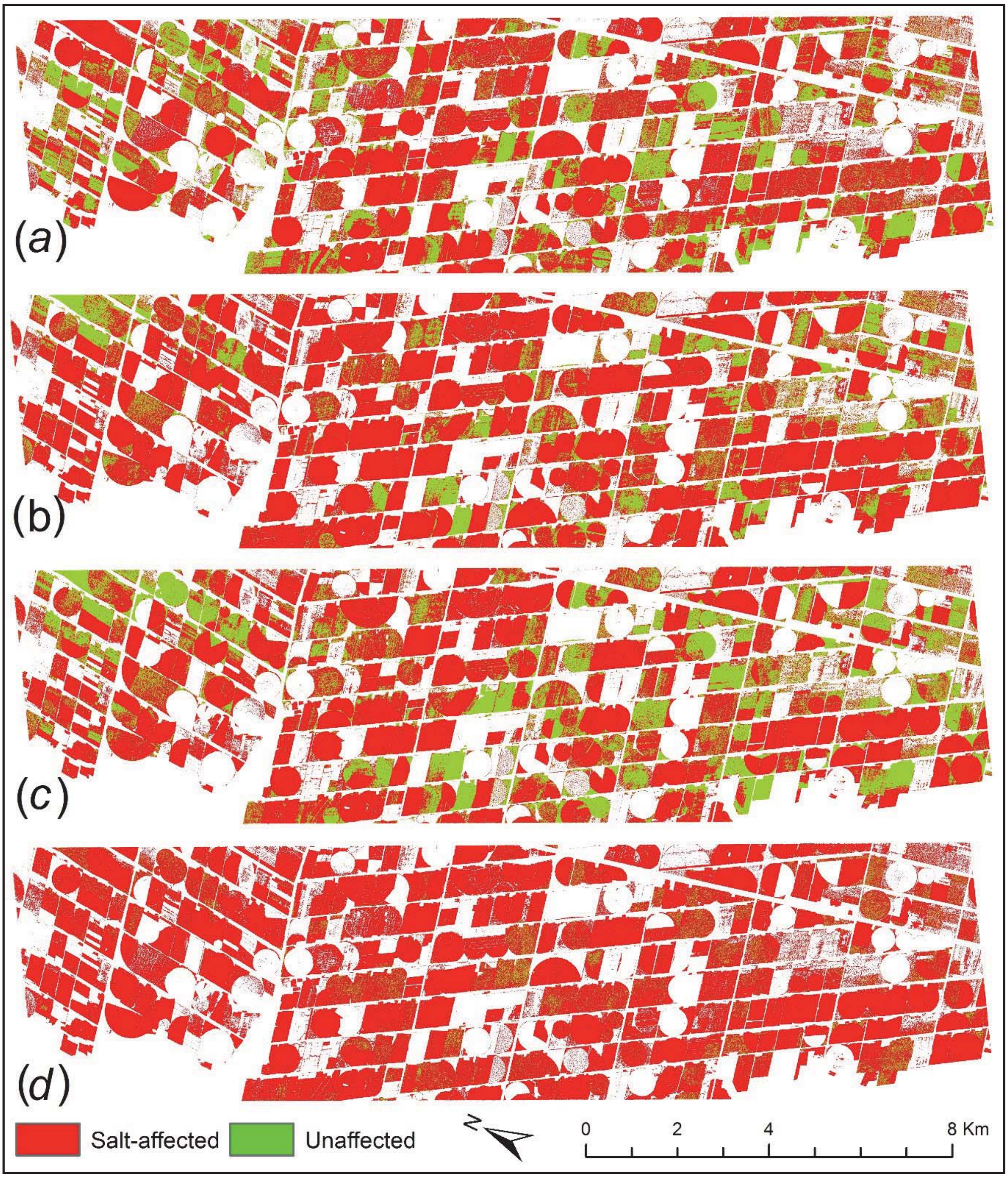

Figure 5.7 Maps produced from the (a) kNN, (b) DT, (c) RF and (d) ML supervised classifiers.

5.1.9 Discussion

Notable differences in the spectral properties of salt-affected and unaffected soils were recorded in the Green, Yellow, Red, RE, NIR1 and NIR2 bands (Fig. 5.4). In contrast to the findings of Rao *et al*. (1995), Metternicht & Zinck (2003) and Elnaggar & Noller (2009), salt-affected soils generally had a lower reflectance in the visible region of the electromagnetic spectrum. This discrepancy is attributed to the relatively low levels of salt precipitation occurring in the study area. Soils with salt precipitation have high reflectance values in the visible and NIR regions of the electromagnetic spectrum (Elnaggar & Noller, 2009;

Metternicht & Zinck, 2003; Rao *et al*., 1995), but in this study only 25% of the samples representing salt-affected soils had sufficiently high levels of salt precipitation for detection using satellite imagery (class A1). Other salt-affected soils (classes A2 and A3) generally appeared smooth and dark as salt accumulation in the study area often coincides with waterlogging and the reflection values of wet soils are generally lower in the visible and NIR spectra (Metternicht & Zinck, 2003).

Salt-affected soils with clear evidence of salt precipitation (class A1) were relatively well differentiated from unaffected soils (class B2) using the $NDSI_1$. $NDSI_1$ also produced a regression model with a moderately strong fit ($R^2 = 0.64$, $p < 0.001$), although the OA of the resulting model was relatively low (75%) compared to some of the other classifiers. When plotted it was observed that the relationship between $NDSI_1$ and EC is erratic when salinity levels are high and that the model generally overestimated EC.

The highest accuracies (80%) were recorded using the kNN, CART and RF classifiers. Most (63%) of the soil samples collected during the field surveys were salt-affected and this slight imbalance (2:3) could have had a negative effect on the classifiers. The kNN classifier is relatively insensitive to unbalanced training data as it only considers the closest known values for classification purposes. RF's use of bagging also makes it less sensitive to skewed or unbalanced training datasets when compared to DTs (Breiman, 2001; Johnson *et al*., 2012). Although techniques such as over- and under-sampling have been proposed to improve the accuracies of supervised classifiers when unbalanced training datasets are used (Chawla *et al.,* 2004; Ganganwar, 2012; Seiffert *et al*., 2010), they were not implemented in this study as such methods are usually needed for very skewed (e.g. 1:20) training data (Johnson *et al*., 2012). Under-sampling also discards potentially important data, while over-sampling can result in over-fitting (Chawla *et al*., 2004; Ganganwar, 2012). A more likely reason for the relatively poor performance of many of the supervised classifiers is the confusion caused by the spectral variation of salt-affected soils, the relatively small sample set and the large number of features (68) considered. RF has been shown to perform well under such conditions (Breiman, 1996; Rodriquez-Galiano *et al*., 2012a).

Another factor that complicates the detection of salt accumulation when bare soils are observed using remote sensing is the disturbance caused by soil preparations (e.g. ploughing), as this can alter the soil surface and reflectance. Vaalharts is a highly dynamic irrigation scheme in which crops are rotated throughout the year. Many of the fields visited during the survey were recently ploughed in preparation for planting. This would also have had an effect on classification accuracy.

All the methods classified most of the study area as being salt-affected. Salt-affected areas are also in most cases portrayed by the classifiers as large, continuous areas. This is, however, not a realistic result as salt accumulation in the study area was observed to occur in small patches (Fig.5.3). From this finding we conclude that the classifiers generally overestimated salt-affected areas, most likely owing to the confusion between salt-affected soils with no evidence of salt precipitation (A3) and unaffected soils with some evidence of precipitation (B2).

Compared to other VHR sensors, the spectral resolution of the WV2 sensor is high, but is limited to the visible and NIR region of the electromagnetic spectrum. Using hyperspectral data on South African soils, Mashimbye *et al*. (2012) found that the 2257 nm band in the shortwave infrared (SWIR) region of the electromagnetic spectrum correlated the strongest with salt-affected soils. The addition of a SWIR (1195-2365 nm) band to the recently-launched WorldView-3 sensor consequently holds much potential for salt accumulation monitoring using multispectral imagery.

5.1.10 Conclusion

This component of the research evaluated the use of VHR (WV2) imagery for modelling and mapping salt-accumulation by observing bare soils. In addition to the WV2 image bands, the first PCA component, a number of texture measures and several SIs were also considered as possible predictor variables. Three rule sets based on regression modelling, the JM separability measure and CART, as well as five supervised classifiers (NN, ML, SVM, DT and RF), were evaluated. The results demonstrated that the rule based on the JM distance measure was the most accurate in differentiating salt-affected and unaffected soils. Overall, $NDSI_1$ was the best predictor of salt accumulation as it featured in the separability analysis, regression modelling, CART and RF classifiers.

It is concluded that the use of WV2 imagery to identify salt-affected soils is not reliable enough for operational purposes as all of the methods evaluated overestimated salt accumulation. The inconsistencies in the visual appearance of salt-affected soils are more likely the reason for the misclassifications. VHR imagery with a SWIR band (e.g. WorldView-3) might produce better results, but it is unlikely that it will overcome all of the limitations of the direct approach (i.e. detecting salt accumulation by observing bare soils). Indirect detection methods (e.g. vegetation stress monitoring, hydrological modelling) that take sub-surface conditions into consideration might produce better results. Ideally a combination of direct and indirect methods should be used. Clearly, more research is needed before such methods can be operationalized for detecting and monitoring salt accumulation in irrigated areas.

5.2 Remote sensing indirect approach: Vegetation monitoring at field level[4]

Several studies have successfully applied the indirect approach to monitor plant stress caused by salt accumulation (Abood *et al*., 2011; Fernández-Buces *et al*., 2006; Lenney *et al*., 1996; Lobell *et al*., 2010; Peñuelas *et al*., 1997; Wiegand *et al*., 1994; Zhang *et al*., 2011). All of these studies relied on VIs (e.g. NDVI, EVI and SAVI). However, poor farming practices and soil preparation can also lead to poor VI responses, which can easily be mistaken for saline conditions (Furby *et al*., 2010). Another limitation of the use of VIs for detecting areas affected by salt accumulation is the negative impact of bare ground backscatter/noise, especially during the early stages of growth (Dehni & Lounis, 2012; Douaoui *et al*., 2006). Very few applications of very high resolution (VHR) imagery for salt accumulation monitoring exist. Notable exceptions are Abood *et al*. (2011) and Douaoui & El Ghadiri (2015) who used 2 m resolution WorldView-2 (WV2) imagery, and Eldiery *et al*. (2005) who used 4 m resolution Ikonos imagery. However, none of these studies investigated the value of spatial features (such as texture measures) for the identification of salt-affected areas. Also, VHR imagery has, to our knowledge, never been used for

[4]The content of this section was adapted from the MSc thesis of Jascha Muller and an article that was submitted for publication in a scientific journal.

monitoring salt accumulation in South Africa. The primary aim of this section is thus to evaluate the use of VHR satellite imagery, specifically WV2, to identify suitable spectral and spatial features for the identification of salt accumulation in a cultivated field. A secondary aim is to improve the understanding of the importance of spatial resolution for detecting salt-affected areas with small spatial extents (i.e. in early stages of deterioration), so that such areas can be proactively identified and managed. These objectives will be evaluated by analysing the WV2 derived features at six different spatial resolutions. Regression modelling, classification and regression tree (CART) analysis will be used. The results are interpreted in the context of finding the best image features and optimal spatial resolution for predicting/identifying salt-affected areas in a South African irrigation system.

5.2.1 Study area

A 2.8 ha irrigated lucerne field in the Vaalharts irrigation scheme was chosen as the study site (Figure 5.8). The selected field is supplied with flood irrigation to supplement the rainfall. Lucerne was targeted for this study because it is moderately sensitive to saline conditions and starts wilting when electric conductivity (EC) persists at levels above 200 mS/m (Hanson *et al.*, 2006). For this study, a single crop was selected so as to eliminate the complexities associated with multiple crop types which have varied spectral properties and tolerances to salt accumulation (Hanson *et al.*, 2006; Zhang *et al.*, 2011).

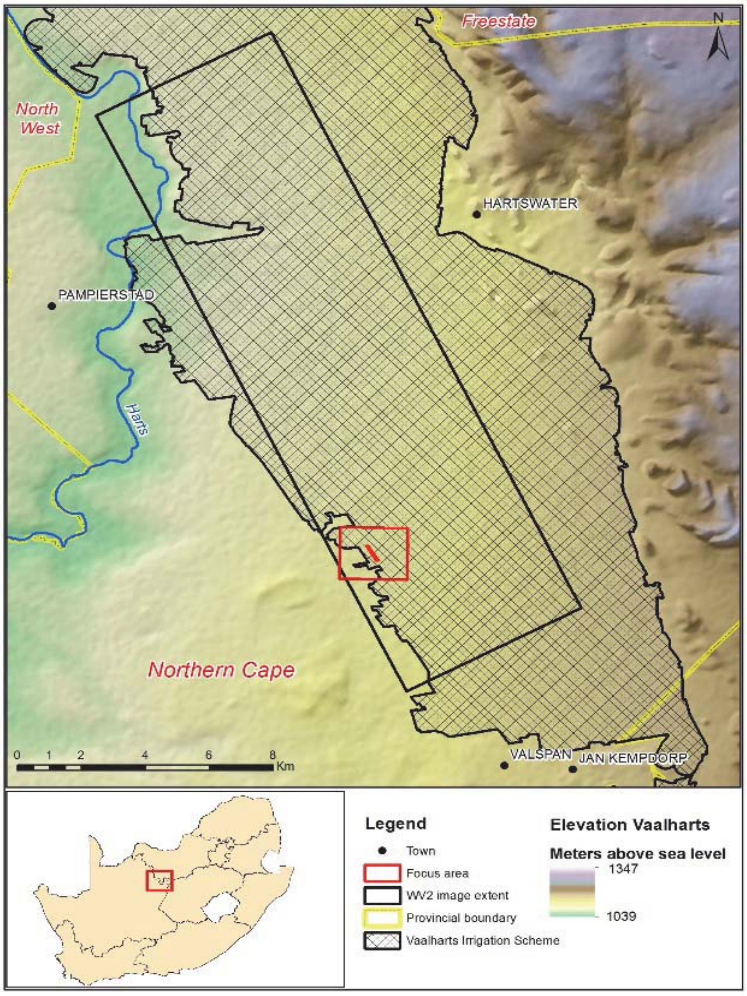

Figure 5.8 Study site location within the Vaalharts irrigation scheme.

5.2.2 Data collection and preparation

The WV2 image described in section 5.1.1 was used in this component of the research. At the time of capture, the WV2 sensor offered higher spectral and spatial resolution compared to other VHR sensors, with eight 2 m resolution relatively narrow bands in the visible and near infrared spectral range (see Table 2.5). The *Pansharp* algorithm as implemented in PCI Geomatica software was used to increase the 2 m spatial resolution of the multispectral data to 0.5 m. The fusion of multispectral and panchromatic images is an effective technique for optimizing the spatial and spectral resolution of images (González-Audícana *et al*., 2004). The *Pansharp* algorithm has been shown to preserve most of the spectral characteristics of the multispectral data in the resulting pansharpened image.

To evaluate the effect of spatial resolution on the identification of salt-affected areas, the original 2 m multispectral bands were down-sampled to 6, 10, 15 and 20 m resolution using the mean aggregate function in ArcMap 10.1. These resolutions were chosen as they represent the resolutions of common sensors (SPOT-6/7, Sentinel-2, ASTER, CBERS-4, IRS). The WV2 image was thus represented by six different spatial resolutions: 0.5, 2, 6, 10, 15 and 20 m.

A field survey was carried out to collect suitable training data. A total of 30 soil samples in the lucerne field were collected.

5.2.3 Feature set development

5.2.3.1 Vegetation indices (VIs)

VIs are the most popular and scientifically-proven remote sensing features for monitoring biomass and vegetation vigour (Campbell, 2007). VIs that have been successfully used for mapping salt-affected areas include the normalized difference vegetation index (NDVI) (Abood *et al.*, 2011; Dehni & Lounis, 2012; Fernandez-Buces *et al*., 2006; Koshal, 2010; Lenney *et al*., 1996; Leone *et al*., 2007; Lobell *et al*., 2010; Peñuelas *et al*., 1997; Turhan *et al*., 2008; Wiegand *et al.,* 1994; Wu *et al*., 2008; Zhang *et al*., 2011), soil-adjusted vegetation index (SAVI) (Abood *et al.*, 2011; Alhammadi & Glenn, 2008; Allbed *et al*., 2014; Koshal, 2010; Zhang *et al*., 2011) and enhanced vegetation index (EVI) (Lobell *et al*., 2010). NDVI is defined as:

$$\mathrm{NDVI} = (N - R)/(N + R) \qquad \text{Equation 5.5}$$

where *N* is the reflectance in the near-infrared (NIR) band and *R* is the reflectance in the red band. Although NDVI is useful for a wide range of applications, it is very sensitive to soil background brightness (Huete, 1988; Bausch, 1993). Huete (1988) proposed using a soil-adjustment factor (L) to reduce soil background brightness. This factor accounts for first-order, non-linear, differential NIR and red radiative transfer through a canopy (Jiang *et al*., 2008). The resulting SAVI is defined as:

$$\mathrm{SAVI} = (1 + L)((N - R)/(N + R + L)) \qquad \text{Equation 5.6}$$

where *N* is the reflectance in the NIR band, *R* is the reflectance in the red band and *L* is the soil-adjustment factor. *L* can vary from 0 to 1 depending on the amount of visible soil. Lower *L* values with increases in vegetation cover are needed as less soil is exposed. A value of 0.5 is a reasonable approximation for *L* when the amount of visible soil is unknown (Koshal, 2010). SAVI provides better results at low vegetation cover than NDVI because of its ability to reduce the soil background effect (Koshal, 2010).

The relatively low spectral resolution of VHR sensors has limited the development of other salt-affected soil detection VIs (Metternicht & Zinck, 2003). Abood *et al*. (2011) took advantage of the additional spectral bands and high spatial resolution of the WV2 imagery to evaluate six adaptations of the NDVI and SAVI indices. Most of the indices that proved to be the most successful in distinguishing salt-affected areas utilized the yellow band, specifically NDVI no. 3 (3) and SAVI no.2 (4):

$$\text{NDVI no. } 3 = (NIR1 - Y)/(NIR1 + Y) \qquad \text{Equation 5.7}$$

where *NIR1* is the reflectance of the WorldView-2's first near-infrared band and *Y* is the reflectance of the WorldView-2's yellow band.

$$\text{SAVI no. } 2 = 1.5((NIR1 - Y)/(NIR1 + Y + 0.5)) \qquad \text{Equation 5. 8}$$

where *NIR1* is the reflectance of the WorldView-2's first near-infrared band and *Y* is the reflectance of the WorldView-2's yellow band. The enhanced vegetation index (EVI) was developed to optimize the vegetation signal with improved sensitivity in high biomass regions. It also improves vegetation monitoring by disconnecting the canopy background signal and reducing atmospheric influences (Jiang *et al*., 2008). EVI is defined as:

$$\text{EVI} = G((N - R)/(N + C_1R - C_2B + L)) \qquad \text{Equation 5.9}$$

where *N* is the reflectance in the NIR band, *R* is the reflectance in the red band, *B* is the reflectance in the blue band, *G* is a gain factor, *L* is the soil-adjustment factor and *C1* and *C2* are aerosol resistance coefficients. The parameters, as adopted in the MODIS EVI algorithm, are *L* =1; *C1* = 6; *C2* = 7.5 and *G* = 2.5, and are used as a *de facto* standard for other sensors. All WV2 derived VIs were produced by performing raster calculations in ArcMap 10.1.

5.2.3.2 Image texture

There is no consensus on a definition for image texture as the meaning seems to vary according to the particular application. For the purposes of this study it is defined as the variation in reflectance from pixel to pixel in a small neighbourhood (Russ, 1999). The observation of image texture is determined by two factors, namely the scale of variation and the scale of observation (Mather & Magaly, 2011). Howari (2003) noted that salt-affected soils tend to have uneven ('spotty') vegetation growth, which suggests a scale of variation. In this study we manipulate the scale of observation by resampling the WV2 image to six spatial resolution levels (0.5, 2, 6, 10, 15 and 20 m).

A total of 25 texture measurements were considered in this study (Table 5.6). The measurements were based on relative frequency distribution statistics (Conners & Harlow, 1980; Haralick, 1979; Haralick *et al.,* 1973) and histogram statistics (Dekker, 2003). The red, NIR and panchromatic bands were used as input for each of the algorithms considered, resulting in a total of 325 texture features. The panchromatic band was selected because it provides the highest resolution (0.5 m), while the red and NIR1 bands were selected because of their well-known sensitivity to vegetation variations.

Table 5.6 Algorithms used for texture feature generation

#	Neighbourhood-based texture algorithms (A)	Histogram-based texture algorithms (B)
1	Homogeneity	Mean
2	Contrast	Median
3	Dissimilarity	Mean deviation from mean
4	Mean	Mean deviation from median
5	Variance	Mean Euclidean distance
6	Entropy	Variance
7	Angular second moment	Coefficient of variation
8	Correlation	Skewness
9	GLDV angular second moment	Kurtosis
10	GLDV entropy	Energy
11	GLDV mean	Entropy
12	GLDV contrast	Weighted-rank fill ratio
13	Inverse difference	

Key: GLDV =Grey level difference vector

5.2.3.3 Principal component analysis (PCA) image transform

Campbell (2007) describes PCA as the process of identifying the optimum linear combinations of the original image layers that accounts for most of the variation in pixel values. PCA is widely used in salinity detection (Abbas *et al.*, 2013; Dehni & Lounis, 2012; Dwivedi *et al.,* 2001; Eldiery *et al.*, 2005; Khan *et al.*, 2001; Tajgardan *et al.*, 2007). In this study only the first two components were included in the feature dataset as they accounted for more than 99% of the variation. These components were generated for all six spatial levels resulting in a total of 12 features.

Table 5.7 provides a summary of the 445 features that were considered in the regression and CART analyses. The feature set consists of the 8 WV2 bands, 10 VIs, 25 texture features and 2 PCA components for each of the six spatial resolution sets.

Table 5.7 Summary of features considered for each of the six feature sets (spatial resolution scenarios) with NIR2 band

Type	Feature	Number
Bands	Coastal Blue	8x6=48
	Blue	
	Green	
	Yellow	
	Red	
	Read Edge	
	NIR1	
	NIR2	
VIs	NDVI & NDVI*	10x6=60
	SAVI & SAVI*	
	EVI & EVI*	
	NDVI no 3 & NDVI* no3	
	SAVI no 2 & SAVI* no 2	
PCA	PCA band 1	2x6=12
	PCA band 2	
Texture	Homogeneity (A)	(2x25x6)+25=325
	Contrast (A)	
	Dissimilarity (A)	
	Mean (A)	
	Variance (A)	
	Entropy (A)	
	Angular second moment (A)	
	Correlation (A)	
	GLDV angular second moment (A)	
	GLDV entropy (A)	
	GLDV mean (A)	
	GLDV contrast (A)	
	Inverse difference (A)	
	Mean (B)	
	Median (B)	
	Mean deviation from mean (B)	
	Mean deviation from median(B)	
	Mean Euclidean distance (B)	
	Variance (B)	
	Coefficient of variation (B)	
	Skewness (B)	
	Kurtosis (B)	
	Energy (B	
	Entropy (B)	
	Weighted-rank fill ratio (B)	
	Total	445

*

5.2.4 Spectral, statistical and CART analyses

According to Hick & Russell (1990) and Zhang *et al*. (2011), salt-affected areas have a higher reflectance in the red band and a lower reflectance in the NIR region. This is due to the decline in vegetation vigour in the presence of high levels of salts. A spectral analysis was carried out to investigate to what extent salt-affected areas can be differentiated using the bands of the WV2 image. The first step was to plot the spectral responses of vegetation in salt-affected and unaffected areas on a graph to allow a visual interpretation of the two profiles. The original 2 m multispectral bands were used as input in the spectral analysis.

The statistical relationships between the image features and salt-affected areas were then explored by regression analyses. The WV2-derived features were specified as independent variables, while the measured EC values were specified as the dependent variable. Stepwise linear regression, partial least squares (PLS) regression and curve estimation regression were carried out in IBM SPSS (version 21) software. The curve estimations tested the fit between the EC values and the dependent variables for various models (linear, logarithmic, inverse, quadratic, cubic, compound, power, s-curve, growth, exponential and logistic). The R^2 values produced by the regression analyses were used to compare the models as they quantify the variation explained by the model and consequently provide a good estimate of the overall predictive power of the model and the nature of the relationship between the input variables (Field, 2006).

A classification and regression tree (CART), as implemented in the Salford Predictive Modeller software suite, was carried out to better understand the relationships between measured EC and the image features. CART has been shown to be a robust decision tree (DT) classifier and was designed for data mining and predictive modelling purposes (Laliberte *et al*., 2007; Myburgh & Van Niekerk, 2013; Steinberg & Golovnya, 2007; Yu *et al*., 2006). CART produces a number of classification trees from which it generates a variable importance list (VIL) based on best relative errors and receiver operating characteristics (ROC) values (a.k.a. area under the curve or AUC). The best relative error (BRE) describes the relationship between classification errors and tree size with 0 representing no error and 1 indicating random guessing. A tree with a ROC value of 0.5 and lower is considered to have poor predicative power, while a tree with a ROC value of 0.7 or higher is likely to produce a good classification (Steinberg & Golovnya, 2007). The VIL summarizes the contribution of a specific feature to the overall tree when all nodes are examined. It contains the primary splitters (the feature that was used to split a node) and surrogate splitters (a back-up feature that could be used when a primary splitter is missing). The VIL therefore acknowledges the influence of variables whose significance is hidden by other variables in the process of tree building (Steinberg & Golovnya, 2007). In contrast to regression analysis, which investigates the continuous relationships between variables, CART can examine both continuous and categorical data. CART results in a crisp classification (e.g. salt-affected or unaffected) rather than a continuous model that is fuzzy in nature and difficult to interpret.

Unlike many other "black box" supervised classifiers, CART is transparent as the contribution of specific features to the classification result can be visualized and inspected. In addition, the decision tree that CART produces can be used to generate a rule set which can be manipulated or modified to accommodate certain conditions. It can also be transferred to other regions, which makes it ideal for developing a salt accumulation monitoring solution.

5.2.5 Results and discussion

The spectral responses of vegetation in salt-affected and unaffected areas based on the WV2 bands are shown in Figure 5.9. The reflectance of the salt-affected areas in the red band is higher than that of unaffected areas. This suggests that the vegetation in salt-affected areas is growing less vigorously. However, the difference between salt-affected and unaffected responses in the NIR band is very small, which contradicts the findings of Wang *et al*. (2002), Tilley *et al*. (2007) and Zhang *et al*. (2011). A likely explanation for this is the influence of background soil. Lucerne has a small canopy cover and background features (e.g. bare ground and salt encrustations) are more likely to be exposed when plant wilting occurs. During the field survey some salt precipitation was observed in salt-affected areas and since salt encrustations have high reflectance in the NIR spectrum (Abood *et al*., 2011; Elnaggar & Noller, 2009; Iqbal, 2011; Khan *et al*., 2005; Metternicht & Zinck, 2003; Setia *et al*., 2013; Sidike *et al*., 2014), this could have contributed to the relatively high reflectance in this band. Nevertheless, the relatively large difference in reflectance in the red band suggests that a VI that makes use of the ratio between the red and NIR bands has the potential to distinguish between salt-affected and unaffected areas. However, the relatively high standard deviations (as indicated by the error bars in Figure 5.9) show that such an approach will not be successful in all cases.

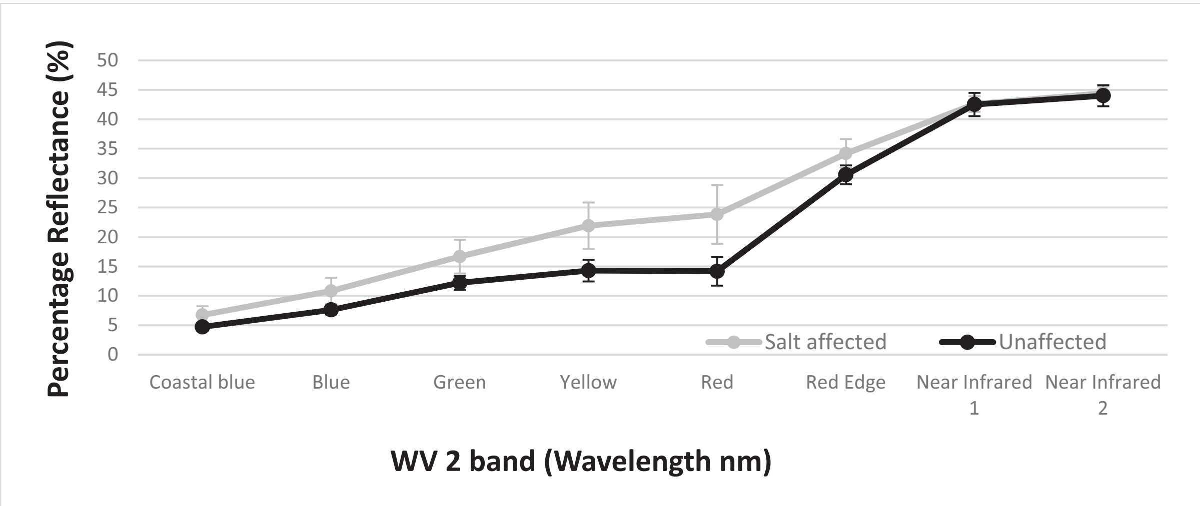

Figure 5.9 Spectral profiles of salt-affected and unaffected soils (error bars represent one standard deviation).

The regression results of models that produced the best R^2 values for each spatial resolution scenario are shown in Table 5.8. A strong relationship between the yellow band and EC values was observed, with R^2 values of 0.7261, 0.6915 and 0.7311 at 0.5, 2 and 6 m resolutions, respectively. This is attributed to the absorption of yellow light by vegetation (Zhang *et al*., 2011) and the high reflectance of yellow wavelengths by salt precipitation on exposed soils (Abood *et al*., 2011; Elnaggar & Noller, 2009; Iqbal, 2011; Khan *et al*., 2005; Metternicht & Zinck, 2003; Setia *et al*., 2013; Sidike *et al*., 2014). The S-curve that models this relationship is shown Figure 5.10(a). Despite the high R^2, it is clear from Figure 5.10(a) that the model becomes less reliable as EC increases. Considering the variability in radiance between images, it is also unlikely that the use of a model based on a single band will be robust enough for the operational identification of salt-affected areas in large irrigation schemes covered by multiple images. The transferability of this model to other areas is consequently questionable. VIs have been shown to be more robust and transferable as it makes use of relative measures such as band ratios (Asrar *et al.*, 1984; Bannari *et al.*, 1995). Figure 5.10 shows that some of the VIs that were considered in the regression analyses also produced relatively strong models. Figure 5.10(b), for instance, shows that the relationship between EVI (with NIR2 band) and EC at 6m resolution can be described using a compound curve with relatively strong predictive power (R^2 = 0.7045).

The VIs that make use of the yellow band (Equations 5.7 & 5.8) generally performed best when compared with the normal NDVI and SAVI indices (Equations 5.5 & 5.6). This is consistent with Abood *et al*. (2011) who found that the detection of salt-affected areas improved when the WV2 red band was substituted with the yellow band in the generation of VIs. The differences in R^2 between the yellow and second NIR band indices compared to the standard VIs, however, were statistically insignificant in this study. Only minor differences in R^2 values of the VI-based models were observed between 0.5 and 6 m spatial resolutions after which the R^2 value dropped significantly (Figure 5.10). This suggests that the greater spectral resolution of the WV2 image is superfluous in the creation of VIs.

Of all the texture features evaluated, B12 produced the strongest model at 0.5 m (R^2 = 0.766). The texture-based regression model outperformed the spectral-based models at all resolution scenarios except at 6 m. Figure 5.10(c) plots the relationship between the textures measure B12 and measured EC at 0.5 m resolution. This result is encouraging as texture measures are a spatial measurement relative to the size of its kernel only and thus theoretically less affected by radiometric variations. Texture should therefore produce models that are more robust and transferable.

The reduction of spatial resolution generally had a detrimental effect on the regression models, with most significant decreases between 6 and 10 m resolutions (mean R^2 of 0.7045 and 0.6007, respectively) and between 10 and 15 m resolutions (mean R^2 of 0.6007 and 0.4887, respectively). The pansharpening of the 2 m multispectral bands to 0.5 m improved the models based on the spectral and textural features, while the VI-based models were highly comparable to those generated from the original 2 m multispectral data.

The relatively poor performance of the models (Table 5.8) generated from 10 m and lower is attributed to the limited extents of salt-affected areas, as observed during the field surveys. This finding suggests that spatial resolutions of 6 m or higher are required. For texture-based models, the highest possible resolution should be used (preferably 0.5 m).

Table 5.8 Significant regression results from all spatial resolutions

Resolution	Bands			VIs			Texture			Mean
	R^2	Feature	Model	R^2	Feature	Model	R^2	Feature	Model	R^2
0.5 m	0.7261	Yellow	S	0.6680	EVI*	Compound	0.7661	B12 (red band)	S	0.720
2 m	0.6915	Yellow	S	0.6782	SAVI* no2	Compound	0.7169	B2 (red band)	S	0.6955
6 m	0.7311	Yellow	S	0.7045	EVI	Compound	0.6780	A4 (red band)	S	0.7045
10 m	0.5872	Red	S	0.5561	EVI	Compound	0.6590	B2 (red band)	S	0.6007
15 m	0.5120	Yellow	S	0.4430	EVI*	Compound	0.5110	B8 (red band)	Compound	0.4887
20 m	0.4400	Red Edge	Compound	0.2240	EVI*	Compound	0.3760	B10 (red band)	Cubic	0.3467

* with NIR2 band

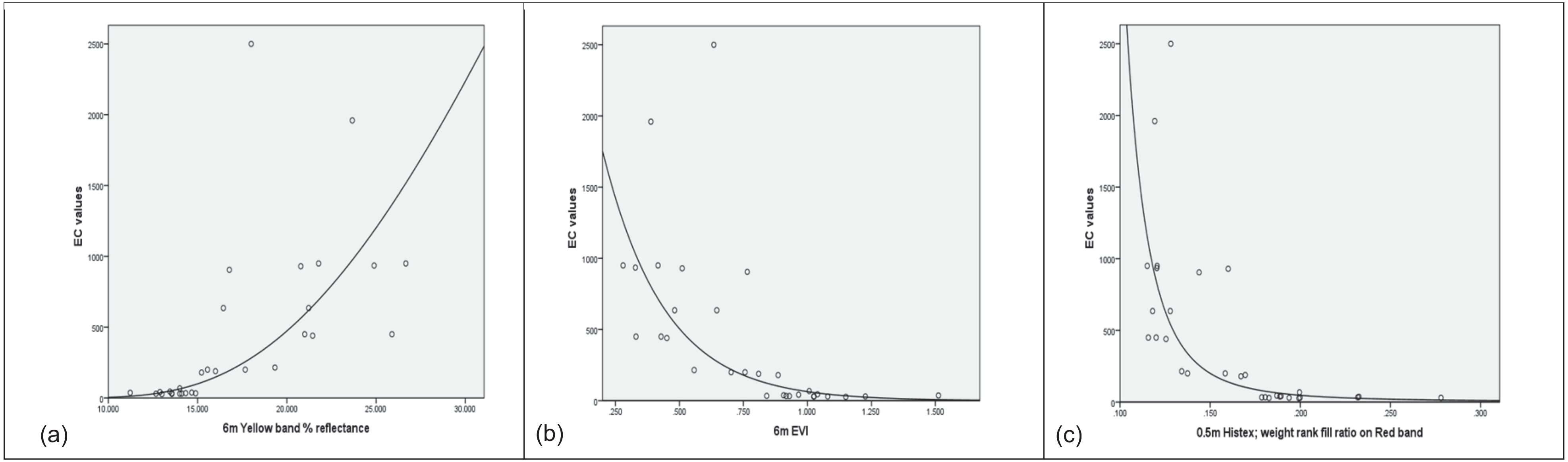

Figure 5.10 (a) S curve regression model (6 m Yellow band) (b) Compound regression model (6 m EVI) (c) S curve regression model (0.5 m B12).

The VIL results, as determined by CART, are summarized in Table 5.9. Of the 445 features, the VIs dominated the classification tree and, in contrast to the regression analysis, the texture features had no significant influence. From Figure 5.11 it is clear that CART produced a relatively good classification (ROC = 0.875; BRE = 0.278) although the classification tree only has one main splitter (NDVI no. 3 at 0.5 m resolution). Based on the VIL results, any of the VIs with 100% variable importance can be used with their specified split value to reproduce the same result (Table 5.9).

The features identified in Table 5.9 are all of 0.5 m spatial resolution, indicating the positive influence of pansharpening on the results. This result suggests that when a more precise (crisp) delineation between unaffected and salt-affected areas is needed, the higher resolution VIs are most effective. This is likely because a VI at 0.5 m resolution can accommodate a finer delineating line than, for instance, a VI at 6 m.

Table 5.9 Variable importance list of 445 features and split values

Feature	% Importance	Split values
EVI 0.5 m	100	0.31630
SAVI 0.5 m	100	0.64892
NDVI 0.5 m	100	0.43633
SAVI no. 2 0.5 m	100	0.63730
NDVI no. 3 0.5 m	100	0.428574
Band 5 0.5 m	89	16.39065

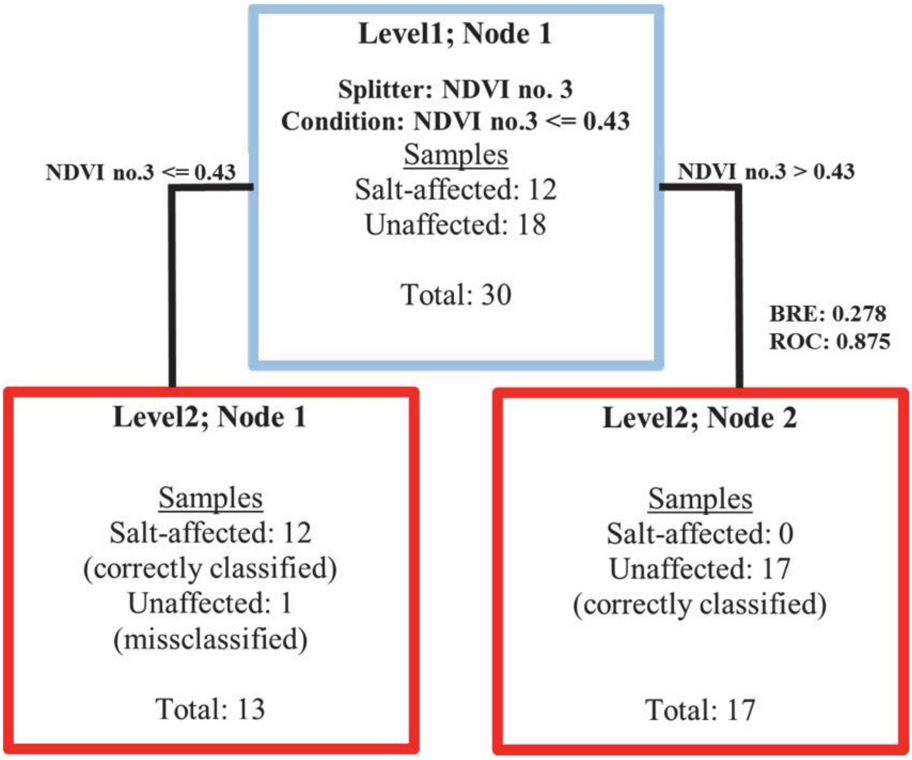

Figure 5.11 CART classification tree and descriptive statistics

More work is needed to determine to what extent the CART models can be transferred to other areas, as "over-fitting" (i.e. producing high accuracies on specific training data while failing to produce similar accuracies on other data) is a well-known limitation of decision tree classifiers (Schaffer, 1993). The performance of other machine-learning classifiers such as k-nearest neighbour (kNN), support vector machines (SVM), and random forests (RF) should also be evaluated.

5.2.6 Conclusions

In this section, 445 WV2-derived spectral and spatial (texture) features were analysed at 0.5, 2, 6, 10, 15 and 20 m resolutions to determine their potential for distinguishing between salt-affected and unaffected soils in an irrigated lucerne field. Regression analyses were carried out to investigate the relationships between the image features and EC values of 30 soil samples collected in the field. The results showed that there are significant and strong continuous relationships between EC and several of the features considered and that the yellow band, as well as a number of VI and texture features, produced the strongest models. Generally, the strength of these relationships diminished as the spatial resolution was reduced.

CART was used to better understand the importance of specific features for producing a categorical (i.e. crisp) output. The CART analysis identified VIs as the most important variables at the highest resolution of 0.5 m.

Overall, the regression analysis and CART results are very promising as they show that VIs generated at 6 m and higher resolution can potentially be used for the identification of salt accumulation in South African irrigation schemes. The results also suggest that high resolution texture features can potentially be used together with VIs for the indirect monitoring of salt-affected soils. Furthermore, the relatively high spectral resolution of the WV2 imagery is not critical as the VIs (based on red and NIR wavelengths only) performed relatively well compared to the performance of the individual bands.

Due to its relatively high cost, the operational use of WV2 imagery for regular monitoring of large areas is not viable. The results show that slightly lower spatial and spectral resolution imagery might produce comparable results. Notable candidates are SPOT-5 (2.5 m panchromatic; 10 m multispectral), SPOT-6 (1.5 m panchromatic; 6 m multispectral), RapidEye (5 m multispectral) and Sentinel-2 (10 m multispectral) data. Although SPOT-5 will soon be decommissioned, its large archive of imagery will be very useful for change analyses where historical baselines are required.

The models generated in this study only considered soil samples collected in a cultivated field with a single crop. It is well known that crops differ in their response to saline conditions and more work is needed to investigate how these variations will affect remote sensing methods. Plant stress observed with satellite imagery might also be the result of factors unrelated to salt accumulation (e.g. irrigation and fertilization). Such factors will have to be taken into consideration in a monitoring system. One possible solution is to make use of multi-temporal imagery to identify areas within fields that are consistently under stress. More work is, however, needed to investigate the value of such approaches for the identification of salt-affected areas in irrigated areas.

5.3 Remote sensing indirect approach: Vegetation monitoring at scheme level[5]

The models generated in the experiments of the previous section only considered soil samples collected in a cultivated field with a single crop. Given that crops differ in their response to saline conditions, an additional series of experiments were carried out in this section to investigate how these variations will affect the results. These experiments were carried out in the Vaalharts and Breede River study areas using slightly lower resolution SPOT-5 imagery. In addition to the image features assessed in section 5.2, soil and terrain data was also included in the analyses.

5.3.1 Study areas, data collection and pre-processing

Two study areas, namely Vaalharts and Breede River were selected for this component of the study (Figure 5.12).

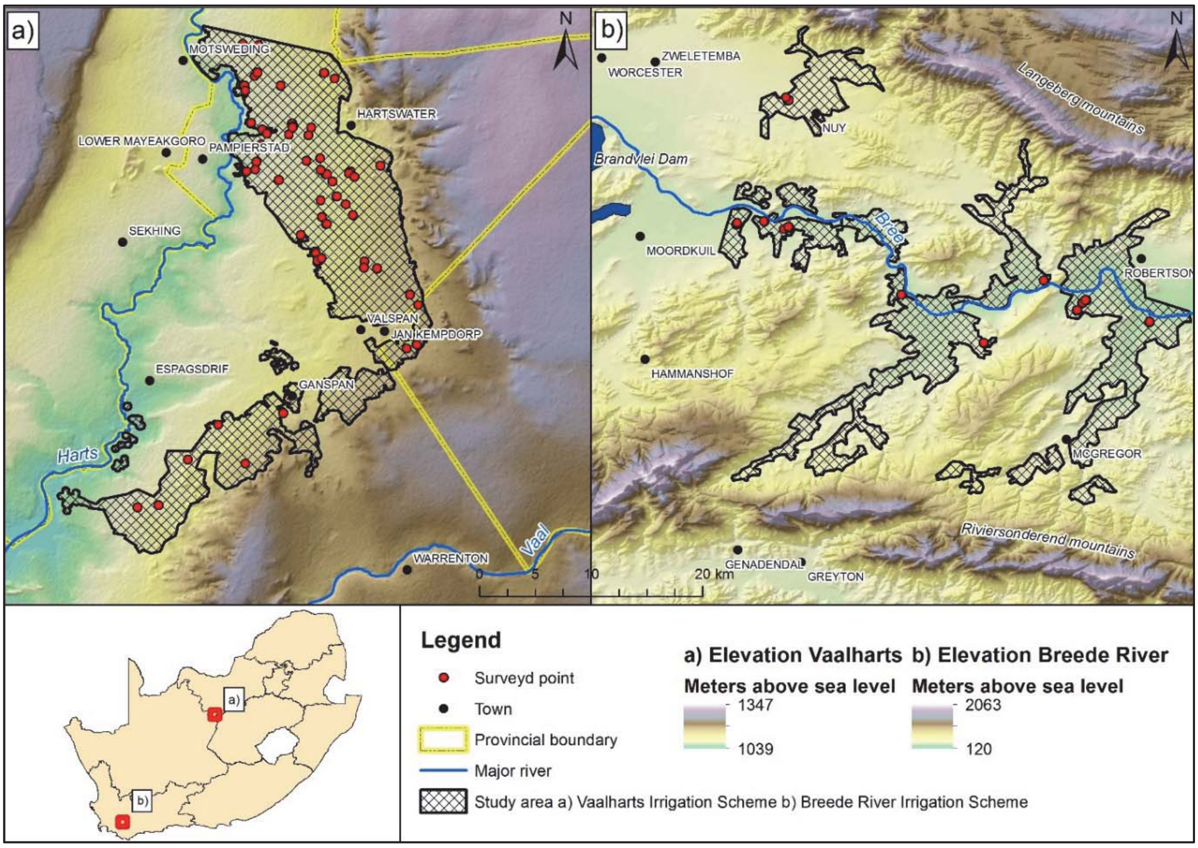

Figure 5.12 Vaalharts and Breede River study area map.

Image data from the time of maximum growth is optimal for indirectly discriminating between saline and non-saline conditions (Furby *et al*., 1995, 2010; Hick & Russell, 1990). Two SPOT-5 satellite images, dated 27 April 2012 (Vaalharts) and 16 January 2013 (Breede River), were acquired from the South African National Space Agency (SANSA). Although SPOT-5 imagery has limited spectral resolution (Table 2.5) it contains the red and near

[5]The content of this section was adapted from the MSc thesis of Jascha Muller and an article that was submitted for publication in a scientific journal.
.

infrared (NIR) bands required for the generation of most VIs. Based on the findings in section 5.2, the 2.5 and 10 m spatial resolutions of the SPOT-5 panchromatic and multispectral images, respectively, were considered to be adequate, particularly if the multispectral images are pansharpened (fused) to 2.5 m. The fusion of multispectral and panchromatic images has been shown to be an effective technique to optimize the spatial and spectral resolution of images (González-Audícana *et al*., 2004).

Geometric and radiometric corrections of all images were done using the software package PCI Geomatica (version 2013 SP2). A north-orientated implementation of the Gauss conform coordinate system (also known as the LO coordinate system), with central meridians 25º E and 19º E for Vaalharts and Breede River, respectively, was used. Nearest neighbour resampling was employed during orthorectification to preserve the original digital numbers (DN) (Campbell, 2007; Lillesand *et al*., 2004). Radiometric corrections were carried out using the ATCOR 2 mathematical model which converted the DNs into percentage reflectances. The *Pansharp* algorithm, as implemented in Geomatica, has been shown to preserve most of the spectral characteristics of the multispectral data in the resulting pansharpened image and was used to increase the 10 m resolution SPOT-5 multispectral data to 2.5 m.

A number of field surveys were carried out to collect suitable *in situ* data. Different sampling approaches were used to accommodate accessibility restrictions (e.g. canal systems and fencing). An attempt was made to include sites that represented as much as possible variation in terms of salt accumulation, soil types and crop types. A total of 69 and 48 samples were collected for Vaalharts and Breede River, respectively. Soil samples were collected by means of a soil auger and analysed for the electrical conductivity (EC_e) in a laboratory using the saturated paste technique. Differential GPS coordinates (10 cm accuracy), notes on the visual appearance of the immediate area, and in some cases photographs were also captured.

5.3.2 Feature set development

5.3.2.1 Vegetation indices

In addition to NDVI, SAVI and EVI-2 (see section 5.2.3.1), the general vegetation moisture index (GVMI) was also considered in this study as it optimizes the retrieval of vegetation water content and minimizes the disturbing effects of geophysical and atmospheric effects (Ceccato *et al*., 2002). GVMI makes use of the shortwave infrared band (SWIR) which distinguishes between variations in vegetation water content (Ceccato *et al*., 2002). GVMI is defined as:

$$GVMI = \frac{(N + 0.1) - (S + 0.02)}{(N + 0.1) + (S + 0.02)} \qquad \text{Equation 5.10}$$

where *N* is the reflectance in the NIR band and *S* is the reflectance in the SWIR band.

5.3.2.2 Image transformations

Two image transformations, namely PCA (see section 5.2.3.3) and intensity, hue and saturation (IHS) transformation, were considered in this study. The IHS (Carper, 1990) transform is a spectral domain procedure that transforms three image bands to IHS space. The three bands chosen as input to the IHS transform were red, green and NIR.

5.3.2.3 Image texture features

Image texture features, which can be described as a high local brightness variation from pixel to pixel in a small neighbourhood (Russ, 1999) of the different spectral bands, were considered as indirect indicators of salt accumulation. The observation of image texture is determined by two factors, namely the scale of variation and the scale of observation (Mather & Magaly, 2011). Spotty growth of vegetation due to salt accumulation (Howari, 2003) suggests a potential scale of variation. Given the relatively small extents of salt-affected areas in the study areas, the finest scale of observation (a 3x3 kernel) was used. Histex algorithms, as implemented in PCI Geomatica software, were implemented for processing first order histogram based texture layers for each of the four spectral bands and the first principal component (Dekker, 2003).

5.3.2.4 Soil/terrain indicator features

According to García Rodríguez *et al*. (2007) and Jenkin (1981), salts are more dominant in specific sediments and in particular landforms. Nussbaum *et al.* (2006), Furby *et al*. (1995) and McFarlane *et al*. (2004) used a digital elevation model (DEM) to evaluate terrain characteristics (e.g. height above streamline, relative height in a sub-catchment and landform position) that may influence the accumulation of salts. For this study soil type data for the study areas was acquired from the Agricultural Research Council (ARC) and a 2 m resolution DEM was generated using unrectified aerial imagery of 2009 and Geomatica 2013 software. The DEM and field boundaries were combined to derive relative height per field. The assumption was that salt accumulation will most likely occur in lower lying areas within fields.

Table 5.10 provides a summary of the 78 indirect indicator features considered for analysis. The feature set consists of the four SPOT-5 bands; four VIs, 12 image texture measurements per spectral band, the two principal components, three IHS image transforms and five features relating to soil and terrain.

5.3.3 Model building

A land cover classification and field boundary data obtained from the Department of Agriculture, Forestry and Fisheries (DAFF) was used to exclude non-cultivated areas (e.g. non-agricultural land uses and fallow fields) from the analyses. Given that increased reflectance in the visible and reduced reflectance in the NIR spectra has been shown to be consistent in the vegetation responses to salt stress (Hick & Russell, 1990; Tilley *et al*., 2007; Wang *et al*., 2002; Zhang *et al*., 2011), a spectral reflectance analysis was done to illustrate the effect of salt accumulation on vegetation growth in each study area. The samples collected during the field surveys were used to extract the reflectance values from the pansharpened image bands to create the profiles.

Regression analyses were carried out to investigate the statistical relationships between the indirect indicator features and salt-affected areas, mainly to provide a basis for comparison with the supervised classification results. The indirect indicator features (Table 5.10) were used as the independent variables, while measured EC values were defined as the dependent variable. Stepwise linear regression (SLR), partial least squares (PLS) regression and curve estimation regression were carried out using IBM SPSS (version 21) software. The curve estimations tested the fit between the EC values and the independent variables for various models (linear, logarithmic, inverse, quadratic, cubic, compound, power, s-curve, growth, exponential and logistic). The R^2 value was used to interpret the overall fit of the regression model and the size of the relationship between the two variables.

Table 5.10 Indirect indicator feature sets considered

Type	Feature	Total
Spectral bands	Green	4
	Red	
	NIR	
	SWIR	
VIs	NDVI	4
	SAVI	
	EVI2	
	GVMI	
Texture	Energy	60
	Entropy	
	Kurtosis	
	Mean Deviance	
	Mean Deviance Median	
	Mean Euclidean distance	
	Mean	
	Median	
	Normalized Coefficient	
	Skewness	
	Variance	
	Weight rank fill	
Image transformations	PCA band 1	5
	PCA band 2	
	Intensity	
	Hue	
	Saturation	
Soils	Soil type and/or	2
	Irrigation potential	
Terrain	Height	3
	Slope	
	Relative height deviation	
Total number of features		78

The regression analyses were followed by a series of categorical (binary) supervised classifications using the indirect indicator features as input. For this purpose, the EC values of the samples were split into two distinct classes (salt-affected and unaffected) using a threshold of 400 mS/m in accordance with the Soil Science Society of America (Bresler *et al.,* 1982; SSSA, 2007). Samples with EC values equal or higher than this threshold were regarded as being salt-affected while all samples with lower EC values were classified as being unaffected.

Because it is known that some classifiers are sensitive to high feature dimensionality, the CART and RF algorithms, as implemented in the Salford Predictive Modeller Software Suite, were used to identify the most important indirect indicators of salt accumulation at scheme level. CART is a robust decision tree classifier designed for data mining and predictive modelling while RF as defined by Breiman (2001) is an ensemble of unpruned CART-like tree classifiers. Unlike CART and other common DT classifiers, RF is less sensitive to over fitting (Breiman, 2001) and has been shown to be an effective feature selection tool. Although it has been shown that the use of CART and RF is not ideal for selecting features when dissimilar classifiers (e.g. ML, SVM, NN) are used, many examples exist where these algorithms have successfully been implemented for feature dimensionality reduction (Cutler *et al*., 2007; Gislason *et al*., 2006; Laliberte *et al*., 2007; Yu *et al*., 2006; Myburgh & Van Niekerk, 2013).

All the features in Table 5.10 were used as predictor variables in the feature selection process. The resulting VILs summarize the contribution of a particular feature to the classification success and give recognition to the variables whose significance is hidden by other variables in the process of tree building (Steinberg & Golovnya, 2007). The VIL's essential function is to reduce the feature dimensionality and computational requirement while preserving the overall accuracy of the classification (Laliberte *et al*., 2007; Yu *et al*., 2006).

The supervised classifications were carried out in an object based image analysis (OBIA) paradigm. The main advantage of an OBIA approach is that the feature values at each surveyed point and its immediate neighbourhood are considered during the training and classifying process (Blaschke & Strobl, 2001; Flanders *et al.,* 2003; Hay & Castilla, 2008). Objects were generated using the multi-resolution image segmentation algorithm as implemented in eCognition software. The same set of objects was used for each supervised classification implementation. Each of the six supervised classifiers was trained separately using different feature sets (see section 5.3.4.4). The classifiers were trained using 60% of the reference data, while the rest was used for accuracy assessment purposes. The training and accuracy assessment sample sets were kept consistent for all the classifiers.

Six supervised classification algorithms (Table 5.11) were evaluated. Customized software developed in C++ using libSVM and OpenCV libraries was used for this purpose (Myburgh & Van Niekerk, 2014a). SVM is known for its superior results in classification accuracy when compared to less sophisticated (e.g. MLC and NN) classifiers (Mountrakis *et al*., 2011; Myburgh & Van Niekerk, 2013, 2014b; Pal & Mather, 2005; Tzotsos & Argialas, 2008). RF (aka Random Trees) is a relatively new classifier in the field of remote sensing and has been shown to compare well, and even outperform SVM (Bosch *et al*., 2007; Novack *et al*., 2011; Pal, 2005).

Table 5.11 Supervised classifiers considered and their implementations

Classifier	Library
Support Vector Machine (SVM1)	Libsvm 3.2 (Chang & Lin, 2011)
Support Vector Machine (SVM2)	OpenCV 2.4.10 (Bradski, 2000)
Nearest Neighbour (NN)	OpenCV 2.4.10
Maximum likelihood classification (MLC)	OpenCV 2.4.10
Decision Trees (DT)	OpenCV 2.4.10
Random Forest (RF)	OpenCV 2.4.10

5.3.4 Results and discussion

5.3.4.1 Spectral analysis

Figure 5.13 shows the spectral profiles of salt-affected and unaffected crops in the Vaalharts irrigation scheme. Compared to healthy crops, salt-affected crops generally have higher reflectance in the blue to red region of the electromagnetic spectrum, while reflectance is lower in the near and shortwave infrared regions. This suggests that vegetation in salt-affected areas experiences weaker growth (vegetation vigour) than in unaffected soils. This result is in accordance with the findings of Hick & Russell (1990), Tilley *et al*. (2007), Wang *et al*. (2002) and Zhang *et al*. (2011) and demonstrates that VIs that make use of the ratio between the red and NIR bands have the potential to distinguish between salt-affected and unaffected crops in Vaalharts. However, the relatively high standard deviation in the NIR region (indicated by error bars in Figure 5.13) suggests that an approach using VIs only might not be successful in all cases.

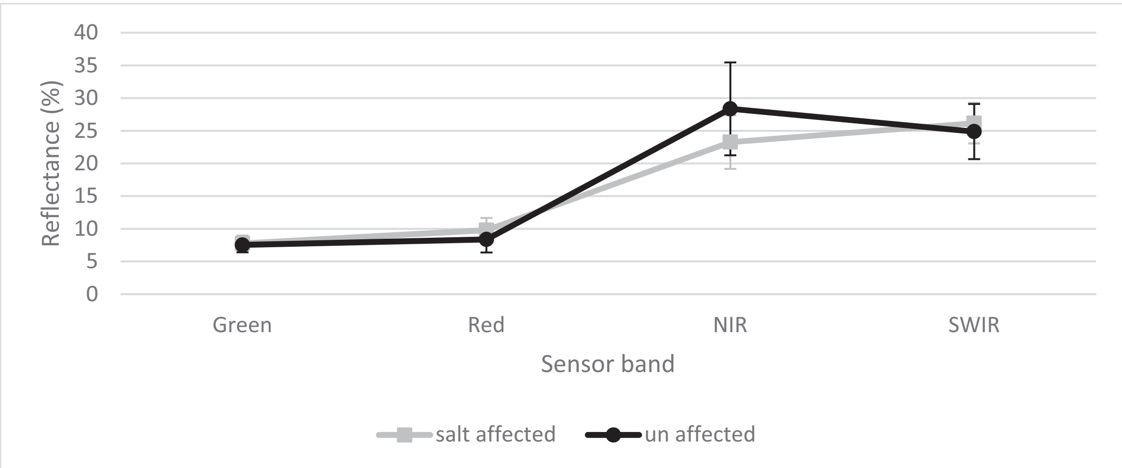

Figure 5.13 Spectral profiles of salt-affected (n = 19) and unaffected (n = 50) soils as extracted from the SPOT-5 image (Vaalharts) with standard deviation error bars.

The spectral profiles of the samples taken in the Breede River irrigation scheme (Figure 5.14) differ from the expected profile in that salt-affected samples generally have higher reflectance in all the bands. This is most likely due to the presence of background soil reflectance, as the predominant crops in Breede River are wine grapes and pruning fruit trees which are planted in rows and separated by bare soil for easy access during harvesting. In addition, visible salt encrustations on bare soil are known to have high reflectance in the visible and NIR regions (Abood *et al.*, 2011; Elnaggar & Noller, 2009; Iqbal, 2011; Khan *et al*., 2005; Metternicht & Zinck, 2003; Rao *et al*., 1995; Setia *et al*., 2013; Sidike *et al*., 2014), which may further contribute to the atypical shape of the salt-affected profile in Figure 5.14. This result suggests that VIs will be less effective for differentiating between salt-affected and unaffected crops in the Breede River irrigation scheme and that other image features such as intensity, principal components, or even the image bands themselves, may provide better discrimination of these classes.

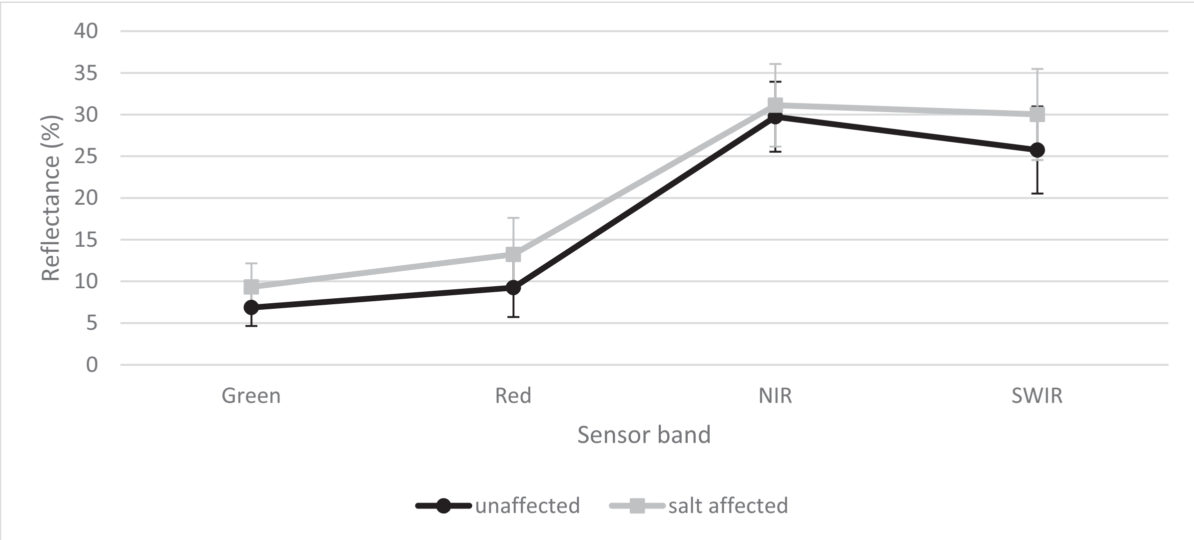

Figure 5.14 Spectral profiles of salt-affected (n = 23) and unaffected (n = 25) soils as extracted from the SPOT-5 image (Breede River) with standard deviation error bars.

5.3.4.2 Regression modelling

A series of regression modelling procedures were carried out to identify the individual or combinations of image, soil and terrain features that best relate to salinity levels (as represented by EC). For both study areas, none of the singular (curve fit) and multiple linear regression models (SLR, PLS) produced any significant results and none of the 78 features paired with the EC values produced a model with an R^2 value greater than 0.4. A likely explanation for the poor performance of the regression modelling in this study is that different crops have varying tolerances to saline conditions (Hanson *et al*., 2006; Zhang *et al*., 2011). Hanson *et al*. (2006) compiled a database of crop types and their “maximum root zone salinity at which 100% yield occurs” (Threshold A) and a “reduction in relative yield per increase in soil salinity” (Slope B) rates. The figures of A and B for the dominant crops planted in the two selected irrigation schemes are listed in Table 5.12. The table also includes a qualitative rating for each crop type, based on the interpretation of A and B. Apricots are the most intolerant to high levels of salt accumulation, with a relatively low threshold value (A = 160) and steep slope (B = 24), while barley is the least sensitive to saline conditions (A = 800; B = 5). In general, the tolerances of the dominant crops produced in Vaalharts are more variable, with A having a standard deviation of 244 mS/m compared to

40 mS/m in the Breede River. There is consequently a substantial difference in salt tolerance levels of the crops produced in the two irrigation schemes.

Better results would likely have been obtained if each individual crop type were considered independently. However, this would require accurate crop type data, which is often not routinely available at scheme level. Also, the different growth stages of crops (even of the same type) planted at different times and in separate fields is also a source of variation and probably had a negative impact on the success of regression models.

Table 5.12 Salinity threshold and slope values for a 100% yield potential of dominant crops in the Vaalharts and Breede River irrigation schemes

	Crop type	100% Yield (A) mS/m	Slope (B)	Classification
Vaalharts	Maize	170	12	Moderately intolerant
	Wheat	600	7.1	Moderately tolerant
	Lucerne	200	7.3	Moderately intolerant
	Groundnuts	320	29	Moderately intolerant
Breede River	Grapes	150	9.6	Moderately intolerant
	Peaches	170	21	Intolerant
	Apricots	160	24	Intolerant
	Tomatoes	250	9.9	Moderately intolerant

5.3.4.3 Feature selection

It is clear from the VIL in Table 5.13 that VIs played an important role in the CART and RF analyses of Vaalharts, confirming the observations made in Figure 5.13. Texture measures also featured strongly in this irrigation scheme.

Table 5.13 Variable importance list for Vaalharts

CART		Random Forest	
Feature	**Importance %**	**Feature**	**Importance %**
EVI2	100	Histex, Variance algorithm; Red layer	100
Histex, Median algorithm; NIR layer	59	SAVI	90
SAVI	52	Histex, Median algorithm, NIR layer	83
NDVI	52	NDVI	82
Histex, Energy algorithm; NIR layer	45	GVMI	77
Histex, Mean algorithm; NIR layer	45	Histex, Mean deviation algorithm; Red layer	74

All of the important indirect indicators of salt accumulation in Breede River relate to texture measures (Table 5.14). Although it was expected (based on the spectral profiles in Figure 514) that VIs will not feature as strongly as in Vaalharts, the strong influence of texture over other features (e.g. intensity and principle components) was unforeseen. At closer inspection it was determined that the importance of texture measures can be attributed to the woody vines and orchards that make up the majority of the crops in the Breede River irrigation scheme. Because these crops are planted in rows, they are characterized by high levels of image texture. A reduction in biomass caused by saline conditions results in a dramatic reduction in texture as it increases reflectance from the soil background and thereby reduces the contrast between the planted and unplanted rows. This effect is amplified by the relatively low root zone salt tolerance threshold (A) and high deterioration slope (B) of these crops (Table 5.12) which can lead to rapid reductions in biomass under saline conditions.

Table 5.14 Variable importance list for Breede River

CART		**Random Forest**	
Feature	Importance %	Feature	Importance %
Histex, Mean euclidean distance algorithm; PCA layer	100	Histex, Mean deviation algorithm; PCA layer	100
Histex, Mean Euclidean distance algorithm; Red layer	90	Histex, Variance algorithm; PCA layer	83
Histex, Mean Euclidean distance algorithm; Green layer	89	Histex, Mean Euclidean distance algorithm; PCA layer	76
Histex, Mean Euclidean distance algorithm; SWIR layer	80	Histex, Mean Euclidean distance algorithm; Green layer	72
Histex, Variance algorithm; Red layer	80	Histex, Mean Euclidean distance algorithm; Red layer	68
Histex, Variance algorithm; Green layer	79	Histex, Mean deviation algorithm, Red layer	66

5.3.4.4 Supervised Classification

Each of the six supervised classifiers were applied to different sets of input features (Table 5.15), namely: all the features (Feature Set A); only the spectral bands (Feature Set B); only the VIs (Feature Set C); only the texture measures (Feature Set D); and a combination of the image transformations, soils and terrain features (Feature Set E). Two additional feature sets (F and G), representing the first six features of the VILs generated by CART and RF respectively, were also used as separate inputs to the classifiers.

The mean overall accuracy (OA) and Kappa coefficient (KC) for each feature set are listed in Table 5.15 and Table 5.16 for Vaalharts and Breede River, respectively.

Table 5.15 Summary of average and individual classifiers for Vaalharts

Features (Feature Set)	SVM 1		SVM 2		NN		ML		DT		RF		Mean		STDDEV	
	OA	KC	OA	KC	OA	KC	OA	KC	OA	KC	OA	KC	OA	KC	OA	KC
All features (A)	80.5	0.591	76.6	0.480	79.8	0.597	63.7	0.086	86.5	0.711	85.6	0.700	78.8	0.527	7.54	0.212
Bands (B)	70.6	0.388	68.7	0.360	79.6	0.576	69.4	0.395	64.6	0.202	77.3	0.529	71.7	0.408	5.18	0.121
VIs (C)	77.9	0.554	70.3	0.404	59.8	0.136	72.7	0.488	76.1	0.482	76.9	0.509	72.3	0.429	6.15	0.138
Texture (D)	82.5	0.622	82.0	0.604	79.8	0.597	62.9	0.062	81.4	0.599	77.3	0.500	77.7	0.497	6.83	0.199
Image transforms, terrain and soil data (E)	84.6	0.658	78.0	0.502	87.4	0.733	80.8	0.605	78.1	0.529	78.9	0.553	**81.3**[a]	0.597	3.57	0.079
CART VIL (F)	77.8	0.557	78.7	0.562	58.6	0.077	71.1	0.463	69.5	0.295	80.4	0.588	72.7	0.424	7.44	0.183
RF VIL (G)	69.3	0.344	69.9	0.384	78.8	0.570	63.8	0.232	**92.9**[c]	0.854	82.2	0.628	76.2	0.502	9.67	0.207
Mean	77.6	0.53	74.9	0.47	74.8	0.47	69.2	0.33	78.4	0.52	**79.8**[b]	0.57				
Standard deviation	5.3	0.11	4.8	0.09	10.2	0.24	6.0	0.19	8.9	0.21	3.0	0.07				

[a] Best feature set result; [b] Best classifier result; [c] Best classification result

Table 5.16 Summary of average and individual classifiers for Breede River

Features (Feature Set)	SVM 1		SVM 2		NN		ML		DT		RF		Mean		STDDEV	
	OA	KC	OA	KC	OA	KC	OA	KC	OA	KC	OA	KC	OA	KC	OA	KC
All features (A)	83.2	0.641	83.2	0.641	86.9	0.735	84.2	0.685	72.5	0.489	72.5	0.489	80.4	0.613	5.72	0.094
Bands (B)	88.4	0.764	75.1	0.530	84.2	0.685	81.9	0.643	88.4	0.764	88.4	0.764	84.4	0.691	4.86	0.086
VIs (C)	79.3	0.600	79.3	0.600	72.0	0.481	74.8	0.525	70.5	0.458	70.5	0.458	74.4	0.520	3.73	0.061
Texture (D)	**91.6**[c]	0.810	91.3	0.804	86.9	0.735	88.4	0.764	72.5	0.489	76.8	0.558	**84.6**[a]	0.693	7.31	0.124
Image transforms, terrain and soil data (E)	75.1	0.530	79.3	0.600	83.7	0.669	85.9	0.717	72.8	0.493	80.8	0.624	79.6	0.605	4.57	0.077
CART VIL (F)	83.1	0.606	83.1	0.606	84.9	0.643	83.6	0.616	79.8	0.535	78.5	0.483	82.2	0.582	2.24	0.055
RF VIL (G)	82.6	0.593	82.6	0.593	84.9	0.643	84.3	0.642	78.3	0.495	85.7	0.672	83.1	0.606	2.41	0.057
Mean	**83.3**[b]	0.65	82.0	0.62	**83.3**[b]	0.66	**83.3**[b]	0.66	76.4	0.53	79.0	0.58				
Standard deviation	5.1	0.09	4.7	0.08	4.8	0.08	4.0	0.07	5.8	0.10	6.0	0.11				

[a] Best feature set result; [b] Best classifier result; [c] Best classification result

In Vaalharts, Feature Set E (image transforms, terrain and soil data) produced the best classification result with a mean OA and KC of 81.3% and 0.597, respectively (Table 5.15). Both feature selection strategies (CART and RF) were not very effective, with Feature Set F (CART VIL) and Feature Set G (RF VIL) producing substantially lower accuracies (OA = 80.4% and 82.2%, respectively) when the full set of features were included as input to the classification algorithms (OA = 85.6). It might be that the feature selection process was too aggressive and that more than six features should have been included in the VIL. Also, the relatively high accuracy achieved when using the full feature set supports the findings of Myburgh and Van Niekerk (2014b), who showed that most of the classifiers considered (in particular SVM, DT and RF) are relatively insensitive to the so-called “curse of dimensionality”. Nevertheless, the best classification result for Vaalharts was when the DT classifier was applied on Feature Set G (RF VIL), achieving an overall accuracy of 92.9%.

On average, the most successful classifier in Vaalharts was RF, with a mean OA of 79.8% (Table 5.15). To our knowledge, RF has never been applied for identifying salt accumulation and this result suggests that this classifier holds much potential for this purpose. The relatively good performance of RF is attributed to their abilities to produce accurate classifications with limited training data (Ham *et al*., 2005; Mountrakis *et al*., 2011). RF is also non-parametric and consequently has the ability to perform well with data that is not normally distributed, as was the case in this study.

In the Breede River study area feature Set D (texture measures) was the most successful set of features, producing a mean OA and KC of 84.6% and 0.693, respectively (Table 5.16). Very similar accuracies were achieved when the original bands (Feature Set A) were used as input (OA = 84.4; KC = 0.691). Feature Set C (VIs) produced the poorest classification results in the Breede River area. This result was anticipated given the spectral profiles of the classes shown in Figure 5.14. Unexpectedly, Feature Set E, containing the image transformations (e.g. PCA and IHS), soil and height data, also produced relatively poor results. Although Figure 5.14 shows that salt-affected areas generally have higher reflectance responses in all bands, it seems that this relationship is not consistent (supported by the large standard deviations in Figure 5.14) and that the classifiers were unable to successfully separate the classes using image transformation features such as intensity and principal components. On average, SVM1, NN and ML produced the best classifications with a mean OA of 83.3% (Table 5.15), but the best classification result (91.6%) was achieved using the SVM1 classifier on the texture measures (Feature Set D). Generally, higher accuracies were achieved in Vaalharts than in Breede River. This was unexpected given the higher level of crop complexity in Vaalharts. The most likely explanation is the larger training dataset used for Vaalharts compared to Breede River as Myburgh and Van Niekerk (2014a) showed that training set size has a significant effect on classifier accuracies. More work is needed to determine the optimal number of samples required for achieving acceptable results.

Figures 5.15 to 5.18 show classification results for detailed areas within each of the irrigation schemes. Generally the agreement between the *in situ* data and the classification results is good (Figures 5.15 and 5.16), but based on extensive interpretations of the mapped results and inputs from local experts it was determined that the classifiers seem to overestimate salt-affected areas. For instance, the misclassifications in Figures 5.16 and 5.18 are mainly attributed to the difference in vegetation response between different crop types. Poor farming practices such as inadequate soil preparation or other soil related issues (e.g. soil compaction) can further lead to such misclassifications.

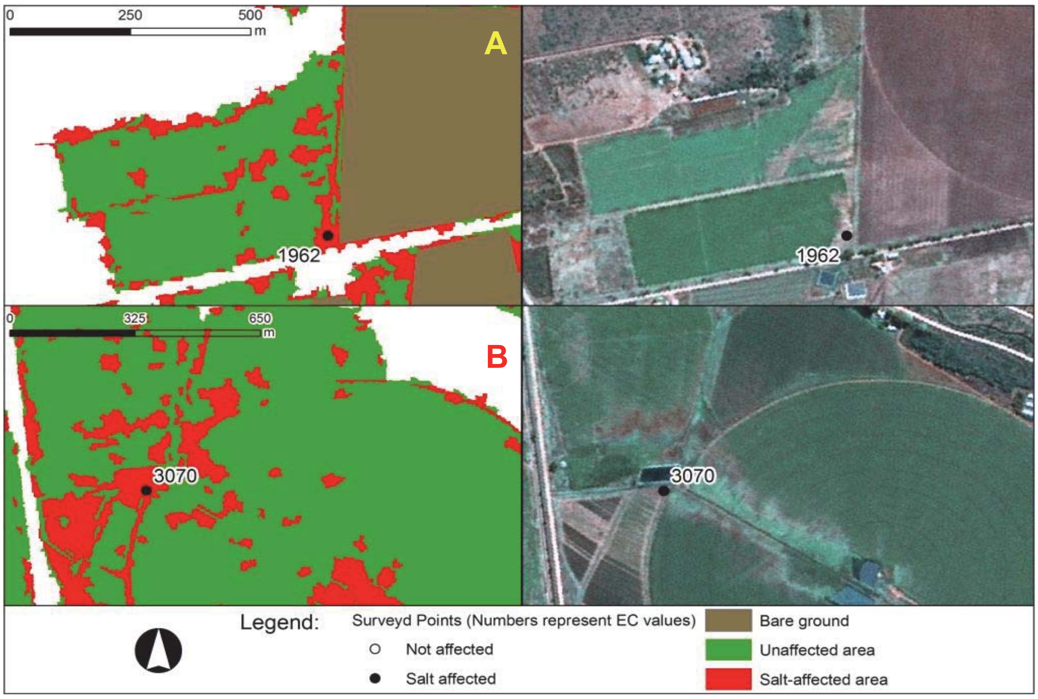

Figure 5.15 RF classification result using Feature Set C in two detail areas (a and b) within the Vaalharts irrigation scheme showing some misclassifications due to differences in vegetation response to saline conditions. False colour image combination: 2-1-3.

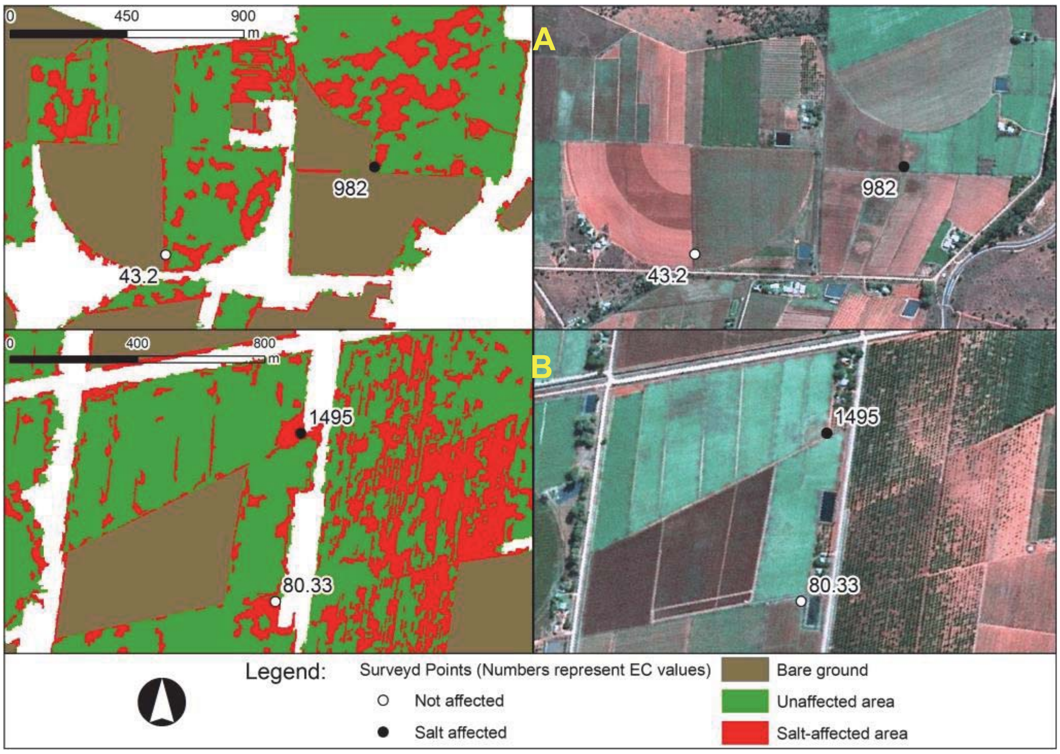

Figure 5.16 RF classification result using Feature Set C in two detail areas (a and b) within the Vaalharts irrigation scheme showing examples of over-classification of salt-affected areas

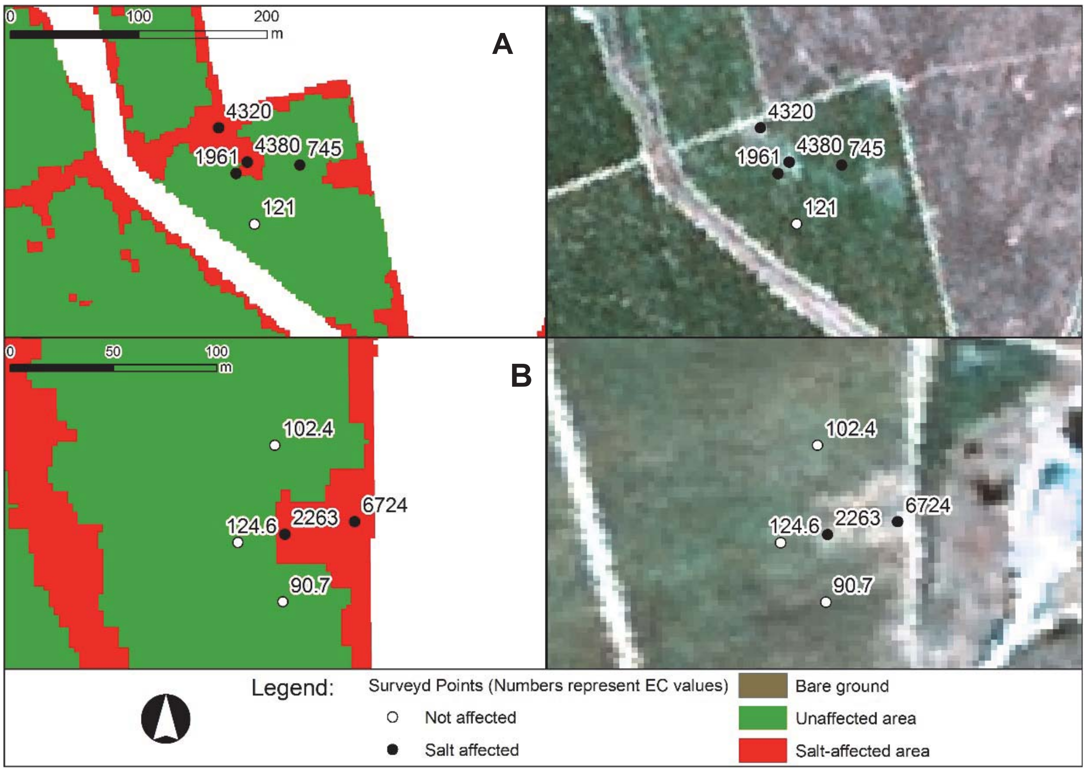

Figure 5.17 Two examples (a & b) of inaccurate delineations of affected areas in the Breede River irrigation scheme when the SVM classifier was used on the texture feature set (D).

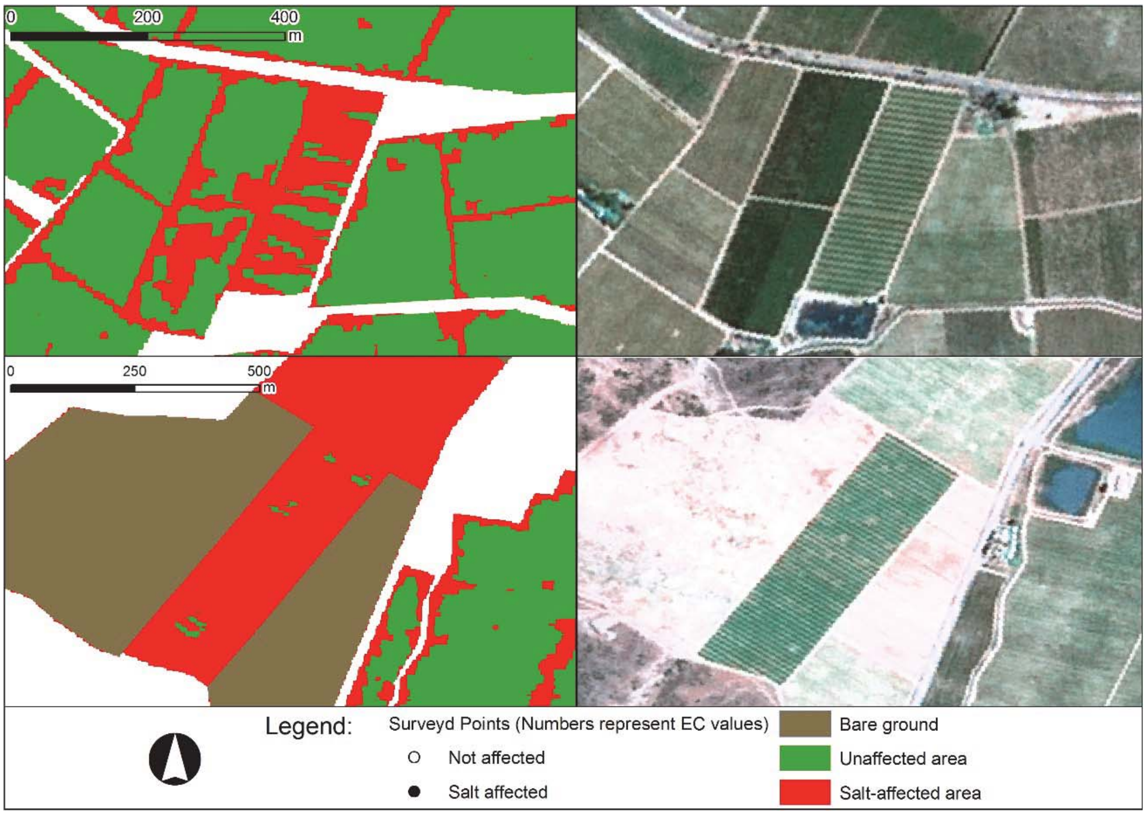

Figure 5.18 Two examples of over-classification of salt-affected areas in the Breede River irrigation scheme when the SVM classifier is applied to the texture feature set

A key finding of this study is that none of the feature sets and/or classification algorithms stood out as being superior for monitoring salt accumulation on irrigation scheme level. Due to the large variations in how different crops respond to saline conditions, the classifications tended to produce many false positives (over-classification). The accuracy levels also varied significantly according to training set size, which is problematic as the routine collection of large sets of soil samples is prohibitively expensive. This suggests that supervised classification methods can at best be used as a scoping mechanism for identifying salt accumulation in cultivated fields and that more work is needed to find more cost-effective solutions that can be applied for operational monitoring of salt accumulation in large, complex irrigation schemes.

One approach to overcome some of the limitations of supervised classification is to shift the focus from scheme level to field level. If each field (planted with a single crop type) can be evaluated relative to itself it would reduce the temporal and spatial variances of crop types and their salinity tolerances. Instead of using a supervised approach, an expert system approach to identify patches within fields that have significantly different spectral properties (compared to the rest of the field) would remove the need for training samples. Furthermore, a multi-temporal approach would help determine whether an area within a field is consistently experiencing poor vegetation growth. According to Furby *et al*. (1995), persistently poor vegetation cover over multiple growing seasons is more likely to be caused by salt accumulation than poor farming practices (Lenney *et al*., 1996). More work is needed to evaluate such an approach.

5.3.4.5 Conclusions

In this study a number of indirect indicators were examined for identifying areas in cultivated fields affected by salt accumulation at irrigation scheme level. Given that such areas tend to occur in small patches within fields, 2.5 m pansharpened SPOT-5 high resolution satellite imagery was evaluated in two distinctly different South African irrigation schemes (Vaalharts and Breede River).

A series of regression analyses were carried out to evaluate the continuous relationships between the surveyed *in situ* salinity levels (represented by EC) and 78 different geospatial features. The results showed that all the resulting regression models were insignificant, most likely due to the high levels of variation in the spectral responses of different crops types at different growing stages, coupled with their individual tolerances to saline conditions (Hanson *et al*., 2006; Zhang *et al*., 2011). A categorical, supervised classification approach to identifying salt-affected areas was also evaluated. CART and RF were used to reduce the dimensionality of the full feature set to two feature subsets, each containing the six most important features. Four other subsets of features (image bands; VIs; texture; image transformations, soil and terrain) were also used as input to six different classification algorithms (ML, NN, RF, DT and two implementations of SVM). The results showed that DT using the RF VIL as input (Feature Set G) produced the best result in Vaalharts (OA = 92.9%; KC = 0.854), while SVM1, using texture measures as input, produced the best result in Breede River (OA = 91.6%; KC = 0.81). The high levels of accuracy achieved suggest that supervised classification of image features (especially texture and VIs) holds much potential for monitoring salt accumulation in agricultural areas. However, based on visual interpretations of the results and inputs from local experts, it was determined that the classifications tend to overestimate salt-affected areas in both irrigation schemes and that the outputs can at best be used as a scoping mechanism for monitoring salt accumulation. More work, possibly using an expert system, multi-temporal approach at individual field level, is needed to find robust solutions for routine monitoring of salt accumulation in large complex irrigation schemes.

5.4 Terrain analyses at scheme level

The aim of the terrain analysis component was to evaluate the use of machine-learning algorithms and terrain data for mapping waterlogged and salt-affected areas in irrigated fields. Separability analysis (Jeffries-Matusita (JM) distance), statistical modelling (regression), classifications and regression trees (CART) and several classifiers were compared to determine the terrain features that best relate to affected soils. The classifiers encompassed the k-nearest neighbour (kNN), maximum likelihood (ML), support vector machine (SVM), decision tree (DT) and random forest (RF) classifiers. Several candidate features were derived from the elevation datasets, including aspect, slope, channel network base level, closed depressions, cross-sectional curvature, longitudinal curvature, LS factor, valley depth, vertical distance to channel network, flow accumulation, downslope distance gradient, real surface area, terrain ruggedness index, terrain surface texture, topographic position index, topographic wetness index (TWI), SAGA wetness index (SWI) and height above nearest drainage (HAND). The methods and features were evaluated in the Vaalharts and Breede River study areas (section 5.3.1).

5.4.1 Study areas

Two study areas, namely the Vaalharts and Breede River irrigation schemes were selected for this component of the study.

5.4.2 Data collection and preparation

5.4.2.1 Digital elevation models (DEMs)

The 5 m resolution Stellenbosch University DEM (SUDEM), developed by the Centre for Geographical Analysis (CGA), was acquired for each of the study areas. This DEM was developed using large-scale, error-corrected (1:10 000) contours, spot heights and the 30 m Shuttle Radar Topography Mission (SRTM) DEM as input (Van Niekerk, 2015). A combination of interpolation algorithms (e.g. the ANUDEM and Spline tools in ArcGIS software) as well as a newly-developed fusion algorithm was used to generate the SUDEM. The 30 m resolution Shuttle Radar Topography Mission (SRTM) DEM was also acquired for the study areas.

5.4.2.2 Stereoscopic aerial image collection

Stereo aerial photographs were acquired from the Chief Directorate: National Geo-spatial Information (CD: NGI) of South Africa in 12-bit true colour (RGB) format. Table 5.17 shows a summary of the acquired stereoscopic aerial photographs. The latest available photographs for the two study areas were captured in 2010. The photographs have a spatial resolution of 0.5 m and consist of three multispectral bands, namely blue, green and red. In total, 489 aerial photographs were acquired for Vaalharts and 1145 for Breede River.

Table 5.17 Details of aerial photographs obtained

Irrigation scheme	Blocks	Capturing date	Number of RGB photographs	Coordinate system
Vaalharts	2724D	2010	489	Lo25
Breede River	3319C 3319D	2010	615 530	Lo19

5.4.2.3 Digital surface model (DSM) generation

The stereoscopic aerial photographs were used to extract the DSM at a spatial resolution of 2 m for both study areas. This is possible as a displacement of objects is noted from one image to another when two or more satellite images or aerial photographs are captured of the same area from different perspectives. This is known as the stereoscopic parallax, which increases as the distance between the object and the observation point increases, allowing for distance or height measurements (Zomer *et al*., 2002; Fabris & Pesci, 2005; Campbell, 2007; Stal *et al*., 2013). PCI Geomatica 2013 was used to extract the DSMs from the stereoscopic aerial photographs.

Several software packages are available for extracting DSMs from remotely-sensed, stereo imagery. ERDAS Imagine 2011, PCI Geomatica 2012 and Inpho were quantitatively and qualitatively compared. The results showed that the DSMs generated using PCI Geomatica 2012 were superior to the other software considered. The updated version of PCI Geomatica 2012, namely PCI Geomatica 2013, was used in this study. This version produced much more detailed and accurate DSMs than in previous reports.

Capturing of ground control points (GCPs) was not required as triangulation information was obtained from CD: NGI. DEMs have been successfully extracted from both stereo aerial photographs (Fabris & Pesci, 2005; Stal *et al*., 2013) and stereo satellite imagery (Zhang & Fraser, 2008; Zhang & Gruen, 2006), producing high precision even in mountainous terrain (Zomer *et al*., 2002). Highest accuracies are usually found within open rural areas (Zhang & Fraser, 2008), with the largest errors found in tree, shadow and building covered areas (Zhang & Gruen, 2006; Zhang & Fraser, 2008; Stal *et al*., 2013).

5.4.2.4 Feature set development

A feature set consisting of 24 input variables derived from the SRTM DEM, SUDEM and a DSM were considered for differentiating salt-affected or water logged soils from unaffected soils (Table 5.18), producing a total of 72 terrain variables.

For processing purposes the high resolution SUDEM (5 m) and DSM (2 m) were down-sampled to 20 m. Vaze *et al*. (2010) showed that reducing the spatial resolution of a DEM (from 1-25 m) improved terrain analyses accuracies. Thompson *et al*. (2001) and found that by reducing DEM horizontal resolution, a smoother, less defined landscape with reduced curvatures and moderate slope gradients was produced. This is of particular importance in this study as groundwater flow tends to follow general topographic patterns and will therefore depend less on small-scale variations (Sorensen & Seibert, 2007). Although a reduction in the spatial resolution has been shown to have a negative effect on wetness indices, especially on the calculation of the upslope area (Sorensen & Seibert, 2007), the 20 m resolution of the down-sampled DEM was still relatively high compared to other studies.

Table 5.18 Features considered in the analyses

Type	Features	# of features
Elevation	SUDEM, SRTM DEM, stereoscopic aerial's DSM	3
Hydrology	Channel network base level, closed depressions, LS-factor, valley depth, vertical distance to channel network, catchment area, slope limited flow accumulation	7
Morphometry	Aspect, slope, convergence index, cross-sectional curvature, longitudinal curvature, relative slope position, mid-slope position, normalized height, slope height, standardized height, downslope distance gradient, real surface area, terrain ruggedness index, terrain surface texture, topographic position index	15
WIs	Topographic wetness index, SAGA wetness index	2

Several terrain features were evaluated for mapping salt-affected or waterlogged areas. This included the topographic wetness index (TWI) (Beven & Kirby, 1979; Grabs *et al*., 2009; Sorensen *et al*., 2006), height above nearest drainage (HAND) (Renno *et al*., 2008) and several terrain analysis (hydrology and morphometry) approaches provided by the software package known as the System for Automated Geoscientific Analyses (SAGA). Terrain analysis calculations performed within SAGA included aspect, slope, channel network base level (CNBL), closed depressions, cross-sectional curvature, longitudinal curvature, LS factor, valley depth, vertical distance to channel network (VDTCN), flow accumulation, downslope distance gradient, real surface area, terrain ruggedness index, terrain surface texture, topographic position index, TWI and the SAGA wetness index (SWI) (Böhner *et al*., 2002). More information on the functionality of SAGA can be found in Böhner *et al*. (2002, 2008).

Several studies have shown a strong relationship between soil EC and terrain variables, especially wetness indices (Elnaggar & Noller, 2009; Jafari *et al*., 2012; Taghizadeh-Mehrjardi *et al*., 2014). Sulebak *et al*. (2000) found that slope, profile curvature and aspect have the highest correlations with soil moisture (Thompson *et al*., 2001).

Several studies have applied and evaluated the utility of wetness indices (WIs) (Grabs *et al*., 2009; Sorensen *et al*., 2006). Two WIs were evaluated for this study, namely TWI and SWI. TWI is the most commonly applied topographic index and is defined as (Beven & Kirkby, 1979):

$$TWI = \ln \frac{a}{\tan ß} \qquad \text{Equation 5.11}$$

where α is the upslope area per contour length; and
tanß is the local slope of the ground surface.

The result from this calculation assigns high values to large upslope areas, which are expected to have high water availability, and low values to small upslope areas. Steep locations will be better drained and therefore receive small index values, whereas gently sloped areas will consist of higher index values (Sorensen & Seibert, 2007). TWI also assumes that the groundwater table is represented by the slope of the ground surface, and that precipitation and hydraulic conductivity are expected to be uniform across the study area (Sorensen & Seibert, 2007).

The SWI is a modified TWI and makes use of a modified catchment area calculation which does not treat the flow as a thin film. The resulting SWI calculation assigns a more realistic soil wetness value to grid cells situated in valley floor with a small vertical distance to a channel (Böhner *et al*., 2002).

The HAND model, first proposed by Renno *et al*. (2008), normalizes DEMs according to the distribution to vertical distances relative to the drainage channels (Renno *et al*., 2008; Nobre *et al*., 2011). The first step in the two-step process is to create a hydrologically coherent DEM, define flow paths and delineate the channel network. The second step makes use of the drainage network and the local drainage directions to produce a nearest drainage map (Renno *et al*., 2008; Nobre *et al*., 2011). A more detailed description on the workings of the HAND model can be found in Renno *et al*. (2008) and Nobre *et al*. (2011). The HAND hydrological model has been successfully used to classify terrain attributes related to local soil water conditions (e.g. water table depth, waterlogging) (Renno *et al*., 2008; Nobre *et al*., 2011) and watershed mapping (Cuartas *et al*., 2012).

5.4.2.5 Separability analysis

Feature selection methods can improve the accuracy of image classifications (Myburgh & Van Niekerk, 2013; Lu & Weng, 2007). This is especially true when the number of features is disproportional high compared to the number of training samples (Myburgh & Van Niekerk, 2013; Pal & Mather, 2005; Oommen *et al*., 2008). The SEaTH (SEparability and THresholds) software package was employed to select the most important terrain features. This makes use of the Jeffries-Matusita (JM) distance to identify the best features for class separation (Nussbaum *et al*., 2006). The JM distance is defined as (Nussbaum *et al*., 2006):

$$J = 2(1 - e^{-B}) \qquad \text{Equation 5.12}$$

where J is the JM distance; and
B is the Bhattacharya distance.

The Bhattacharya distance (B) is the mean and standard deviation of the training samples of the two classes (Bhattacharya, 1943). The J value can range from 0 to 2; J = 2 shows that two classes are separable due to being completely uncorrelated, whilst completely correlated classes will produce a low J value (J = 0). Therefore, the lower the value of J the higher the number of misclassified objects will be Nussbaum *et al*., 2006; Gao *et. al*., 2011; Heumann, 2011). According to Nussbaum *et al*. (2006) and Heumann (2011), a J value less than 1 indicates a requirement for new training data. A J value less than 1.7 shows poor separability and greater than 1.9 shows good separation between classes. A J value of 2 indicates perfect intra-class separation (Nussbaum *et al.,* 2006).

SEaTH first identifies the features that provide the highest separability between classes and then establishes a threshold value that best separates each of the classes (Nussbaum *et al*., 2006, Gao *et al.,* 2011; Heumann, 2011). Because the JM distance assumes that the sample values are normally distributed within classes, the threshold value might be substantially different when the sample values are not normally distributed, but the separability measure may still be valid (Gao *et al*., 2011). A more detailed discussion on the JM distance measures can be found in Nussbaum *et al*. (2006).

5.4.2.6 Statistical modelling

Regression analyses were carried out using IBM SPSS v20.0 to statistically analyze the relationship between soil EC and the terrain features. Linear, logarithmic, inverse, quadratic, cubic, power and exponential regression models were implemented. Stepwise multiple regression and partial least squares (PLS) analyses were also performed. Stepwise multiple regression fits an observed dependent variable using a linear combination of independent variable by simultaneously removing unimportant variables. PLS regression reduces a large number of measured collinear spectral variables to a few non-correlated latent variables by utilizing a bilinear calibration method using data compression (Hansen & Schoerring, 2003). A linear relationship is specified between a set of dependent variables and predictor variables, thereby extracting the orthogonal predictor variables accounting for as much of the variation of the dependent variables as possible (Cho *et al*., 2007).

5.4.2.7 Supervised classification

Supervised classification, which is the process of using samples of known identity to classify cases of unknown identity (Campbell, 2007; Rees, 2001), was also evaluated. Several classifiers were considered, including the kNN, ML, SVM, DT and RF (see section 2.3.2.2). A total of 125 soil samples were used for training the classifiers in the Vaalharts study area, while 43 soil samples were used for Breede River classifications. A total of 50 and 20 samples were kept aside for determining the accuracy of the classifications in the Vaalharts and Breede River study areas, respectively.

The kNN, SVM, DT and RF classifications were performed within eCognition 8.9, which makes use of OpenCV implementations of the classifiers (Bradski, 2000). ML was applied in ENVI 5.0. A pixel-based approach was followed during the classifications to avoid distorting the values of the training features. To avoid ties with the kNN classifier, only odd numbers were applied (Campbell, 2007). This included a k value of one, three and five. The number of active variables for RF, which is the number of randomly selected features used to find the best splits at each node, was set to three. The number of trees was set to 100. As recommended by Hsu *et al*. (2010), the kernel type was set to the radial basis function for the SVM classifier. Default parameters were applied for the ML and DT classifiers.

5.4.2.8 Accuracy assessment

Maps were created from the rule-based and supervised classifications to identify affected areas within the study areas. Confusion matrices were used to calculate the overall accuracy (OA), producer accuracy (PA) and user accuracy (UA). The Kappa coefficient (KC) and the receiver operating characteristic (ROC) curve were also calculated.

5.4.3 Results

5.4.3.1 Separability analysis results

The gradient dataset derived from the SUDEM attained the highest relationship (J = 0.36) to EC in the Vaalharts study area. Given that the J value is much lower than the required 1.8, this result indicates that the relationship is poor or that the training data was not insufficient (Nussbaum *et al.*, 2006; Heumann, 2011). Although separability improved in the Breede River using the flow accumulation raster derived from the SUDEM, the resulting J value of 1.27 was still not high enough to expect a good classification. From the separability analysis results it was concluded that a classification involving a simple threshold approach will not produce an accurate classification in either study area.

5.4.3.2 Regression modelling

Slope height derived from the SRTM DEM (30 m) produced the best regression model (R^2 = 0.711, p <0.01) in the Vaalharts study area. The resulting cubic model is defined as:

$$EC = b_0 + (b_1 \times x) + (b_2 \times x^2) + (b_3 \times x^3) \qquad \text{Equation 5.12}$$

where EC is the predicted soil EC;
x is the slope height derived from the SRTM DEM;
b0 = 5188.408; b1 = 0.0; b2 = -961.625; and b3 = 155.546.

Figure 5.19 compares this model to the slope height dataset derived from SRTM DEM and measured soil EC (mS/m) values. A large proportion (85.8%) of unaffected samples have a slope height less than 4 m.

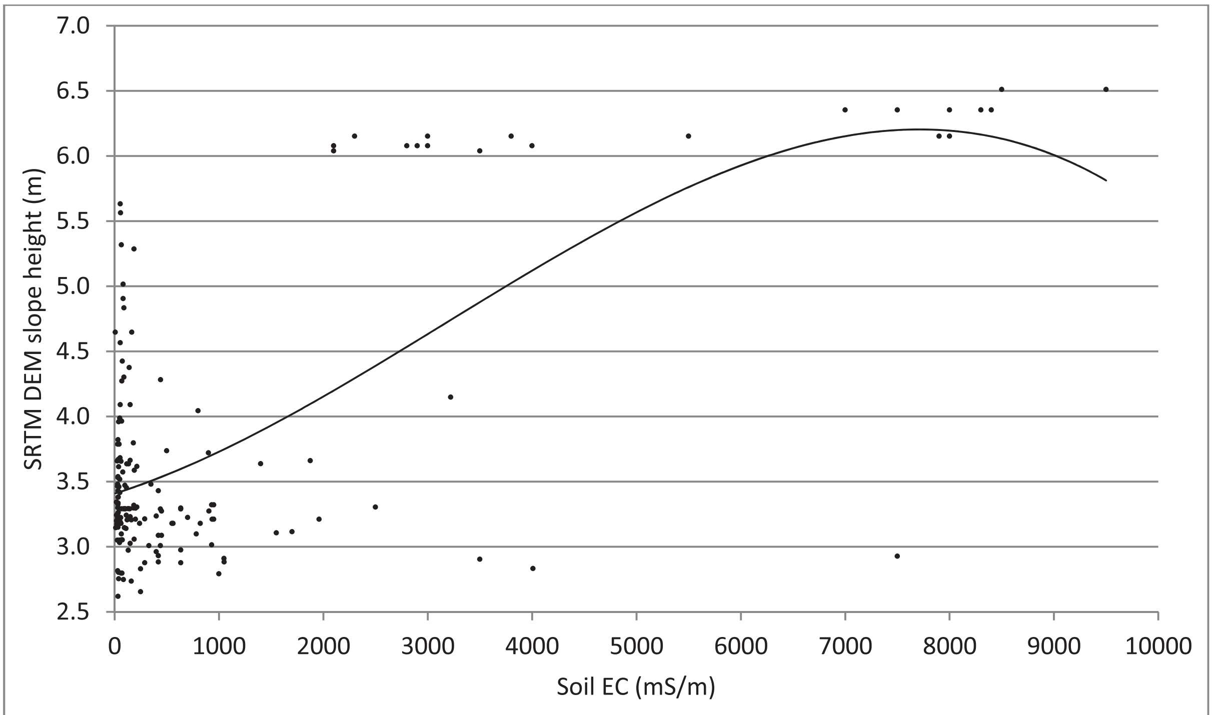

Figure 5.19 Cubic relationship between slope height and soil EC_e in the Vaalharts study area.

Multistep and PLS regression was also performed on all features, but did not improve the results. The regression modelling in the Breede River study area did not produce good results, with a cubic model of the vertical distance to channel network (VDTCN) dataset, derived from the SUDEM, achieving the best fit ($R^2 = 0.153$, $p < 0.05$).

The best model generated for each of the study areas was implemented and a threshold of 400 mS/m was used to discriminate between salt-affected and unaffected areas. The resulting maps were included in the classification accuracy assessments.

5.4.3.3 CART rule sets

Figure 5.20 shows the optimal tree from the CART analysis for Vaalharts. Each of the features included as splitters were derived from the SUDEM, namely mid-slope position (MSP), valley depth and channel network base level (CNBL). Low MSP values (≤0.73) were classed as salt-affected, with high valley depth values (>1.69) classed as unaffected. The final split was performed on the CNBL feature with a threshold value of 1107.82. High values were classed as salt-affected (>1107.82) and low values as unaffected (≤1107.82).

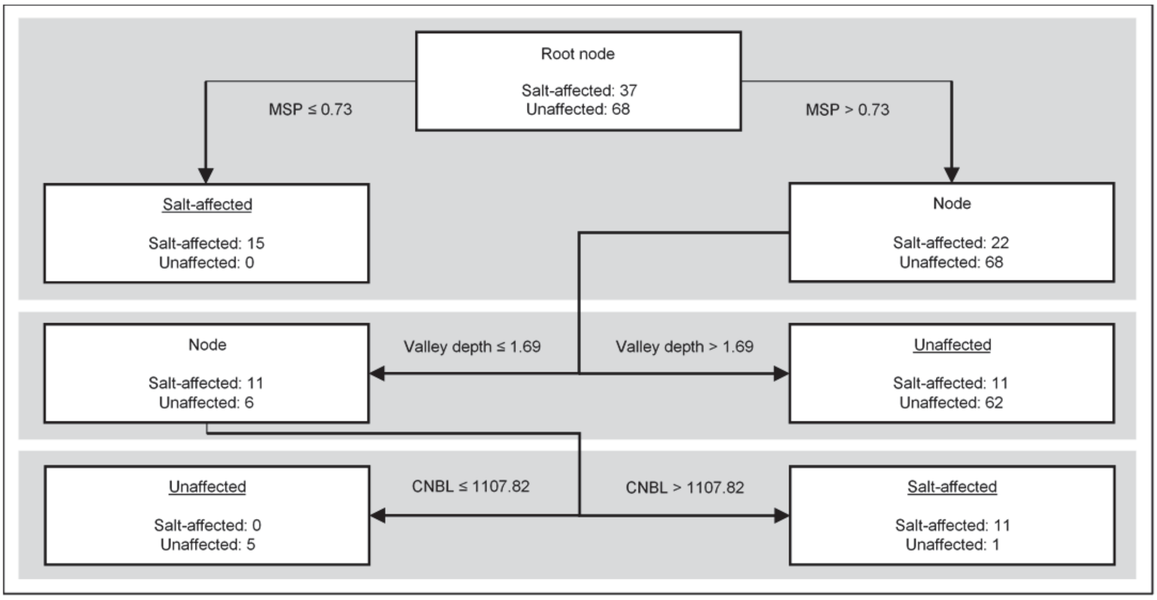

Figure 5.20 Decision tree produced from the CART analysis for Vaalharts

The resulting CART tree for Breede River is shown in Figure 5.21. As with Vaalharts, the features derived from the SUDEM showed the most promising results. LS-factor, slope height, aspect, cross-sectional curvature (CSC) and CNBL were included as splitters in the resulting tree. Low LS-factor (>0.23) and slope height values (≤3.16) were classed as unaffected, while low aspect values (≤0.24) were classed as salt-affected. CSC values less than or equal to zero were classed as unaffected. The final split classed high CNBL values (>196.23) as unaffected and low CNBL values (≤196.23) as salt-affected. The CART trees were implemented as rule sets and included in the classification results.

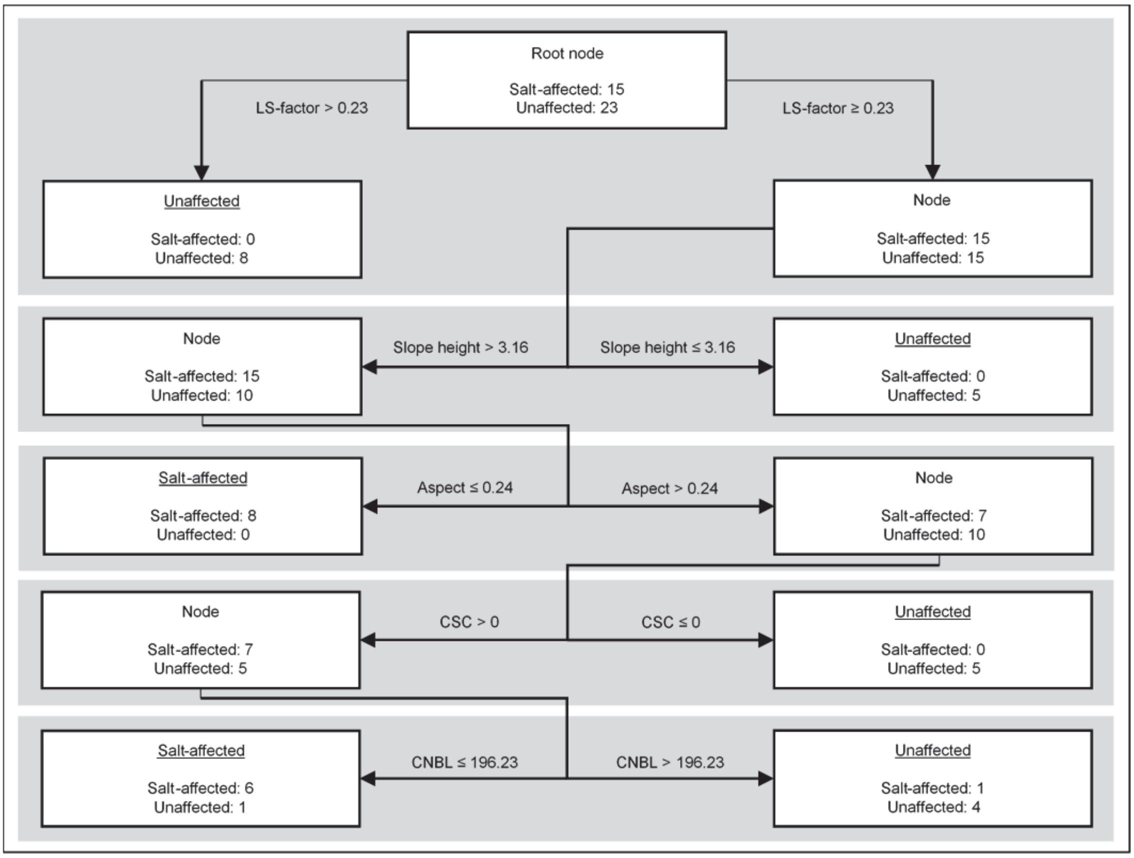

Figure 5.21 Decision tree produced from the CART analysis for Breede River.

5.4.3.4 Classification results

Table 5.19 summarizes the accuracy assessment results of the classifications. The ML algorithm is excluded as it produced erratic results, most likely due to the large number of features considered. The kNN (k = 1) classifier achieved the highest accuracy for both Vaalharts (OA = 92%; Kappa = 0.84; AUROC = 0.93) and Breede River (OA = 75%; Kappa = 0.50; AUROC = 0.75). However, the relatively high proportions of the study areas that were classified as being salt-affected (19.8% and 33.1% in Vaalharts and Breede River, respectively) suggest that the classifier overestimates affected areas.

Although the rule-based classification of the slope height (SRTM) regression model for Vaalharts achieved an OA of 68%, the low KC of 0.36 suggests that there is a high agreement by chance and that the classification is not robust. Similar results (OA = 70%; Kappa = 0.40; AUROC = 0.74) were achieved for the VDTCN (SUDEM) regression model in the Breede River study area. The CART rule-based classification achieved the lowest accuracy (OA = 66%) in Vaalharts, and performed only marginally better in the Breede River study area (OA = 50%). The DT classifier produced the poorest classification (OA = 35%) in the Breede River, but in Vaalharts performed on par with most of the other classifiers (OA = 72%). The high proportion of the area that was classified as being salt-affected (68.3%) is, however, unrealistic.

Table 5.19 A summary of the accuracies of each rule-based and classifier approach applied to Vaalharts and Breede River

Study area	Method	Approach	Class	Producer's accuracy (%)	User's accuracy (%)	Overall accuracy (%)	Kappa Coefficient	AUROC	% salt-affected
Vaalharts	Regression (slope height)	Rule-based	Salt-affected	76	66	68	0.36	0.69	44.2
			Unaffected	60	71				
Vaalharts	CART	Rule-based	Salt-affected	36	90	66	0.32	0.75	30.0
			Unaffected	96	60				
Vaalharts	kNN (k = 1)	Supervised Classification	Salt-affected	84	100	**92**	**0.84**	0.93	19.8
			Unaffected	100	86				
Vaalharts	DT	Supervised Classification	Salt-affected	76	70	72	0.44	0.72	68.3
			Unaffected	68	74				
Vaalharts	RF	Supervised Classification	Salt-affected	80	83	80	0.64	0.80	49.0
			Unaffected	84	81				
Vaalharts	SVM	Supervised Classification	Salt-affected	68	100	84	0.68	0.88	0.01
			Unaffected	100	76				
Breede River	Regression (VDTCN)	Rule-based	Salt-affected	90	64	70	0.40	0.74	49.1
			Unaffected	50	83				
Breede River	CART	Rule-based	Salt-affected	40	50	50	0.29	0.50	7.80
			Unaffected	60	50				
Breede River	kNN (k = 1)	Supervised Classification	Salt-affected	70	78	**75**	**0.50**	0.75	33.1
			Unaffected	80	73				
Breede River	DT	Supervised Classification	Salt-affected	0	0	35	-0.30	0.21	12.9
			Unaffected	70	41				
Breede River	RF	Supervised Classification	Salt-affected	50	71	65	0.30	0.67	4.70
			Unaffected	80	62				
Breede River	SVM	Supervised Classification	Salt-affected	0	0	50	0.0	0.0	**0.00**
			Unaffected	100	50				

RF was one of the better classifiers, achieving an OA of 80% and 65% for Vaalharts and Breede River, respectively. High accuracies were recorded for the Vaalharts SVM classification (OA = 84%; Kappa = 0.68; AUROC = 0.88), scoring a perfect UA (100%) and a low PA (68%) for the salt-affected class. However, the classifier suffered from over-fitting as only 0.01% of Vaalharts was highlighted as being salt-affected. An even smaller proportion was labelled as affected in Breede River.

Figure 5.22 provides a spatial representation of the best rule-based (slope height regression model) and best supervised (kNN) classifications in the Vaalharts study area. The first observation is that there is very little agreement between the two results. The classified regression model produced large continuous affected areas, while the affected areas in the kNN result are generally much smaller and discrete. The slope height regression model classified 42.2% of the Vaalharts study area as being salt-affected, while the kNN classifier labelled a much smaller proportion (19.8%) as affected. Based on the field surveys and expert knowledge, the kNN result is a more realistic representation of salt accumulation conditions in the study area.

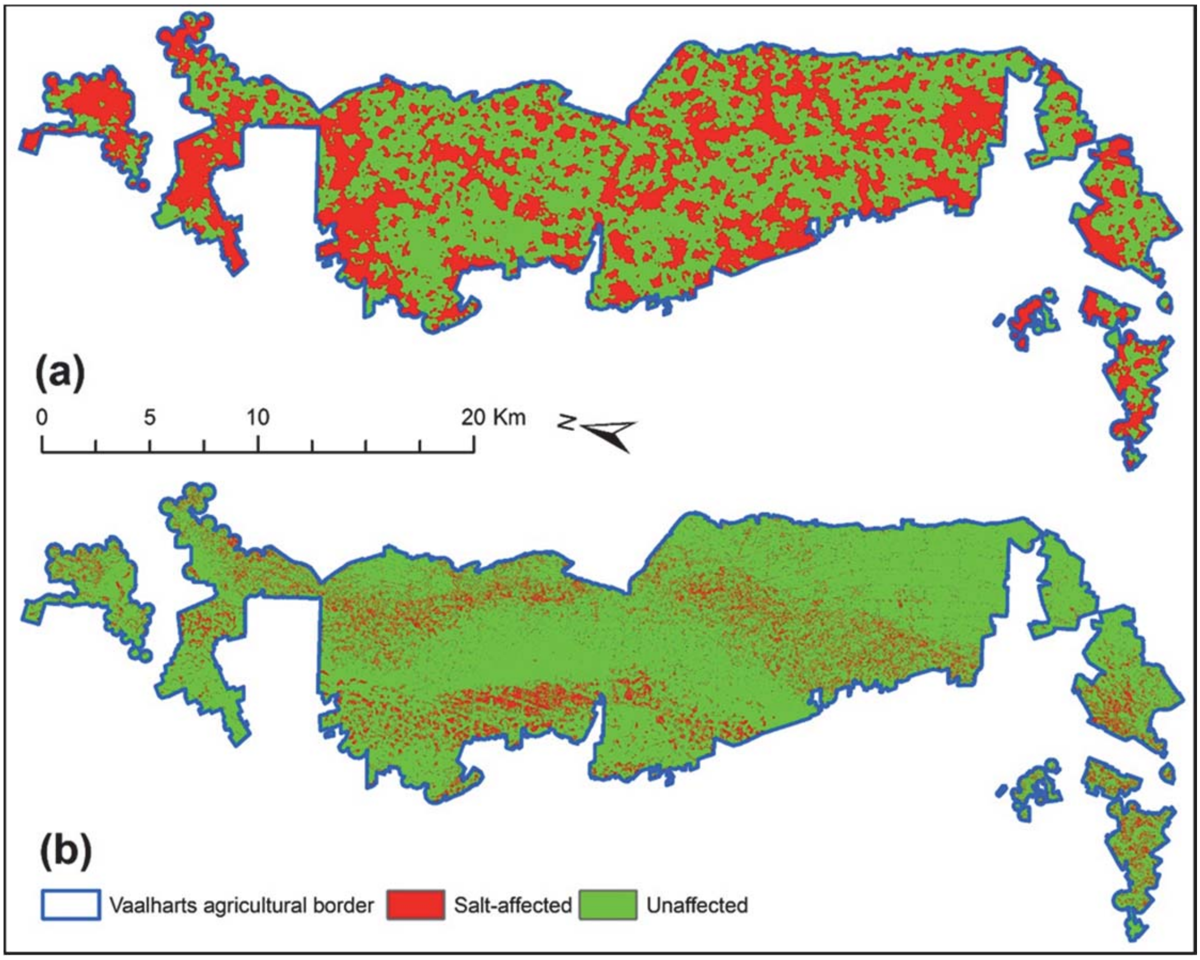

Figure 5.22 (a) Rule-based classification of the slope height regression model and (b) supervised kNN (k = 1) classification maps of Vaalharts.

Table 5.20 Error matrix produced from the kNN classification for Vaalharts

	Confirmed as salt-affected	**Confirmed as unaffected**	**Total**	**User's accuracy (%)**
Classified as salt-affected	21	0	21	100
Classified as unaffected	4	25	29	86.2
Total	25	25	50	
Producer's accuracy (%)	84	100		92%
			Kappa	0.84

The confusion (error) matrix of the kNN classifier results in Vaalharts (Table 5.20) reveals that, of the 50 samples, only four salt-affected samples were incorrectly classified as unaffected, while all the samples that were classified as salt-affected were verified as being salt-affected.

Similar observations were made in the Breede River study area (Figure 5.23), where the VDTCN regression model based on the SUDEM classified salt-affected areas as large continuous regions covering 49.1% of the study area. As with Vaalharts, the kNN classifier mostly labelled small patches as salt-affected, although some large sections in the western parts of the scheme were also delineated. A total of 33.1% of the Breede River study area was classified as salt-affected.

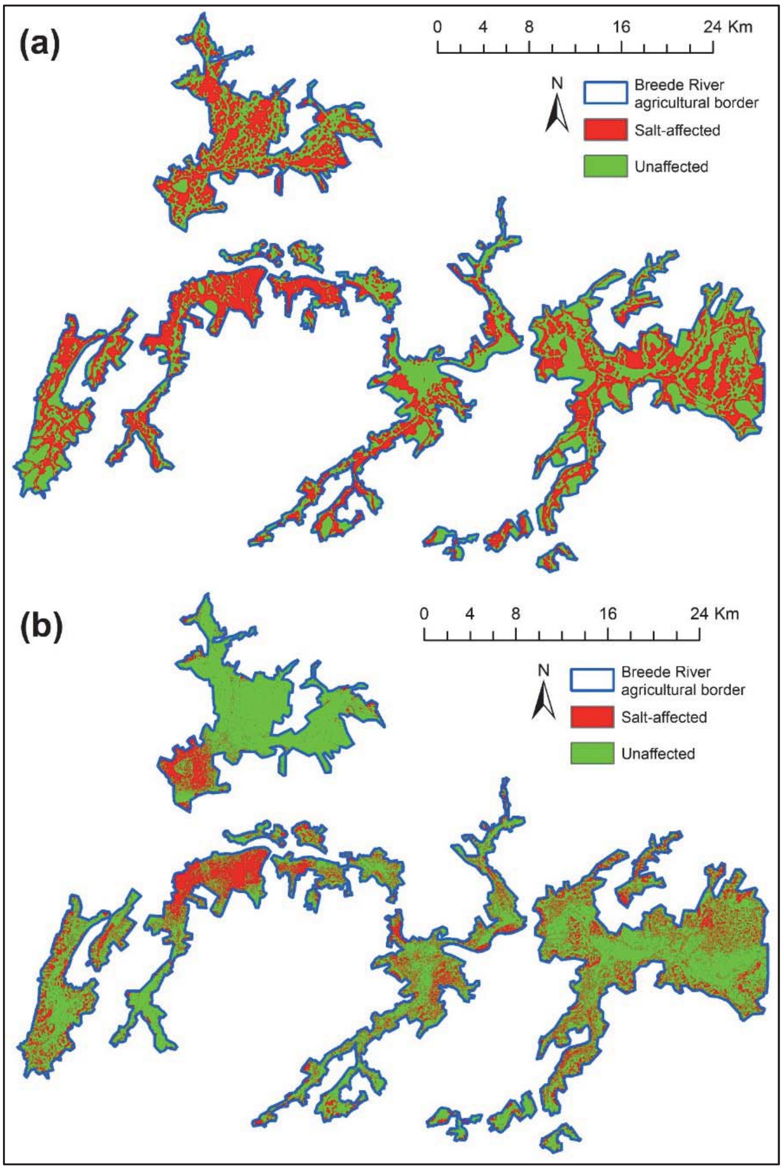

Figure 5.23 (a) Rule-based classification of the VDTCN regression model and (b) supervised kNN (k = 1) classification maps of Breede River.

The kNN classifier achieved a substantially lower overall accuracy (75%) in the Breede River study area (Table 5.21) and the relatively low Kappa coefficient of 0.50 suggests high agreement by chance (Garrett & Viera, 2005), most likely due to the small number of samples (20) used for accuracy assessment.

Table 5.21 Error matrix produced from the kNN classification for Breede River.

	Confirmed as salt-affected	Confirmed as unaffected	Total	User's accuracy (%)
Classified as salt-affected	7	2	9	77.8
Classified as unaffected	3	8	11	72.7
Total	10	10	20	
Producer's accuracy (%)	70	80		75%
			Kappa	0.50

5.4.4 Discussion

The terrain features derived from the DTMs performed better than those extracted from the DSMs. This finding is attributed to the influence of land cover features (e.g. vegetation), particularly in the Breede River study area where the crops are mainly perennial and woody (e.g. fruit trees and vineyards). Better results may have been obtained with LiDAR data, which has the ability to penetrate foliage.

The SRTM DEM produced better results in Vaalharts, while the SUDEM was generally more successful in Breede River in establishing relationships between terrain features and salt accumulation. The main difference between the SUDEM and SRTM DEM is that the former incorporates contours, but in flat terrain such as Vaalharts, the horizontal distances between contours are large and will consequently not provide any significant value. Also, the higher resolution of the SUDEM will not have much benefit in flat terrain.

The rule-based classifications that were performed on the regression models did not produce meaningful results. This is attributed to the large number of contributing factors to salt accumulation and the large variations in the samples that were collected. CART also performed poorly, but has the advantage of providing a set of rules (decision tree) that can be interpreted, modified and transferred to other areas. However, CART and other DT classifiers are known to be susceptible to over-fitting, which can reduce their transferability.

Generally the classification results were better in the Vaalharts study area (mean OA = 77%) compared to Breede River (mean OA = 57.5%). The terrain in the Breede River is more complex and this may have contributed to the lower accuracies, but it is more likely that the higher accuracies in Vaalharts were due to the larger set of training data used. This result highlights the main disadvantage of supervised classifiers. Although they generally produce accurate results (compared to regression modelling), the results are heavily dependent on the size and quality of the training data. The routine collection of large sets of training (and reference) data for operational monitoring of salt accumulation at national level is not viable. Another drawback of supervised classifiers (DTs being an exception) is that they are "black box" techniques, meaning that the classification cannot be replicated in other study areas without collecting a new set of training data.

It is important to note that salt accumulation, as represented by EC, is measured on a ratio scale. The accuracy assessments in this component of the research were performed on crisp categorical (salt-affected and unaffected) outputs using 400 mS/m as a threshold. The classification results might have been significantly different if another threshold (e.g. 410 mS/m) was used. The fuzzy nature of salt accumulation is consequently not well addressed when using classification approaches and the uncertainties of such results should be taken into consideration when the data is interpreted.

5.4.5 Conclusion

This section evaluated the use of elevation data and its derivatives for modelling salt accumulation. The SRTM DEM, SUDEM and DSMs derived from high-resolution stereoscopic aerial photography were used as the primary data sources. Numerous derivatives were produced from the primary datasets and several terrain analysis methods were assessed. Two rule sets based on regression modelling and CART, as well as five supervised classifiers (NN, ML, SVM, DT and RF) were considered. The kNN supervised classifier was the most successful in differentiating salt-affected from unaffected soils in both study areas.

From the results of this section it can be concluded that the use of elevation data and its derivatives to identify salt-affected soils is ineffective and unreliable. Most of the methods evaluated either underestimated or overestimated salt accumulation or achieved low accuracies, especially for Breede River. The low spatial resolution and quality of the DEMs might have had a negative impact on the results and other elevation data sources, such as LiDAR, should be explored in future research. However, such data may be prohibitively expensive to acquire for large irrigation schemes. Another contributing factor to the poor performance of this approach was the exclusion of artificial drainage in the modelling process.

5.5 Multi-temporal object-based image analysis

The previous four sections demonstrated that both the direct and indirect methods for identifying waterlogged and salt-affected soils have limitations. Farming practices such as tillage and irrigation compromise the spectral properties of soils and salt crusts and the dynamic nature of irrigation schemes limits the application of a direct detection of affected areas (Zhang et al., 2011). Hydrophytic grasses and weeds can also create spectral confusion in waterlogged areas (Dwivedi & Sreenivas, 1998). In an indirect approach, poor vegetation responses related to factors other than soil salinity or waterlogging (e.g. poor farming practices or soil compaction) can cause confusion. Because different crop types have varying tolerances to salt accumulation, a single model will not be able to sufficiently discriminate between affected areas on an irrigation scheme with a large variety of crop types (Zhang et al., 2011; Gratton & Handson, 2006). The occurrence of salt accumulation and waterlogging in generally small patches in South African irrigation schemes poses additional challenges and will require a robust modelling strategy. This section describes a geographical object-based image analysis (GEOBIA) approach that makes use of delineated field boundaries and multi-temporal high resolution (SPOT-5) imagery to identify potential salt-affected or waterlogged areas. This approach was applied in the Vaalharts and Loskop irrigation schemes to produce maps of areas that are likely to be affected. The resulting maps were quantitatively compared to reference data collected during several field surveys.

5.6 Synthesis

This chapter evaluated a range of remote sensing and terrain analysis techniques for identifying waterlogged and salt-affected areas. Some of the techniques produced very promising results.

The experiments showed that the direct approach (bare soil analysis) produced meaningful results, in particular when normalized difference salinity indexes are derived from very high resolution WorldView-2 imagery. However, the approach:

- is only effective when visible evidence of salt accumulation (e.g. salt precipitation) is present on the soil surface; and
- can only be used if the soil is entirely bare (i.e. directly after cultivation) as the presence of vegetation confuses the statistical models and classifiers.

Given the dynamic nature of irrigation schemes, only a small number of fields are bare at any given time, which means that multiple analyses will be required to monitor a particular area. The acquisition of multi-temporal imagery (especially very high resolution imagery) will be prohibitively expensive for operational monitoring purposes.

Section 5.2 demonstrated how an indirect approach that monitors the response of a single crop to salt accumulation can address some of the limitations of the direct approach. Very strong statistical relationships (R^2>0.7) were found between salinity (EC) levels and the vegetation indices and texture measures that were derived from a very high resolution WorldView-2 image. The main advantages of using vegetation response as an indicator for detecting salt accumulation and waterlogging are that:

- it can be employed any time during the growing season (but preferably when crops are mature); and
- it takes sub-surface (root zone) conditions into consideration.

However, the vegetation response monitoring approach is not without limitations. The main drawback is that crops respond differently to saline conditions. Section 5.3 showed that when multiple crops are monitored at scheme level no significant statistical relationships (regression models) between the indirect indicators and salt-accumulation levels could be determined. The machine-learning algorithms (specifically SVM, NN and RF) were less sensitive to these variations, but their ability to differentiate between affected and unaffected crops relies on large training (*in situ*) datasets, which are expensive to routinely collect over large areas.

The terrain analysis experiments (section 5.4) showed that there are generally very weak statistical relationships between terrain derivatives and salinity levels. Better results may be achieved using very high resolution digital terrain (e.g. LiDAR) data, but such data was not available for any of the study areas. Some of the machine-learning classifiers (particularly kNN) performed well according to the accuracy assessments, but the results were not consistent in the two study areas. Moreover, supervised classifiers' reliance on training data makes them less suitable for operational purposes. Rule-based classification approaches have been shown to be more cost-effective for application in large areas as they do not rely on *in situ* data and are consequently more transferable. The next chapter explains how rule-based classification was used to develop a method for monitoring salt accumulation and waterlogging at field, farm and scheme level.

6 WITHIN-FIELD ANOMALY DETECTION[6]

Chapter 5 demonstrated that both the direct and indirect methods for identifying waterlogged and salt-affected soils have limitations. Farming practices such as tillage and irrigation compromise the spectral properties of soils and salt crusts and the dynamic nature of irrigation schemes limits the application of a direct detection of affected areas (Zhang *et al.,* 2011). Hydrophytic grasses and weeds can also create spectral confusion in waterlogged areas (Dwivedi & Sreenivas, 1998). In an indirect approach, poor vegetation related to factors other than soil salinity or waterlogging (e.g. poor farming practices or soil compaction) can cause confusion. Because different crop types have varying tolerances to salt accumulation, a single model will not be able to sufficiently discriminate between affected areas on an irrigation scheme with a large variety of crop types (Zhang *et al.,* 2011; Gratton & Hanson, 2006). The occurrence of salt accumulation and waterlogging in generally small patches in South African irrigation schemes poses additional challenges and will require a robust modelling strategy. This chapter describes a geographical object-based image analysis (GEOBIA) approach that makes use of delineated field boundaries and multi-temporal high resolution (SPOT-5) imagery to identify potential salt-affected or waterlogged areas. The within-field anomaly detection (WFAD) method was applied to nine different irrigation schemes across South Africa to produce maps of areas that are likely to be affected. The resulting maps were quantitatively compared to reference data collected during several field surveys. The results of the accuracy assessments are discussed and interpreted in the context of operational monitoring of waterlogging and salt accumulation at field, farm and irrigation scheme level. The results were also used to quantify the extent of waterlogging and salt accumulation in the schemes considered.

6.1 Study areas

Nine irrigation schemes were selected for this component of the study, namely Vaalharts irrigation scheme, Loskop irrigation scheme, Makhathini irrigation scheme, Tugela River, Olifants River, Breede River, Sundays River, Limpopo River and the Orange and Vaal Rivers near Douglas.

6.2 Data collection and preparation

Bi-annual SPOT-5 scenes covering all or large parts of nine irrigation schemes were acquired from the South African National Space Agency (SANSA). A scene consists of a SPOT-5 multispectral and corresponding panchromatic image. Multiple scenes were required in some of the irrigation schemes (Table 6.1). With a multispectral resolution of 10 m (see Table 2.5), SPOT-5 imagery is regarded as high resolution imagery compared to the very high resolution (multispectral resolution <5 m) imagery provided by Quickbird, Ikonos and WorldView-2 (as used in sections 5.1 and 5.2). SPOT-5 imagery is, however, available at a higher temporal resolution and reduced cost and is consequently a cost-effective solution for covering extensive areas. Although the spectral resolution of SPOT-5 imagery (see section 2.3.5) is less than the WorldView-2 imagery, it contains the most important bands for the creation of VIs. Section 5.2 showed that such imagery holds much potential for

[6] The content of this section was adapted from the MSc thesis of Jascha Muller.

identifying salt accumulation and waterlogging, especially when the multispectral data is sharpened to its panchromatic resolution of 2.5 m.

Table 6.1 SPOT-5 scenes acquired for the study areas

Irrigation scheme	Scene dates	K/J
Vaalharts	27 April 2012; 20 Feb 2011	127-406 127-406
Loskop	30 Sept 2012; 3 June 2012; 18 May 2012; 15 June 2011 ; 5 May 2011; 17 Aug 2011	135-400 135-400 134-400 135-400 135-400 134-400
Makhathini	26 July 2012; 2 Aug 2011	142-405 142-405
Tugela River	22 March 2012; 1 Aug 2011	137-408 137-408
Olifants River	26 Jan 2013; 10 April; 2012	116-413 116-413
Breede River	16 Jan 2013; 26 Feb 2013; 26 March 2012; 11 Dec 2012	120-418 119-417 120-418 119-417
Sundays River	18 Feb 2013; 12 April 2012	132-417 132-417
Limpopo River	23 Feb 2013; 12 March 2012	133-394 133-394
Douglas	16 April 2013; 13 Aug 2013;	126-408 126-408

Geometric and radiometric corrections of all images were carried out using the software package PCI Geomatica (v 2013 SP2). All necessary resampling during pre-processing was done using the nearest neighbour method to preserve the original digital numbers (DNs) (Lillesand *et al.,* 2004; Campbell, 2007). A north-oriented implementation of the Gauss conform coordinate system (also known as the LO coordinate system), with the central meridian adjusted for each scheme, was used. The software ATCOR 2, which is based on the MODTRAN algorithm, was used to convert the DNs into percentage surface reflectance.

Image fusion (see section 5.2) was performed to increase the spatial resolution of the multispectral bands. The fusion of multispectral and panchromatic images is an effective technique to optimize the spatial and spectral resolution of the images (Gonzales- *et al.,* 2004). PCI Geomatica's algorithm Pansharp has been shown to preserve most of the spectral characteristics of the multispectral data in the resulting pansharpened image (Zhang, 2002; 2004). Pansharp was used to increase all the 10 m multispectral data to a 2.5 m resolution.

Reference data collected during several fields' surveys (section 4.2) was used for accuracy assessment.

6.3 A geographical object-based image analysis (GEOBIA) approach to detecting anomalies within fields

The challenge with using remote sensing for identifying and delineating waterlogged and salt-affected areas is that they are local manifestations and can only be differentiated from unaffected areas by taking its context (surrounding area) into consideration. For instance, an affected area within a wheat field will have very different spectral properties to an affected area in a vineyard, while the latter will have a very different spectral response compared to an affected area within a bare/fallow field. Section 5.2 demonstrated that advanced machine-learning classifiers can overcome these variations to some extent, but only if a sufficiently large set of *in situ* data is available. This data needs to be collected within the area of interest as close as possible to the date when the imagery was acquired. Given the high costs associated with field surveys and soil analyses, an alternative method is needed that does not rely on *in situ* data.

The WFAD technique is based on the principle that heterogeneous areas are in many cases indicative of waterlogging or salt accumulation. Affected areas often stand out as being spectrally different compared to the rest of a field, either because of a reduction in biomass due to saline or saturated conditions (in cultivated fields) or due to specific species of vegetation occurring in fallow fields. Although such "anomalies" can be easily identified using visual interpretation of imagery, they are not easily extracted from remotely-sensed data. Traditional remote sensing techniques involve classifying individual pixels (cells) without taking topology (relationships between spatial entities) into consideration. Section 2.3.3 explained that the incorporation of contextual information is one of the key strengths of GEOBIA as objects (groups of pixels that are spectrally similar) can be compared to surrounding (neighbour) or encompassing (parent) objects. Object-based image analysis mimics higher order logic, similar to human visual interpretation, to identify useful shapes, sizes and textures from spatial data (Campbell, 2007).

GEOBIA is employed in the WFAD technique to consider the spectral variations within each field individually, thereby eliminating the impact of varying spectral characteristics of affected areas of different crop types as fields are normally planted with the same crop. The WFAD method was implemented using eCognition Developer (v9) software. The following sub-sections overview each of the steps in the procedure.

6.3.1 Step 1: Image segmentation

The first step in the WFAD technique is to delineate suitable objects that can be used as primary entities for image classification and analysis. As explained in section 2.3.3.1, image objects (or segments) are spectrally similar features (polygons) and are generated using an image segmentation algorithm. The multi-resolution segmentation (MRS) algorithm was used to generate a unique hierarchical segmentation of each study area. Hierarchical segmentation structures consist of more than one level of segmentation that share inherent properties.

The DAFF field boundaries vector layer that was manually improved was used as the parent segmentation layer for each irrigation scheme. Below the parent level the MRS algorithm was used to generate the child layer consisting of finer, more detailed objects (Figure 7.1).

Due to the hierarchal structure, the child objects inherit the properties of the parent objects so that each child object can be related to its corresponding parent.

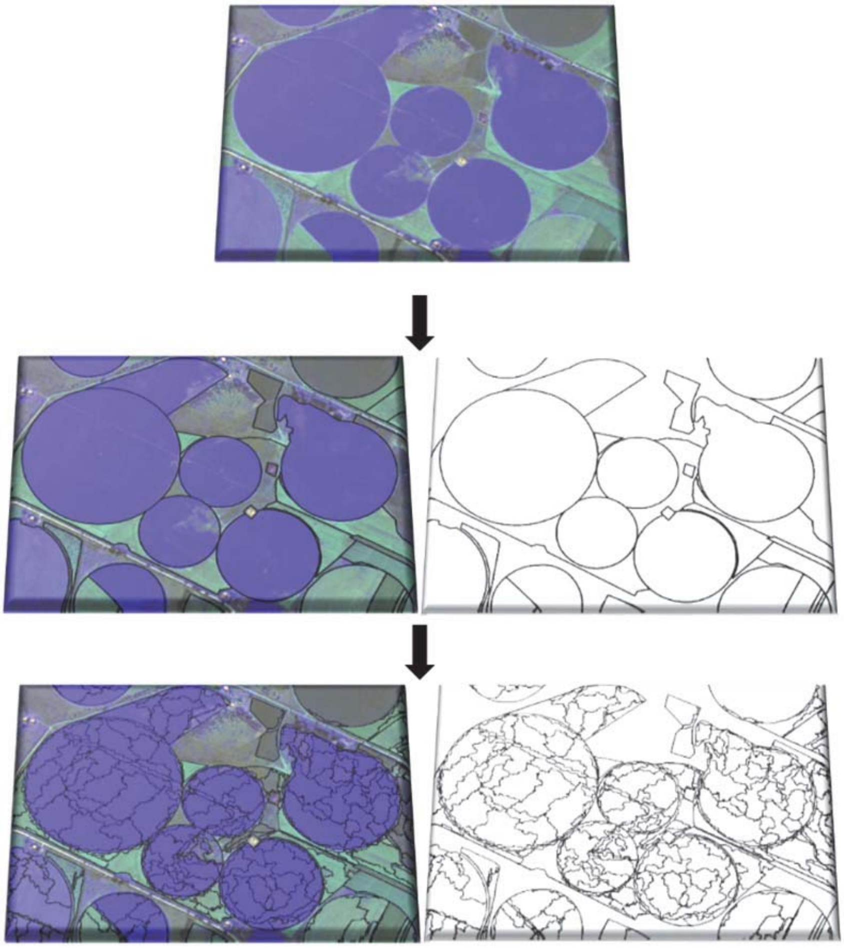

Figure 6.1 Hierarchical segmentation process.

6.3.2 Step 2: Anomaly detection

The second step in the WFAD method was to classify the child objects within each field into anomalies and non-anomalies. A rule-based classification approach was implemented for this purpose. As explained in section 2.3.2.3, a rule-based (expert system) approach has the advantage of making use of a set of instructions (rules) to classify images. Rules can be based on empirical data or can be constructed based on expert knowledge. Another advantage of the rule-based approach is that rules can be developed on observable differences and changes within the data and can progressively be applied and refined while maintaining full control in the time of the classification process (Lucas *et al.,* 2007).

A rule set was developed to first classify the field (parent) objects as vegetated or bare/fallow. The spectral response of each child object was then compared to the mean spectral response of its relative parent object. If there was a substantial difference between the child object and the relative parent object, the child object was identified as an anomaly (Figure 6.2).

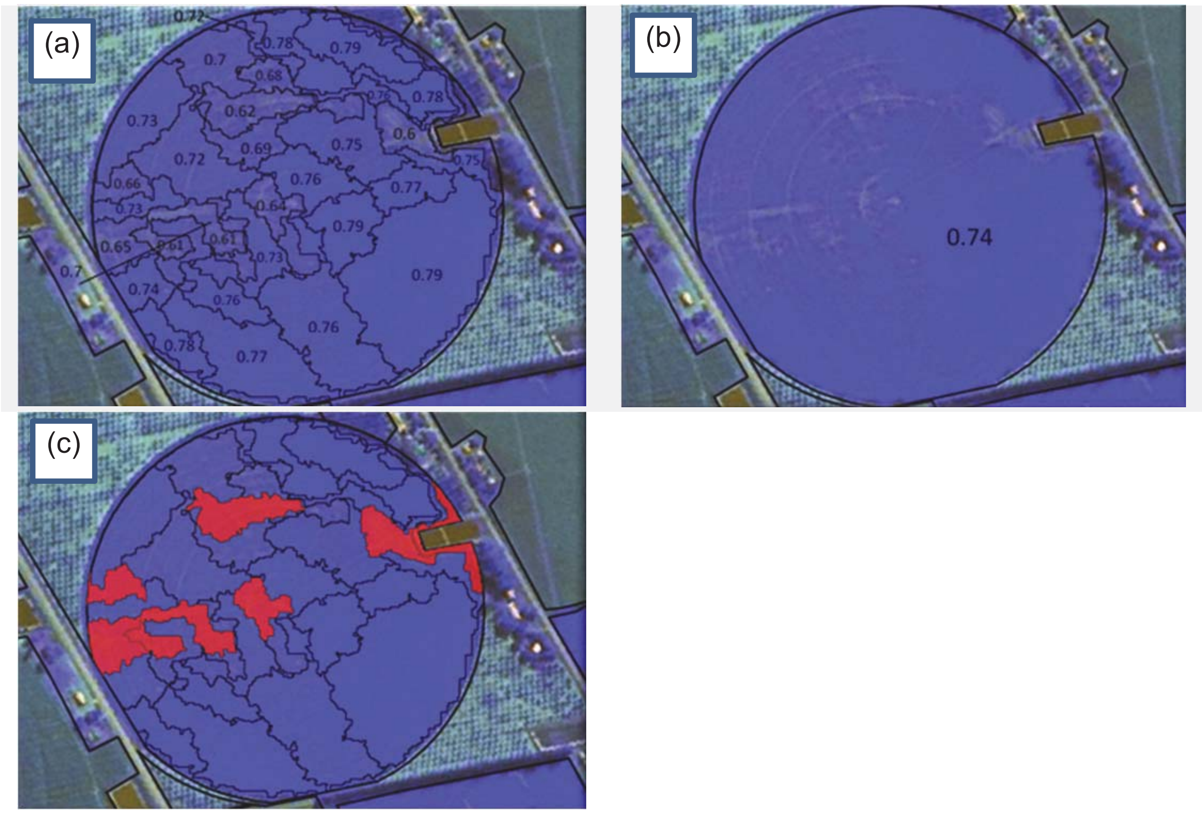

Figure 6.2 The anomaly detection classification compares the spectral response of each (a) child against its respective (b) parent to identify (c) objects that are substantially different in terms of spectral response.

For vegetated fields, mean NDVI was employed for calculating spectral responses. Mean NDVI was calculated for each parent and child object and a suitable mean difference (MD) threshold was used to identify anomalies. MD is defined as:

$$MD = MSR_c - MSR_p \qquad \text{Equation 6.1}$$

where MSRc is the mean spectral response (e.g. NDVI) of a child object and the MSRp is the mean spectral response of the relative parent object. A positive MD threshold was implemented to identify a child object with a substantially higher MSR compared to the relative parent object. A negative MD threshold identifies a child object with a substantially lower MSR compared to the relative parent object. Only negative MD thresholds were used in vegetated fields as these highlight areas experiencing vegetation stress. A positive MD threshold in a vegetated field would indicate an area with relatively high biomass, which is generally not associated with salt accumulation or waterlogging.

To identify anomalies in bare/fallow fields, NDVI and a brightness ratio (Br) were used to calculate the MSR, where:

$$Br = (Green + Red + NIR)/3 \qquad \text{Equation 6.2}$$

Salinity indices were not considered due to the absence a blue band in SPOT-5 imagery. The SWIR band was excluded for calculating *Br* because of its lower (20 m) resolution. Both negative and positive MD thresholds were used for fallow fields owing to the wide range of possible indicators of waterlogging and salt accumulation. Indicators that were targeted in the WFAD technique included low reflectance values in all bands due to waterlogging (Dwivedi & Sreenivas, 1998); high reflectance in the visible and near-infrared regions due to salt encrustations (Metternicht & Zinck, 2003); and occasional vegetation response in fallow fields due to hydrophytic vegetation occurring in waterlogged areas (Dwivedi & Sreenivas, 1998).

6.3.3 Step 3: Multi-temporal analysis

During the field surveys it was observed that not all anomalies were related to salt accumulation or waterlogging. Some of the anomalies were, for instance, found to be caused by poor farming practices (e.g. insufficient irrigation, inadequate fertilizer, over-application of pesticides). To reduce this effect, anomalies were detected for multiple (at least two) seasons. The assumption was that the impact of poor farming practices will likely be temporary, and that areas within fields that are persistently identified as being anomalies are most likely caused by other factors such as salt accumulation or waterlogging (Lobell *et al.,* 2010; Furby *et al.,* 1995; Lenney *et al.,* 1996).

The multi-temporal analysis was implemented by overlaying the anomaly layers of two or more seasons. Anomalies that only occurred in one season were discarded from further consideration.

6.4 Accuracy assessment

The accuracy of the WFAD method was assessed by visiting predefined locations within each study area (see section 4.1 for an overview of the field surveys). The observations made in the field and from the laboratory analyses (section 4.2) were used to determine how successful the WFAD technique was in identifying affected areas. Confusion (error) matrices were created to quantify the errors of omission (unidentified affected areas), errors of commission (falsely identified areas) and overall accuracy.

6.5 Incorporating abandoned fields

Because the WFAD method only considers cultivated or fallow fields, it does not incorporate fields that have been abandoned due to salt accumulation or waterlogging. Because this exclusion can have a significant effect on the overall quantification of affected areas, abandoned fields were manually identified using visual image interpretations. Where available, historical irrigation scheme maps were also employed in the identification process. The abandoned fields were added to the set of anomalies.

6.6 Quantification of affected areas

The multi-temporal analysis was very successful in reducing the number of “false positives”, i.e. anomalies that are unrelated to waterlogging or salt accumulation. However, many false positives still remained after applying this correction and an additional step was needed to take this into account during the quantification process. An anomaly ratio (Ar), describing the ratio between the number of anomalies caused by salt accumulation and waterlogging and those caused by other factors, was consequently introduced. Ar is defined as:

$$Ar = \frac{A_{sw}}{(A_{sw} + A_o)} \qquad \text{Equation 6.3}$$

where Asw represents the number of anomalies that were verified during the field surveys to be related to salt accumulation or waterlogging and Ao represents the number of anomalies that were found to be related to other factors.

The resulting Ar ranges between 0 and 1, with a value of 1 indicating that all anomalies were affected. A unique Ar value was calculated for each of the irrigation schemes.

To determine the percentage of an irrigated scheme that is affected by waterlogging or salt accumulation, the following equation was used:

$$\%\ affected\ area = Ar(100(Area_{anomalies}/Area_{total})) \qquad \text{Equation 6.4}$$

where $Area_{anomalies}$ represents the total area (ha) of the identified anomalies and $Area_{total}$ represents the total area (ha) of fields in the study area. The most recent extent of the anomalies was used for the area calculations. This procedure was repeated for each of the nine study areas.

6.7 Results

Table 6.2 summarizes the results of the WFAD method for the nine study areas in which it was applied. The results for each study area are discussed in the following sub-sections. Appendix A shows the confusion matrices generated during the accuracy assessment of the WFAD method.

Table 6.2 Results of the WFAD method

Study area			n	Anomalies						Ar	Affected		Adjusted*	
Name	ha	ha*	#	#	ha	OA%	KC	EoO%	EoC%	%	ha	%	ha	%
Vaalharts	26434	27033	70	594	572	71.6	0.58	35	25	72.5	414.7	1.57	848.9	3.14
Loskop	38831	40867	90	1714	1239	82.2	0.72	18.3	12.5	71.6	887.1	2.28	2344.7	5.74
Makhathini	4312	4624	56	336	194	80.4	0.67	11.9	19.3	71.4	138.5	3.21	361.1	7.81
Olifants River	11284	11911	82	1179	320	76.8	0.6	10.5	27.7	70.2	224.6	1.99	664.9	5.58
Tugela River	27384	28244	83	1983	2032	78.3	0.6	12.1	18.9	72.7	1477.3	5.39	2102.8	7.44
Breede River	29129	30188	85	10995	1807	76.5	0.58	33.3	16.1	77.3	1396.8	4.8	2215.3	7.34
Sundays River	18608	18832	51	3699	556	80.4	0.6	30.4	16.7	95.0	528.2	2.84	740.5	3.93
Limpopo River	8681	8805	77	1630	604	61	0.33	47	44	77.5	468.1	5.39	564.0	6.40
Douglas	22748	23445	66	3891	1614	66.7	0.39	35.1	30	91.9	1483.3	6.52	2124.0	9.06
MEAN	20823	21550	73	2891	993	74.9	0.56	26.0	23.4	77.8	779.8	3.78	1329.6	6.27

Key: n = Samples used for accuracy assessment; OA = Overall accuracy; KC = Kappa coefficient; EoO = Error of omission; EoC = Error of commission; Ar = Anomaly ratio (see section 7.6); * Area adjusted by adding abandoned fields

6.7.1 Vaalharts, Loskop and Makhathini Irrigation Schemes

The WFAD technique was initially developed in the Vaalharts irrigation scheme and evaluated at Loskop and Makhathini. The findings were used to improve the procedure for implementation in subsequent study areas. Generally the WFAD method produced good results at Vaalharts (Figure 6.3) as there is generally a strong relationship between heterogeneous areas and high EC values (Figure 6.3d). This is supported by the two photographs (Figure 6.4) taken in the anomaly delineated in Figure 6.3a. The owner of the particular farm also confirmed that the highlighted areas are known to be salt-affected and frequently waterlogged.

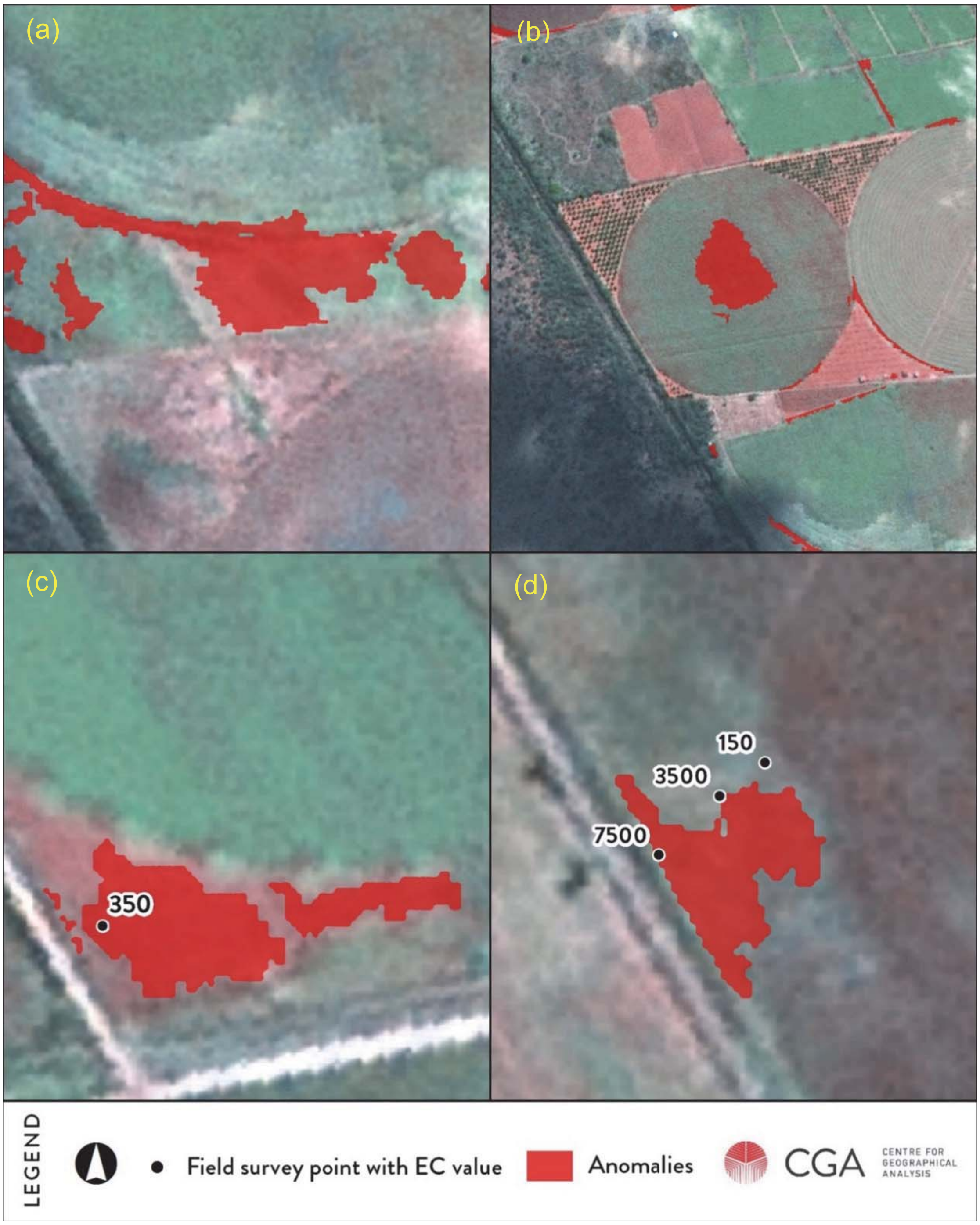

Figure 6.3 Examples of areas at Vaalharts where within-field anomalies were detected for the period 2010-2012.

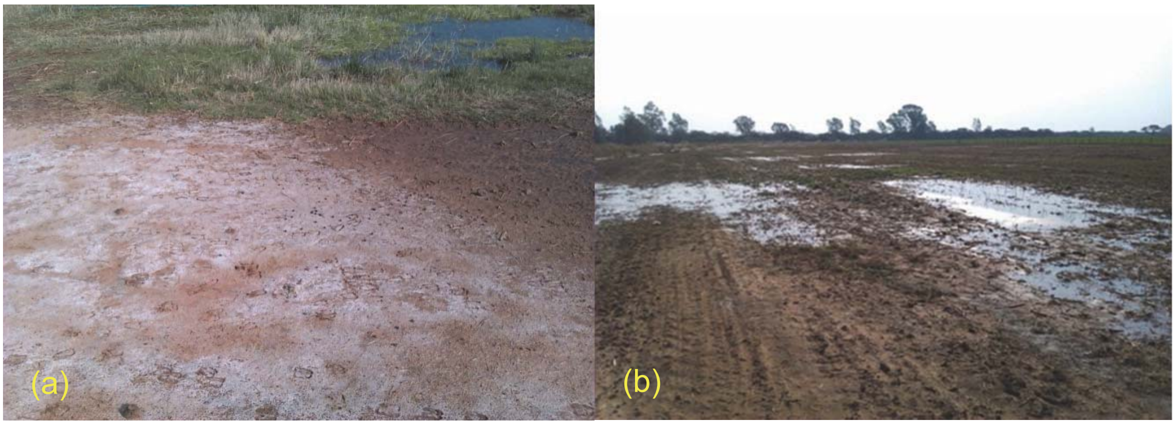

Figure 6.4 Two areas visited during the field survey at Vaalharts that showed clear evidence of (a) salt accumulation and (b) waterlogging.

Figure 6.5 shows an example of a heterogeneous patch in a ploughed field that was delineated by the WFAD technique, illustrating the potential of this methodology for the application to both bare and vegetated areas. This specific affected area was not identified by any of the other methods evaluated in Chapter 5 which suggests that the WFAD method is more effective for highlighting areas that may potentially be affected by waterlogging or salt accumulation.

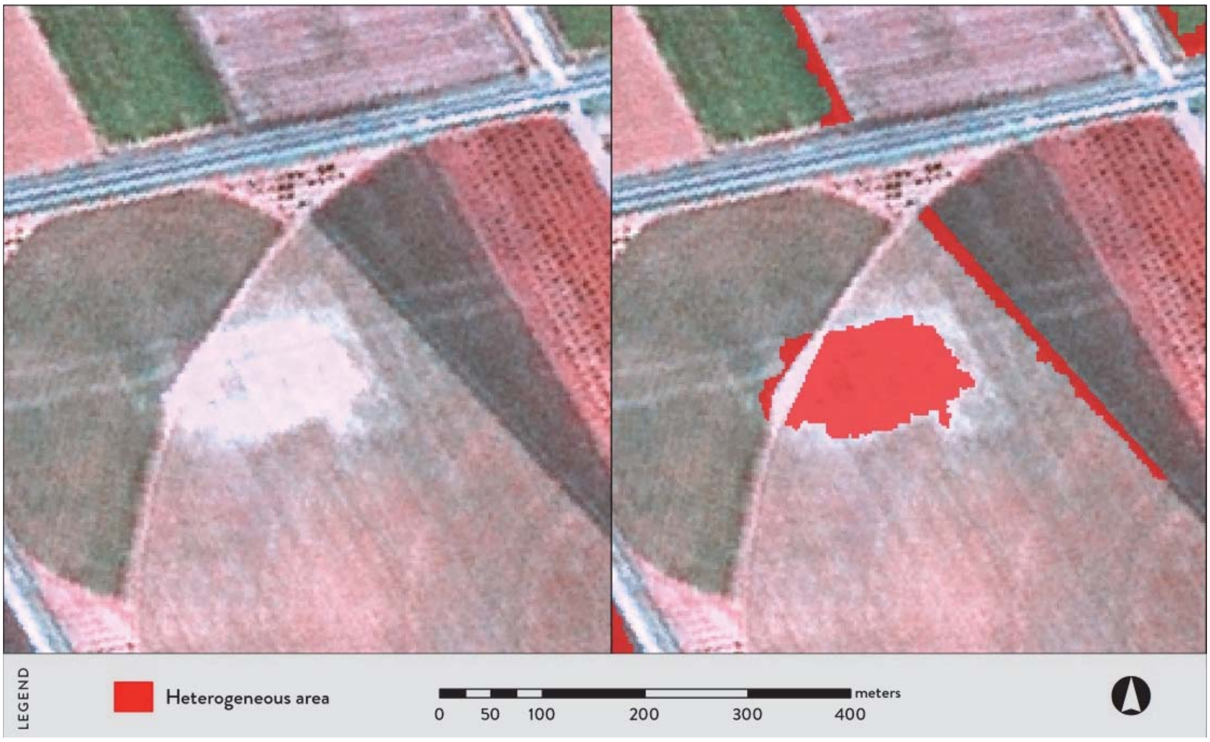

Figure 6.5 Example of a heterogeneous area that was identified in a ploughed field at Vaalharts.

The evaluation of the WFAD technique at Vaalharts highlighted some limitations as a number of inconsistencies were noticed (Figure 6.6), mostly related to the accuracy of the field boundaries GIS data obtained from DAFF. In Figure 6.6a, it is clear that the digitized field boundaries do not perfectly match the actual field boundaries. Some areas on the edges of fields were consequently highlighted as being heterogeneous (affected). This was rectified in subsequent study areas by improving the quality of the shapefile through manual editing. More research is needed to develop semi-automated remote sensing procedures to reduce the required human inputs of such corrections.

Figure 6.6 Inconsistencies as a result of mismatching field boundaries at Vaalharts.

Fields planted with multiple crop types also caused false positives. For example, the anomaly marked with “A” in Figure 6.6b contains two different crops and due to their differences in spectral response this area was falsely identified as being an anomaly. Such errors can also be rectified by editing the field boundaries so that each “field” contains only a single crop. In spite of these limitations, the WFAD method was very successful in highlighting areas in Vaalharts that may potentially be affected by salt accumulation and/or waterlogging.

Table 6.2 shows that the WFAD technique achieved an overall accuracy (OA) of 71.6. The accuracy assessment of the WFAD technique results in Vaalharts showed that only 6 out of the 40 (15%) of the anomalies that were visited during the field verification were incorrect (i.e. should not have been mapped as anomalies as there was no evidence of salt accumulation, waterlogging or any other factors that may impact production. Of the 40 anomalies visited, 11 (27.5%) were verified as being anomalies, but were judged to have been caused by factors unrelated to salt accumulation or waterlogging. This percentage was used for calculating the anomaly ratio (Ar) (see section 6.6). Using this as a correction factor, the total affected area in the Vaalharts study area was estimated to be 414.7 ha (1.57%). By adding abandoned fields (see section 6.5), the total affected area was adjusted to 848.9 ha (3.14%).

Better accuracies were achieved in the Loskop study area, with an overall accuracy of 82.2%. In total 887.1 ha (2.28%) were identified as being potentially affected (anomalies), of which 71.6% were confirmed to be salt-affected or waterlogged. A large number of abandoned fields were also identified, which increased the affected area to 2344.7 ha (5.74%). Figure 6.7 shows examples of anomalies detected in the Loskop study area. It is clear that some of the detected anomalies in Figure 6.7a are slightly smaller than the actual affected areas. This is most likely because the area was less affected in the earlier image used for the temporal analyses.

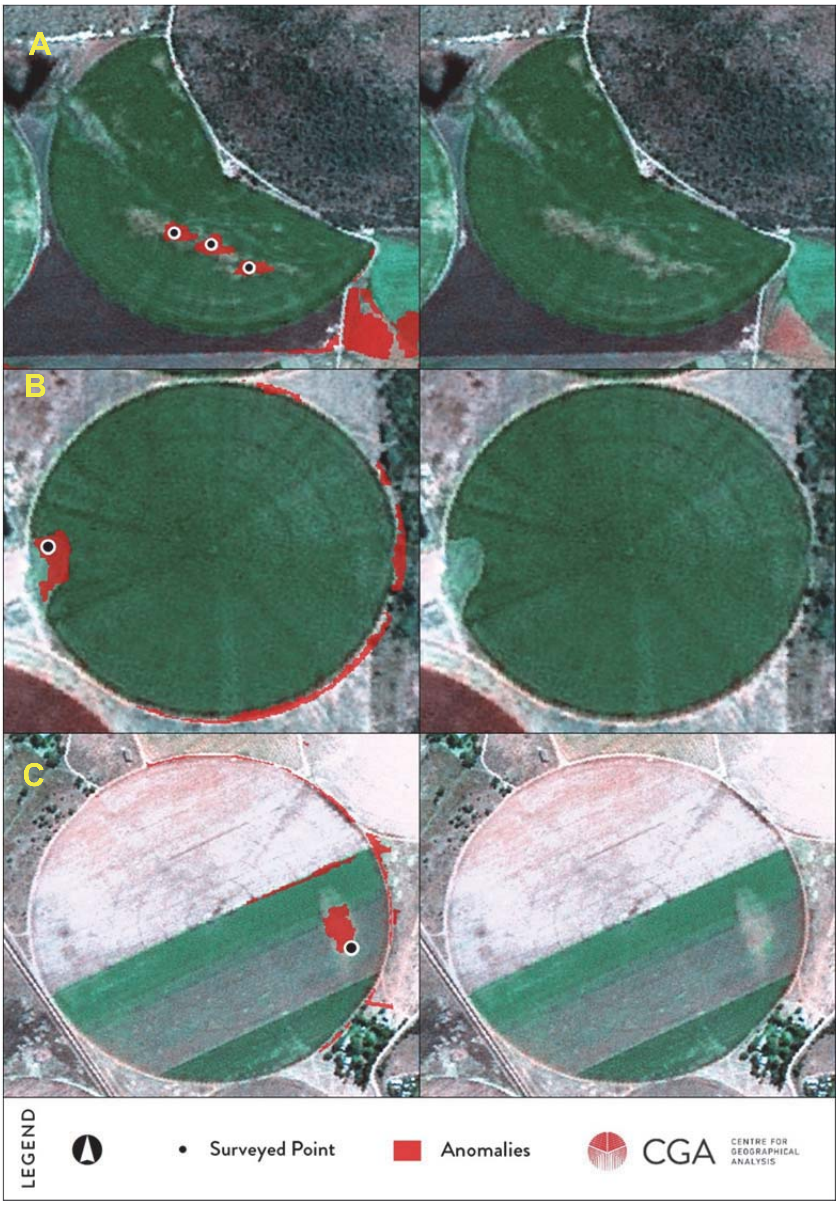

Figure 6.7 Examples of anomalies detected at Loskop.

Applying the WFAD method in the Makhathini irrigation scheme was challenging as it has very small fields which made accurate field boundary delineation difficult using the 2.5 m resolution pan-sharpened SPOT-5 images (Figure 6.8). In addition, the dominant crop is sugarcane, which has a medium to high tolerance to waterlogging and a medium tolerance to salts (Kahlown *et al*., 1998). In spite of these factors, the WFAD managed to achieve an overall anomaly detection accuracy of 80.4%. Only 71.4% of the anomalies visited were found to have been caused by waterlogging or salt accumulation. Based on these findings it was estimated that 138.5 ha (3.21%) of the Makhathini study area is affected by waterlogging or salt accumulation. This increased to 361.1 ha (7.81%) when abandoned fields were added.

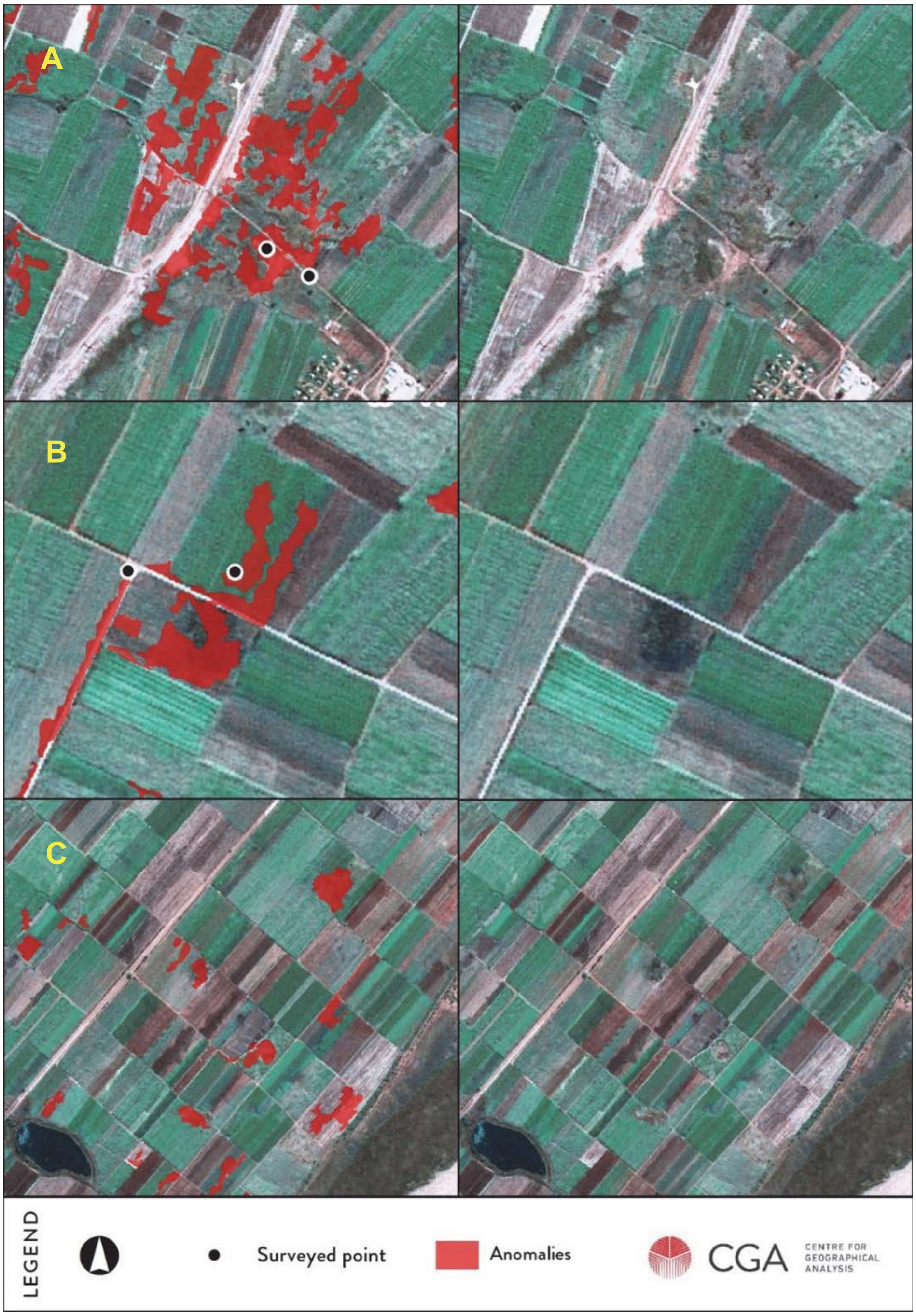

Figure 6.8 Examples of anomalies detected in small fields at Makhathini.

6.7.2 Olifants River

The within-field anomaly detection was applied to a 11 284 ha area within Olifants River irrigation scheme. Figures 6.9 and 6.10 show some examples of anomalies that were detected. The anomalies were generally less defined than at Vaalharts, Loskop and Makhathini and the transitions between affected and unaffected areas were more gradual. This is likely owing to the fact that the area is dominated by perennial crops (vineyards) which are dormant during the winter months.

Figure 6.9 Examples of large anomalies detected at Olifants River Irrigation Scheme (Vredendal) that were confirmed to be related to waterlogging.

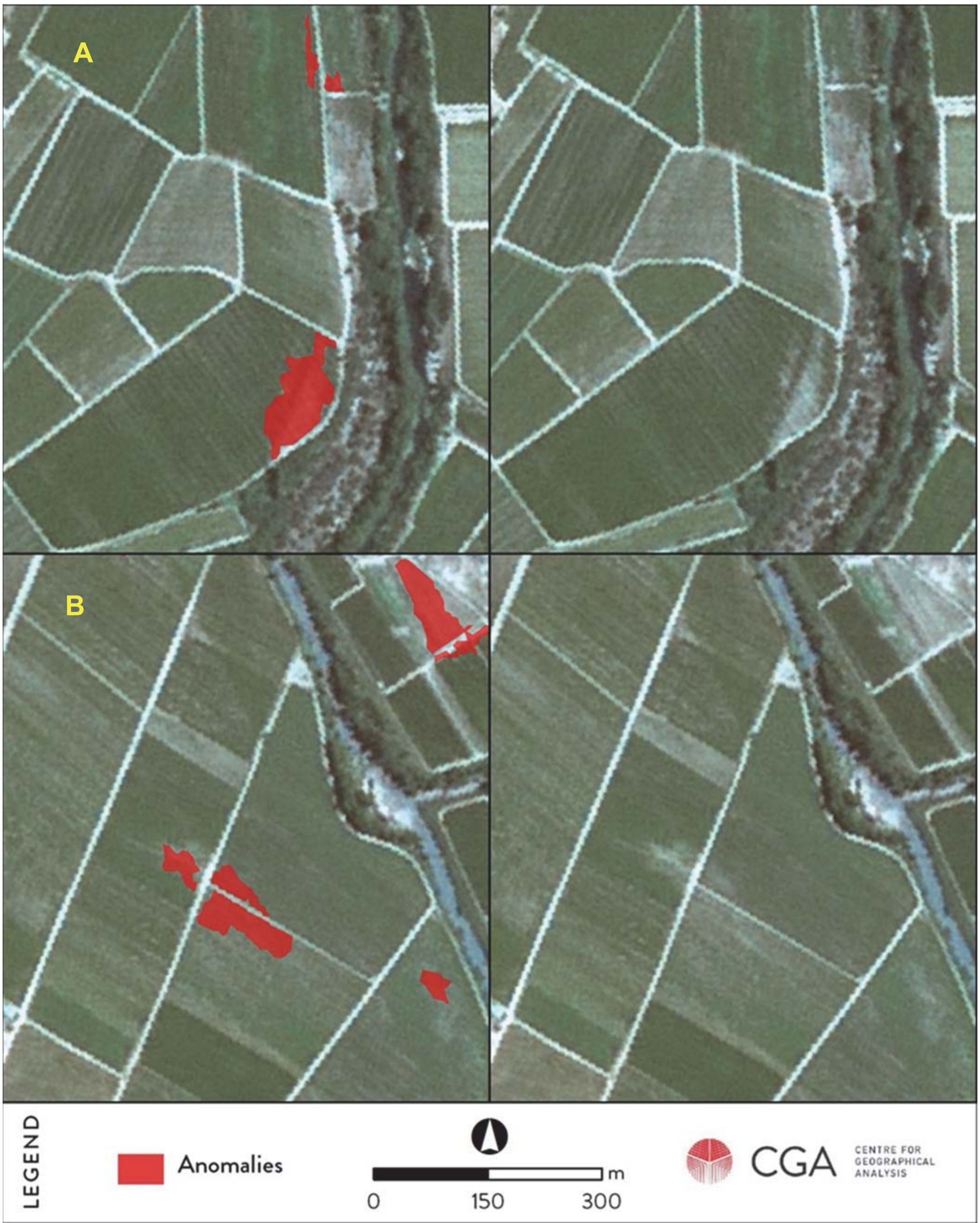

Figure 6.10 Examples of small anomalies detected at Olifants River that were confirmed to be related to waterlogging.

A total area of 223.6 ha (1.99%) was identified as being anomalies, but only 70.2% were verified to be affected by salt accumulation or waterlogging. A large number of abandoned fields were identified, which inflated the estimation to 665.9 ha (5.58%). Some lower lying areas were abandoned due to waterlogging problems in the past, but at present more efficient irrigation systems and practices and the installation of drainage structures reduced some of the problems that occurred in the past.

6.7.3 Tugela River

Of the 27 384 ha Tugela River study area, a total of 2032 ha (7.4%) were identified as anomalies (examples shown in Figure 7.11). The overall accuracy of the anomaly detection was 78.3% and 72.7% of the confirmed anomalies were affected by waterlogging. Figure 7.12 shows that even small patches of affected areas were successfully identified. Contour farming in the past had resulted in concentration of runoff water in specific areas.

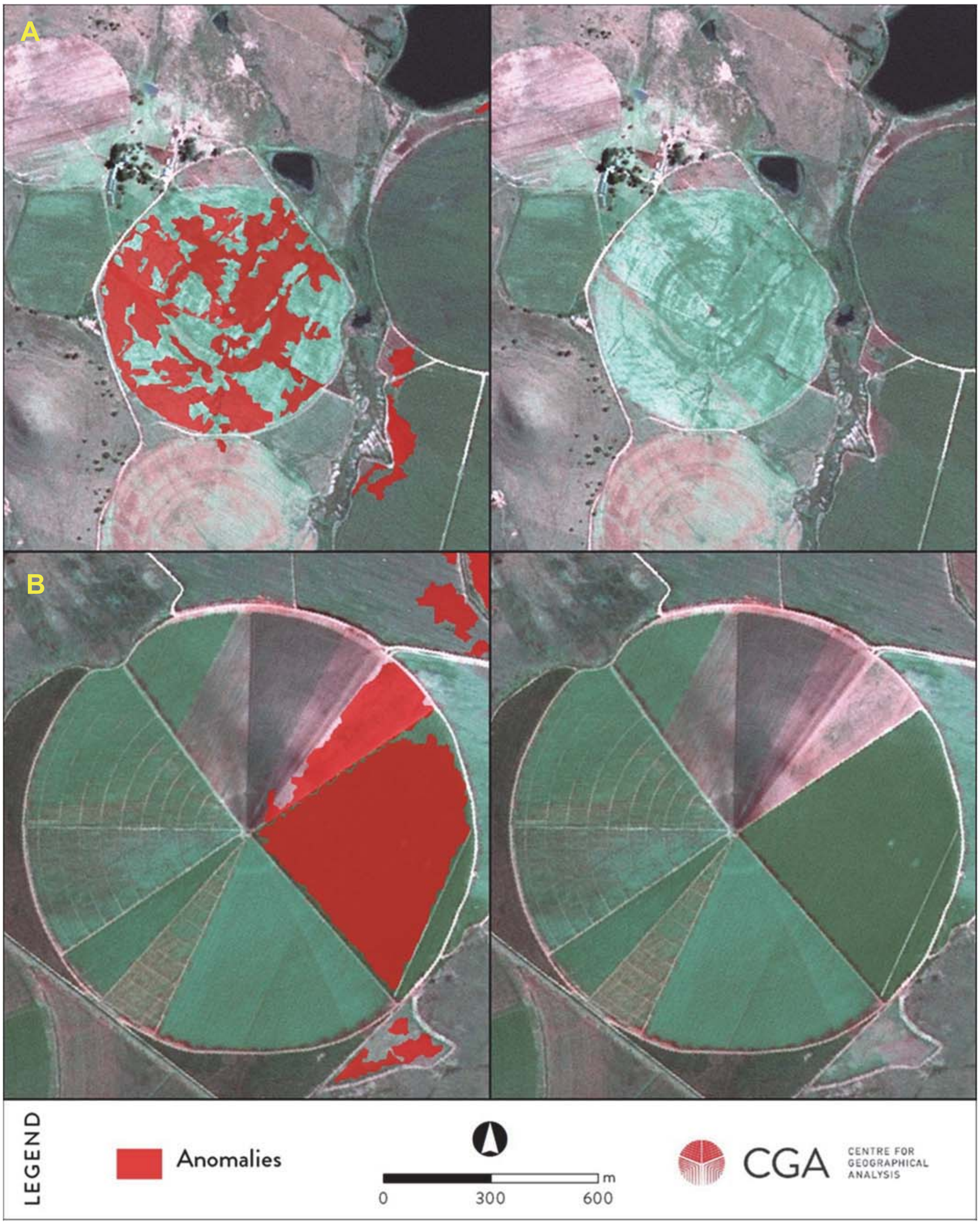

Figure 6.11 Examples of large anomalies detected at Tugela River that were confirmed to be related to waterlogging.

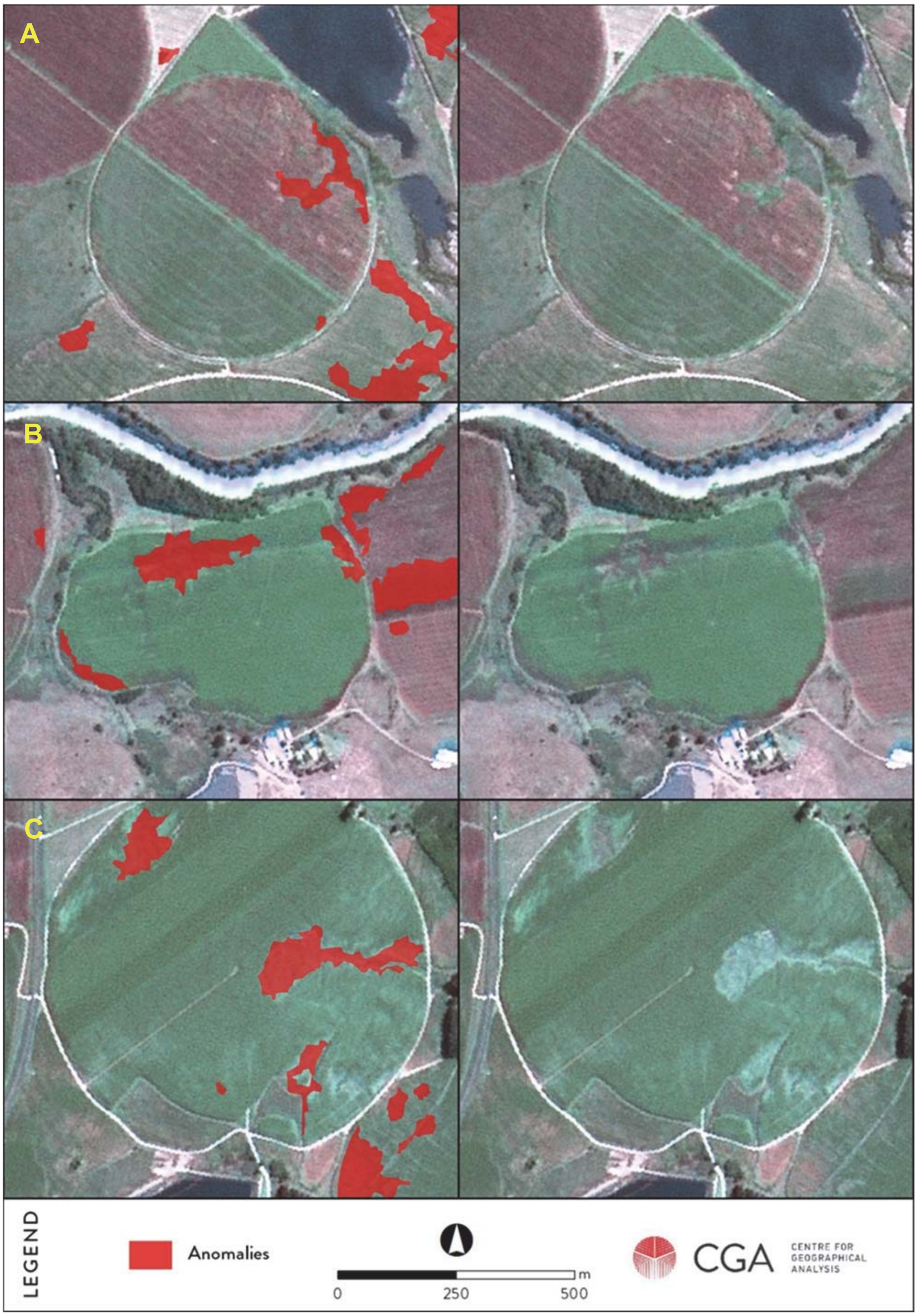

Figure 6.12 Examples of small anomalies detected at Tugela River that were confirmed to be related to waterlogging.

6.7.4 Breede River

The WFAD method was applied to a 29 129 ha area within the Breede River irrigation scheme and a total area of 1396.8 ha (7.34%) was identified as being potentially affected by waterlogging or salt accumulation (i.e. anomalies). Table 6.2 shows that 76.5% of the anomalies were correctly classified and 77.3% of the verified anomalies were observed to be affected by salt accumulation or waterlogging.

An intensive and clustered sampling approach was adopted for Breede River to improve the verification of the delineation of anomalies. Figures 6.13 and 6.14 show examples of where the WFAD technique successfully identified and delineated salt-affected areas. It is clear that the measured EC relates very well with the boundaries of the identified anomalies. However, the precision of delineations depends on the crop type in which the anomaly is identified as the transitions between affected and unaffected areas vary according to crop types. Yields of peaches and grapes, for instance, are affected when the root zone salinity reaches 170 and 150 mS/m, respectively, and are consequently rated sensitive to moderately sensitive to saline conditions (Grattan & Hanson, 2006). The transitions between affected and unaffected areas will therefore be less gradual for these crops, but for less sensitive crops such as lucerne the automated demarcation of anomalies was observed to be less accurate. These variances in sensitivity can only be determined through sufficient field verification.

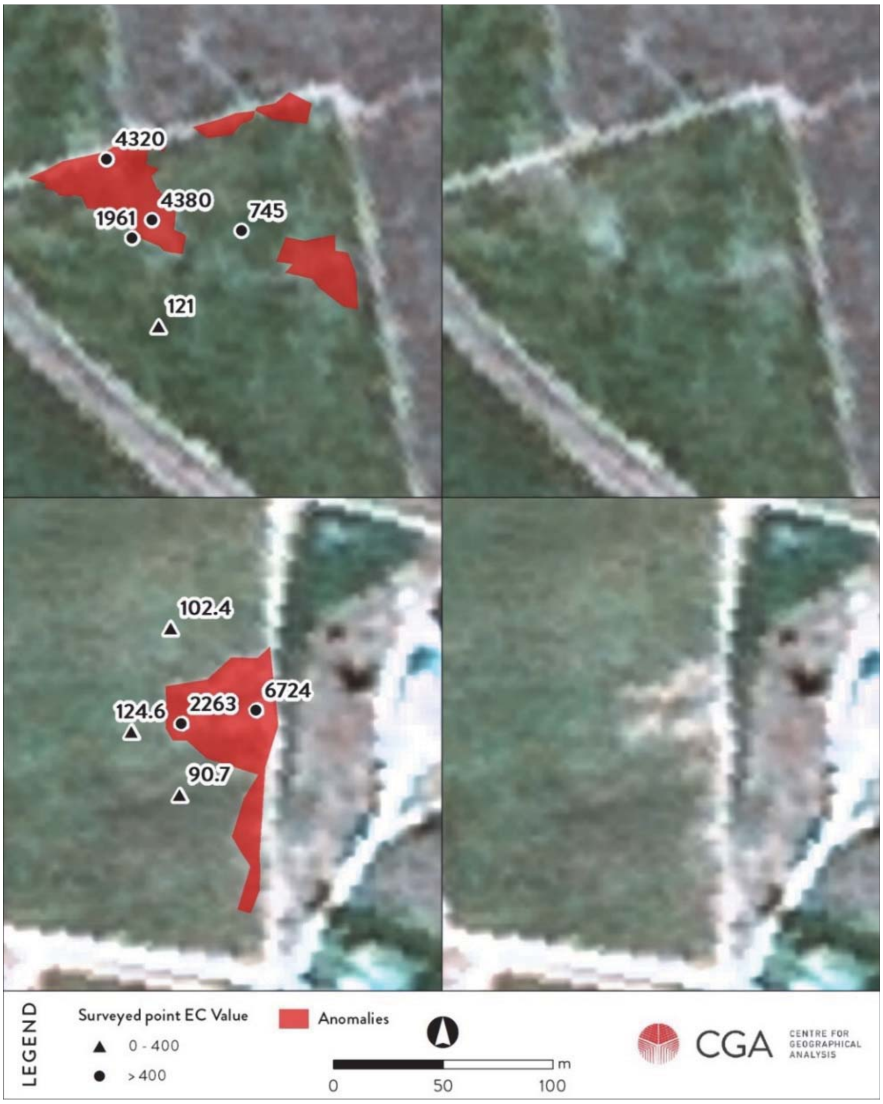

Figure 6.13 Examples of large anomalies detected at Breede River that were confirmed to be related to waterlogging and/or salt accumulation.

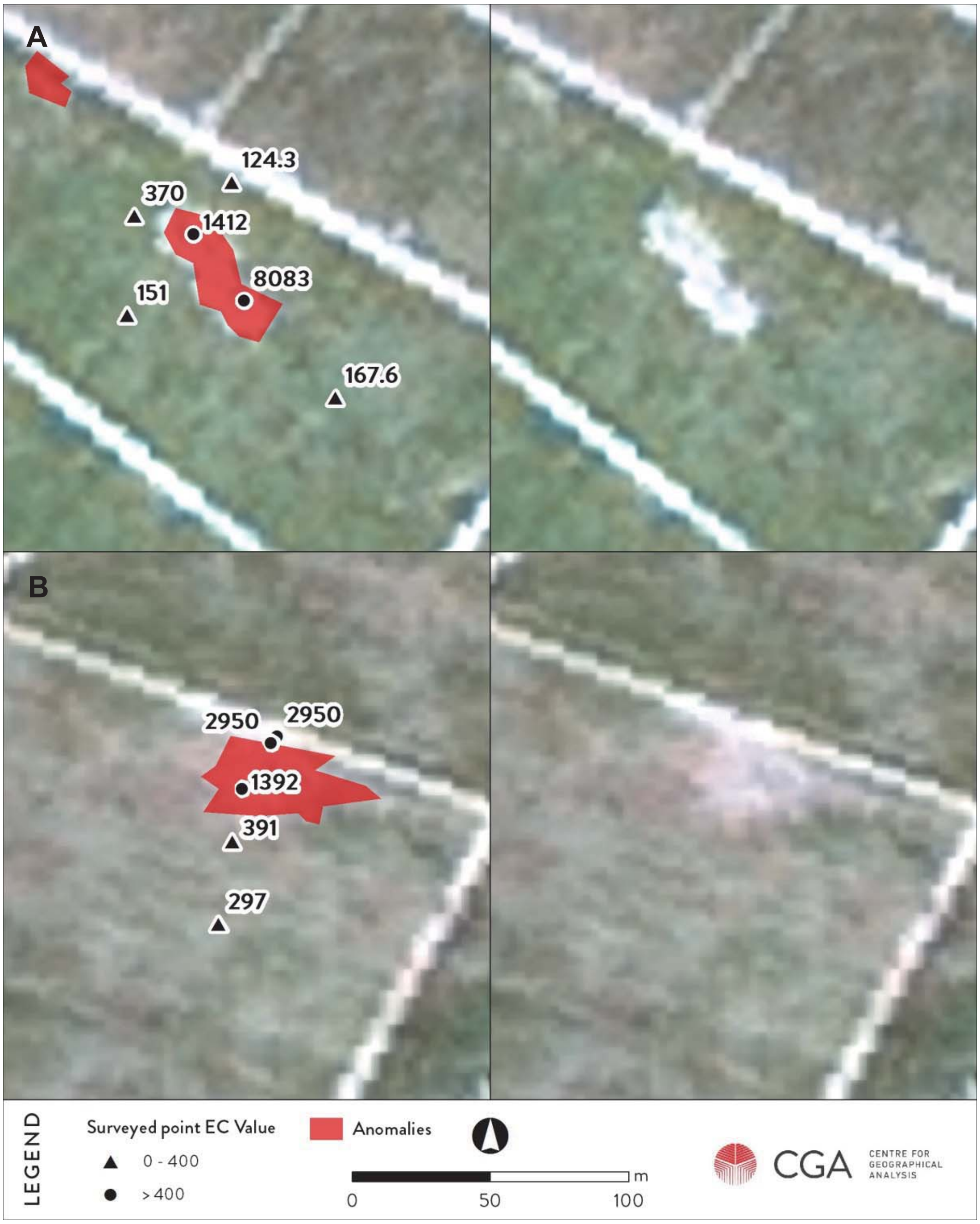

Figure 6.14 Examples of small anomalies detected at Breede River that were confirmed to be related to waterlogging and/or salt accumulation.

6.7.5 Sundays River

Even small patches of affected areas in the Sundays River irrigation scheme were successfully highlighted using the WFAD technique (Figure 6.15). However, the intricate grids of roads that are present in many fields complicated the detection process as some roads were incorrectly classified as being anomalies (Figure 6.16). This resulted in a slight overestimation of salt-affected or waterlogged areas. Such errors can, however, be reduced by manually removing the roads from consideration, but this will be a very time consuming task for large areas. Automated methods should be investigated in future research.

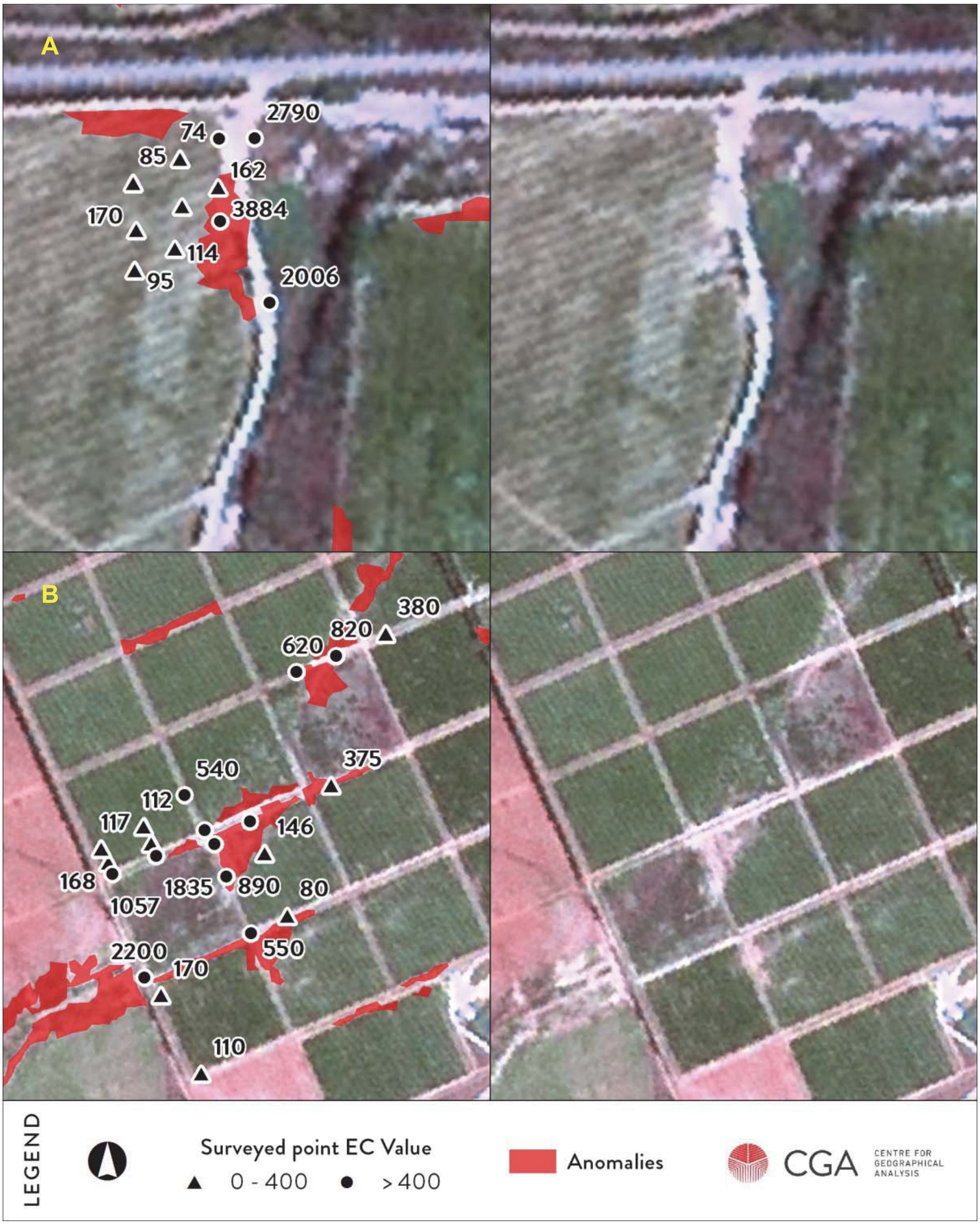

Figure 6.15 Examples of anomalies detected at Sundays River that were confirmed to be related to waterlogging and/or salt accumulation.

The WFAD method was applied to an area of 18 608 ha within the Sundays River irrigation scheme, of which 528.2 ha (2.84%) were identified as being anomalies. Table 6.2 shows that the overall accuracy of the anomaly detection was 80.4%. Almost all (95%) of the anomalies were confirmed to be affected by salt accumulation or waterlogging.

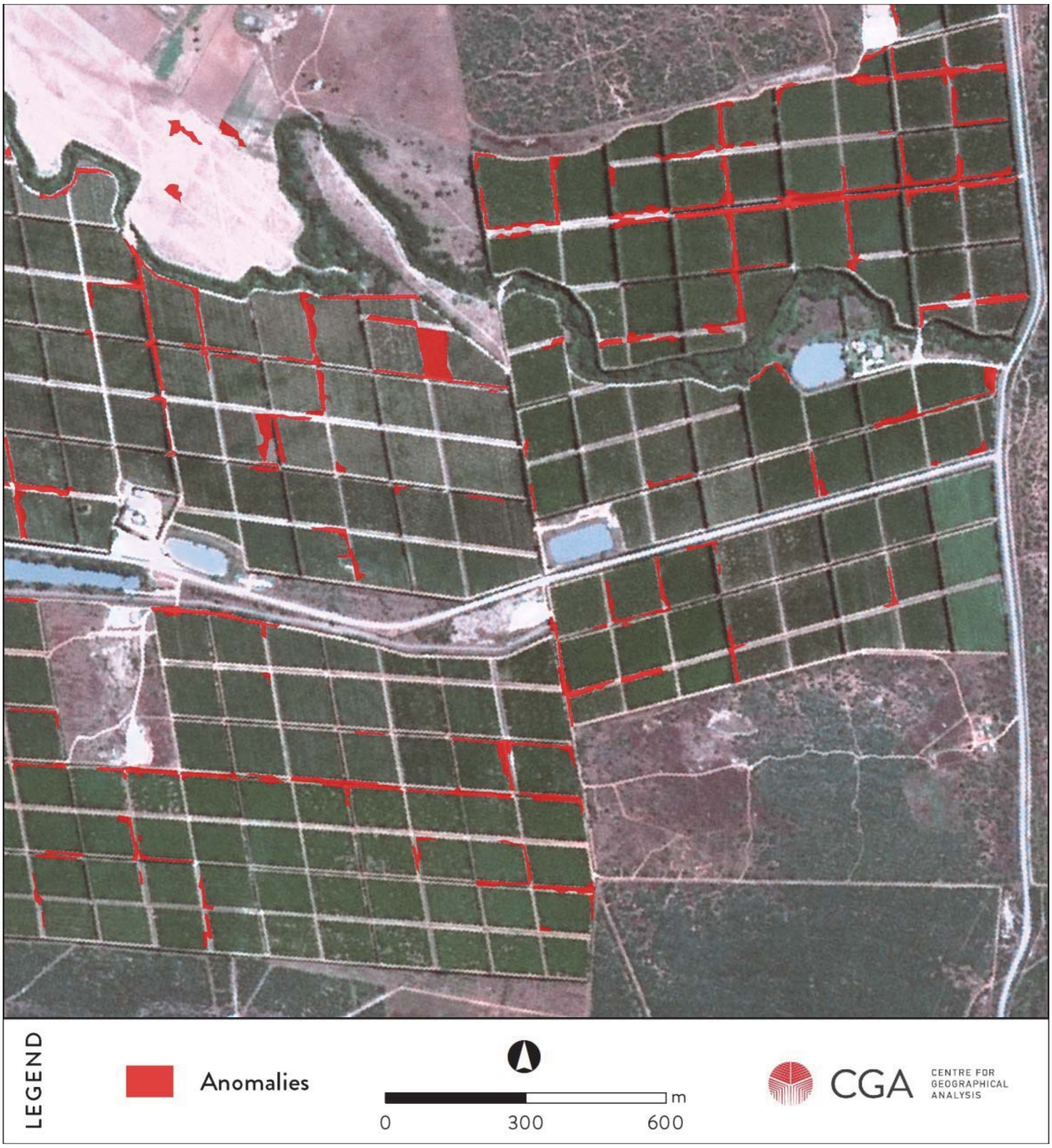

Figure 6.16 Examples of roads at Sundays River that were incorrectly identified as anomalies (i.e. false positives).

6.7.6 Limpopo River

Figure 6.17 shows examples of salt-affected areas that were successfully identified and delineated with the WFAD technique. It is clear that the boundaries of the identified areas relate well to the extent of the verified affected areas. Figure 6.17a and b show a highly heterogeneous area that was classified as an anomaly. During the field survey it was observed that the soil in this area was washed away during a flood and was levelled with transported soil. Such anomalies are consequently false positives as they are not salt-affected or waterlogged. This example demonstrates that the WFAD method is very sensitive to anomalies caused by flood events and should preferably not be implemented in areas that were recently damaged by flooding. Outside flooded areas the WFAD performed relatively well (Figure 6.17c and d), especially in woody croplands (Figure 6.17e and f).

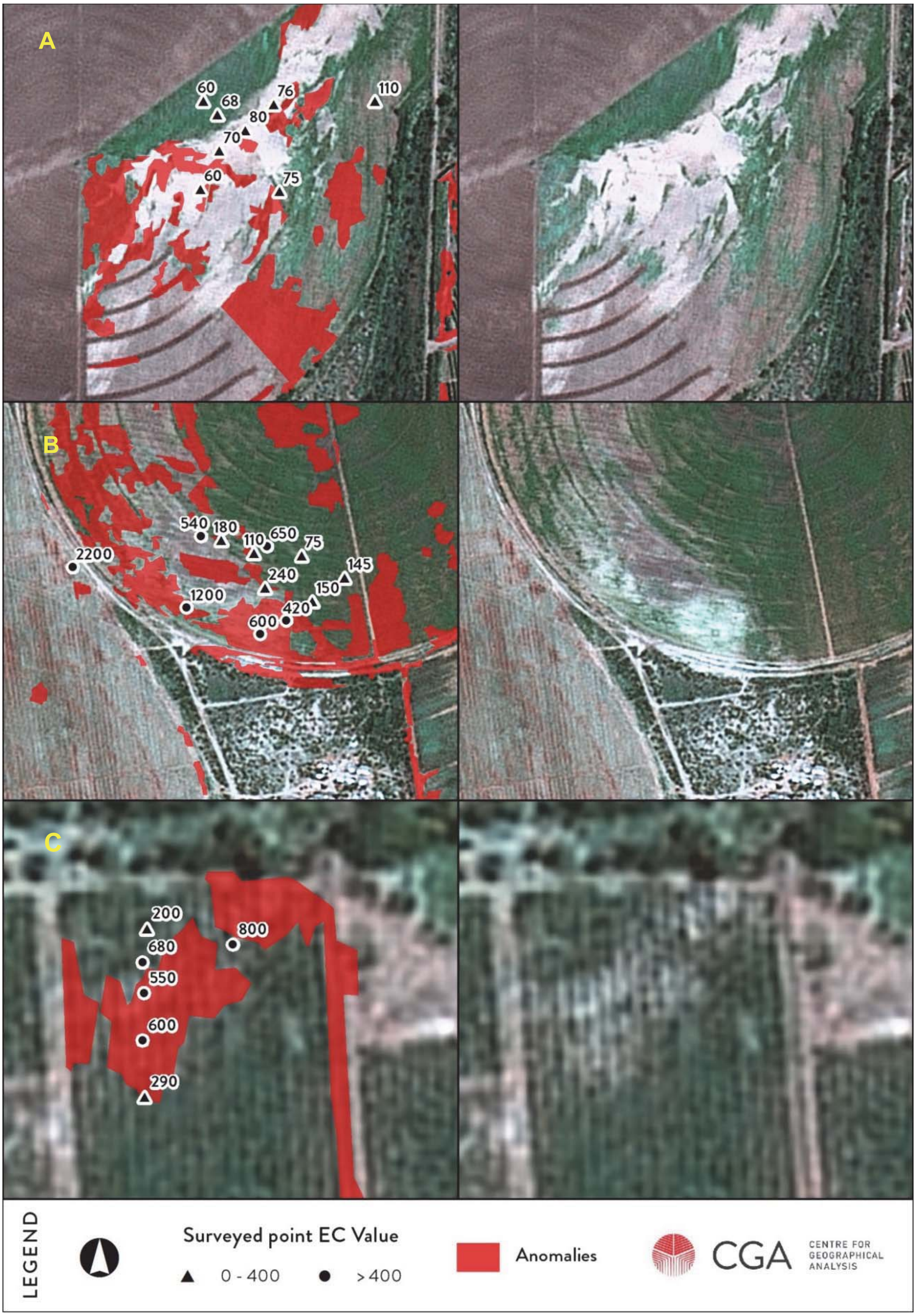

Figure 6.17 Examples of large anomalies detected at Pontdrift that were confirmed to be related to flooding, waterlogging and/or salt accumulation.

The Limpopo River study area was 8681 ha in size and a total of 468.1 ha (5.39%) were identified as anomalies. Table 6.2 shows that the overall accuracy of the anomaly detection was 61%. The relatively low overall accuracy can partly be attributed to false positives due to flood damage. Several areas affected by salt accumulation went undetected, most likely because the flooding temporarily reduced salt accumulation and has since increased. The imagery used in the WFAD technique was from 2012 and 2013 (more recent imagery was unavailable), while the field survey was carried out during 2015. It is thus very likely that temporal changes had a negative effect on the accuracy assessment. The 77.5% proportion of the anomalies in the Limpopo River that are affected by salt accumulation or waterlogging (Ar) closely matched those of the Breede River study area (77.3%).

6.7.7 Douglas (Vaal and Orange Rivers)

Figure 6.18a and e show examples of where large anomalies within two pivot fields were confirmed to be salt-affected. The WFAD method was also very affective in identifying areas that are waterlogged (Figure 6.18c).

As with the Limpopo River, a number of false positives (anomalies that were not affected) also occurred. In Figure 6.19a, for instance, a large anomaly was detected, but no evidence of salt accumulation or waterlogging was found during the field survey (see T1). The WFAD technique works on the assumption that an anomaly is a relatively small (<50%) part of a field. In this case the majority of the field was under stressed conditions (a result of a combination of salt accumulation and drought) which resulted in the healthy part to be classified as being an anomaly. Other anomalies in the same field were, however, confirmed to be affected (see T2). Errors such as those at T1 are very rare and are relatively easy to identify using a quick qualitative assessment of the results. However, a solution to automatically correct such errors needs to be investigated in future research.

Figure 6.19c shows another example of drought stress that resulted in a false positive. In some cases, anomalies were detected but were not large enough to adequately cover the affected area (see Figure 6.19e for an example). This is because some of the areas were not consistently under stress over the period of analysis (2012 and 2013). The addition of images of 2014 would probably have prevented such errors.

As with the Limpopo River, flood damage contributed to a large number of false positives. Figure 6.20 shows some examples of areas affected by the 2011 flood. Figure 6.20a-c show areas that were covered in water in January 2011, while Figure 6.20d-f depict areas when the water receded by July 2011. Most of the surveyed points fall within the flooded areas. This may have had a significant effect on the relatively low accuracy of WFAD in these areas. Much of the secondary salt concentrations of the last decade were likely leached out during the floods, only to resurface due to capillary movement of the primary salts in the system. The timing of field visits are consequently critical. Some areas remained waterlogged after the flood as is the case in Figure 6.20a and d and Figure 6.20b and e which show roughly the same trend.

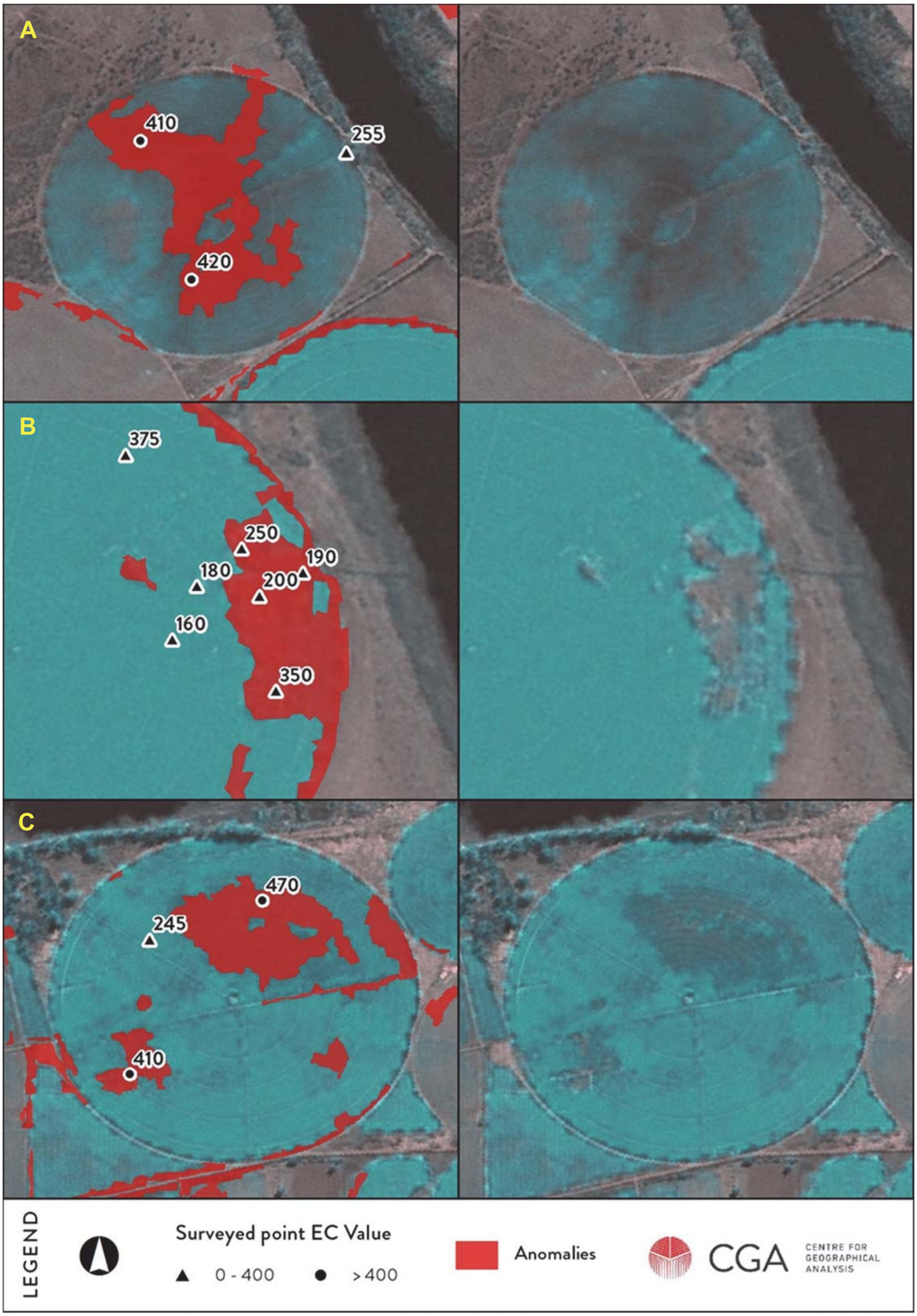

Figure 6.18 Examples of large anomalies detected at Douglas that were confirmed to be related to salt accumulation or waterlogging.

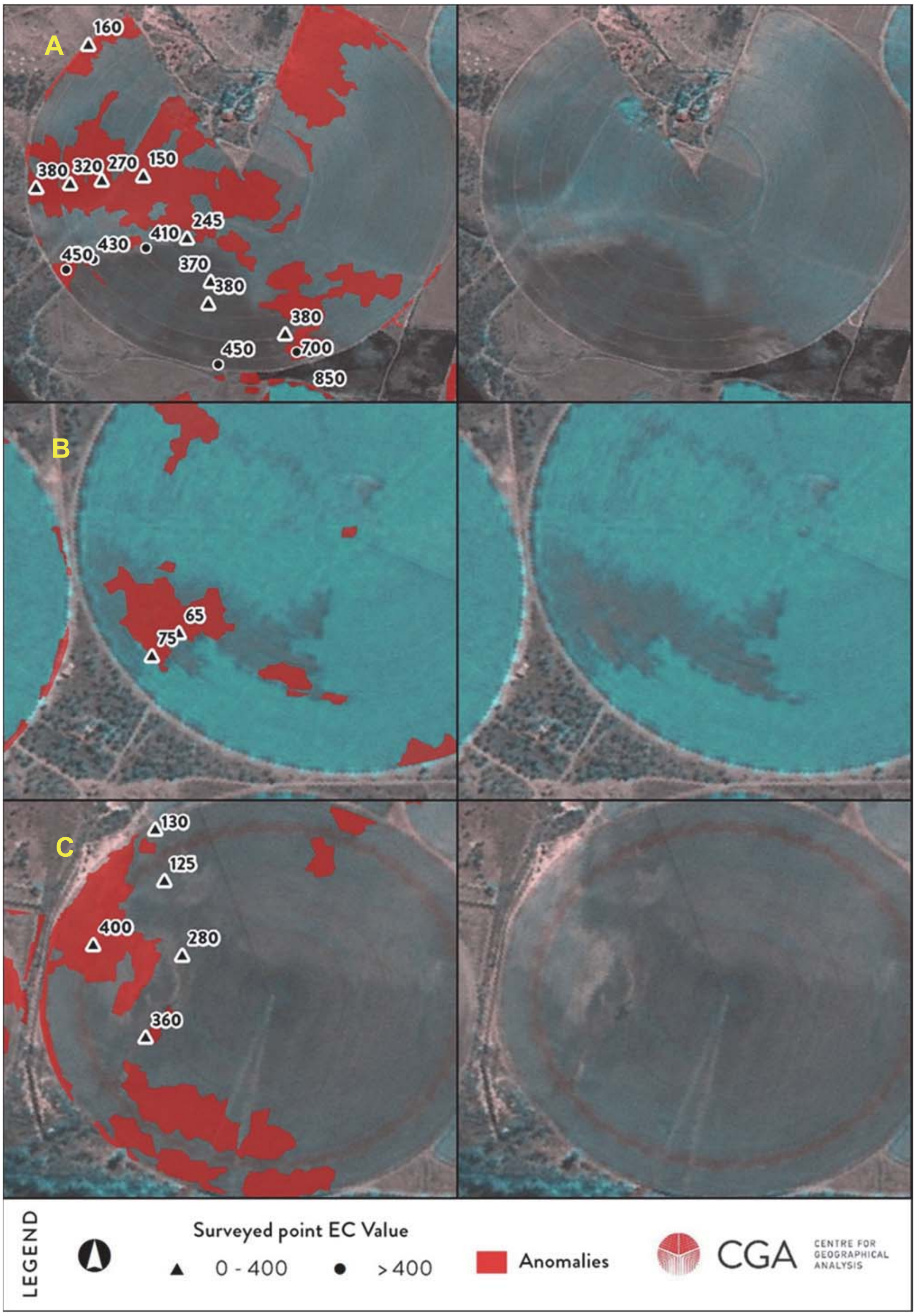

Figure 6.19 Examples of false positives at Douglas.

The WFAD method was applied to a 22 748 ha area within the Douglas irrigation scheme. A total area of 1483.3 ha (6.52%) was identified as being potentially affected by waterlogging or salt accumulation. Table 6.2 shows that the overall accuracy of the classification was 66.7%, with a Kappa coefficient of 0.39. The main reason for the relatively low accuracy is the large number (13) of salt-affected areas that were not picked up as anomalies. This resulted in a salt accumulation producer's accuracy of only 62%. As with the Limpopo River this can be partly attributed to the effects of the 2011 flood (Figure 6.20) which likely reduced the salt accumulation for a period (2011-2012), after which it increased through 2013 and 2014. Given that the field verification was carried out in 2014, the salt accumulation is probably higher than that detected using 2012-2013 imagery. This result demonstrates the dynamic nature of salt accumulation and waterlogging and the importance of regular (at least once a year) monitoring. It is noteworthy that 91.9% of the confirmed anomalies were affected by waterlogging or salt accumulation, which indicates that WFAD holds much potential for monitoring irrigation schemes (such as Douglas) that are dominated by annual crops.

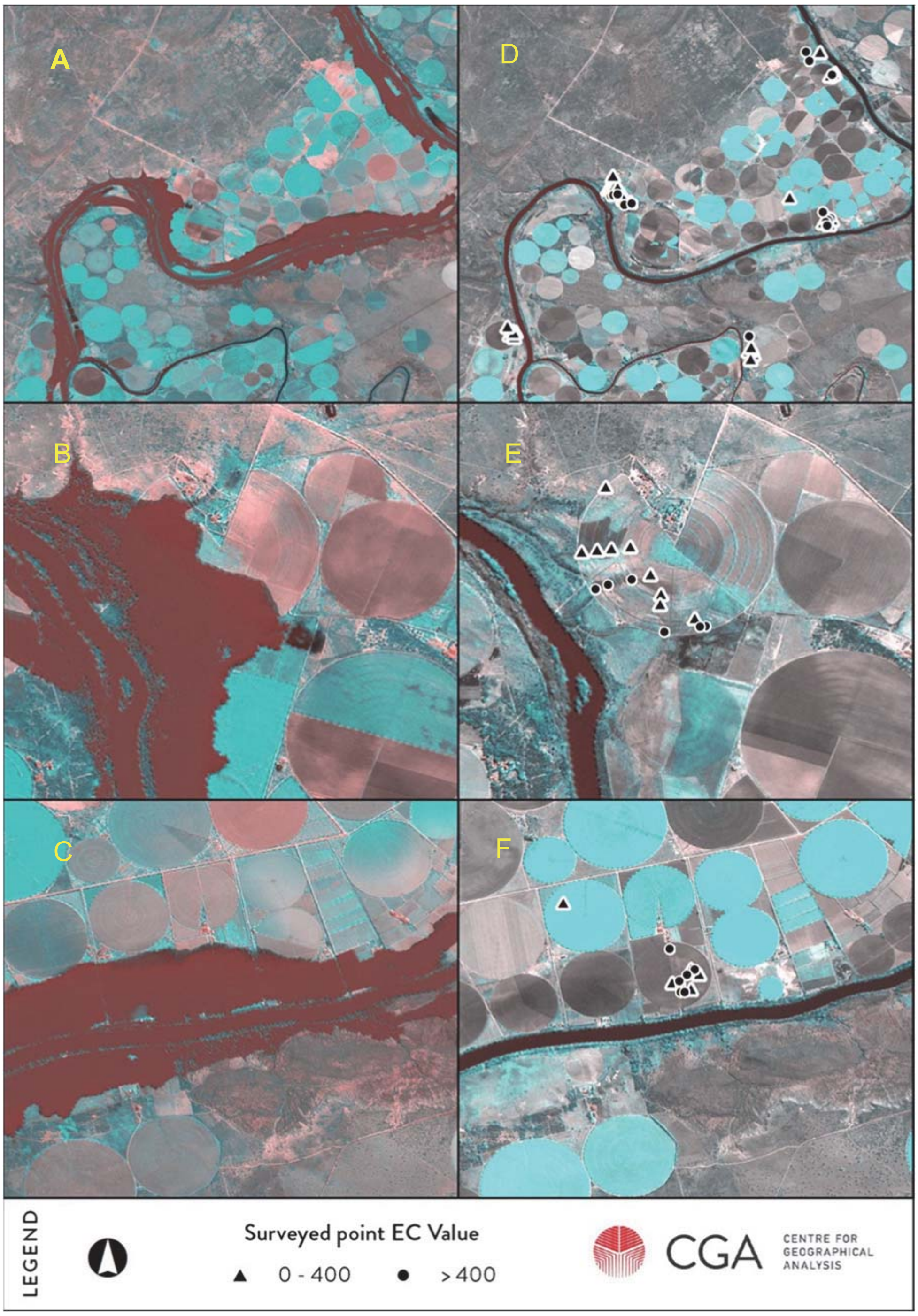

Figure 6.20 Flood damage at Douglas as exposed by images from (a-c) January 2011 and (d-f) July 2011.

6.8 Discussion

Compared to the other methods evaluated, the WFAD technique produced the most promising results for monitoring and quantification purposes. The mean overall accuracy of the technique was 74.9% (Table 6.2). Although this may seem modest compared to some of the other techniques evaluated in Chapter 6, it should be noted that, in contrast to those techniques, the WFAD method:

- was applied in nine irrigation schemes, consisting of a wide range of crop types and conditions;
- was applied in both vegetated and non-vegetated fields;
- required no empirical data for model building purposes; and
- has the potential to be fully automated.

The latter two advantages of the WFAD technique are probably the most noteworthy as they relate directly to the cost-effectiveness of the methodology. The implication of not needing any empirical data for model building is that it can be used for routine monitoring without having to collect and analyse large quantities of soil samples. All the information required by the WFAD technique is acquired from satellite imagery. Although some of the processing steps still need to be streamlined and improved (particularly the field boundary delineation), the WFAD technique has the potential to be fully automated. Once this is done, the only costs involved would be to acquire the satellite imagery. With the recent renewal of the agreement between the South African National Space Agency (SANSA) and Airbus Defence and Space (owner of the SPOT-5/6/7 constellation) it is likely that suitable imagery for use in the WFAD method will remain freely available for South African applications. The recent successful launch of the Sentinel-2 satellite by the European Space Agency (ESA) will also increase the availability of free multispectral imagery. Together these sources of imagery will increase the temporal resolution of available data and enable frequent monitoring of salt accumulation and waterlogging at very low cost.

Although the WFAD technique is very successful in identifying salt-affected and waterlogged areas, one of its main limitations is that it cannot discriminate such areas from anomalies that are caused by other factors (e.g. drought, flooding, soil compaction, disease, inadequate fertilizer application). WFAD should consequently be regarded as a scoping mechanism that can direct attention to areas that are likely to be affected by salt accumulation and/or waterlogging. Such areas should preferably be visited to investigate the likely causes. However, this "limitation" of the WFAD technique can also be regarded as a strength as it can be used for monitoring other factors such as within-field drought and flood damage, disease outbreaks, over-application of pesticides, inadequate fertilization, soil compaction and faulty irrigation infrastructure.

Based on the field surveys conducted in nine irrigation schemes, waterlogging and salt accumulation was the cause in 77.8% of the cases (see mean Ar in Table 6.2). This anomaly ratio was calculated for each study area and used to estimate the total affected areas. On average, 3.3% of the areas considered were found to be affected. This was adjusted to 5.8% by adding abandoned fields. However, it should be noted that this quantification is probably an underestimation of the actual affected area since the majority of the anomalies identified by the WFAD technique represent crops that have been severely affected (to the extent of loss of biomass) for two consecutive seasons. Consequently WFAD cannot (in its current form) detect sudden increases in salt accumulation or waterlogging.

Another implication of the WFAD technique's reliance on crop health is that it does not take a crop's tolerance to saline conditions into consideration. All anomalies are assumed to have the same level of salt accumulation. This is not the case in reality as Table 6.12 showed that an anomaly within a barley field (A = 800 mS/m) will likely have higher levels of accumulated salts than an anomaly in a vineyard (A = 150 mS/m). The crop type should therefore be taken into consideration when interpreting the results of the WFAD method.

In spite of these limitations, WFAD is a robust and cost-effective technique for identifying areas that are potentially affected by salt accumulation and/or waterlogging.

7 AGRICULTURAL GEO-REFERENCED INFORMATION SYSTEM

The aim was to report on the capturing of temporal and spatial data in a geographical information system (GIS) database and establish links to the Agricultural Geo-referenced Information System (AGIS) of DAFF. Unfortunately this was not possible because AGIS has not been properly functional for more than 6 years. Stellenbosch University was contacted to develop a prototype web application, because they have already produced the remote sensing maps and also have the majority of the other soil and irrigation potential maps from ARC-ISCW.

The spatial application server used for AGIS was ArcIMS, which is a product developed by ESRI but is no longer supported by them. AGIS had run on an application server called Appache Tomcat and was using Informix with the Spatial Data Blade extension for spatial operations. All this runs on an operating system that was developed by Sun Micro Systems called Solaris. The fact that AGIS would still be using very old technology to run on probably accounts for its poor functionality.

Modern GIS has moved into all sorts of directions. ESRI has released a few versions of ArcGIS Server since ArcIMS was discontinued. ArcGIS Server has made it possible for users to create functionality such as mapping, geometry and caching services. It gives tools to the administrator to optimize performance best suited to deliver maps speedily, thus making it very interactive. ESRI has also released developer tools for developers to create mapping applications seamlessly to plug into any development environment they see fit.

The open source industry has constantly contributed to products such as spatial databases like PostGIS that runs on top of PostGre SQL. All this has moved GIS systems in a direction that has inspired the masses. Therefore one has to remember that staying competitive in a market that is evolving rapidly, where cloud computing is growing and performance tuning becomes easier, much work is needed for AGIS to be considered with the leading players. Farmers and other stakeholders have over the years become dependent on AGIS to provide them with various kinds of agricultural information. However, because of the current unavailability of AGIS there is still a long road ahead to firstly revive it and then make it relevant.

The current DAFF website (http://www.daff.gov.za/daffweb3/) is quite basic and the scientific information very rudimentary, especially related to agricultural information (http://www.daff.gov.za/ daffweb3/Resource-Centre). In contrast, the Western Cape Department of Agriculture's CapeFarmMapper is a web mapping application that provides functionality to query agricultural, natural resource, farm and erven cadastre in the Western Cape, as well as to create geographical point, line and polygon features on a spatial interface. Other features include calculation of distances and areas, editing features and importing/exporting KML/KMZ files. The OpenLayers API is used to display and manipulate the spatial data and several base map options are available for overlaying the spatial layers (http://www.elsenburg.com/bulletin-board/capefarmmapper).

The web application was developed in the ArcGIS Server environment. ArcGIS Server allows geographical data to be published online and provides web users with access to the data through the Internet. The functionality of the prototype was developed (programmed) using HTML5 and JavaScript. HTML5, the latest revision of the Hypertext Mark-up Language (HTML) standard, is a mark-up language used for displaying content on the World Wide Web. HTML5 improves on previous versions of the language through support of additional multimedia and provides consistent compatibility with various web browsers. HTML5 also allows for the easy integration of JavaScript: a browser-based scripting language that can be used to programmatically control the behaviour of web content. Together, HTML5 and JavaScript provide a powerful platform for the development of content-rich, dynamic and interactive web applications. Extended geographical functionality was obtained through ArcGIS API for JavaScript. The geospatial data (feature classes and raster datasets) are maintained in an ArcSDE enterprise geodatabase and published online as a map service with ArcGIS Server.

Data collected during this project were loaded into the geodatabase for demonstration purposes. It includes three point feature classes (the sampled soil data), a polygon feature class (soil types of the area) and four raster datasets (aerial photography, SPOT-5 imagery, WorldView-2 imagery, and a digital surface model). The application displays the locations of soil samples classified as either Salt-affected or Unaffected according to their measured EC.

Discussions are currently taking place with DAFF to make the information from this project available on a new web platform.

8 CONCLUSIONS AND RECOMMENDATIONS

The main aim of this research was to develop and test a methodological approach for identification, classification and monitoring the extent and degree of waterlogging and salt accumulation at farm, irrigation scheme and national level.

The research agenda was to first carry out a comprehensive literature review, the first component of which focussed on gaining a better understanding of the waterlogging and salt accumulation processes. The second component of the literature review concentrated on the availability of data and existing techniques for monitoring waterlogging and salt accumulation over large areas. It was determined that data with a high spatial resolution would be essential, given that affected areas in South Africa are often small in extent. It was concluded that the use of synthetic aperture radar (SAR) is not viable given the cost and availability of such data in South Africa. Also, despite the efforts of the scientific community, there is currently no robust model for accurately and consistently extracting soil water content or soil salinity from SAR imagery. This science is still very much in an experimental phase, and most authors agree that great strides still need to be made before such an application can be operational. In contrast, there is a relatively large body of work on the use of hyperspectral imagery for detecting salt-affected soils, but such data is even more difficult to obtain in South Africa. From a data availability point of view, multispectral satellite imagery seems to be the most viable source of information for monitoring salt accumulation and waterlogging over large areas. Digital elevation models (DEMs) were also identified as a potential source of valuable information.

Three approaches to mapping waterlogged and salt-affected areas were identified as potential solutions. The first is a modelling approach whereby hydrological, terrain and soil data is used to determine where waterlogging or salt accumulation is likely to occur. Another approach is to differentiate affected and unaffected soils by making use of remotely-sensed imagery (hyperspectral or multispectral) to analyse their spectral properties. This direct remote sensing method is consequently applied to exposed (bare) soil. The third approach, referred to as the indirect remote sensing approach, examines vegetation response (e.g. loss of biomass) to saline or waterlogged conditions. The latter approach mainly makes use of VIs derived from multispectral imagery.

All three of these approaches were evaluated in this research. For the direct remote sensing approach, a WorldView-2 (WV2) satellite image was used to investigate if there are any spectral features of affected soils that can be used in their discrimination. The WV2 image was ideal for this purpose as it had the highest possible spatial (0.5 m) and spectral (8 bands) resolution. Although such imagery is too expensive to be used for monitoring purposes over large areas, its use in this study contributed to the establishment of a “best case scenario”. Also, it enabled an investigation into how less expensive imagery (e.g. that offering only red, green, NIR bands) might perform in comparison. Statistical analyses as well as rule-based and supervised classification methods were evaluated.

Experiments with the direct remote sensing approach showed that there were a number of statistically significant relationships between image features and salt accumulation, with NDSI1 being the best predictor. However, the use of WV2 imagery to identify salt-affected soils was found to be unreliable as all of the methods evaluated grossly overestimated salt accumulation. This was attributed to inconsistencies in the visual appearance of salt-affected soils as in many cases there was no visible evidence of salt accumulation (e.g. salt precipitation). Another factor that complicates the detection of salt accumulation when bare soils are observed using remote sensing is the disturbance caused by soil preparations (e.g. ploughing) as this can alter the soil surface and reflectance. The main limitation of the direct approach is that a relatively small proportion of fields in irrigation schemes are bare at any given time during the year. The implication is that multiple analyses will be required to map an entire irrigation scheme. This will be costly, even with the use of less expensive satellite imagery.

The indirect remote sensing approach was evaluated in the Vaalharts and Breede River study areas. The WV2 image of a lucerne field at Vaalharts was used for evaluating vegetation response to saline conditions. Several experiments were also carried out to investigate the impact of reduced spatial and spectral resolution of satellite imagery – effectively testing the hypothesis that very high spatial resolution imagery is required for monitoring salt accumulation and waterlogging in South African irrigation schemes. A total of 445 WV2-derived spectral and spatial (texture) features were analysed at 0.5, 2, 6, 10, 15 and 20 m resolutions to determine their potential for distinguishing between salt-affected and unaffected soils. Regression analyses were carried out to investigate the relationships between the image features and electrical conductivity (EC) values of 30 soil samples collected in the field. The results showed that there are significant and strong continuous relationships between EC and several of the features considered and that the yellow band, as well as a number of vegetation indices (VIs) and texture features, produced the strongest models. Generally, the strength of these relationships diminished as the spatial resolution was reduced. Overall, the regression analysis and CART results were very promising as they show that VIs generated at 6 m and higher resolution can potentially be used. The results also suggest that high resolution texture features can potentially be used together with VIs for the indirect monitoring of salt-affected soils. Furthermore, the relatively high spectral resolution of the WV2 imagery is not critical as the VIs (based on red and NIR wavelengths only) performed relatively well compared to the performance of the individual bands.

It was concluded that, due to its relatively high cost, the operational use of WV2 imagery for regular monitoring of large areas is not viable. The results show that slightly lower spatial and spectral resolution imagery might produce comparable results. Notable candidates are SPOT-5 (2.5 m panchromatic; 10 m multispectral), SPOT-6 (1.5 m panchromatic; 6 m multispectral), RapidEye (5 m multispectral) and Sentinel-2 (10 m multispectral) data. Although SPOT-5 will soon be decommissioned, its large archive of imagery will be very useful for change analyses where historical baselines are required.

The models generated in the experiments only considered soil samples collected in a cultivated field with a single crop. Given that crops differ in their response to saline conditions, an additional series of experiments was carried out to investigate how these variations will affect the results. These experiments were done in the Vaalharts and Breede River study areas using slightly lower resolution SPOT-5 imagery. In addition to the image features assessed in section 5.2, soil and terrain data was also included in the analyses. It was found that the spectral responses of affected crops differed considerably between the two study areas and that none of the feature sets and/or classification algorithms stood out as being superior for monitoring salt accumulation on irrigation scheme level. Due to the large variations in how different crops respond to saline conditions, the classifications tended to produce many false positives (over-classification). The accuracy levels also varied significantly according to training set size, which is problematic as the routine collection of large sets of soil samples is prohibitively expensive.

The final set of experiments investigated the efficacy of elevation data and its derivatives for modelling salt accumulation at irrigation scheme level. Vaalharts and Breede River were again chosen as the study areas and the SRTM DEM, SUDEM and DSMs derived from high-resolution stereoscopic aerial photography were used as the primary data sources. Numerous derivatives were produced from the primary datasets and several terrain analysis methods were assessed. Two rule sets based on regression modelling and CART, as well as five supervised classifiers (NN, ML, SVM, DT and RF) were considered. The kNN supervised classifier was the most successful in differentiating salt-affected from unaffected soils in both study areas, but it was concluded that the use of elevation data and its derivatives to identify salt-affected soils is ineffective and unreliable. Most of the methods evaluated either underestimated or overestimated salt accumulation or achieved low accuracies, especially for Breede River. The low spatial resolution and quality of the DEMs might have had a negative impact on the results and other elevation data sources, such as LiDAR, should be explored in future research. However, such data may be prohibitively expensive to acquire for large irrigation schemes.

A selection of the more successful experiments are discussed and explained, but many other experiments were carried out during the course of this research project. These included the use of CART on all possible input data (satellite imagery, terrain derivatives, soil data), multi-temporal vegetation response monitoring, and object-based terrain analyses using high-resolution (2m) DSMs (which was evaluated in most of the study areas). These experiments were unsuccessful and discussions thereof were excluded from this report in the interest of brevity.

Both the successful and unsuccessful experiments provided a better understanding of the complexities involved in monitoring salt accumulation and waterlogging in irrigation schemes. It became clear that image texture (heterogeneity) is an important feature for identifying areas that are likely to be salt-affected or waterlogged. The newly-developed within-field anomaly detection (WFAD) method) is based on the principle that heterogeneous areas are in many cases indicative of waterlogging or salt accumulation. Affected areas often stand out as being spectrally different compared to the rest of a field, either because of a reduction in biomass due to saline or saturated conditions (in cultivated fields) or due to specific species of vegetation occurring in fallow fields. Although such “anomalies” can be easily identified using visual interpretation of imagery, they are not easily extracted from remotely-sensed data. Traditional remote sensing techniques involve classifying individual pixels (cells) without taking topology (relationships between spatial entities) into consideration. The WFAD method was implemented and evaluated in all of the study areas. The results showed that, compared to the other methods evaluated, WFAD produced the most promising results for monitoring and quantification purposes. The technique not only produced accurate (74.9% on average) results, but is also cost-effective as it can be applied on both vegetated and non-vegetated fields; requires no empirical data; makes use of freely-available imagery (SPOT-5); and has the potential to be fully automated.

The WFAD technique was used to quantify the extent of affected areas on nine irrigation schemes. On average, 3.3% of the areas considered were found to be affected. This estimate was adjusted to 6.27% by adding abandoned fields. Although the WFAD technique is very successful in identifying salt-affected and waterlogged areas, one of its main limitations is that it cannot discriminate such areas from anomalies that are caused by other factors (e.g. drought, flooding, soil compaction, disease, inadequate fertilizer application). Based on the field surveys conducted in nine irrigation schemes, waterlogging and/or salt accumulation was the cause in 77.8% of the cases (see mean Ar in Table 6.2). The WFAD method should consequently be regarded as a scoping mechanism that can direct attention to areas that are likely to be affected by salt accumulation and/or waterlogging. Such areas should preferably be visited to investigate the actual causes.

Based on the results of this study it is recommended that the WFAD technique be operationalized for routine monitoring of salt accumulation and waterlogging. Its ability to accurately identify potentially affected areas and its reliance on data that is readably available (e.g. SPOT-5 imagery) are its main strengths. The main drawback of the WFAD method is that it relies heavily on manual inputs (e.g. digitizing of field boundaries and crop types) and requires considerable effort to implement (e.g. image acquisition, pre-processing, segmentation and classification), especially when imagery of more than two seasons are used and when large areas need to be covered. More research is needed to improve the efficiency of the workflow and to automate as many as possible of the steps so that the technique can be cost-effectively carried out on a regular basis and for large areas. The technique should also be extended so that multiple images with different extents and resolutions (e.g. SPOT-5/6/7 and Sentinel-2) can be analysed.

The anomaly maps produced by the WFAD technique should be updated on a regular (at least annual) basis. By doing so, a historical record of anomalies and crop conditions can be accrued and used to identify abnormal conditions as soon as they occur. Such abnormal conditions can then be brought to the attention of the farmer.

For the WFAD method to become an operational tool in the proactive management of salt accumulation and waterlogging, the detected anomalies must be made available to all stakeholders (e.g. farmers, extension officers, agribusinesses) in a timely and cost-effective manner. Ideally the information should be delivered through a web-based service that is simple, intuitive and easy to use

From previous studies it appears that severe waterlogging, salinity and sodicity affects 8-18% of the area under regular irrigation in South Africa (Backeberg *et al*., 1996). Ghassemi *et al*. (1995) citing Van Pletsen (1989) stated that a survey of five major irrigation schemes in South Africa indicated that, on average, 28% of irrigated land shows signs of either waterlogging or harmful high salt contents or both. Salt-affected and waterlogged figures of 18-28% for South Africa seem unrealistic if compared to the current study of 6.27% (Table 8.1). If the figure of 6.27% of areas affected is applied to the 1.5 million hectares under irrigation in South Africa, the area that is salt-affected and waterlogged on South African irrigation schemes is 94 050 ha. The areas affected by waterlogged and salt-affected soils on the different irrigation schemes studied were: Vaalharts 849 ha (3.1%), Loskop 2 345 ha (5.7%), Tugela 2103 ha (7.4%), Limpopo River 564 ha (6.4%), Makhathini 361 ha (7.8%), Olifants River 665 ha (5.6%), , Breede River 2215 ha (7.3%), Sundays River 741 ha (3.9%) and Douglas (Vaal and Orange Rivers) 2124 ha (9.1%).

Table 8.1 Summary of the areas affected by salt accumulation and waterlogging

Study Area			Affected		Adjusted	
Name	ha	ha*	ha	%	ha	%
Vaalharts	26434	27033	414.7	1.57	848.9	3.14
Loskop	38831	40867	887.1	2.28	2344.7	5.74
Makhathini	4312	4624	138.5	3.21	361.1	7.81
Olifants River	11284	11911	224.6	1.99	664.9	5.58
Tugela River	27384	28244	1477.3	5.39	2102.8	7.44
Breede River	29129	30188	1396.8	4.8	2215.3	7.34
Sundays River	18608	18832	528.2	2.84	740.5	3.93
Limpopo River	8681	8805	468.1	5.39	564.0	6.40
Douglas	22748	23445	1483.3	6.52	2124.0	9.06
MEAN	20823	21550	779.8	3.78	1329.6	6.27

* Area adjusted by adding abandoned fields

9 PROPOSALS FOR FUTURE RESEARCH AND TECHNOLOGY EXCHANGE

Formation, movement and accumulation of salts and water have a substantial influence on several aspects of soils, mainly on their physical, chemical and biological properties. There are five basic tools for salt accumulation and waterlogging assessments: (i) remote sensing and GIS, (ii) conventional soil analyses and watertable depth measurement, (iii) geophysical methods, (iv) salt and waterlogging modelling, and (v) morphological and micro chemical assessment from field to sub microscopic levels.

Salt accumulation and waterlogging are characterized by their evolution in both time and space. Therefore, the use of traditional methods (laboratory analysis and field surveys) for their monitoring are insufficient and unsuited to the rate of evolution of these phenomena. These methods are also costly, especially for implementation over large areas. In contrast, optical satellite imagery have been shown to be effective for mapping and continuously monitoring of the progression of this phenomena.

Viable permanent irrigated agriculture requires periodic information on salts and watertables on a regional, national, scheme and farm levels for decision making and managing purposes. It is important to know where salt accumulation and waterlogging occur, so that the extent and further risk of increased salt accumulation and waterlogging can be contained.

A monitoring network to record spatial and temporal changes in salt accumulation and waterlogging on irrigation schemes are almost non-existing in South Africa. South Africa must have standardized monitoring, assessments, modelling and mapping methodologies/ procedures to improve the quantification and qualification of salt-affected and waterlogged soils on especially a scheme and national scale. A network of representative monitoring points (benchmark soil sites) should therefore be established on irrigation schemes in conjunction with remote sensing. Assessment and monitoring of salt-affected soils with remote sensing should include associated salts/metals, e.g. magnesium, boron, nitrates, etc. in order to potentially explain observed anomalies. The lead organizations to establish a salt-affected soils and waterlogging monitoring network on South African irrigation schemes are mainly the responsibility of the agricultural provincial departments, together with DAFF, DEA and DAWS.

Remote sensing can provide useful information for large-area water and salt balances and identification of parameters such as evapotranspiration, rainfall distribution, interception losses, and crop types and intensities that can be used as indirect measures of salt accumulation and waterlogging and as evidence for direct estimates.

The possibility to integrate remote sensing, geophysical surveys, and solute modelling, needs to be further explored. More accurate estimation of waterlogging and salt affected soils and wider applications can be expected from such an integrated approach.

Further studies are required in order to determine the calibrating coefficients that can be used to eliminate the background spectra caused by soil moisture contents. In this regard, there are various techniques and data that need to be explored, especially the potential of ground-penetrating radar (GPR), LiDAR, and high-resolution thermal infrared (TIR) data. A third area that still needs research is related to selecting an optimal integration technique. Effective methods of technology transfer need to be developed to ensure that irrigation farmers adopt a best practices approach with respect to irrigation and salt management.

It is recommended that the WFAD technique be operationalized for routine monitoring of salt accumulation and waterlogging. Its ability to accurately identify potentially affected areas and its reliance on data that is readably available. More research is needed to improve the efficiency of the workflow and to automate as many as possible of the steps so that the technique can be cost-effectively carried out on a regular basis and for large areas. The technique should also be extended so that multiple images with different extents and resolutions (e.g. SPOT-5/6/7 and Sentinel-2) can be analysed. The anomaly maps produced by the WFAD technique should be updated on a regular (at least annual) basis. By doing so, a historical record of anomalies and crop conditions can be accrued and used to identify abnormal conditions as soon as they occur. Such abnormal conditions can then be brought to the attention of the farmer.

For the WFAD method to become an operational tool in the proactive management of salt accumulation and waterlogging, the detected anomalies must be made available to all stakeholders (e.g. farmers, extension officers, agribusinesses) in a timely and cost-effective manner. Ideally the information should be delivered through a web-based service that is simple, intuitive and easy to use

The identification of areas on existing irrigation schemes that were abandoned due to waterlogging and salt-affected soils using historical aerial photography and satellite images are also necessary as the WFAD method only considers cultivated or fallow fields, it does not incorporate fields that have been abandoned due to salt accumulation or waterlogging. This exclusion can have a significant effect on the overall quantification of affected areas.

10 REFERENCES

ABBAS, A., 1999. Analysis of Environmental Land Degradation in the Semi-arid Region of Faisalabad, Pakistan using Remote Sensing and GIS Japan.

ABBAS, A. 2007. Using remote sensing techniques for appraisal of irrigated soil salinity. Australia: International Centre of Water for Food Security

ABBAS, A. & KHAN, S., 2007. Using remote sensing techniques for appraisal of irrigated soil salinity. In: Proceedings of the MODSIM 2007 International Congress on Modelling and Simulation, pp. 2632-2638.

ABBAS, A., KHAN, S., HUSSAIN, N., HANJRA. M.A. & AKBAR, S., 2013. Characterizing soil salinity in irrigated agriculture using a remote sensing approach. *Physics and Chemistry of the Earth* 56-57: 43-52.

ABOOD, S., MACLEAN, A. & FALKOWSKI, M., 2011. Soil salinity detection in the Mesopotamian Agricultural Plain utilizing WorldView-2 imagery. In: 8-Bands Challenge Competition.

ABDEL-RAZAK, M.Z., BONN, F., GIUGNI, L.P. & MAHMOOD, A., 2003. Potentiality of RADARSAT-1 images in the detection of salt affected soils in the arid zone: Wadi El-Natrun, Egypt. Geoscience and Remote Sensing Symposium, 2003. IGARSS '03. Proceedings. 2003 IEEE International.

ADEDIRAN, A.O., PARCHARIDISB, I., POSCOLIERIC, M. & PAVLOPOULOSD, K., 2004. Computer-assisted discrimination of morphological units on north-central Crete (Greece) by applying multivariate statistics to local relief gradients. *Geomorphology* 58: 357-370.

AGASSI, M., MORIN, J. & SHAINBERG, I., 1985. Effect of raindrop impact energy and water salinity on infiltration rates of sodic soils. *Soil Sci. Society of American Journal* 49, 186-90.

AKRAMKHANOV, A., MARTIUS, C., PARK, S. & HENDRICKX, J., 2011. Environmental factors of spatial distribution of soil salinity on flat irrigated terrain. *Geoderma* 163(1-2): 55-62.

ALBERT, T.H., 2002. Evaluation of remote sensing techniques for ice-area classification applied to the tropical Quelccaya Ice Cap, Peru. *Polar Geography* 26(3): 210-226.

ALDAKHEEL, Y.Y., 2010. Assessing NDVI spatial pattern as related to irrigation and soil salinity management in Al-Hassa oasis, Saudi Arabia Indian Society of Remote Sensing 39: 171-180.

ALDAKHEEL, Y.Y., 2011. Assessing NDVI spatial pattern as related to irrigation and soil salinity management in Al-Hassa Oasis, Saudi Arabia. *Journal of the Indian Society of Remote Sensing* 39(2): 171-180.

ALHAMMADI, M.S. & GLENN, E.P., 2008. Detecting date palm trees health and vegetation greenness change on the eastern coast of the United Arab Emirates using SAVI. *International Journal of Remote Sensing* 29(6): 1745-1765.

AL-KHAIER, F., 2003. Soil salinity detection using satellite remote sensing. International Institute for Geo-Information Science and Earth Observation. M.Sc. Thesis, Michigan Technological University.

ALLAIN, S., FERRO-FAMIL, L. & HAJNSEK, I., 2002. Extraction of surface parameters from multi-frequency and polarimetric SAR data Proceedings of IGARSS 2002 1: 426-428.

ALLBED, A., KUMAR, L. & ALDAKHEEL, Y.Y., 2014. Assessing soil salinity using soil salinity and vegetation indices derived from IKONOS high-spatial resolution imageries: Applications in a date palm dominated region. *Geoderma* 230-231: 1-8.

ÁLVAREZ-MOZOS, J., CASALÍ, J., GONZÁLEZ-AUDÍCANA, M. & VERHOEST, N.E.C., 2005. Correlation between Ground Measured Soil Moisture and RADARSAT-1 derived Backscattering Coefficient over an Agricultural Catchment of Navarre (North of Spain). Biosystems Engineering 92: 119-133.

ALY, Z., BONN, F. & MAGAGI, R., 2007. ANALYSIS OF THE BACKSCATTERING COEFFICIENT OF SALT-AFFECTED SOILS USING MODELING AND RADARSAT-1 SAR DATA. *IEEE TRANSACTIONS ON GEOSCIENCE AND REMOTE SENSING* 45: 332-341.

ARGIALAS, D.P., 1995. Towards structured-knowledge models for landform representation. *Zeitschrift für Geomorfologie N.F* 101: 85-108.

ARMOUR, R.J., 2002. The economic effects of poor and fluctuating irrigation water salinity levels in the Vaal and Riet rivers. M.Sc. Agric University of the Free State, Bloemfontein.

ASRAR, G., FUCHS, M., KANEMASU, E. & HATFIELD, J., 1984. Estimating absorbed photosynthetic radiation and leaf area index from spectral reflectance in wheat. *Agronomy Journal* 76: 300-306.

AURECON, 2010. Feasibility study and business plan on the rehabilitation/upgrading of bulk water infrastructure and agri-business development within the Vaalharts/Tung irrigation region. Volume 1, Status quo report, Final report.

BAATZ, M. & SCHÄPE, A., 2000. Multiresolution Segmentation: an optimization approach for high quality multi-scale image segmentation. *Journal of Photogrammetry and Remote Sensing* 58: 12-23.

BACKEBERG, G.R., BEMBRIDGE, T.J., BENNIE, A.T.P., GROENWALD, J.A., HAMMES, P.S., PULLEN, R.A. & THOMPSON, H., 1996. Policy proposal for irrigated agriculture in South Africa. WRC Report No. KV 96/96, Water Research Commission, Pretoria.

BANNARI, A., MORIN, D., BONN, F. & HUETE, A.R., 1995. A review of vegetation indices. *Remote Sensing Reviews* 13: 95-120.

BARALDI, A. & PARMIGGIANI, F., 1995. An investigation of the textural characteristics associated with gray level cooccurrence matrix statistical parameters. *IEEE Transactions on Geoscience and Remote Sensing* 33(2): 293-304.

BARNARD, R.O., VAN DER MERWE, A.J., NELL, J.P., DE VILLIERS, M.C., VAN DER MERWE, G.M.E. & MULIBANA, N.E., 2002. Technical country report/in-depth study on problem soils including degraded soils in South Africa: Extent, present use, management and rehabilitation (with emphasis on salt-affected soils). 4th Meeting of FAO Global Network Integrated Soil Management for Sustainable Use of Salt-Affected Soils. Valencia, Spain. May 2001.

BASTIAANSSEN, W.G.M., 1998. Remote Sensing in Water Resources Management : The State of the Art. International Irrigation Management Institute, Colombo, Sri Lanka.

BASTIAANSSEN, W.G.M., MOLDEN D.J; MAKIN, I.W., 2000. Remote Sensing for irrigated agriculture: examples from research and possible applications. *Agricultural Water Management* 46: 137-155.

BAUSCH, W.C., 1993. Soil background effects on reflectance-based crop coefficients for corn. *Remote Sensing of Environment* 46: 213-222.

BEHARI, J., 2005. Microwave Dielectric Behaviour of Wet Soils (Springer Verlag)

BELL, D., MENGES, C., AHMAD, W. & VAN ZYL, J.J., 2001. The Application of Dielectric Retrieval Algorithms for Mapping Soil Salinity in a Tropical Coastal Environment Using Airborne Polarimetric SAR. *Remote Sensing of Environment* 75: 375-384.

BENADE, N., 1991. Optimisation of distribution losses in irrigation canals. *Proceedings of the Southern African Irrigation Symposium,* 4-6 June 1991, Elangeni Hotel, Durban.

BEN-DOR, E., LEVIN, N. & SAARONI., H., 2001. A spectral based recognition of the urban environment using the visible and near-infrared spectral region (0.4-1.1 μm). A case study over Tel-Aviv, Israel. *International Journal of Remote Sensing* 22: 2193-2218.

BERTRAM, E., 1989. Die verband tussen geologie, grondwatergehalte en boorgat-lewerings in die Breederiviervallei tussen die Groter Brandvleidam en die Sanddrift-meetwal. Department of Water Affairs, Directorate Geohydrology, Technical Report No. GH 3651, 46: 137-155.

BESTER, J., GORGENS, A.H.M. & GREYLING, A.J., 1990. Breede River System: Development of a Daily Hydrosalinity Model (DISA). DWA Report No.H 000/00/0790.

BESTER, H.C. & LIEGME, D.P., 1989. The evaluation of land for irrigation: A literature review. SIRI Report No. GB/A/90/03, ARC-Institute for Soil, Climate and Water, Pretoria.

BEVEN, K. & KIRKBY, M., 1979. A physically based, variable contributing area model of basin hydrology. *Hydrological Sciences Bulletin* 24, 1: 43-69.

BHATTACHARYA, A.A., 1943. On a measure of divergence between two statistical populations defined by their probability distributions. *Bulletin of the Calcutta Mathematical Society* 35: 239-258.

BLASCHKE, T., 2010. Object based image analysis for remote sensing. *ISPRS Journal of Photogrammetry and Remote Sensing* 65: 2-16.

BLASCHKE, T. & STROBL, J., 2001. What's wrong with pixels? Some recent developments interfacing remote sensing and GIS. GIS. *Zeitschrift Fur Geoinformationssysteme,* 14: 12-17.

BLASCHKE, T, LANG, S., LORUP, E., STROBEL, J. & ZEIL, P., 2000. Object-orientated image processing in an integrated GIS/Remote sensing environment and perspectives for environmental applications. *EnviroInfo 2000:Umweltinformatik Umweltinformation fur Planung, Politik und Offentlichkeit, 555-569.*

BOCK, M., XOFIS, P., MITCHLEY, J., ROSSNER, G. & WISSEN, M., 2005. Object-oriented methods for habitat mapping at multiple scales – Case studies from Northern Germany and Wye Downs, UK. *Journal for Nature Conservation* 13: 75-89.

BÖHNER, J., BLASCHKE, T. & MONTANARELLA, L., 2008. SAGA – Seconds Out. *Hamburger Beiträge zur Physischen Geographie und Landschaftsökologie* 19.

BÖHNER, J., KÖTHE, R., CONRAD, O., GROSS, J., RINGELER, A. & SELIGE, T., 2002. Soil regionalisation by means of terrain analysis and process parameterisation. In: E. Micheli, F. Nachtergaele & L. Montanarella (eds). European Soil Bureau. The European Soil Bureau, Joint Research Centre, EUR 20398 EN, Ispra, pp. 213-222. Available from: http://www.scilands.de/referenzen/veroeffentlichung/601Bohner.pdf.

BOLSTAD, P.V. & LILLISAND, T.M., 1991. Rapid maximum likelihood classification. *Photogrammetric Engineering and Remote Sensing 57: 67-74.*

BOSCH, A., ZISSERMAN, A. & MUOZ, X., 2007. Image classification using Random Forests and Ferns. In: IEEE 11th International Conference on Computer Vision, Miami, 1-8.

BOTHA, M.J., COETZEE, C.J. & VAN RENSBURG, H., 1988. Verkenningsopname van gronde langs riviere in die Noord-Transvaalse aangewese gebied. NIGB Verslagnommer GB/A/88/20, ARC-Institute for Soil, Climate and Water, Pretoria.

BRADSKI, G., 2000. The OpenCV library. *Dr. Dobb's Journal of Software Tools for the Professional Programmer* 25(11): 122-125.

BREIMAN, L., 1996. Bagging predictors. *Machine Learning* 24, 2: 123-140.

BREIMAN, L., 2001. Random Forests. *Machine Learning* 45: 5-32.

BRESLER, E., MCNEAL, B.L. & CARTER, D.L., 1982. Saline and Sodic Soils. Springer-Verlag, New York.

BROWN, DE COLSTOUN, E.C., STORY, M.H., THOMPSON, C., COMISSO, K., SMITH, T.G. & IRONS J.R., 2003. National Park vegetation mapping using multitemporal Landsat 7 data and a decision tree classifier. *Remote Sensing of Environment* 85: 316-327.

BUSCHMANN, C., LANGSDORF, G. & LICHTENTHALER, H.K., 2000. Imaging of blue, green, and red fluorescence emission of plants: an overview. *Photosynthetica* 38: 483-491.

CAI, S., ZHANG, R., LIU, L. & ZHOU, D., 2010. A method of salt-affected soil information extraction based on a support vector machine with texture features. *Mathematical and Computer Modelling* 51(11-12): 1319-1325.

CAMPBELL, J.B., 2002. Introduction to remote sensing. London: Taylor & Francis.

CAMPBELL, J.B., 2007. Introduction to remote sensing. Fourth Edition London: Taylor & Francis.

CARPER, W.J., 1990. The use of intensity-hue-saturation transformations for merging SPOT panchromatic and multispectral image data. *Photogrammetric Engineering & Remote Sensing* 56: 457-467.

CASS, A., 1980. The influence of pore structural stability and internal drainage rate on selection of soils for irrigation. Ph.D. Agric. Dissertation, University of Natal, Pietermaritzburg

CECCATO, P., GOBRON, N., FLASSE, S., PINTY, B. & TARANTOLA, S., 2002. Designing a spectral index to estimate vegetation water content from remote sensing data: Part 2. Validation and applications. *Remote Sensing of Environment* 82: 198-207.

CHANG, C. & LIN, C., 2011, 'LIBSVM: A library for support vector machines', ACM Transactions on Intelligent Systems Technology, vol. 2, pp. 27:1-27:27.

CHAWLA, N. V., JAPKOWICZ, N. & DRIVE, P., 2004. Editorial : Special Issue on Learning from Imbalanced Data Sets. *ACM SIGKDD Explorations Newsletter* 6(1): 1-6.

CHEN, Y., S.U., W., LI, J. & SUN, Z., 2009. Hierarchical object oriented classification using very high resolution imagery and LIDAR data over urban areas. Advances in Space Research 43: 1101-1110.

CHILDS, S.W. & HANKS, R.J., 1975. Model of salinity effects on crop growth. *Soil Sci.Soc.Am.Proc.* 39: 617-622.

CHO, M. A., SKIDMORE, A., CORSI, F., VAN WIEREN, S. E. AND SOBHAN, I. 2007. Estimation of green grass/herb biomass from airborne hyperspectral imagery using spectral indices and partial least squares regression. *Int. J. Appl. Earth Observ. Geoinform. 9: 414-424*

CHUVIECO, E. & HUETE, A., 2010. Fundamentals of Satellite Remote Sensing. Boca Raton: Taylor & Francis.

CLAUSI, D., 2002. An analysis of co-occurrence texture statistics as a function of grey level quantization. *Canadian Journal of Remote Sensing* 28(1): 45-62.

COHEN, Y. & SHOSHENY, M., 2002. A national knowledge-based crop recognition in Mediterranean environment. *International Journal of Applied Earth Observation and Geoinformation* 4: 75-87.

CONCHEDDA, G., DURIEUX, L. & MAYAUX, P., 2008. An object-based method for mapping and change analysis in mangrove ecosystems. *ISPRS Journal of Photogrammetry and Remote Sensing* 63: 578-589.

CONNERS, R.W. & HARLOW, C.A, 1980. A theoretical comparison of texture algorithms. *IEEE Transactions on Pattern Analysis and Machine Intelligence* 2: 204-222.

CORWIN, D.L. & RHOADES, J.D., 1982. An improved technique for determining soil electrical conductivity-depth relations from above ground electromagnetic measurements. *Soil Sci Soc Am J 46:517-520*.

COVER, T. & HART, P., 1967. Nearest neighbour classification. *IEEE Transactions on Information Theory* 13(1): 21-27.

CSILLAG, F.L., PASZTOR, L. & BIEHL, L.L., 1993. Spectral band selection for the characterization of salinity of soils. *Remote Sensing of Environment* 43: 231-242.

CSORNAI, G., SUBA, Z., NÁDOR, G., LÁSZLÓ, I. & CSEKÓ, Á., 2004. Envisat and ERS Symposium. Envisat and ERS Symposium, Salzburg.

CUARTAS L.A., TOMASELLA, J., NOBRE, A.D., NOBRE, C.A., HODNETT, M.G.,WATERLOO, M.J. &MOTA DE OLIVEIRA, S. (2012). Distributed hydrological modelling of a micro-scale rainforest watershed in Amazonia: Model evaluation and advances in calibration using the new HAND terrain model, *Journal of Hydrology* 462-463:

CUNNINGHAM, P. & DELANY, S.J., 2007. K-Nearest Neighbour Classifiers. Technical Report UCD-CSI-2007-4. University College Dublin.

CUTLER, D.R., EDWARDS, T.C., BEARD, K.H., CUTLER, A., HESS, K.T., GIBSON, J. & LAWLER, J.J., 2007. Random forests for classification in ecology. *Ecology* 88: 2783-2792.

DEHNI, A. & LOUNIS, M., 2012. Remote sensing techniques for salt affected soil mapping: Application to the Oran region of Algeria. *Procedia Engineering* 33: 188-198.

DEKKER, R.J., 2003. Texture analysis and classification of ERS SAR images for map updating of urban areas in the Netherlands. *IEEE Transactions on Geoscience and Remote Sensing* 41: 1950-1958.

DEL VALLE, H., BLANCO, P., SIONE, W., ROSTANGO, C. & ELISSALDE, N. (eds) 2009. Assessment of salt-affected soils using multisensor radar data: a Case study from north eastern Patagonia (Argentina). Boca Raton, FL: Taylor and Francis.

DEMERS, M.N. 2009. Fundamentals of geographic information systems. 3rd ed. New York: Wiley & Sons.

DENDGIZ, O., BAYRAMIN, Ü. & YÜKSEL, M., 2003. Geographic information system and remote sensing based land evaluation of BeypazarÝ area soils by ILSEN model. *Turkish Journal of Agriculture and Forestry* 27: 145-153.

DIGITALGLOBE, 2015. WorldView-2. (Web) https://www.digitalglobe.com/sites/default/files/DG_WorldView2_DS_PROD.pdf

DOHSE, T.E., SCHOEMAN, J.L. & TURNER, D.P., 1991. Changing aspects to the assessment of land suitability for irrigation planning. In: Proceedings of the Southern African Irrigation Symposium, 4-6 June 1991, Elangeni Hotel, Durban. SABI, Pretoria.

DOBSON,M., ULABY, F., HALLIKAINEN, M. & EL-RAYES, M., 1985. Microwave Dielectric Behaviour of Wet soil – part ii: Dielectric mixing models *IEEE Transactions on Geoscience and Remote Sensing* GE-23: 35-46.

DOOLITTLE, J. A., SUDDUTH, K.A., KITCHEN, N. R., & INDORANTE, S.J., 1994. Estimating depths to clay pans using electromagnetic induction methods. *J. Soil and Water Cons. 49:572-575.*

DOUAOUI, A.G., 2011. Combination of remote sensing and kriging to improve soil salinity in the Hmadna plain (Algeria). Chlef, Algeria: University Hassiba Benbouali.

DOUAOUI, A. & EL GHADIRI, I., 2015. Combination of remote sensing and kriging to improve soil salinity mapping in the Hmadna plain (Algeria). *Soil-Water Journal* Special Issue 1-5.

DOUAOUI, A.E.K., NICOLAS, H. & WALTER, C., 2006. Detecting salinity hazards within a semiarid context by means of combining soil and remote-sensing data. *Geoderma* 134: 217-230.

DRAGUT, L. & BLASCHKE, T., 2006. Automated classification of landform elements using object-based image analysis. *Geomorphology* 81: 330-344.

DU PLESSIS, H.M., 1991. Researching and applying measures to conserve natural irrigation resources. In: Proceedings of the Southern African Irrigation Symposium, 4-6 June 1991, Elangeni Hotel, Durban. SABI, Pretoria.

DU PREEZ, C.C., STRYDOM, M.G., LE ROUX, P.A.L., PRETORIUS, J.P., VAN RENSBURG, L.D. & BENNIE, A.T.P., 2000. Effect of water quality on irrigation farming along the lower Vaal River: The influence on soils and crops. WRC Report No. 740/1/00, Water Research Commission, Pretoria.

DURO, D.C., FRANKLIN, S.E. & DUBE, M., 2012. Multi-scale object-based image analysis and feature selection of multi-sensor earth observation imagery using random forests. *International Journal of Remote Sensing* 33(14): 4502-4526.

D'URSO, G. & MINACAPILLI, M., 2006. A semi-empirical approach for surface soil water content estimation from radar data without a-priori information on surface roughness. Journal of Hydrology 321: 297-310.

DWIVEDI, R.S., 1992. Monitoring and the study of the effect of image scale on delineation of salt-affected soils in the Indo-Gangetic plains. *Int J Remote Sens 13:1527-1536*

DWIVEDI, R.S., 1997. Mapping waterlogged areas in part of the Indo-Gangetic plains using remote sensing data. *Geocarto International* 12: 65-70.

DWIVEDI, R.S., RAMANA, K.V., THAMMAPPA, S.S. & SINGH, A.N., 2001. The utility of IRS-1C LISS-III and PAN-merged data for mapping salt-affected soils. *Photogrammetric Engineering and Remote Sensing* 67: 1167-1175.

DWIVEDI, R.S. & SREENIVAS, K., 1998. Delineation of salt-affected soils and waterlogged areas in the Indo-Gangetic plains using IRS-1C LISS-III data. *International Journal of Remote Sensing* 19: 2739-2751.

DWIVEDI, R.S., SREENIVAS, K. & RAMANA, K.V., 1999. Inventory of salt-affected soils and waterlogged areas: A remote sensing approach. *International Journal of Remote Sensing* 20(8): 1589-1599.

DYMOND, J.R., DEROSE, R.C. & HARMSWORTH, G.R., 1995. Automated mapping of land components from digital elevation data. *Earth Surface Processes and Landforms* 20: 131-137.

ELDIERY, A., 2005. Estimating soil salinity from remote sensing data in corn fields. Ph.D. Thesis, Colorado: Colorado State University.

ELDIERY, A., GARCIA, L.A. & REICH, R.M., 2005. Estimating soil salinity from remote sensing data in corn fields. *Hydrology Days* 970: 31-42.

ELLIS, F., 1988. Die gronde van die Karoo. Ph.D.-thesis, University of Stellenbosch, Stellenbosch.

ELNAGGAR, A.A. & NOLLER, J.S., 2009. Application of remote-sensing data and decision-tree analysis to mapping salt-affected soils over large areas. *Remote Sensing* 2(1): 151-165.

ENGELBRECHT, J., 2009. Synthetic aperture radar data employed for soil moisture estimation in the Piketberg region, South Africa. Geoscience and Remote Sensing Symposium, 2009 IEEE International,IGARSS 2009.

ENGINEERING NEWS 2002. Big agricultural plan for Makhathini Flats [online]. (Web) http://www.engineeringnews.co.za/article/big-agricultural-plan-for-Makhatini-flats-2002-10-18.

EVANGELISTA, P., 2006. The unbalanced classification problem: Detecting breaches in security. Ph.D. Thesis, Rensselaer Polytechnic Institute.

FABRIS, M. & PESCI, A., 2005. Automated DEM extraction in digital aerial photogrammetry: Precisions and validation for mass movement monitoring. *Annals of Geophysics* 48(6): 973-988.

FAO, 1985. Water quality for agriculture. FAO, Irrigation and Drainage Paper (29 Rev.1), Rome, Italy.

FAO, 2002. Agricultural drainage water management in arid and semi-arid areas. K.K. Tanji & N.C. Kielen. FAO Irrigation and Drainage Paper No. 61. Rome, Italy.

FARIFTEH, J., 2007. Imaging spectroscopy of salt-affected soils: Model-based integrated method. D. Phil. Thesis, University Utrecht, Netherlands.

FARIFTEH, J., FARSHAD, A. & GEORGE, R.J., 2006. Assessing salt-affected soils using remote sensing, solute modelling, and geophysics. *Geoderma* 130(3-4): 191-206.

FERNANDEZ-BUCES, N., SIEBE, C., CRAM, S. & PALACIO, J.L., 2006. Mapping soil salinity using a combined spectral response index for bare soil and vegetation: A case study in the former lake Texcoco, Mexico. *Journal of Arid Environments* 65(4): 644-667.

FIELD, A., 2006. *Discovering statistics using SPSS*, 2nd Ed. SAGE Publications Ltd, London.

FITZPATRICK, R.W., 2002. Land degradation processes. In: T.R. McVicar, Li Rui, J. Walker, R.W. Fitzpatrick & Liu Changming (eds). Regional Water and Soil Assessment for Managing Sustainable Agriculture in China and Australia, *ACIAR Monograph No. 84:* 119-129.

FLANDERS, D., HALL-BEYER, M. & PEREVERZOFF, J., 2003. Preliminary evaluation of eCognition object-based software for cut block delineation and feature extraction. *Canadian Journal of Remote Sensing* 29: 441-452.

FLUGEL, W.A., 1989a. Groundwater dynamics influenced by irrigation and associated problems of river salination; Breede River, Western Cape Province, RSA Groundwater Contamination IAHS Publication No. 185, pp. 137-145.

FLUGEL, W.A., 1989b. Studies of shallow groundwater dynamics for salinity research in the Breede River Valley, Western Cape Province, RSA. Fourth South African National Hydrological Symposium, Pretoria, pp. 400-408.

FRIEDL, M.A. & BRODLEY, C.E., 1997. Decision tree classification of land cover from remotely sensed data. *Remote Sensing of Environment* 61: 399-402.

FURBY, S., CACCETTA, P., WALLACE, J., 2010. Salinity monitoring in Western Australia using remotely sensed and other spatial data. *Journal of Environment Quality* 39: 16-25.

FURBY, S., WALLACE, J., CACCETTA, P., WHEATON, G., 1995. Detecting and monitoring salt-affected land. Project CDM1. LWRRDC.

GANGANWAR, V., 2012. An overview of classification algorithms for imbalanced datasets. *International Journal of Emerging Technology and Advanced Engineering* 4(2): 42-47.

GAO, Y., MARPU, P., NIEMEYER, I., RUNFOLA, D.M., GINER, N.M., HAMILL, T. & PONTIUS, R.G., 2011. Object-based classification with features extracted by a semi-automatic feature extraction algorithm – SEaTH. *Geocarto International* 26(5): 413-413.

GARCÍA RODRÍGUEZ, P., PÉREZ GONZÁLEZ, M.E. & GUERRA ZABALLOS, A., 2007. Mapping of salt-affected soils using TM images. *International Journal of Remote Sensing* 28: 2713-2722.

GARRETT, J. & VIERA, A., 2005. Understanding interobserver agreement: The kappa statistic. *Family Medicine* 37(5): 360-363.

GERBER, H. 2006. Business Plan: New Farmer Settlement Project at Vaalharts research Station Department of Agriculture and Land Reform

GHASSEMI, F., JAKEMAN, A.J. & NIX, H.A., 1995. Salinisation of land and water resources: Human causes, extent, management and case studies. University of New South Wales Press Ltd, Sydney.

GIBSON,L., MÜNCH, Z., ENGELBRECHT, J., PETERSEN,N. & CONRAD, J 2009. Remote Sensing as a tool for resource assessment towards the determination of the legal compliance of surface and groundwater use. Pretoria.

GIBSON, P. & POWER, C., 2000. *Introductory remote sensing: Digital image processing and applications*. New York: Routledge.

GILES, P.T. & FRANKLIN, S.E. 1998. An automated approach to the classification of the slope units using digital data. Geomorphology 21: 251-264.

GISLASON, P.O., BENEDIKTSSON, J.A. & SVEINSSON, J.R., 2006. Random forests for land cover classification. *Pattern Recognition Letters* 27 4: 294-300.

GONZALEZ-AUDICANA, M., SALETA, J., CATALAN, R. & GARCIA, R., 2004. Fusion of multispectral and panchromatic images using improved HIS and PCA mergers based on wavelet decomposition. IEEE Transactions on Geoscience and Remote Sensing 42: 1291-1299.

GÓMEZ, C., WULDER, M.A., MONTES, F. & DELGADO, J.A., 2012. Modelling forest structural parameters in the Mediterranean pines of central Spain using QuickBird-2 imagery and classification and regression tree analysis (CART). *Remote Sensing* 4(1): 135-159.

GÖRGENS, A.H.M & FOSTER, S.F., 1989. Establishment of a master plan for salinity research: future salinisation trends and impacts. WRC Co-ordinating Committee for Salinity Research, Pretoria.

GRABS, T., SEIBERT, J., BISHOP, K. & LAUDON, H., 2009. Modeling spatial patterns of saturated areas: A comparison of the topographic wetness index and a dynamic distributed model. *Journal of Hydrology* 373(1-2): 15-23.

GRAFF, L.H. & USERY, E.L., 1993. Automated classification of generic terrain features in digital elevation models. *Photogrammetric Engineering & Remote Sensing* 59: 1409-1417.

GRATTAN, S.R. & HANSON, B.R., 2006. Crop Salt Tolerance. (Eds) S.R. Grattan & B.R. Hanson) In: Agricultural Salinity and Drainage. USDA, University of California.

GREEFF, G.J., 1989. Changes in seepage characteristics after development of soils overlying Bokkeveld shales. *SA Besproeiing/SA Irrigation* 11: 19-25.

GREEFF, G.J., 1990. Detailed geohydrological investigations in the Poesjenels River Catchment in the Breede River Valley with special reference to mineralization. WRC Report No. 120/1/90, Water Research Commission, Pretoria.

GREEFF, G.J., 1991. The geology of a typical catchment in the Cape Supergroup, Bree River Valley. Dissertation (Ph. D.) University of Stellenbosch.

GRISSA, M., ABDELFATTAH, R., MERCIER, G., ZRIBI, M., CHAHBI, A. & LILI-CHABAANE, Z., 2011. Empirical model for soil salinity mapping from SAR data. Geoscience and Remote Sensing Symposium (IGARSS), 2011 IEEE International

HAJNSEK, I., POTTIER, E. & CLOUDE, S.R., 2003. Inversion of surface parameters from polarimetric SAR. Geoscience and Remote Sensing, IEEE Transactions on 41: 727-744.

HALL, G.C. & DU PLESSIS, H.M., 1984. Studies of mineralization in the Great Fish and Sundays Rivers. Volume 2. Modelling river flow and salinity. CSIR Special Report WAT 63, Council for Scientific and Industrial Research, Pretoria.

HALL, G.C. & DU PLESSIS, H.M. & HUTSON, J.L., 1980. Modelling river flow and salinity. Collection of Papers Presented at the Workshop on Understanding Mineralization Processes, 19 August 1980. National Institute for Water Research, Council for Scientific and Industrial Research, Pretoria.

HALL, G.C. & GöRGENS, A.H.M., 1978. Studies of mineralisation in South African rivers. South African National Scientific Programmes, Report No. 26. Council for Scientific and Industrial Research, Pretoria.

HALLIKAINEN, M.T., ULABY, F.T., DOBSON, M.C., EL-RAYES, M.A. & LIL-KUN, W., 1985. Microwave Dielectric Behavior of Wet Soil-Part 1: Empirical Models and Experimental Observations. *Geoscience and Remote Sensing, IEEE Transactions on* GE-23: 25-34.

HAM, J., CHEN, Y., CRAWFORD, M.M., & GHOSH, J., 2005. Investigation of the random forest framework for classification of hyperspectral data *IEEE Transactions on Geoscience and Remote Sensing* 43: 492-501.

HANSEN, P.M. & SCHJOERRING, J.K., 2003. Reflectance measurement of canopy biomass and nitrogen status in wheat crops using normalized difference vegetation indices and partial least squares regression. *Remote Sensing of Environment* 86(4): 542-553.

HANSON, B.R., GRATTAN, S.R. & FULTON, A., 2006. *Agricultural Salinity and Drainage*, 2nd Ed. Department of Land, Air and Water Resources, University of California, California.

HARALICK, R.M., SHANMUGAM, K. & DINSTEIN, I., 1973. Textural features for image classification. *IEEE Transactions on Systems, Man and Cybernetics* 3(6): 610-621.

HARALICK, R.M., 1979. Statistical and structural approach to texture. In: Proceedings of IEEE Vol. 67 No. 5: pp. 786-804.

HARRIS, R., 1987. *Satellite remote sensing: An introduction*. New York: Routledge & Kegan Paul.

HARTMANN, M.O. & NELL, J.P., 1993. Report of the task team investigating the management of water and soil for irrigation in the Sundays River Valley. ARC-ISCW Report No. GW/A/93/26, ARC-Institute for Soil, Climate and Water, Pretoria.

HAY, G.J. & CASTILLA, G., 2008. Geographic Object-Based Image Analysis (GEOBIA): A new name for a new discipline. In: T. Blaschke, S. Lang & G. Hay (eds). Object-Based Image Analysis. Springer, Berlin, Heidelberg. pp. 75-89.

HENGL, T., GRUBER, S & SHRESTHA, D.P., 2004. Reduction of errors in digital terrain parameters used in soil-landscape modelling. *International Journal of Applied Earth Observation and Geoinformation* 5: 97-112.

HENSLEY, M. & LAKER, M.C., 1980. A proposed integrated procedure for the identification, delineation, evaluation and planning of irrigable land. In: Proc. 9th National Congress, Soil Sci. Soc. S.A., Durban, Tech. Comm. No. 174, Dept. Agriculture and Fisheries, Pretoria.

HEROLD, C.E. & BAILEY, A.K., 1996. Long term salt balance of the Vaalharts Irrigation Scheme. WRC Report No. 420/1.96, Water Research Commission, Pretoria.

HEUMANN, B., 2011. An object-based classification of mangroves using a hybrid decision tree-support vector machine approach. *Remote Sensing* 3(11): 2440-2460.

HICK, P.T. & RUSSELL, W.G.R., 1990. Some spectral considerations for remote sensing of soil salinity. *Australian Journal of Soil Research* 28: 417-431.

HILLEL, D., 1998. *Environmental Soil Physics*. Academic Press, San Diego.

HLADIK, C. & ALBER, M., 2014. Classification of salt marsh vegetation using edaphic and remote sensing-derived variables. *Estuarine, Coastal and Shelf Science* 141: 47-57.

HOERSCH, B., BRAUN, G. & SCHMIDT, U., 2002. Relation between landform and vegetation in alpine regions of Wallis, Switzerland. A multiscale remote sensing and GIS approach. *Computers, Environment and Urban Systems* 26: 113-139.

HOLAH, N., BAGHDADI, N., ZRIBI, M., BRUAND, A. & KING, C., 2005. Potential of ASAR/ENVISAT for the characterization of soil surface parameters over bare agricultural fields. Remote Sensing of Environment 96: 78-86.

HOPMANS, J.W. & BRISTOW, K.L., 2002. Current capabilities and future needs of root water and nutrient uptake modelling. *Advances in Agronomy* 77: 104-175.

HOWARI, F.M., 2003. The use of remote sensing data to extract information from agricultural land with emphasis on soil salinity. *Australian Journal of Soil Research* 41: 1243-1253.

HSU, C.W., CHANG, C.C. & LIN, C.J., 2010. A Practical Guide to Support Vector Classification. (Web) http://www.csie.ntu.edu.tw/~cjlin/papers/guide/guide.pdf

HUANG, C., DAVIS, L.S. & TOWNSHEND, JRG 2002. An assessment of support vector machines for land cover classification. International *Journal of Remote Sensing* 23(4): 725-749.

HUETE, A., 1988. A soil-adjusted vegetation index (SAVI). *Remote Sensing of Environment* 25: 295-309.

HUETE, A.R., JACKSON, R.D. & POST, D.F., 1985. Spectral response of a plant canopy with different soil backgrounds. *Remote Sensing of Environment* 17: 37-53

IMMITZER, M., ATZBERGER, C. & KOUKAL, T., 2012. Tree species classification with Random forest using very high spatial resolution 8-band WorldView-2 satellite data. *Remote Sensing* 4(9): 2661-2693.

IQBAL, F., 2011. Detection of salt affected soil in rice-wheat area using satellite image. *African Journal of Agriculture Research* 6(21): 4973-4982.

IRVIN, B.J., VENTURA, S.J., SLATER, B.K., 1997. Fuzzy and isodata classification of landform elements from digital terrain data in Pleasant Valley, Wisconsin,. *Geoderma 77, 137-154.*

IRONS, J.R. & PETERSEN, G., 1981. Texture transforms of remote sensing data. *Remote Sensing of Environment* 11: 359-370.

IRONS, J.R., WEISMILLER, R.A. & PETERSEN, G.W., 1989. Soil reflectance. In: G. Asrar (ed.). Theory and Applications of Optical Remote Sensing. J. Wiley & Sons, New York.

IRRIGATION PLANNING STAFF, 1980. A method of evaluating land for irrigation development. Proc. 9th National Congress, Soil, Science Society of South Africa, Durban, Tech. Comm. No. 174.

JAFARI, A., FINKE, P.A., DE WAUW, J.V., 2012. Spatial prediction of USDA-great soil groups in the arid Zarand region, Iran: comparing logistic regression approaches to predict diagnostic horizons and soil types. European Journal of Soil Science, 63(2): 284-298.

JAMES, A.J., 2001. Die identifisering van ontwikkelingsensitiewe areas teen berghellings: Stellenbosch- en Hottentotshollandberge. MA thesis. Stellenbosch, Stellenbosch.

JAYNES, D.B., 1996. Improved soil mapping using electromagnetic induction surveys. *In* P.C. Robert, R.H. Rust, and W.E. Larson (ed.) Proc. 3rd Inter. Conf. on Precision Agriculture. Minneapolis, MN. June 23-26, 1996. ASA, CSSA, SSSA, Madison, WI. University.

JENKIN, J.J., 1981. Terrain, groundwater and secondary salinity in Victoria, Australia. *Agricultural Water Management* 4: 143-171.

JENSEN, J.R., 2007. Remote sensing of the environment: An earth resource perspective. 2nd Ed. Upper Saddle River: Pearson Prentice Hall.

JIANG, Z., HUETE, A.R., DIDAN, K. & MIURA, T., 2008. Development of a two-band enhanced vegetation index without a blue band*. Remote Sensing of Environment* 112: 3833-3845.

JOHNSON, R., CHAWLA, N. & HELLMANN, J., 2012. Species distribution modelling and prediction: A class imbalance problem. In: Proceedings of the Conference on Intelligent Data Understanding (CIDU). pp. 9-16.

JOLLY, J.L., 1990. The groundwater contribution to the salt load and flow volume of the Breede River in the Robertson area. Department of Water Affairs, GH Report 3683.

KAHLOWN, M.A., AHMED, S. & ARSHAD, C.M., 1998. Performance evaluation of SCARP tube wells of Mona Reclamation Experimental Project, WAPADA,

KASISCHKE, E.S., SMITH, K.B., BOURGEAU-CHAVEZ, L.L., ROMANOWICZ, E.A., BRUNZELL, S. & RICHARDSON, C.J., 2003. Effects of seasonal hydrologic patterns in south Florida wetlands on radar backscatter measured from ERS-2 SAR imagery. Remote Sensing of Environment 88: 423-441.

KALKHAN, M., STOHLGREN, T., CHONG, G., LISA, D. & REICH, R., 2000. A predictive spatial model of plant diversity: integration of remotely sensed data, GIS, and spatial statistics. Eighth Biennial Remote Sensing Conference, Albuquerque, New Mexico.

KANTHACH, F.E., 1909. Irrigation development in the Cape Colony: Past, present and future. In: Proc.1st S. Afr.Irrig.Cong., 24-35. Cape Times Ltd, Cape Town.

KACHANOSKI, R.G., GREGORICH, E.G. & VAN WESENBEECK. I.J., 1988. Estimating spatial variations of soil water content using non contacting electromagnetic inductive methods. *Can. J. Soil Sci. 68: 715*-722.

KELLY, R.B., DAVIE, T. & ATKINSON, P. 2003. Explaining temporal and spatial variation in soil moisture in a bare field using SAR imagery. International Journal of Remote Sensing 24: 3059-3074.

KHAN, N.M., RASTOSKUEV, V.V., SHALINA, E.V. & SATO, Y., 2001*.* Mapping salt-affected soils using remote sensing indicators – A simple approach with the use of GIS IDRISI. In: 22nd Asian Conference on Remote Sensing, 5-9 November, Singapore.

KHAN, N.M., RASTOSKUEV, V.V., SATO, Y. & SHIOZAWA, S., 2005. Assessment of hydrosaline land degradation by using a simple approach of remote sensing indicators. *Agricultural Water Management* 77(1-3): 96-109.

KIENZLE, S., 1989. Breede River Salination Program. 3. Internal Report. Summary of daily data for the hydrological year 1987/88. HRI Report NH000//RIQ0589.

KIENZLE, S., 1990. Breede River Salination Program. 5. Internal Report. Summary of daily data for the hydrological year 1988/89. HRI Report NH000//RIQ0390.

KIENZLE, S. & FLUGEL, W.A., 1988. Breede River Salinity Research Program, 1. Internal Report: The Salinity of the Breede River and its Tributaries between Brandvlei References 93 Dam and H5M04: Summary of Daily Data up to September 1987. HRI Report NH000//RIQ0888.

KIRCHNER, J.O.G., 1995. Investigation into the contribution of ground water to the salt load of the Breede River, using natural isotopes and chemical tracers. WRC Report No. 344/1/95, Water Research Commission, Pretoria.

KOSHAL, A.K., 2010. Indices Based Salinity Areas Detection Through Remote Sensing & GIS in Parts of South West Punjab. In: 13th Annual International Conference and Exhibition on Geospatial Information Technology and Applications, Gurgaon, pp. 1-11.

KRUGER, M, VAN RENSBURG, J.B.J. & VAN DEN BERG, J., 2009. Perspective on the development of stem borer resistance to Bt maize and refuge compliance at the Vaalharts irrigation scheme in South Africa. *Crop Protection* 28: 684-689.

LALIBERTE, A.S., FREDRICKSON, E.L. & RANGO, A., 2007. Combining decision trees with hierarchical object-oriented image analysis for mapping arid rangelands. *Photogrammetric Engineering and Remote Sensing* 73: 197-207.

LAMBRECHTS, J.J.N., 1979. Geology, geomorphology and soils. In: J. Day, W.R. Siegfried, G.N. Louw & M.L. Jarman (eds). Fynbos ecology: a preliminary synthesis. South African National Science Progress Report 40: 16-26.

LANG, S., 2008. Object-based image analysis for remote sensing applications: Modelling reality – dealing with complexity. In: T. Blaschke, S. Lang & G. Hay (eds). Object-based image analysis: Spatial concepts for knowledge-driven remote sensing applications, 3-26. Berlin/Heidelberg: Springer Verlag.

LASNE, Y., PAILLOU, P., FREEMAN, A., FARR, T., MCDONALD, K.C., RUFFIE, G., MALEZIEUX, J.M., CHAPMAN, B. & DEMONTOUX, F., 2008. Effect of Salinity on the Dielectric Properties of Geological Materials: Implication for Soil Moisture Detection by Means of Radar Remote Sensing. *Geoscience and Remote Sensing, IEEE Transactions on* 46: 1674-1688.

LAUCHLI, A. & LUTTGE, U. 2002. Introduction to Salinity: Environment-Plants-Molecules. Dordrecht, Netherlands: Kluwer Academic Publishers.

LAWRENCE, R.L., WOOD, S.D. & SHELEY, R.L., 2006. Mapping invasive plants using hyperspectral imagery and Breiman Cutler classifications (RandomForest). *Remote Sensing of Environment* 100(3): 356-362.

LAWRENCE, R.L. & WRIGHT, A., 2001. Rule-based classification systems using classification and regression tree (CART) analysis. *Photogrammetric Engineering and Remote Sensing* 67(10): 1137-1142.

LENNEY, M.P., WOODCOCK, C.E., COLLINS, J.B. & HAMDI, H., 1996. The status of agricultural lands in Egypt: The use of multi temporal NDVI features derived from Landsat TM. *Remote Sensing of Environment* 56: 8-20.

LEONE, A.P., MENENTI, M., BUONDONNO, A., LETIZIA, A., MAFFEI, C. & SORRENTINO, G., 2007. A field experiment on spectrometry of crop response to soil salinity. *Agricultural Water Management* 89: 39-48.

LESCH, S.M., RHOADES, J. D., LUND L.J. & CORWIN. D.L., 1992. Mapping soil salinity using calibrated electromagnetic measurements. Soil Sci. Soc. Am. J. 56(2):540-548.

LI, H., GU, H., HAN, Y. & YANG, J., 2010. Object-oriented classification of high-resolution remote sensing imagery based on an improved colour structure code and a support vector machine. *International Journal of Remote Sensing* 31: 1453-1470.

LILLESAND, T.M., KIEFER, R.W. & CHIPMAN, J.W., 2004. *Remote Sensing and Image Interpretation.* 5th Ed. New York: John Wiley & Sons, Inc.

LIU, D. & XIA, F., 2011. Assessing object-based classification: advantages and limitations. *Remote Sensing Letters* 1: 187-194.

LIU, X-H, SKIDMORE, A.K. & VAN OOSTEN, H., 2002. Integration of classification methods for improvement of land-cover map accuracy. *ISPRS Journal of Photogrammetry and Remote Sensing* 56: 257-268.

LIZARAZO, I., 2008. SVM-based segmentation and classification of remotely sensed data. *International Journal of Remote Sensing* 29(24): 7277-7283.

LOBELL, D.B., LESCH, S.M., CORWIN, D.L., ULMER, M.G., ANDERSON, K. A, POTTS, D.J., DOOLITTLE, J. A, MATOS, M.R. & BALTES, M.J., 2010. Regional-scale assessment of soil salinity in the Red River Valley using multi-year MODIS EVI and NDVI. *Journal of Environmental Quality* 39: 35-41.

LONGLEY, P.A., GOODSCHILD, M.F., MAGUIRE, D.J. & RIHIND, D.W., 2002. Geographic Information Systems and Science. Wiley, Chichester

LU, D. & WENG, Q., 2007. A survey of image classification methods and techniques for improving classification performance. *International Journal of Remote Sensing* 28(5): 823-870.

LUCAS, R., ROWLANDS, A., BROWN, A., KEYWORTH, S. & BUNTING, P., 2007. Rule-based classification of multi-temporal satellite imagery for habitat and agricultural land cover mapping. *Journal of Photogrammetry Remote Sensing* 62: 165-185.

MAAS, E.V., 1990. Crop Salt Tolerance. In: K.K. Tanji (ed.). Agricultural Salinity Assessment and Management. ASCE Manuals and Reports on Engineering Practice No. 71. ASCE, New York.

MAAS, E.V. & HOFFMAN, M., 1977. Crop salt tolerance – current assessment. *J.Irrig.Drain. Div.ASCE* 103:115-134.

MACELLONI, G., PALOSCIA, S. & PAMPALON, P., 1999. The SIR-C/X-SAR experiment on Montespertoli: sensitivity to hydrological parameters. *International Journal of Remote Sensing* 20: 2597-2612

MACVICAR, C.N., 1972. Legend for the sketch map giving a tentative appreciation of the occurrence of salt-affected soils in South Africa. SIRI Report No. 768/139/72, Dept of Agricultural Technical Services, Pretoria.

MAISELA, J., 2007. Realizing agricultural potential in land reform: the case of Vaalharts irrigation scheme in the Northern Cape Province. Magister Philosophiae (Land and Agrarian Studies), University of the Western Cape.

MALLINIS, G., KOUTSIAS, N., TSAKIRI-STRATI, M. & KARTERIS, M., 2008. Object-based classification using Quickbird imagery for delineating forest vegetation polygons in a Mediterranean test site. *ISPRS Journal of Photogrammetry and Remote Sensing* 63: 237-250.

MASHIMBYE, Z.E., 2005. Remote sensing-based identification and mapping of salinised irrigated land between Upington and Keimoes along the lower Orange River, South Africa. M.Sc. Thesis, Stellenbosch University, Department of Geography and Environmental Sciences.

MASHIMBYE, Z.E., CHO, M.A., NELL, J.P., DE CLERCQ, W.P., VAN NIEKERK, A. & TURNER, D.P., 2012. Model-based integrated methods for quantitative estimation of soil salinity from hyperspectral remote sensing data: a case study of selected South African soils. *Pedosphere* 22(5): 640-649.

MATHER, P., 2004. Computer processing of remotely sensed images. West Essex: John Wiley & Sons.

MATHER, P. & MAGALY, K., 2011*. Computer processing of remotely-sensed images*. John Wiley & Sons.

MATHIEU, R., SBIH, M., VIAU, A., ANCTIL, F., PARENT, L. & BOISVERT, J., 2003. Relationships between Radarsat SAR data and surface moisture content of agricultural organic soils. International Journal of Remote Sensing 24: 5265-5281.

MCDONALD, R.C., ISBELL, R.F., SPEIGHT, J.G., WALKER, J. & HOPKINS, M.S., 1984. Australian soil and land survey. Melbourne: Inkata Press.

MCFARLANE, D.J., GEORGE, R.J. & CACCETTA, P.A., 2004. The extent and potential area of salt-affected land in Western Australia estimated using remote sensing and digital terrain models. In: 1st National Salinity Engineering Conference. Perth.

MCGHIE, S. & RYAN, M., 2005. Salinity indicator plants. Department of Infrastructure, Planning and Natural Resources, Australia.

MEIRI, A. & PLAUT, Z., 1985. Crop production and management under saline conditions. *Plant and Soil* 89: 253-271.

METTERNICHT, G.I., 1998. Fuzzy classification of JERS-1 SAR data: an evaluation of its performance for soil salinity mapping. Ecological Modelling 111: 61-74.

METTERNICHT, G.I & ZINCK, J., 2003. Remote sensing of soil salinity: Potentials and constraints*. Remote Sensing of Environment* 85(1): 1-20.

MITCHELL, C.W., 1991. Terrain evaluation. New York: Longman.

MOEREMANS, B. & DAUTREBANDE, S., 2000. Soil moisture evaluation by means of multi-temporal ERS SAR PRI images and interferometric coherence. *Journal of Hydrology* 234: 162-169.

MOOLMAN, J. & QUIBELL, G., 1995. Salinity problems in the Douglas Weir and Lower Riet River. Report Number: N/C900/29/DIQ1495, DWAF, Pretoria.

MOOLMAN, J.H., VAN ROOYEN, P.C. & WEBER, H.W., 1983. The effect of irrigation practices in the Bree River valley on the salt content of a small river. *Irrigation Science* 4: 103-116.

MOOLMAN, J.H. & WEBER, H.W., 1979. Die toepassing van die grens-konsentrasiekonsep op die beoordeling van water vir besproeiing van brak fynsand-gronde in Suid-Kaapland. *Water SA* 5: 26-38.

MOOLMAN, J.H., 1982. The implementation of a Deterministic Conceptual Computer Simulation Model to characterise the relationship between irrigation return flow and the process of river mineralization. Ph.D. Thesis, University of Stellenbosch, (unpublished), Stellenbosch.

MORAN, M., MCELROY, S., WATTS, J. & PETERS, L., (eds) 2006. *Radar remote sensing for estimation of surface soil moisture at the watershed scale, in Modeling and Remote Sensing Applied in Agriculture (US and Mexico).* Mexico: INIFAP.

MORANT, I.D., 1984. Estuaries of the Cape. Part II. Synopses of available information on individual systems. Report No. 26. Olifants. CSIR Research Report 425, Stellenbosch: Council for Scientific and Industrial Research.

MOUGENOT, B., POUGET, M. & EPEMA, G., 1993. Remote sensing of salt affected soils. *Remote Sensing Reviews* 7: 241-259.

MOUNTAIN, M.J., 1967. Pedogenic materials. *Proc. 4th Reg. Conf. Afr. Soil Mech. Fndn., 65-70,* Cape Town.

MOUNTRAKIS, G., IM, J. & OGOLE, C., 2011. Support vector machines in remote sensing: A review. *ISPRS Journal of Photogrammetry and Remote Sensing*, 66: 247-259.

MUCINA, L. & RUTHERFORD, M.C., (eds) 2006. The vegetation of South Africa, Lesotho and Swaziland. Strelitzia 19, SANBI, Pretoria.

MYBURGH, G. & VAN NIEKERK, A., 2013. Effect of feature dimensionality on object-based land cover classification: a comparison of three classifiers. *South African Journal of Geomatics* 2(1): 13-27.

MYBURGH, G. & VAN NIEKERK, A., 2014a. Impact of training set size on object-based land cover classification: A comparison of three classifiers. *International Journal of Applied Geospatial Research* 5(3): 49-67.

MYBURGH, G. & VAN NIEKERK, A., 2014b. Impact of training set size and feature dimensionality on object-based land cover classification: a comparison of three classifiers. GEOBIA2014, 21-24 May 2014, Thessaloniki, Greece.

MYERS, V. I., HEILMAN, M. D., LYON, R. J. P., NAMKEN, L. N., SIMONETT, D., & al., et. 1970. Soil, water, and plant relations. 253-97. Retrieved from http://www.cabdirect.org/abstracts/19710703625.html;jsessionid=3021DC84BAF491BCD6B1AF2B5A83E988?freeview=true

NANGENDO, G., SKIDMORE, A.K. & VAN OOSTEN, H., 2007. Mapping East African tropical forests and woodlands – A comparison of classifiers. *ISPRS Journal of Photogrammetry and Remote Sensing* 61: 393-404.

NELL, J.P., 1991. Besproeibaarheid van Gestruktuurde Gronde. M.Sc. Agric. Thesis, University of the Free State, Bloemfontein.

NELL, J.P., 1993a. Analitiese gegewens van moniteringspunte sowel as ‘n vergelyking tussen besproeide en onbesproeide gronde in die Sondagsriviervallei. LNR-IGKW Verslagnommer GW/A/93/1, ARC-Institute for Soil, Climate and Water, Pretoria.

NELL, J.P., 1993b. Waterkwaliteit in die Sondagsriviervallei. LNR-IGKW Verslagnommer GW/A/92/2, ARC-Institute for Soil, Climate and Water, Pretoria.

NELL, J.P., 1994. Die invloed van waterkwaliteit op die chemiese eienskappe van gronde in die Limpopovallei. LNR-IGKW Verslagnommer GW/A/94/57, ARC-Institute for Soil, Climate and Water, Pretoria.

NELL, J.P., 1995. Kriteria vir besproeiingswater van gronde in die Rietrivier en Laer Vaalrivier wat deur die Oranje-Rietkanaal bedien word. LNR-IGKW Verslagnommer GW/A/95/5, ARC-Institute for Soil, Climate and Water, Pretoria.

NELL, J.P., 1997. Nkomazi irrigation expansion programme environmental audit: Agronomic/agricultural resources. ARC-ISCW Report No. GW/A/97/40, ARC-Institute for Soil, Climate and Water, Pretoria.

NELL, J.P., 1998. Limpoporivier: Grond en waterkwaliteitprobleme in die beweerde onkruid-doder vergiftingsaak. LNR-IGKW Verslagnommer GW/A/98/16, ARC-Institute for Soil, Climate and Water, Pretoria.

NELL, J.P., 2007. The effect of soil and water quality on sustainable irrigation development. SABI Congress, Fish River Sun, 14-17 August, 2007.

NELL, J.P., 2010. The primary salinity, sodicity and alkalinity status of South African soils. Ph.D. Thesis in Soil Science, University of the Free State, Bloemfontein.

NELL, J.P. & CHILDS, R.F.M., 1992. Karakterisering van grond- en watereienskappe en die invloed daarvan op sitrusproduksie in die Sondagsriviervallei. LNR-IGKW Verslagnommer GW/A/92/15, ARC-Institute for Soil, Climate and Water, Pretoria.

NELL, J.P. & DE CLERCQ, W.P., 2008. Soil Protection Strategy: Salt affected soils and waterlogging. ARC-ISCW Report No. GW/A/2008/47, ARC-Institute for Soil, Climate and Water, Pretoria.

NELL, J.P. & HENNING, A.J., 2003. Salt-affected soils: South Africa. ARC-ISCW Map No. GW/B/2004/01, ISCW, Pretoria.

NÉMETH, T., BIDLÓ, A., GAÁL, Z., HEIL, B., HERMANN, T., MAKÓ, A., MÁTÉ, F., SPEISER, F., SZÛCS, I., TÓTH, G., TÓTH, T., VÁRALLYAY, G. & VASS, J., 2006. Framework and Components of a New Land Evaluation System in Hungary. The 18th World Congress of Soil Science (July 9-15, 2006), Philadelphia.

NINHAM SHAND, 1985. Report on a situation study of irrigation return flow quantity and quality in river basins with extensive irrigation development in South Africa. WRC Report No. 943/406, Water Research Commission, Pretoria.

NOBRE, A.D., CUARTAS, L.A., HODNETT, M., RENNÓ, C.D., RODRIGUES, G.,SILVEIRA, A., WATERLOO, M. & SALESKA, S., 2011. Height Above the Nearest Drainage – a hydrologically relevant new terrain model. *Journal of Hydrology, 404, 13-29*

NON-AFFILIATED SOIL ANALYSIS WORK COMMITTEE, 1991. Methods of soil analysis. SSSSA, Pretoria.

NOVACK, T., ESCH, T., KUX, H. & STILLA, U., 2011. Machine learning comparison between WorldView-2 and QuickBird-2-simulated imagery regarding object-based urban land cover classification. *Remote Sensing* 3(10): 2263-2282.

NUSSBAUM, S., NIEMEYER, I. & CANTY, M.J., 2006. Seath – a New Tool for Automated Feature Extraction in the Context of Object-Based Image Analysis. In: Proceedings of the 1st International Conference on Object-based Image Analysis.

ODINDI, J. & MHANGARA, P., 2013. Potential of texture-based classification in urban landscapes using multispectral aerial photos. *South African Journal of Science* 109(3): 1-9.

OOMMEN, T., MISRA, D., TWARAKAVI, N., PRAKASH, A., SAHOO, B. & BANSOPASHYAY, S., 2008. An objective analysis of support vector machine based classification for remote sensing. *Mathematical Geosciences* 40: 409-424.

PAL, M., 2005. Random forest classifier for remote sensing classification. *International Journal of Remote Sensing* 26(1): 217-222.

PAL, M. & MATHER, P.M., 2003. An assessment of the effectiveness of decision tree methods for land cover classification *Remote Sensing of Environment* 86: 554-565.

PAL, M. & MATHER, P., 2005. Support vector machine for classification in remote sensing. *International Journal of Remote Sensing* 26(5): 1007-1011.

PCI GEOMATICS, 2012. PCI Geomatics User Guide 2012. Canada: PCI Geomatics.

PEARCE, M.W., 1987. Analysis of spatial variation in the quality of surface water and groundwater in the Coerney River Irrigation area. Unpub. Hons thesis, Rhodes University.

PEÑUELAS, J., ISLA, R., FILELLA, I. & ARAUS, J.L., 1997. Visible and near-infrared reflectance assessment of salinity effects on barley. *Crop Science* 37(1): 198-202.

PETROPOULOS, G.P., KALAITZIDIS, C. & PRASAD VADREVU, K., 2012. Support vector machines and object-based classification for obtaining land-use/cover cartography from Hyperion hyperspectral imagery. *Computers and Geosciences* 41: 99-107.

PICKUP, G. & CHEWINGS, V.H., 1996. Correlations between DEM-derived topographic indices and remotely-sensed vegetation cover in rangelands. *Earth Surface Processes and Landforms* 21: 517-529.

PLATT, R.V. & RAPOZA, L., 2008. An evaluation of an object-oriented paradigm for land use/land cover classification. *The Professional Geographer* 60: 87-100.

POTTIER, E. & LEE, J., 1999. *Application of of the ‹‹ H / A / à ›› Polarimetric Decomposition Theorem for Unsupervised Classification of Fully Polarimetric SAR data Based on the Wishart Distribution.* SAR Workshop: CEOS Committee on Earth Observation Satellites; Working Group on Calibration and Validation., Toulouse, France

PUISSANT, A., HIRSCH, J. & WEBER, C., 2005. The utility of texture analysis to improve per-pixel classification for high to very high spatial resolution imagery. *International Journal of Remote Sensing* 26(4): 733-745.

PUNIA, M., JOSHI, P. & PORWAL, M., 2011. Decision tree classification of land use cover for Delhi, India using IRS-P6 AWiFS data. *Expert Systems with Applications* 38: 5577-5583.

QI J., CHEHBOUNI A., HUETE A.R., KERR Y.H., 1994. Modified Soil Adjusted Vegetation Index (MSAVI). Remote Sens Environ 48:119-126.

QI J., KERR Y., CHEHBOUNI A., 1994. External factor consideration in vegetation index development. Proc.of Physical Measurements and Signatures in Remote Sensing, ISPRS, 723-730.

RAHMAN, M.M., MORAN, M.S., THOMA, D.P., BRYANT, R., HOLIFIELD COLLINS, C.D., JACKSON, T., ORR, B.J. & TISCHLER, M., 2008. Mapping surface roughness and soil moisture using multi-angle radar imagery without ancillary data. Remote Sensing of Environment 112: 391-402.

RAO, B.R.M., SANKAR, T., DWIVEDI, R., THAMMAPPA, S., VENKATARATNAM, L., SHARMA, R. & DAS, S., 1995. Spectral behaviour of salt-affected soils. *International Journal of Remote Sensing* 16(12): 2125-2136.

REES, W., 2001. Physical principles of remote sensing. New York: Cambridge University Press.

RENNÓ, C.D., NOBRE, A.D., CUARTAS, L.A., SOARES, J.V., HODNETT, M.G., TOMASELLA, J., WATERLOO, M., 2008. A new terrain descriptor using SRTM-DEM; mapping terra-firme rainforest environments in Amazonia. Remote Sensing of Environment 112, 3469-3481.

RHOADES, J.D., CHANDUVI, F. & LESCH, S., 1999. Soil salinity assessment. Methods and interpretation of electrical conductivity measurements. FAO Irrigation and Drainage Paper 57, Rome.

RHOADES, J.D., & LOVEDAY J., 1990. Salinity in Irrigated Agriculture. p. 1089-1142. In B.A. Stewart and D.R. Nielsen (ed.) Irrigation of Agricultural Crops. Agron. Monogr. 30. ASA, CSSA and SSSA, Madison, WI.

RICHTER, R., 2011. Atmospheric/Topographic correction for Satellite imagery. Munich: DLR.

RODRIQUEZ-GALIANO, V.F., CHICA-OLMO, M., ABARCA-HERNANDEZ, F., ATKINSON, P.M. & JEGANATHAN, C., 2012a. Random Forest classification of Mediterranean land cover using multi-seasonal imagery and multi-seasonal texture. *Remote Sensing of Environment* 121: 93-107.

RODRIQUEZ-GALIANO, V.F., GHIMIRE, B., ROGAN, J, CHICA-OLMO, M. & RIGOL-SANCHEZ, J.P., 2012b. An assessment of the effectiveness of a Random Forest classifier for land-cover classification. *ISPRS Journal of Photogrammetry and Remote Sensing* 67(1): 93-104.

ROMBACH, M. & MAUSER, W., 1997. Multi-annual analysis of ERS surface soil moisture measurements of different land uses. 3rd ERS Scientific Symposium, Florence, Italy.

ROSE, P.D., 2002. Salinity, sanitation and sustainability a study in environmental biotechnology and integrated wastewater beneficiation in South Africa. WRC Report No. TT 187/02, Water Research Commission, Pretoria.

ROSSOUW, J.D., 1997. Water demands of the Orange River Basin. Department of Water Affairs Report No. PD 00/00/4497, Pretoria.

RUDDOCK, A., 1947. Terraces in the lower part of the Sundays River Valley, Cape Province. *Transactions of the Royal Society of South Africa* August 1947: 347-370.

RUDMAN, R.B., SCHLOMS, B.H.A. & DOHSE, T.E., 1978. Verkenningsopname van die Olifantsrivier-Vredendal tot Vanrhynsdorp. NIGB Verslagnommer 869/7/78, ARC-Institute for Soil, Climate and Water, Pretoria.

RUSS, J.C., 1999. *The Image Processing Handbook*, 3rd Ed. Taylor & Francis Group.

RUST, M.E., DE MUNNIK, R.O., LINDEMAN, H. & WEIR-SMITH, J., 1999. AGIS – An Agricultural GIS for South Africa. (Web) http://proceedings.esri.com/library/userconf/proc99/proceed/papers/pap497/p497.htm

SAMADI, M., REMMELZWAAL, A., BEUKES, H., VAN DER WALT, M., VERMEULEN, M., VAN HUYSSTEEN, C.W., VAN ENGELEN, V.W.P. & BARNARD, R.O., 1999.The development of the South African SOTER and WOCAT. Proc. FAO/ISCW Expert Consultation on Land Resources inventories/SOTER, National Soil Degradation Assessment and its Impacts on Soil Productivity 83-92. Pretoria, South Africa.

SCHAFFER, C., 1993. Overfitting avoidance as bias. *Machine Learning* 10: 153-178.

SCHIEWE, J., 2002. Segmentation of high-resolution remotely sensed data – concepts, applications and problems. Joint ISPRS Commission IV Symposium: Geospatial Theory, Processing and Applications, Ottawa.

SCHOEMAN, J.L. & VAN DEVENTER, P.W., 2004. Soils and the environment: the past 25 years. *South African Journal of Plant and Soil* 21(5): 369-387.

SCHOOLMASTER, F.A. & MARR, P.G., 1992. Geographic information systems as a tool in water use data management. *Water Resources Bulletin* 28(2): 331-336.

SCHULZE, B.R., 1965. Climate of South Africa. Department of Transport, Government Printer, Pretoria.

SCOTNEY, D.M. & VAN DER MERWE, A.J., 1991. Irrigation: Long-term viability of soil and water resources in South Africa. In: Proceedings of the Southern African Irrigation Symposium, 4-6 June 1991, Elangeni Hotel, Durban.

SEIFFERT, C., KHOSHGOFTAAR, T.M., VAN HULSE, J. & NAPOLITANO, A., 2010. RUSBoost: A hybrid approach to alleviating class imbalance. *IEEE Transactions on Systems, Man, and Cybernetics Part A: Systems and Humans* 40(1): 185-197.

SEOS 2014. Introduction to remote sensing. Available from: http://www.seos-project.eu/modules/remotesensing/remotesensing-c01-p05.html [Accessed 7 November 2015].

SETIA, R., LEWIS, M., MARSCHNER, P., RAJA SEGARAN, R., SUMMERS, D. & CHITTLEBOROUGH, D., 2013. Severity of salinity accurately detected and classified on a paddock scale with high resolution multispectral satellite imagery. *Land Degradation and Development* 24(4): 375-384.

SHAO, Y., HU, Q., GUO, H. CHUNMING, H., 2003. Effect of dielectric properties of moist salinized soils on backscattering coefficients extracted from RADARSAT image. IEE Transactions of Geoscience and Remote Sensing 41 (8) 1879-1888.

SHARMA, R. C. & BHARGARVA, G. P., 1988. Landsat imagery for mapping saline soils and wetlands in north-west India. *Int. J. Remote Sens. 9: 39-44.*

SHONE, R.W., 1976. The sedimentology of the Mesozoic Algoa Basin. M.Sc. Thesis, University of Port Elizabeth.

SIDIKE, A., ZHAO, S. & WEN, Y., 2014. Estimating soil salinity in Pingluo County of China using QuickBird data and soil reflectance spectra. *International Journal of Applied Earth Observation and Geoinformation* 26: 156-175.

SLAVICH, P.G., 1990. Determining EC_a-depth profiles from electromagnetic induction measurements. *Aust J Soil Res 28;443-452*.

SØRENSEN, R. & SEIBERT, J., 2007. Effects of DEM resolution on the calculation of topographical indices: TWI and its components. *Journal of Hydrology* 347(1-2): 79-89.

SØRENSEN, R., ZINKO, U. & SEIBERT, J., 2006. On the calculation of the topographic wetness index: evaluation of different methods based on field observations. *Hydrology and Earth System Sciences* 10(1): 101-112.

SPEIGHT, J.G., 1977. Landform pattern description from aerial photographs. *Photogrammetria* 32: 161-182.

SPIES, B. & WOODGATE, P., 2005. Salinity mapping methods in the Australian context. Department of the Environment and Heritage; and Agriculture, Fisheries, and Forestry, Canberra.

SSSA, 2007. Glossary of Soil Science Terms. Soil Science Society of America. Date of access 4/03/2004 [Web] http://www.soils.org/sssloss/index/php.

STAL, C., TACK, F., DE MAEYER, P., DE WULF, A. & GOOSSENS, R., 2013. Airborne photogrammetry and lidar for DSM extraction and 3D change detection over an urban area – a comparative study. *International Journal of Remote Sensing* 34(4): 1087-1110.

STONE, A.W., 1988. Climate and Weather. In Lubke RA, Gess FW & Bruton ME(eds), 1988. A field guide to the Eastern Cape coast. Wildlife Society of Southern Africa.

STEINBERG, D. & GOLOVNYA, M., 2007. CART user's guide. San Diego, California.

STRAATSMA, M.W. & BAPTIST, M.J., 2008. Floodplain roughness parameterization using airborne laser scanning and spectral remote sensing. *Remote Sensing of Environment* 112: 1062-1080.

STREUTKER, A., 1982. Huidige situasie van besproeiingsgrond in Suid Afrika. 2de Werksessie van KKBN, Department Landbou en Visserye, Pretoria.

STREUTKER, A., 1977. The dependence of permanent crop production on efficient irrigation and drainage at the Vaalharts Government Water Scheme. *Water SA* 3(2): 90-102.

STRONKHORST, L., TRYTSMAN, G., LOTTER, L., TAYLOR, J., BOTHA, C., ROBERTS, V. & MASHIYANA, B., 2010. Local level land degradation assessment on commercial farms in Winterton, KwaZulu-Natal Province. ARC-ISCW Report No. GW/A/2010/36, ARC-Institute for Soil, Climate and Water, Pretoria.

SULEBAK, J., TALLAKSEN, L. & ERICHSEN. B., 2000. Estimation of areal soil moisture by use of terrain data. *Geografiska Annaler* 82(1): 89-105.

SUMNER, M.E., 1993. Sodic Soils: New Perspectives. *Aust. J. Soil Res.* 31: 683-750.

SVORAY, T. & SHOSHANY,M., 2004. Multi-scale analysis of intrinsic soil factors from SAR-based mapping of drying rates. *Remote Sensing of Environment* 92: 233-246.

TAGHIZADEH-MEHRJARDI, R., MINASNY, B., SARMADIAN, F. & MALONE, B., 2014. Digital mapping of soil salinity in Ardakan region, central Iran. *Geoderma* 213: 15-28.

TAJGARDAN, T., SHATAEE, S. & AYOUBI, S., 2007. Spatial prediction of soil salinity in the arid zones using ASTER data, Case study: North of Ag ghala, Golestan Province, Iran. In: 28th Asian Conference on Remote Sensing 2007, ACRS 2007. Kuala Lumpur, Malaysia, pp. 1712-1717.

TANJI, K.K. (ed.), 1990. Agricultural salinity *assessment* and management. *Manual No. 7. Am.Soc. Civil Eng,* New York.

TAYLOR, G.R., MAH, A.H., KRUSE, F.A., KIEREIN-YOUNG, K.S., HEWSON, R.D. & BENNETT, B.A., 1996. Characterization of saline soils using airborne radar imagery. Remote Sensing of Environment 57: 127-142.

THOMPSON, J., BELL, J. & BUTLER, C., 2001. Digital elevation model resolution: Effects on terrain attribute calculation and quantitative soil-landscape modeling. *Geoderma* 100(1-2): 67-89.

TILLEY, D.R., AHMED, M., SON, J.H. & BADRINARAYANAN, H., 2007. Hyperspectral reflectance response of freshwater macrophytes to salinity in a brackish subtropical marsh. *Journal of Environmental Quality* 36: 780-789.

TRIMBLE, 2011a. *eCognition Developer 8.64.1 Reference Book.* München: Trimble Germany GmbH.

TRIMBLE, 2011b. *eCognition Developer 8.64.1 User Guide.* München: Trimble Germany GmbH.

TSATSOULIS, C., 1993. Expert Systems in Remote Sensing Applications. *IEEE Geoscience and Remote Sensing Newsletter* June: 7-15.

TSENG, M.H., CHEN, S.J., HWANG, G.H. & SHEN, M.Y., 2008. A genetic algorithm rule-based approach for land-cover classification. ISPRS *Journal of Photogrammetry and Remote Sensing* 63: 202-212.

TSWAI, D., 2011. RADAR observation Vaalharts: ARC-ISCW internal report: Project for Water Research Commission Pretoria.

TURHAN, H., GENC, L., SMITH, S.E., BOSTANCI, Y.B. & TURKMEN, O.S., 2008. Assessment of the effect of salinity on the early growth stage of the common sunflower (Sanay cultivar) using spectral discrimination techniques*. African Journal of Biotechnology* 7: 750-756.

TZOTSOS, A. & ARGIALAS, D., 2008. Support vector machine classification for object-based image analysis. In: T. Blaschke, S. Lang & G. Hay (eds). Object-based image analysis: Lecture notes in geoinformation and cartography. Berlin: Springer, pp. 663-677.

ULABY, F.T., BATLIVALA, P.P. & DOBSON, M.C., 1978. Microwave backscatter dependence on surface roughness, soil moisture, and soil texture: Part I – Bare soil. *IEEE Transactions on Geoscience Electronics* 16: 286-295.

ULABY, F.T., MOORE, R. & FUNG, A., 1986. Microwave Remote Sensing: Active and Passive, Volume II: Radar Remote Sensing and Surface Scattering and Emission Theory. Artech House Publishers.

VAN DER EYK, J.J., MACVICAR, C.N. & DE VILLIERS, J.M., 1969**.** Soils of the Tugela Basin. A study in subtropical Africa. Town and Regional Planning Commission, Natal.

VAN DER SANDE, C.J., DE JONG, S.M. & DE ROO, A.P.J., 2003. A segmentation and classification approach of IKONOS-2 imagery for land cover mapping to assist flood risk and flood damage assessment. *International Journal of Applied Earth Observation and Geoinformation* 4: 217-229.

VAN DER MERWE, A.J., SMITH, H.J.C. & NELL, J.P., 1989. Verslag oor navorsing in verband met die Besproeibaarheid van Valsrivier- en soortgelyke probleemgronde van die Sondags- en Laer Visrivier besproeiingskemas. LNR-IGKW Verslagnommer GW/A/91/2, ARC-Institute for Soil, Climate and Water, Pretoria.

VAN DER MERWE, C.R., 1934. Rapport oor die bodemopname van Loskop besproeiing-skema. NIGB Verslagnommer 123, Dept. Landbou, Pretoria.

VAN DER MERWE, C.R., 1942. Soil Groups and Subgroups of South Africa. Science Bulletin No.231, Chemistry Series No.165. Dept of Agricultural Technical Services, Pretoria.

VAN NIEKERK, A., 2012. Stellenbosch University Digital Elevation Model (SUDEM) – 2012 Edition. Stellenbosch: Centre for Geographical Analysis.

VAN NIEKERK, A., 2012. Developing a very high resolution DEM of South Africa. *Position IT* November: 55-60.

VAN NIEKERK, A., 2015. Stellenbosch University Digital Elevation Model (SUDEM) Product Description. Stellenbosch, Centre for Geographical Analysis

VAN NIEKERK, A. & SCHLOMS, B.H.A., 2001. Automated mapping of land components from elevation data. Paper presented at the Fourth Biennial International Conference of the Society of South African Geographers, Rawsonville.

VAN DER WALT, H.v.H. & VAN ROOYEN, T.H., 1995. A glossary of soil science. The Soil Science Society of South Africa of South Africa, Pretoria.

VAPNIK, V., 2000. *The nature of statistical learning theory*. New York: Springer-Verlag.

VAZE, J., TENG, J. & SPENCER, G., 2010. Impact of DEM accuracy and resolution on topographic indices. *Environmental Modelling and Software* 25(10): 1086-1098.

VERMA, K. S., SAXENA, R. K., BARTHWAL, A. K. & DESHMUKH, S. N. 1994. Remote sensing technique for mapping salt affected soils. Int. J. Remote Sens. 15: 1901-1914.

VERSTRAETE, M. & PINTY, B.,1996. Designing optimal spectral indexes for remote sensing applications. IEEE Transactions on Geoscience and Remote Sensing 34: 1254-1265

VOLSCHENK, T., FEY, M.V. & ZIETSMAN, H.L., 2005. Situation analyses of problems for water quality management in the Lower Orange River region with special reference to the contribution of the foothills to salinisation. WRC Report No. 1358/1/05, Water Research Commission, Pretoria.

WAGNER, W. & PATHE, C., 2004. Has SAR failed in soil moisture retrieval? Envisat and ERS Symposium, Salzburg, Austria.

WANG, F., CHEN, X., LUO, G., DING, J. & CHEN, X., 2013. Detecting soil salinity with arid fraction integrated index and salinity index in feature space using Landsat TM imagery. *Journal of Arid Land* 5(3): 340-353.

WANG, D., POSS, J.A., DONOVAN, T.J., SHANNON, M.C. & LESCH, S.M., 2002. Biophysical properties and biomass production of elephant grass under saline conditions. *Journal of Arid Environments* 52: 447-456.

WENG, Y. L., GONG, P. & ZHU, Z. L., 2010. A spectral index for estimating soil salinity in the Yellow River Delta Region of China using EO-1 Hyperion data. Pedosphere. 20: 378-388.

WESTERN, A.W., GRAYSON, R.B., SADEK, T. & TURRAL, H., 2004. On the ability of AirSAR to measure patterns of dielectric constant at the hillslope scale. *Journal of Hydrology* 289: 9-22.

WHITESIDE, T. & AHMAD, W., 2005. A comparison of object-oriented and pixel-based classification methods for mapping landcover in northern Australia. SSC2005 Spatial intelligence, innovation and praxis: The national biennial Conference of the Spatial Sciences Institute, Melbourne.

WICKEL, A., JACKSON, T. & WOOD, E., 2001. Multi-temporal monitoring of soil moisture with RADARSAT SAR during the 1997 Southern Great Plains Hydrology Experiment international Journal of Remote Sensing 22: 1571-1583.

WIEGAND, C., RHOADES, J., ESCOBAR, D. & EVERITT, J., 1994. Photographic and videographic observations for determining and mapping the response of cotton to soil salinity. *Remote Sensing of Environment* 49: 212-223.

WU, J., VINCENT, B., YANG, J., BOUARFA, S. & VIDAL, A., 2008. Remote sensing monitoring of changes in soil salinity: a case study in Inner Mongolia, China. *Sensors* 8: 7035-7049.

YU, Q., GONG, P., CLINTON, N., BIGING, G., KELLY, M. & SCHIROKAUER, D., 2006. Object-based detailed vegetation classification with airborne high spatial resolution remote sensing imagery. *Photogrammetric Engineering and Remote Sensing* 72: 799-811.

YUN, S., QINGRONG, H., HUADONG, G, YUAN L., QING, D. & CHUNMING, H., 2003. Effect of dielectric properties of moist salinized soils on backscattering coefficients extracted from RADARSAT image. *IEEE Transactions on Geoscience and Remote Sensing* 41: 1879-1888.

ZHANG, C. & FRASER, C., 2008. Generation of digital surface model from high resolution satellite imagery. *The International Archives of the Photogrammetry, Remote Sensing and Spatial Information Sciences* 37, B1: 785-790.

ZHANG, L. & GRUEN, A., 2006. Multi-image matching for DSM generation from IKONOS imagery. *ISPRS Journal of Photogrammetry and Remote Sensing* 60(1): 195-211.

ZHANG, T.T., ZENG, S.L., GAO, Y., OUYANG, Z.T., LI, B., FANG, C.M. & ZHAO, B., 2011. Using hyperspectral vegetation indices as a proxy to monitor soil salinity. *Ecological Indicators* 11: 1552-1562.

ZHANG, Y., 2002. Problem of fusion of commercial high-resolution satellite as well as Landsat 7 image and initial solutions. *The International Archives of the Photogrammetry, Remote Sensing and Spatial Information Sciences* 34: 587-592.

ZHANG, Y., 2004. Understanding image fusion. *Photogrammetric Engineering and Remote Sensing* 70(6): 657-661.

ZHOU, Q. & LIU, X., 2004. Analysis of errors of derived slope and aspect related to DEM data properties. *Computers & Geosciences* 30: 369-378.

ZIETSMAN, H.L., VLOK, A.C. & NEL, I., 1996. The identification of irrigated land in an intensively cultivated agricultural area in the south-western Cape by means of satellite remote sensing. WRC Report No. 440/1/96, Water Research Commission, Pretoria.

ZINK, J., 2000. Monitoring soil salinity from remote sensing data. Netherlands: International Institute for Aerospace Survey and Earth Sciences.

ZRIBI, M., BAGHDADI, N., HOLAH, N. & FAFIN, O., 2005a. New methodology for soil surface moisture estimation and its application to ENVISAT-ASAR multi-incidence data inversion. Remote Sensing of Environment 96: 485-496.

ZRIBI, M., BAGHDADI,N., HOLAH, N., FAFIN, O. & GUÉRIN, C., 2005b. Evaluation of a rough soil surface description with ASAR-ENVISAT radar data. Remote Sensing of Environment 95: 67-76.

ZOMER, R., USTIN, S. & IVES, J., 2002. Using satellite remote sensing for DEM extraction in complex mountainous terrain: Landscape analysis of the Makalu Barun National Park of eastern Nepal. *International Journal of Remote Sensing* 23(1): 125-143.

APPENDIX: A

Confusion matrices generated during the accuracy assessment of the within-field anomaly detection (WFAD) method.

Vaalharts irrigation scheme

		Field verification data				
		Salt-affected\Waterlogged	Stressed	Unaffected	Total	*User's accuracy (%)*
Predicted data	Anomaly	**18**	0	6	24	75
	Anomaly	0	**8**	0	8	100
	Not Anomaly	11	3	**24**	38	63.2
	Totals	29	11	30	**70**	
	Producer's accuracy (%)	62.1	72.73	80		
	Overall accuracy	**71.64**				
	Kappa	**0.58**				

Loskop irrigation scheme

		Field verification data				
		Salt-affected\Waterlogged	Stressed	Unaffected	Total	*User's accuracy (%)*
Predicted data	Anomaly	**35**	0	5	40	87.5
	Anomaly	0	**14**	0	14	100
	Not Anomaly	8	3	**25**	36	69.5
	Totals	43	17	30	**90**	
	Producer's accuracy (%)	81.4	82.4	83.3		
	Overall accuracy	**82.20**				
	Kappa	**0.72**				

Makhathini irrigation scheme

		Field verification data				
		Salt-affected\Waterlogged	Stressed	Unaffected	Total	*User's accuracy (%)*
Predicted data	Anomaly	**25**	0	6	31	80.7
	Anomaly	0	**12**	0	12	100
	Not Anomaly	5	0	**8**	13	61.54
	Totals	30	12	14	**56**	
	Producer's accuracy (%)	83.3	100	57.14		
	Overall accuracy	**80.4**				
	Kappa	**0.672**				

Tugela River irrigation scheme

		Field verification data				
		Salt-affected\Waterlogged	Stressed	Unaffected	Total	*User's accuracy (%)*
Predicted data	Anomaly	**43**	0	10	53	81.13
	Anomaly	0	**15**	0	15	100
	Not Anomaly	5	3	**7**	15	46.67
	Totals	48	18	17	**83**	
	Producer's accuracy (%)	89.58	83.33	41.18		
	Overall accuracy	**78.3**				
	Kappa	**0.6**				

Olifants River irrigation scheme

		Field verification data				
		Salt-affected\Waterlogged	Stressed	Unaffected	Total	*User's accuracy (%)*
Predicted data	Anomaly	**34**	0	13	47	72.34
	Anomaly	0	**17**	0	17	100
	Not Anomaly	6	0	**12**	18	66.67
	Totals	40	17	25	**82**	
	Producer's accuracy (%)	85	100	48		
	Overall accuracy	**76.8**				
	Kappa	**0.6**				

Breede River irrigation scheme

		Field verification data				
		Salt-affected\Waterlogged	Stressed	Unaffected	Total	*User's accuracy (%)*
Predicted data	Anomaly	**26**	0	5	31	83.87
	Anomaly	0	**4**	0	4	100
	Not Anomaly	8	7	**35**	50	70
	Totals	34	11	40	**85**	
	Producer's accuracy (%)	76.47	36.36	87.5		
	Overall accuracy	**76.5**				
	Kappa	**0.58**				

Sundays River irrigation scheme

		Field verification data				
		Salt-affected\Waterlogged	Stressed	Unaffected	Total	*User's accuracy (%)*
Predicted data	Anomaly	**15**	0	3	18	83.33
	Anomaly	0	**1**	0	1	100
	Not Anomaly	7	0	**25**	32	78.13
	Totals	22	1	28	**51**	
	Producer's accuracy (%)	68.18	100	89.29		
	Overall accuracy	**80.4**				
	Kappa	**0.6**				

Limpopo River irrigation scheme

		Field verification data				
		Salt-affected\Waterlogged	Stressed	Unaffected	Total	*User's accuracy (%)*
Predicted data	Anomaly	**14**	0	11	25	56
	Anomaly	0	**7**	0	7	100
	Not Anomaly	17	2	**26**	45	57.78
	Totals	31	9	37	**77**	
	Producer's accuracy (%)	45.16	77.78	70.27		
	Overall accuracy	**61.0**				
	Kappa	**0.326**				

Douglas irrigation scheme

		Field verification data				
		Salt-affected\Waterlogged	Stressed	Unaffected	Total	*User's accuracy (%)*
Predicted data	Anomaly	**21**	0	9	30	70
	Anomaly	0	**3**	0	3	100
	Not Anomaly	13	0	**20**	33	60.61
	Totals	34	3	29	**66**	
	Producer's accuracy (%)	61.76	100	68.97		
	Overall accuracy	**66.7**				
	Kappa	**0.387**				

APPENDIX: B

Vaalharts Irrigation Scheme Observation Points

Latitude	Longitude	EC (mS/m)	Field Note
-27.888673758	24.799996587	188	Bare ground
-27.888595237	24.800402161	1048	2) Ground use: Bare ground; Overnight Dam; reeds present
-27.884902895	24.798954988	930	3) Ground use: Side of road; White salt precipitation; Next to maize field
-27.860178187	24.782748665	350	4) Ground use: Bare ground; Slat affected confirmed by farmer
-27.856399802	24.779404029	1550	5) Ground use: Oats; salt affected area; not even germinated; reeds
-27.855913099	24.779371013	950	6) Ground use: Oats; potential good area
-27.841239454	24.766760009	86	7) Lucerne; dry patch; maybe other than salt affected problem; flood irrigation
-27.821375941	24.763332014	115	8) Ground use: Pecan nuts; drip irrigation; fallow; young pecan nut trees
-27.801591932	24.751521144	33	9) Combination between lucerne and Pecan nuts; centre pivot irrigation; good to moderate growth
-27.782207021	24.731045289	52	10) Ground use: bare ground; centre pivot irrigation
-27.760923289	24.732642493	250	11) Ground use: bare ground; very sandy; powdery calcium carbonate on surface, not salt affected
-27.756015098	24.735796453	130	12) Was lucerne; possibility of waterlogging and salt affection;, perched watertable
-27.750847834	24.726782564	65	13) Ground use: Lucerne, invasive grass patches; centre pivot irrigation

27.720553415	24.750703756	40	Cotton	
-				
27.801596793	24.767798835	50		15) Ground use: bare ground; fallow
-				
27.832538449	24.787280034	1875		16) Ground use: Lucerne, salt precipitation on surface, sign of salt damage on leaves
-				
27.832309492	24.787920051	53		17) Ground use: Invasive grass; possibility waterlogging
-				18) Ground use: Pecan nuts; flood
27.860294130	24.804981375	40		irrigation
-				
27.867126744	24.822016096	7		19) Ground use: Bare ground; very sandy yellow soil, pecan nuts; pivot irrigation
-				
27.867263209	24.821768957	165		20) Ground use: Bare ground; very sandy brown soil; pecan nuts; pivot irrigation
-				
27.825207573	24.808774201	31		21) Ground use: Peanut field; centre pivot irrigation
-				
27.810508924	24.795511654	58		22) Ground use: Dry patch compacted soil; above average hard setting; lucerne field
-				23) Ground use: hardsetting; compaction; well grown patch
27.810172053	24.795762152	55		Lucerne
-				
27.792094837	24.785935613	80		24) Ground use: Maize; centre pivot detection; salt detection; waterlogging
-				
27.792157029	24.787138472	105		25)Ground use: Maize; bare patch, heavy clay content; sign of waterlogging on surface; slight salt
-				26) Ground use: Wheat/barley; flood irrigation; poor ground preparation, poor farming methods; str
27.754857050	24.775142510	35		lines
-				
27.754484607	24.775465371	185		27) Ground use: Wheat/barley; flood irrigation; poor farming methods; better patch
-				28) Ground use: Lucerne; compaction; normal
27.752126729	24.760086693	75		sprinklers;
-				
27.751065515	24.759039149	55		29) Ground use: Lucerne; compaction; dead patch;; slight depression; possibly old flood irrigation; di
-	24.759951480	70		30) Ground use: Lucerne; good growth; higher elevation (Near Dr Nell peso meter)

27.751103858			
-			
27.713087150	24.729829940	50	31) Ground use: Bare ground; peanuts; grey soil
-			
27.713212805	24.729518673	29	32) Ground use: Bare ground; peanuts; red soil
-			
27.718325875	24.727181381	42	33) Ground use: Bare ground; ground identified by farmer as a bad patch
-			
27.718187767	24.727785142	63	34) Ground use: Bare ground; ground identified by farmer as a better patch
-			
27.720265769	24.718619876	3220	35) Ground use: Reeds; highly salt affected; waterlogged area
-			
27.720354294	24.719004074	55	36) Ground use: Lucerne; centre pivot irrigation; bare spot; possibly waterlogged
-			
27.720293616	24.720299732	68	37) Ground use: Lucerne; centre pivot irrigation; bare spot
-			
27.768545709	24.734344292	83	Lucerne /Pecan nuts; flood irrigation; waterlog area; possibly because of its position in landscape
-			
27.768438425	24.734648165	82	39) Ground use: Lucerne and Pecan nuts; flood irrigation; flood irrigation; light salt precipitation;
-			
27.803028351	24.760426692	60	40) Ground use: Cabbage; bad patch
-			
27.802549348	24.760372889	34	41) Ground use: Cabbage; better patch
-			
27.799958742	24.757677197	90	Lucerne; hard setting; water shortage; bare spots; normal sprinklers because pivot is out of reach
-			
27.860229915	24.787435307	110	43) Ground use: Bare ground; lime spot in slight depression; very young pecan nuts
-			
27.861507734	24.781934881	38	44) Ground use: Oats, Lime, grazing, dead patch, possibility of salt affection.
-			
27.861880987	24.781628143	39	45) Ground use: Oats , better (good) patch
-			
27.861652048	24.780427708	160	46) Ground use: Oats, higher clay, shallow lime old farming methods)

-27.862666251	24.818212645	34	47) Ground use: non- agricultural patch , remnants of previous crops, central pivot irrigation
-27.867562503	24.817753508	55	48) Ground use: Dry grass land; abandoned land
-27.868602720	24.818273376	12	49) Ground use: Very sandy, Flood irrigation, Pecan nuts, small, newly planted tree
-27.868399615	24.817934408	290	50) Ground use: Very sandy, Flood irrigation, Pecan nuts, larger tree, well grown
-27.869513216	24.820868088	441	51) Ground use: Very sandy, Flood irrigation, Pecan nuts, Pecan nuts, salt crust present on surface
-27.868642167	24.828584797	25	52) Ground use: Lucerne; invasive grass, dead patch
-27.868218695	24.828256018	32	53) Ground use: Lucerne; beter growth
-27.759961704	24.757391016	48	54) Ground use: Bare Soil, peanut field, peanut remrants, slight silt crust, red soils, fine
-27.781516801	24.771120596	72	55) Ground use: Lucerne, corner area, dead patch, waterlogged
-27.781461122	24.771360266	63	56) Ground use: Lucerne, good patch, hard ground, flood irrigation
-27.780829070	24.753756745	186	57) Ground use: Bare ground, fine soils, red, old cotton field, centre pivot irrigation

Maize Grid Vaalharts

Latitude	Longitude	EC (mS/m)	Field Note
-27.791724409	24.786131150	118	MG_1) Maize; bare patch, high clay content 25 -35%; long rectangular cracks; earth worm (sigh of wetness);
-27.791772700	24.786257265	135	MG_2) Maize; bare patch, high clay content 25 -35%; long rectangular cracks; earth worm (sigh of wetness);
-27.791819766	24.786397149	190	MG_3)clear salt precipitation; on side of maize; hard surface
-27.791954123	24.786811526	100	MG_4) Very hard surface; strong structure; pedocutanic; possibly subsoil, top soil removed during old flood irrigation
-27.791998590	24.786919296	90	MG_5) High clay, bare patch; high water holding, poor internal drainage; 35 -40%
-27.792050558	24.787016635	145	MG_6) previously; waterlogged on the surface, bare patch
-27.792105778	24.787153413	90	MG_7) large bare patch, salt cracks, salt precipitation on surface
-27.792121807	24.787665234	95	MG_8) large bare patch, signs of perch water table
-27.792174506	24.787792855	74	MG_9) Inside maize, slight salt precipitation, slightly less clay, soil more red than black
-27.792204263	24.787909424	66	MG_10) Inside maize, earth worm, less clay, phosphate shortage
-27.792249054	24.787140374	113	MG_11) Large bare area, white salt cracks, black clay
-27.792017257	24.787161973	100	MG_12) Large bare area, white salt cracks, black clay

Vegetation Grid Vaalharts

Latitude	Longitude	EC (mS/m)	Field Note
-27.856098640	24.779563645	420	VG_1) Ground use: Oats; salt precipitation visible; flood irrigation; yellow/red copper leaf colouring
-27.855935796	24.779446336	450	VG_2) more salt precipitation visible
-27.855763181	24.779356211	635	VG_3) salt precipitation clearly visible, leaf colouring
-27.855602021	24.779243117	440	VG_4) Bare patch, leaf colouring, clear salts, strange flat plant formation
-27.855446429	24.779128431	215	VG_5) Bare patch, leaf colouring, clear salts
-27.855284818	24.779024773	450	VG_6) Bare patch, leaf colouring, clear salts
-27.855108104	24.778913916	905	VG_7) More salts on ridge
-27.854941474	24.778807066	180	VG_8) Slightly less salts; plants looking better; slight salt crust, harder setting
-27.854785756	24.778705412	38	VG_9) Slightly better conditions, no salt visible
-27.854630976	24.778601489	33	VG_10) Good patch, 60 cm – depth of soil, calcium carbonate rock; water table problems; lime spots
-27.854467982	24.778494538	30	VG_11) Good patch
-27.854317547	24.778383605	31	VG_12) Good patch; end of grid line 1

-27.854420519	24.778209792	45	VG_13) Medium patch, light salt precipitation
-27.854528107	24.778032684	34	VG_14) Medium condition, edge of green area
-27.854646946	24.777886776	65	VG_15) Bare patch; reeds start; 50 cm ,lime watertable
-27.854736730	24.777757816	783	VG_16) Heavy salt precipitation on surface, reeds
-27.854860321	24.777597301	420	VG_17) Dead spot, water present, reeds
-27.854989748	24.777421786	33	VG_18) Very sandy, low water holding; dry patch, no salt precipitation
-27.855101261	24.777267696	37	VG_19) Very sandy, stress symptoms on plans due to water shortage, 3-4 % clay
-27.855227993	24.777104590	42	VG_20) Very sandy, very dry, stress because of poor irrigation, no salt precipitation
-27.855748824	24.777472958	34	VG_21) Very sandy dry patch
-27.855715069	24.777677074	30	VG_22) Very sandy, top soil dry
-27.855667783	24.777870534	44	VG_23) Sandy top soil, more moisture deeper in the ground, 60 cm lime layer
-27.855623633	24.778099960	900	VG_24) Failed maize crops, reeds , sign of water, no salt precipitation
-27.855589193	24.778306657	215	VG_25) maize dead patch; no salt precipitation
-27.855544301	24.778511525	28	VG_26) Sandy top soil; dry patch; end of dry area
-27.855491069	24.778718211	33	VG_27) irrigated area, relatively good patch
-27.855437096	24.778929176	189	VG_28) Crust patch, light salt precipitation, fairly bad area
-27.854351775	24.778181098	27	VG_29) Good green patch, no salt precipitation
-27.854510113	24.778285637	30	VG_30) Good patch
-27.854670333	24.778399663	29	VG_31) Good patch
-27.854827923	24.778502049	68	VG_32) Slight salt patch
-27.855006098	24.778621001	635	VG_33) Slight dry top soil, light salt precipitation
-27.855163788	24.778725612	200	VG_34) Medium crop, slightly salt precipitation
-27.855367250	24.778850586	2500	VG_35) dead patch ; high salt precipitation, small plats, no germination
-27.855588244	24.778998143	930	VG_36) high salt; dead patch
-27.855746358	24.779109591	950	VG_37) high salt; dead patch
-27.855896320	24.779198649	1960	VG_38) Very high salty very poor growth, 80 cm lime layer
-27.856051787	24.779308234	200	VG_39) Better patch, slight salt
-27.855936647	24.779333508	935	VG_40) high salt precipitation, dead patch, very poor growth

Bare ground Grid Vaalharts

Latitude	Longitude	EC (mS/m)	Field_Note
-27.888281556	24.799980875	290	BGG_1) Bare ground, cultivated, salt on sub-soil and yellowish
-27.888204935	24.799798585	635	BGG_2) Bare ground, cultivated, salt on sub-soil and yellowish
-27.888123348	24.799613348	420	BGG_3) Bare ground, cultivated, salt on sub-soil and yellowish
-27.888041589	24.799416686	1050	BGG_4) Bare ground, cultivated, salt on sub-soil and yellowish
-27.887951603	24.799207346	420	BGG_5) Bare ground, cultivated, salt on sub-soil and yellowish
-27.887870787	24.799015571	440	BGG_6) Bare ground, cultivated, salt on sub-soil and yellowish
-27.887781672	24.798811984	550	BGG_7) Pecan nuts, salt on surface, drip irrigation
-27.887695743	24.798598927	62	BGG_8) Pecan nuts, salt on surface, drip irrigation
-27.887615163	24.798406145	36	BGG_9) Pecan nuts, salt on surface, drip irrigation
-27.887529594	24.798208174	20	BGG_10) Pecan nuts, salt on surface, drip irrigation
-27.887868360	24.798104204	35	BGG_11) Pecan nuts, salt on surface, drip irrigation
-27.887701470	24.798154819	20	BGG_12) At drip line
-27.887341560	24.798255483	20	BGG_13) At drip line
-27.887079066	24.798580241	150	BGG_14) At drip line
-27.887231129	24.798526560	30	BGG_15) Pecan nuts, salt on surface, drip irrigation
-27.887432255	24.798459710	36	BGG_16) Pecan nuts, salt on surface, drip irrigation
-27.887814984	24.798352221	22	BGG_17) At drip line
-27.887969992	24.798238544	19	BGG_18) At drip line
-27.887856555	24.798521018	42	BGG_19) Pecan nuts, salt on surface, drip irrigation
-27.887523367	24.798669657	160	BGG_20) Pecan nuts, salt on surface, drip irrigation
-27.887349000	24.798711703	120	BGG_21) Pecan nuts, salt on surface, drip irrigation
-27.887172594	24.798780317	150	BGG_22) Whitish colour
-27.887255521	24.798966249	400	BGG_23) Whitish colour
-27.887416986	24.798921356	132	BGG_24) Whitish colour
-27.887597859	24.798865185	240	BGG_25) Pecan nuts, salt on surface, drip irrigation
-27.887746843	24.798663583	561	BGG_O_1) Pecan nuts, salt on surface, drip line irrigation
-27.887656968	24.798817402	821	BGG_O_2) Salt on top soil
-27.887658475	24.798924137	635	BGG_O_3) Salt on top soil, reddish soil in sub soil
-27.887911820	24.798923635	330	BGG_O_4) Red soil outside the drip line

Vaalharts Piezometer (Watertable Depth, ECwater and Soil

Depth	SAR	EG-Soil	pH-Soil	Ecwater	Watertabel	South	East
0-300	1.3	45	7.9	92	1.4	27 42 52.6	24 46 20.7
300-600	4.4	39	7.18				
600-900	2.2	38	7.62				
900-1200	1.3	48	7.62				
0-300	1.0	56	7.46	62	0.7	27 47 43.1	24 45 17.2
300-600	1.8	49	9.01				
600-900	2.1	59	9.12				
900-1200	4.2	77	9.08				
0-300	1.4	53	8.72	162	1.9	27 47 29.9	24 47 34.2
300-600	4.6	324	7.93				
600-900	6.0	196	8.58				
900-1200	9.3	143	9.26				
0-300	0.5	33	8.57	62	1.2	27 49 10.9	24 45 19.8
300-600	0.4	32	8.07				
600-900	0.5	29	7.59				
900-1200	0.8	29	7.96				
0-300	1.5	41	7.67	176	2.25	27 47 42.4	24 48 20.9
300-600	1.9	38	8.02				
600-900	2.1	60	8.06				
900-1200	2.7	130	8.04				
0-300	1.4	70	7.79	70	1.35	27 40 42.4	24 47 07.9
300-600	1.8	85	7.69				
600-900	2.8	151	7.52				
900-1200	3.0	94	7.5				
0-300	1.0	33	7.33	480	1.65	27 40 44.6	24 46 55.6
300-600	1.6	41	7.52				
900-1200	1.3	32	7.26				
1500-1600	1.5	44	7.46				
0-300	0.8	41	7.12	138	1	27 41 43.8	24 45 25.2
300-600	2.6	93	7.26				

600-900	2.2	98	7.6				
900-1200	2.3	67	7.76				
0-300	0.6	17	7.27	920	1	27 42 06.7	24 41 32.2
300-600	1.1	30	7.78				
900-1200	1.6	195	8.14				
0-300	21.8	1095	8.48	1180	0.7	27 39 59.0	24 41 45.7
300-600	36.8	596	8.92				
600-900	15.3	380	9.02				
900-1200	12.1	439	8.8				
0-300	5.7	389	8.21			28 01 52.3	24 40 50.3
300-600	1.5	102	8.42				
600-900	0.7	88	7.98				
900-1200	67.5	53	8.08				
0-300	5.3	990	8.44			28 01 48.2	24 40 48.1
300-600	11.2	217	8.93				
600-900	11.8	Herhaal	9.32				
900-1200	114.6	137	9.37				
0-300	10.6	627	8.72			28 01 48	24 40 43.5
300-600	2.4	297	8.46				
600-900	1.9	102	8.43				
900-1200	0.9	79	8.57				
0-300	8.7	48	7.1			28 01 43.1	24 40 51.9
300-600	5.2	276	7.04				
600-900	4.6	332	7.54				
900-1200	0.6	272	7.67				
0-300	9.7	58	7.42			28 01 39.1	24 40 48.6
300-600	4.5	227	7.37				
600-900	1.9	281	7.5				
900-1200	1.1	132	7.96				
0-300	1.6	71	7.38			28 01 33.9	24 40 46.3
300-600	8.4	69	7.68				
600-900	6.2	265	7.74				
900-1200	0.3	56	7.72				

APPENDIX: C

Sundays River Irrigation Scheme

Point	SAR	EC (mS/m	Watertable (cm)	Comments
1	2.4	370		Orchard was problematic
1.1	16.9	3200	30	Waterlogged and salt affected in old paleodrainage canal/vlei
1.2	15.4	2050	30	Waterlogged and salt affected in old paleodrainage canal/vlei
2	2.8	150		Citrus good condition
4	3.2	60		Citrus good condition
5	4.8	250	110	Slightly waterlogged (from dam)
6	2.7	95		Citrus good condition
7	4.9	193		Citrus good condition
8	4.3	350		Slightly salt precipitation
9	3.8	120		Citrus good condition
11	3.4	110		Citrus good condition
12	3.9	145		Citrus good condition
13	3.2	167		Old flood irrigation system with sighs of waterlogging in the past.
14	2	129		Citrus good condition
15	1.9	70		Citrus good condition
16	4.8	350		Citrus variable growth
17	4.2	138		Citrus good condition
18	3.5	166		Citrus healthy. ARC-Experimental Farm Orchard
33	9.9	670	85	Waterlogged and salt affected in old paleodrainage canal
34	2.9	90		Citrus good
35	7.4	600	45	Waterlogged and salt affected
39	3.1	115		Citrus good
M10	6.2	248	70	Pasture healthy
M11	3.5	88	80	Pasture healthy

M12	6.7	750		Possible boundary between waterlogged and dry area
M13	5.8	380		Boundary between pastures and citrus
M14	1.2	140		Citrus good condition
M15	1.6	65		Citrus good condition
M3	9.7	1380	105	Possible boundary between waterlogged and dry area
M4	3.8	100	90	Lowest point
M5	12.5	375	80	Pasture healthy
M5(b)	16.5	2360	90	Fallow land halophytic plants and salt precipitation
M6	4.1	150		Just outside floodplain. Bare batch – animal water point
M7	9.8	627	120	Pasture relatively healthy
M8	2.3	66		Pasture healthy
M9	5.3	180		Pasture healthy
S1	7.5	420		Bare patches (sandy, slight depression with salt crust)
S11	9.3	450	80	Waterlogged and salt affected near natural drainage canal
S12	8.7	620		Citrus relatively poor condition
S2	6.2	560	80	Waterlogged and salt affected
S3	2.3	45		Different rootstock trial on experimental farm
S6	4.2	309	100	Waterlogged and salt affected
S9	5.1	480	110	Waterlogged and salt affected
Se1	23.8	3884	90	Salt precipitation on surface, halophytic plants and waterlogged
Se10	18.8	2790	70	Salt precipitation on surface, halophytic plants and waterlogged
Se11	43.5	2006	50	Salt precipitation on surface, halophytic plants and waterlogged, dispersion
Se2	4.3	114		Citrus relatively healthy
Se3	3.5	95		Citrus relatively healthy
Se4	2.4	162		Citrus relatively healthy
Se5	2.9	225		Citrus relatively healthy
Se6	2.7	170		Citrus relatively healthy
Se7	9.8	589		Citrus relatively poor condition
Se8	5.2	74		Citrus relatively healthy
Se9	2.8	85		Citrus relatively healthy

W1	62.4	2200	30	Lowest point. Drainage ditch. Waterlogged. Salt precipitation. No trees
W10	15.4	620	110	Knick point in topography
W11	8.5	820	70	Waterlogged and salt affected
W12	4.7	380	1200	Citrus relatively healthy
W13	4.1	375	1200	Citrus relatively healthy
W14	9.7	1350	70	Waterlogged and salt affected
W15	6.1	146	100	Possible boundary between waterlogged and dry area
W16	3.5	80		Citrus relatively healthy
W17	8.4	550	100	Drainage ditch. Waterlogged
W18	7.6	890	90	Waterlogged and salt affected
W19	9.3	1200	40	Waterlogged and salt affected
W2	23.1	1057	45	Just outside destroyed area
W20	3	170	70	Possible boundary between waterlogged and dry area
W21	2.9	110		Citrus relatively healthy
W3	7.7	168	110	Possible boundary between waterlogged and dry area
W4	2.7	117		No watertable 0-120 cm
W5	36.9	1835	30	Waterlogged
W6	4.4	140	105	Possible boundary between waterlogged and dry area
W7	2.3	112		Citrus healthy
W8	8.2	580	80	Salt precipitation
W9	7.9	540	120	Knick point in topography

APPENDIX: D

Limpopo River Irrigation Scheme

No	South	East	EC(mS/m)	Water (cm)	Description
B2	22.177194	29.493583	280	120	Light salt precipitation on some crusts
B23	22.177208	29.491654	440	45	Very shallow watertable
B611	22.180444	29.493582	390	110	Bare Ground
B621	22.180444	29.494222	380	110	Bare Ground
B631	22.180079	29.494705	180	110	Bare Ground
B641	22.179814	29.495265	320	110	Bare Ground with salt crust
B651	22.179508	29.496015	190		Bare Ground
B67	22.179673	29.493132	410	70	Bare Ground
B68	22.179222	29.492880	400	80	Bare Ground
B69	22.180834	29.493973	350	120	Bare Ground
B70	22.181121	29.494159	340	120	Bare Ground
b72	22.173296	29.487659	380		Ridge, but relatively shallow
b75	22.173451	29.487274	420	110	Ridge, but relatively shallow
b76	22.173679	29.486492	430	120	Ridge, but relatively shallow
B79	22.173385	29.488166	400	110	Ridge, but relatively shallow
B80	22.17356	29.488585	360		Ridge, but relatively shallow
D21	22.20013	29.282419	400	80	Patches of standing water
D3	22.199051	29.284657	390	80	Patches of standing water
D41	22.198442	29.288698	500		Citrus removed because of salinity and waterlogging
D44	22.198787	29.287402	1800	100	Citrus removed because of salinity and waterlogging
D5	22.197113	29.287314	1970	100	Abandoned because of salinity and waterlogging
D6	22.197291	29.279903	350		Area was flooded
D81	22.196465	29.288020	380	110	Light salt precipitation on surface.
D82	22.196888	29.289097	420	90	Light salt precipitation on surface.
D83	22.197216	29.289347	370	110	Light salt precipitation on surface.

D84	22.195891	29.288458	410	110	Light salt precipitation on surface. High clay content 38%
D85	22.19529	29.288003	380	110	Light salt precipitation on surface. High clay content 38%
D86	22.196706	29.288615	360	120	Area was flooded
D87	22.197313	29.288657	350	120	Area was flooded
D90	22.197246	29.288040	410	90	Light salt precipitation on surface. High clay content 38%
D95	22.198587	29.278792	425		Signs of salt precipitation
D96	22.197904	29.279170	375		Ok
F1	22.187295	29.539067	150		Was totally flooded. Disturbed soils – soil levelling
F100	22.19594	29.503889	75		Ridge, but relatively shallow
F1011	22.196212	29.503571	90		Ridge, but relatively shallow
F102	22.196666	29.502680	80		Ok
F103	22.194896	29.504293	360	100	Light salt precipitation. Green Peppers
F2	22.197329	29.503310	55		Shallow and stoney. Tomatoes
F3	22.19036	29.504628	100		Signs of wetness at 110 cm
F551	22.186592	29.540072	140		Was totally flooded. Disturbed soils – soil levelling
F591	22.188252	29.538844	155		Was totally flooded. Disturbed soils – soil levelling
F601	22.189017	29.539111	80		Was totally flooded. Disturbed soils – soil levelling
M1	22.171133	29.545976	60		Crusting on surface. Cotton (Is die spierwit katoenlande 'n probleem vir julle?
M2	22.171364	29.546229	68		Bare patch (high silt content)
M3	22.171973	29.546265	70		Bare patch (high silt content and indication of transported soils)
M41	22.17265	29.547356	75		Bare patch (slight depression)
M441	22.17163	29.546736	80		Soil washed away during flood. Land was levelled with transported soil
M461	22.171187	29.547241	76		Soil washed away during flood. Land was levelled with transported soil
M481	22.17113	29.549070	110		Soil washed away during flood. Land was levelled with transported soil
M501	22.172618	29.545924	60		Soil washed away during flood. Land was levelled with transported soil
N1	22.1607	29.606652	650	100	Bare ground with removed citrus trees (possibly poor area)
N110	22.160813	29.606139	700	100	Bare ground with removed citrus trees (possibly poor area)
N1111	22.160619	29.606576	600	100	Bare ground with removed citrus trees (possibly poor area)
N113	22.15986	29.607837	800	80	Poor growth
N114	22.159919	29.606515	350	120	Crusting on surface

N115	22.161056	29.606583	500	110	Bare ground with removed citrus trees (possibly poor area)
N130	22.149361	29.620528	200		Was irrigation – bare ground
N2	22.160071	29.607429	550	80	Bare ground with salt precipitation.
N242	22.137734	29.663530	380		Bare ground. Natural drainage
N252	22.137722	29.662806	410		Bare ground.
N261	22.137343	29.662471	350		Bare ground. Natural drainage
N291	22.136778	29.661917	330		Bare ground.
N292	22.137032	29.660699	280		Bare ground.
N3	22.159796	29.607441	200	115	Citrus in a relatively poor condition. Waterlogged area during floods.
N4	22.159937	29.607421	680	90	Salt precipitation. Citrus poor condition.
N5	22.160274	29.607424	600	100	Bare Patch
N6	22.160518	29.607434	290		OK
N7	22.161406	29.602681	2400	50	Was citrus. Waterlogged and salt-affected
N71	22.160667	29.603621	3000	50	Was citrus. Waterlogged and salt-affected
N8	22.151488	29.623447	50		Was irrigation. Well drained red soils
W_37	22.180333	29.583583	145		OK
W1	22.180159	29.578502	2200	90	Salt precipitation on surface. New citrus plantings
W2	22.179614	29.580902	540	50	Waterlogged area. Potatoes
w3	22.179694	29.581274	180		Potatoes not stress
W321	22.181318	29.582014	600		Bare Patch. Signs of wetness from 90 cm
W331	22.180517	29.582099	240		OK
W35	22.181083	29.582500	420	100	Poor growth
W361	22.18075	29.582981	150		OK
w4	22.179912	29.581890	110		Potatoes not stress
W411	22.179788	29.582129	650		Salt precipitation on surface
W5	22.179952	29.582784	75		Potatoes not stress
W6	22.180862	29.580634	1200	80	Bare Patch. Salt precipitation on surface

APPENDIX: E

Vaal and Orange River Irrigation Scheme (Douglas)

No	South	East	EC (mS/m)	Water (cm)	Description
V1	28.95755	23.914607	850	45	Area was a wetland before it was drained for irrigation. Salt precipitation
V10	28.96145	23.966826	510	70	Bare patch. High clay content
V1051	29.032888	24.010808	320		Very shallow soils with $CaCO_3$ rocks on surface
V1061	29.033639	24.010011	6080		Depression. Salt precipitation
V1081	29.032751	24.010141	390		OK
V11	28.961435	23.966518	375	110	Ok
V1171	29.051769	23.67945	400	60	Very shallow soil (gravel)
V12	28.961899	23.9662	600	55	Better patch. Salt precipitation on surface
V1201	29.053295	23.680311	360	20	Hydric plants
V1281	29.071679	23.669541	220		Very shallow soil (gravel)
V1291	29.071525	23.670326	455		Very shallow soil (gravel), with salt precipitation on surface
V13	28.962594	23.964951	250		OK
V1301	29.071385	23.671098	210		Fallow land
V1312	29.071308	23.672111	270		Fallow land
V136	29.102395	23.625043	475		Poor growth
V137	29.102625	23.625703	445		Poor growth
V14	28.92311	23.968003	375	20	Lowest point
V1411	29.103677	23.623718	150		Ok
V15	28.923349	23.967657	350	20	Bare patch. Perched watertable
V150	28.99728	23.94656	220		Ok
V153d	28.996119	23.946118	150		Ok
V153s	28.996459	23.94528	200		Shallow
V153Sui	28.992601	23.945303	410	40	Waterlogged
V154g	28.995525	23.945851	180		OK

V155	29.115296	23.761694	190		Lowest point
V156	29.115352	23.762828	345		In drainage line with salt precipitation on surface
V16	28.923761	23.966731	340		Ok
V160	29.116261	23.764118	140		Ok
V163	29.062058	23.695596	410	100	Salt precipitation
V165	29.058594	23.69824	470		Salt precipitation and crusting
V168	29.059377	23.695995	245		Crusting (poor infiltration)
V17	28.917643	23.964014	255		Lowest point, some erosion
V18	28.991454	23.883684	190	50	Lowest point. Bare patch
V19	28.991172	23.882962	250	20	Knick point in topography
V2	28.957982	23.912408	450	115	Relative low point.
V20	28.991612	23.882435	180		Ok
V21	29.04986	23.680469	130	50	Lowest Point. $CaCO_3$ on surface. Bare ground
V22	29.050715	23.680622	125	70	Stoney. Slight depression
V23	29.051942	23.680914	280	25	Hydric plants
V25	28.99868	23.94578	300		Fallow not irrigated. Very high silt and clay content
V3	28.956002	28.956002	395	110	Drainages point to river
V313	28.917426	23.960314	410	80	Bare patch
V363	28.92362	23.967233	460	40	Bare patch. Perched watertable, although near to drain
V4	28.95027	23.90936	160		OK
V413	28.919925	23.961232	420	80	Bare patch
V5	28.95976	23.96477	550	80	Bare patch. High clay content. Perched watertable
V532	28.962717	23.965619	620	40	Bare patch. Depression. High clay content
V552	28.961854	23.967166	270		Better patch
V6	28.96242	23.96557	700	80	Bare patch. Depression. High clay content
V671	28.957561	23.914307	700	80	Bare patch
V681	28.957134	23.914032	380	100	Poor growth
V7	28.96332	23.96568	525	90	Very poor lucerne
V721	28.955617	23.908835	450	80	Lowest point
V731	28.955374	23.909484	430	100	Drainage line
V741	28.955103	23.91073	410	110	Drainage line

V751	28.954858	23.911705	245		Lowest point of drainage path
V761	28.953665	23.908112	380		OK
V771	28.953564	23.908925	320		OK
V781	28.953487	23.909684	270		OK
V791	28.953385	23.910661	150		OK
V8	28.963315	23.966002	550	80	Bare patch. High clay content
V811	28.955881	23.912257	370		OK
V821	28.956406	23.912207	380		OK, but some indication of salt precipitation on surface
V9	28.963106	23.966508	370		Better patch
V901	28.992241	23.882149	160		Ok
V921	28.992855	23.883366	350	60	Bare patch, very poor drainage
V951	28.991729	23.883173	200	80	Bare patch
V971	28.99007	23.881598	375		Relatively Ok
V981	29.018533	24.028147	75		On crest. Shallow sandy soil low water holding capacity (drought stress)
V991	29.01815	24.02859	65		Deeper soil, no indication of drought stress

APPENDIX: F

Makhathini Irrigation Scheme

NO	Lab	Sender	ESP	pH (H2O)	SAR	EC	Cl		SO_4
						mS/m	mmol(c)/l	mg/kg	mmol(c)/l
M167	M353	113F	2.56	7.27	2.71	32	0.396	9.83	0.441
	M354	196F	6.16	7.46	4.41	36	0.391	8.82	1.193
	M355	218F	8.35	7.95	6.61	37	0.641	15.03	1.777
M161	M356	14F	2.57	6.56	8.38	50	0.826	16.24	0.760
	M357	415F	8.42	6.94	8.79	81	1.232	27.05	4.259
	M358	530F	16.57	8.32	7.12	58	0.282	5.81	1.016
M175	M359	21F	2.33	7.23	2.81	42	0.547	10.23	0.440
	M360	24F	8.43	6.69	7.24	92	2.893	58.67	2.628
	M361	57F	11.73	8.04	9.78	88	2.745	55.05	1.984
M183	M368	386F	6.48	7.67	9.78	725	39.069	975.39	4.013
	M369	660F	6.58	7.90	7.55	296	14.556	379.17	2.107
	M370	687F	5.10	8.52	5.72	157	6.476	167.51	1.290
M192	M371	604F	9.03	7.16	3.33	99	0.607	12.47	0.497
	M372	617F	2.76	7.67	3.71	39	0.667	13.55	0.560
	M373	790F	19.12	7.83	5.06	39	1.205	28.07	0.665
M251	M374	773F	2.35	7.36	2.15	43	0.259	6.47	0.684
	M375	878F	17.65	8.86	2.60	101	1.756	52.15	1.670
	M376	922F	16.37	9.21	18.82	202	6.412	198.73	3.648
M266	M377	936F	1.63	7.86	1.62	61	0.286	6.10	0.708
	M378	950F	4.14	6.64	6.17	73	2.021	46.02	1.240
	M379	973F	8.82	7.32	11.24	79	3.315	71.70	0.924
M257	M388	225F	5.07	8.12	7.88	97	3.328	93.20	0.592
	M389	232F	7.94	8.14	18.32	792	39.764	1315.74	11.480
	M390	255F	11.25	7.94	18.61	871	41.331	1459.51	11.553
M243	M403	923F	5.17	7.84	6.58	889	43.769	1423.34	13.641

	M404	946F	11.88	8.15	9.75	665	34.592	1101.34	6.042
	M405	976F	9.75	8.62	11.26	360	18.494	531.24	2.635
	M422	829F	15.70	7.37	12.85	311	18.438	430.10	2.245
M127	M432	1349F	2.10	6.52	4.17	207	9.364	176.63	2.103
	M433	1403F	17.32	7.33	9.24	1558	71.291	1587.66	23.824
	M434	1442F	28.75	8.18	13.52	1778	77.290	1902.44	26.307
M125	M435	1486F	3.37	8.02	3.89	84	2.156	52.32	1.220
	M436	1505F	9.88	9.00	11.02	165	6.977	186.50	1.843
	M437	1552F	20.20	8.98	25.40	483	25.748	844.78	9.430
M51	M444	1285F	3.20	7.54	3.95	54	0.368	8.59	0.602
	M445	1482F	13.82	8.91	11.20	126	2.589	62.85	2.835
	M446	1512F	16.79	9.18	18.04	156	5.064	123.27	2.131
M1	M447	409F	2.28	7.76	3.79	114	1.280	24.27	5.704
	M448	673F	3.35	7.72	4.90	77	1.882	45.27	2.095
	M449	736F	4.40	7.67	6.58	93	2.629	54.37	2.641
M19	M453	1230F	1.84	6.44	1.83	49	0.468	10.28	0.837
	M454	1317F	6.61	7.53	4.18	52	0.345	8.85	1.231
	M455	1463F	7.20	8.38	6.92	113	1.339	29.40	1.444
M48	M465	1330F	1.57	7.73	1.34	50	0.358	7.96	0.464
	M466	1408F	11.47	7.36	6.23	173	7.248	131.40	3.115
	M467	1423F	16.83	8.16	12.94	542	23.739	573.98	11.391
M55	M468	1426F	1.89	7.32	2.36	78	2.170	53.17	0.901
	M469	1432F	7.96	6.82	6.42	270	0.926	21.88	0.234
	M470	1451F	27.05	5.67	9.85	583	31.506	811.10	3.111
M50	M471	1466F	4.96	7.44	3.64	42	0.782	20.02	0.786
	M472	1537F	35.72	8.73	7.35	244	12.512	387.46	2.705
	M473	1571F	23.76	8.48	12.84	1128	58.607	1660.65	14.315
M100	M489	1016F	3.56	8.04	4.47	66	0.829	17.29	0.546
	M490	1022F	13.87	8.12	15.30	1010	48.358	1183.10	6.149
	M491	1042F	15.44	8.07	11.06	1746	84.186	3031.94	6.716
M101	M492	1054F	25.16	8.63	23.29	283	12.666	287.46	3.077
	M493	1066F	21.10	8.60	19.93	231	8.121	196.93	4.787
	M494	1080F	22.70	8.63	21.42	257	10.381	226.52	4.080
M112	M495	1295F	20.84	6.16	6.03	2530	96.615	1691.54	38.848

	M496	1344F	11.06	7.59	10.72	645	33.839	740.65	11.829
	M497	1434F	12.42	7.78	12.17	610	29.000	646.21	10.066
M091	M498	1460F	3.78	6.19	5.39	384	20.171	406.82	2.966
	M499	1476F	5.92	6.92	8.57	921	47.531	1071.46	7.279
	M500	1492F	25.68	7.84	9.89	1685	70.275	1620.45	13.087
M89	M501	1524F	15.48	7.63	15.11	251	11.350	283.39	2.695
	M502	1550F	21.15	8.56	20.12	891	38.476	1068.40	15.877
	M503	1564F	22.41	8.44	21.40	884	36.559	1138.76	19.986

APPENDIX: G

Sundays River Irrigation Scheme

GPS point #	Sample	Soil EC (mS/m)	Water	Comments
43		75	100	No vineyard on specific spot.
Waterlogged		1670	80	Waterlogged and salt-affected.
10	1461F	1148	80	Beter growth; Good ground surface.
12	141F	323	80	Corn field; Dead area; Sandy soil.
Geen	992F	296	80	Better spot.
27	P36	135.6	80	On hill; Vegetation growth well to spotty; Elevation high; Clayish soil.
6	1486F	382	75	Beter area; More sandy soil; No salt
41		330	75	Poor patch of vineyards; West abandoned vineyard with halophytic plants.
13	256F	846	70	
13	P27	433	65	Height point. Depression. Old river bed; Winelands; Slight salt precipitation; Weaker growth.
Waterlogged		1750	60	Waterlogged and salt-affected.
46a		600	60	Drainage ditch with water and hydric plants.
15	913F	577	60	Peace poor growth
47		700	55	Salt-precipitation.
22	P25	675	50	Clay at 50 cm; Higher ground; Weaker growth.
40		75	50	Vineyards; Poor condition.
7	950F	688	45	Lower area; No salt on service .
25	P34	302	45	River bed; Weak growth; Dead patch; Sand.
21	P31	297	45	Clay at 45 cm; Less clay at topsoil; Better growth.

Symbology

Colour	Type
Blue	Waterlogged
Yellow	Salt-affected
Orange	Both
Green	Unaffected

46		880	40	Slight salt-precipitation.
24	P33	355	40	River bed; Less growth; Sand.
19	P29	1392	30	Dead patch; Salt crusts; Clay.
20	P30	391	30	Vineyard. Copper colour Clay.
20	P23	2530	25	Plants are dying; Light salt crust Lower point in field;
10	P5	329	20	Corn; Bare spot next to dam; Crusting; Clearly a bad area.
29	P38	1412	15	Sandy; Bare spot; No growth; Severe salt crust; Salt-affected.
	306F			
4	30GF	113.5	10	Better growth; Weak infiltration.
2	844F	107.7	10	Light salt on surface. Crusting;
19	P16	68.5	10	Dry; Depression; Weak growth; Rocks at 15 cm.
53		62	10	Bare patch; Depression.
21			10	Compacted soil. No infiltration. Height point.
5	1083F		15	Lower area; High clay content; Permanent hanging watertable; Salt crus
1	1332F	8164		Vineyard; Just outside the field; Salt crusts on surface.
32	P41	8083		Salt on surface; No growth; Bare patch.
9	1263F	7824		Salt crust with a dead patch.
34	P43	6724		Lower point; Salt-affected; Weak growth; Vineyard ; Rock bed at 30 cm.
11	47F	5470		Dead spot; No growth; Salt crust; Rock bed at 30 cm.
27	P21	4380		Bad area; Salt patches/crust; No growth; Bed rock at 20 cm.
24	P18	4320		15 to 20 cm rock bed; Peach; Salt crust Salt-affected.
21	P14	3510		Salt-precipitation; Abandoned area
17	P28	2950		Dead patch. Salt crusts.
18	P28	2950		Dead patch Salt crusts.
35	P44	2263		Rocks at 30 cm; Less salt crust; Weak growth.
25	P19	1961		Less salt crust; Small trees; More ground plants; Rock bed at 10 cm.
8	191F	966		Slight salt crust; Edge of field; Poor growth; Bed rock at 20 cm; Vineyard
28	P22	745		Good area; Better growth; No salt crust.
18	P11	588		Slight salt-precipitation; Bad area; Rock at 15 cm (Calcite?);
52		550		Old vineyard abandoned due to waterlogging and salinity.
6	1713F	457		Better spot – Row 2; Light crust; Good growth; Close to sandy soil spot.

44		381	Vineyard; Relatively good condition.
31	P40	370	Slight salt crusts on surface; Good growth.
54		340	New vineyard; Drained.
21	P24	317	Better growth; No salt crust.
Win1		300	New vineyard; Drained one year.
Win2		280	New vineyard; Drained two years.
45		250	Boundary between waterlogged and non-waterlogged.
28	P26	194.9	Rock bed at 80 cm; No signs of salt precipitation; Spotty growth, but good growth; Sandy soil.
3	401F	185.2	Weaker spot; Salt precipitation on surface.
18	P15	176.8	Higher point; Good growth; Compacted soil
33	P42	167.6	Slight salt precipitation; Good growth.
30	P39	151	No coppering; Good patch; Vines growing well.
13	P8	146.6	Telephone pole; Compacted calcite.
42		138	Vineyard; Relatively good condition.
36	P45	124.6	High point; Beter area; Good growth.
28	P37	124.3	No coppering; Good growth; Edge of vineyard; Sandy soil.
26	P20	120.9	Good spot; Trees growing well.
7	3873 383	103.2	Good area; Bush growth is good.
39	P47	102.4	Beter area; Good growth; No salts; Rocks.
3	P3	99	Sandy soil; Better, thicker growth.
37	P46	90.7	Good area; Denser growth.
D3		90	Dune.
26	P35	84.8	Good growth; Out of river bed; Hard soil; Sand; Incline.
5	P4	82.1	Sandy soil; Lime/rocks 70 cm.
23	P32	80	Higher vines; Good growth.
D1		80	Dune; Salt-precipitation 10 m north of dunes.
11	P6	67.7	Slight crust; Same field as P5; Calcite layer at 15 cm; Transition.
17	P10	63.8	Butternut; Calcite within the field; Better area.
12	P7	61.6	Calcite at 15 cm; Good patch within same corn field as P5 & P6




9781431207398